

Importance of NFAT and NF- κ B signaling in Diffuse large B-cell lymphoma

Dissertation

der Mathematisch-Naturwissenschaftlichen Fakultät
der Eberhard Karls Universität Tübingen
zur Erlangung des Grades eines
Doktors der Naturwissenschaften
(Dr. rer. nat.)

vorgelegt von
Philip Bucher
aus Tübingen

Tübingen
2021

Gedruckt mit Genehmigung der Mathematisch-Naturwissenschaftlichen Fakultät der Eberhard Karls Universität Tübingen.

Tag der mündlichen Qualifikation:

20.10.2021

Dekan:

Prof. Dr. Thilo Stehle

1. Berichterstatter:

Prof. Dr. Stephan Hailfinger

2. Berichterstatter:

Prof. Dr. Dirk Schwarzer

3. Berichterstatter:

Prof. Dr. Lienhard Schmitz

Abstract

Diffuse large B-cell lymphomas (DLBCLs) represent the most frequent B-cell lymphoma and can be subdivided into two groups by their gene expression profile, the Activated B-cell-like (ABC) and the Germinal center B-cell-like (GCB) DLBCL subtype. Around 30% of all patients do not respond to standard immunotherapy or relapse, which highlights the need for further therapeutic options. Among the subtypes, ABC DLBCLs have a less favorable prognosis. ABC DLBCLs are characterized by chronic B-cell receptor signaling and concomitant NF- κ B dependency. Since targeting NF- κ B in patients is challenging due to severe side effects, we investigated other potential targets for ABC DLBCL treatment. We found elevated basal Ca²⁺ levels and NFAT activity in ABC and GCB DLBCLs. Surprisingly, chronic BCR signaling in ABC DLBCLs was not responsible for elevated Ca²⁺ levels and calcineurin activity, but for NFATc1 overexpression. By use of the clinically approved drugs Cyclosporin A and FK506 we could show that calcineurin inhibition impaired survival of ABC but not GCB DLBCLs. In ABC DLBCL, decreased NFAT activity after calcineurin inhibition correlated with reduced expression of relevant target genes, such as *JUN*, *IL6* and *IL10*, which resulted in decreased c-Jun levels and decreased cytokine mediated STAT3 activity.

Furthermore, we identified dimethyl fumarate (DMF) as another therapeutic option for DLBCL treatment. In ABC DLBCLs, DMF induced cell death via inhibition of chronic NF- κ B and STAT3 activity, which was mediated by succination of reactive cysteines of the respective upstream kinases IKK β and JAK1. Intriguingly, not only ABC but also GCB DLBCLs exhibited cytotoxicity upon DMF treatment. We could show that the electrophilic drug DMF induced ferroptosis selectively in GCB DLBCLs by decreasing intracellular GSH levels. ABC DLBCL were more resistant to DMF induced ferroptosis, since chronic BCR signaling and the resulting NF- κ B activity were responsible for increased antioxidant responses. Finally, we could demonstrate that DMF as well as calcineurin inhibitors synergized with Mcl-1 and Bcl-2 inhibitors in inducing cell death in ABC DLBCLs, whereas GCB DLBCLs showed increased sensitivity towards DMF and an inhibitor of ferroptosis suppressor protein 1. Collectively, we could show that the drugs DMF, Cyclosporin A and FK506, all approved for treatment of autoimmune diseases, exhibited a broad anti-lymphoma effect, highlighting their potential for DLBCL treatment.

Zusammenfassung

Diffuses großzelliges B-Zell-Lymphome (DLBCLs) stellen das häufigste B-Zell-Lymphom dar und können anhand ihrer Genexpression in zwei Gruppen unterteilt werden, welche als ABC- und GCB-DLBCL bezeichnet werden. Etwa 30% aller Patienten sprechen nicht auf die Therapie an oder erleiden einen Rückfall, was den Bedarf an weiteren therapeutischen Optionen unterstreicht. Der ABC-DLBCL Subtyp hat eine schlechtere Prognose und ist durch ein chronisches B-Zell-Rezeptor (BCR) Signal und eine gleichzeitige NF- κ B Abhängigkeit gekennzeichnet. Da gezielte NF- κ B Inhibition bei Patienten aufgrund schwerer Nebenwirkungen eine Herausforderung darstellt, haben wir andere potenzielle Angriffspunkte für die Behandlung von ABC-DLBCL untersucht. Wir fanden erhöhte basale Ca^{2+} -Spiegel und NFAT-Aktivität bei ABC- und GCB-DLBCLs. Überraschenderweise war das chronische BCR Signal in ABC-DLBCLs nicht für die erhöhten Ca^{2+} -Spiegel und die Calcineurin-Aktivität verantwortlich, sondern nur für die Überexpression von NFATc1. Durch den Einsatz der klinisch zugelassenen Medikamente Cyclosporin A und FK506 konnten wir eine Calcineurin Abhängigkeit in ABC, nicht aber in GCB DLBCLs zeigen. In ABC-DLBCL korrelierte die Calcineurin-Inhibierung mit einer verminderten Expression von *JUN*, *IL6* und *IL10*, welche für das Überleben der Tumorzellen essenziell sind.

Darüber hinaus identifizierten wir Dimethylfumarat (DMF) als eine weitere therapeutische Option für die DLBCL-Behandlung. In ABC-DLBCLs induzierte DMF den Zelltod durch Hemmung der chronischen NF- κ B und STAT3 Aktivität, die durch Succinierung reaktiver Cysteine in IKK β und JAK1 vermittelt wurde. Interessanterweise war DMF nicht nur für ABC-, sondern auch GCB-DLBCLs toxisch. Wir konnten zeigen, dass DMF den intrazellulären GSH-Spiegel senkte und somit Ferroptose in GCB-DLBCLs induzierte. Durch eine NF- κ B vermittelte, erhöhte antioxidative Kapazität waren ABC-DLBCLs resistenter gegenüber der DMF-induzierten Ferroptose. Sowohl DMF als auch Calcineurin-Inhibitoren zeigen in ABC-DLBCLs Synergien mit Mcl-1- und Bcl-2-Inhibitoren, während GCB-DLBCLs eine erhöhte Sensitivität gegenüber DMF und einem Inhibitor des Ferroptose-Suppressorproteins 1 aufwiesen. Insgesamt konnten wir zeigen, dass die Medikamente DMF, Cyclosporin A und FK506, die alle für die Behandlung von Autoimmunerkrankungen zugelassen sind, auch eine breite Anti-Lymphom-Wirkung aufweisen, was ihr Potenzial für die Behandlung von DLBCLs unterstreicht.

Table of Contents

Abbreviations	6
List of publications	10
I) Included publications	10
II) Accepted publications	10
1. Introduction	12
1.1. B-cell receptor signaling	12
1.2. NF- κ B signaling in B-cells	13
1.3. AP-1 family	15
1.4. PI3K signaling in B-cells	16
1.5. Ca ²⁺ mediated NFAT activation in B-cells	16
1.6. B-cell development	18
1.7. DLBCL classification and mutations	20
2. Aims	25
3. Results and Discussion	26
3.1. Calcineurin inhibitors impair survival by targeting chronic NFAT activity in ABC DLBCL	26
3.1.1. DLBCL cell lines exhibit high intracellular Ca ²⁺ levels	26
3.1.2. Calcineurin inhibitors impair ABC DLBCL cell line survival	28
3.1.3. NFAT and NF- κ B share target genes relevant for ABC DLBCL survival	29
3.1.4. BCR signaling is not directly linked to increased intracellular Ca ²⁺ levels	33
3.1.5. Pathways affecting Ca ²⁺ influx in DLBCLs	37
3.2. Dimethyl fumarate inhibits ABC and GCB DLBCL survival via targeting NF- κ B/STAT3 and inducing ferroptosis, respectively	47
3.2.1. DMF is toxic for DLBCL cell lines	47
3.2.2. DMF induces ferroptosis in GCB DLBCLs	48
3.2.3. DMF directly targets IKK β and JAK1 thus inhibiting NF- κ B and STAT3 activity	49
3.2.4. BCR signaling counteracts ferroptosis sensitivity in ABC DLBCLs	50
3.2.5. DMF treatment synergizes with FSP1 and Bcl-2 inhibition	50
3.2.6. Cytokine treatment sensitizes DLBCLs for DMF induced ferroptosis	51
4. References	56

Abbreviations

5-lipoxygenase (5-LOX)

Activated B-cell-like (ABC)

Activating transcription factor (ATF)

Activation-induced cytidine deaminase (AID)

Activator protein-1 (AP-1)

B-cell linker protein (BLNK)

B-cell lymphoma 10 (Bcl-10)

B-cell receptor (BCR)

Bruton's tyrosine kinase (BTK)

Ca²⁺ release activated channels (CRAC)

Caspase recruitment domain-containing protein 11 (CARD11)

Chimeric antigen receptor (CAR)

Chromatin immunoprecipitation (ChIP)

Chronic lymphocytic leukemia (CLL)

c-Jun N-terminal kinase (JNK)

Class-switch recombination (CSR)

Cyclosporin A (CsA)

Dark zone (DZ)

Diacylglycerol (DAG)

Dimethyl fumarate (DMF)

Early growth response protein (EGR)

Endoplasmic reticulum (ER)

Extracellular signal-regulated kinase (ERK)

Ferroptosis suppressor protein 1 (FSP1)

Fetal Calf Serum (FCS)

Germinal center (GC)

Germinal center B-cell-like (GCB)

Glutathione (GSH)

Glutathione peroxidase 4 (GPX4)

Growth factor receptor-bound protein 2 (Grb2)

Hematopoietic stem cell (HSC)

Immunoglobulin variable region (IgV)

Immunoreceptor tyrosine-based activation motif (ITAM)

Inhibitor of nuclear factor κ B kinase (IKK)

Inositol 1,4,5-trisphosphate (IP3)

Inositol 1,3,4,5-tetrakisphosphate (IP4)

Interferon regulatory factor 4 (IRF4)

Interleukin (IL)

Interleukin-1 receptor-associated kinase (IRAK)

Iodoacetamide (IA)

IP3 receptor (IP3R)

Janus kinase (JAK)

Light zone (LZ)

Mantle cell lymphoma (MCL)

Mechanistic target of rapamycin (mTOR)

Mucosa-associated lymphoid tissue lymphoma translocation protein 1 (MALT1)

Natural killer (NK)

NFAT homology region (NHR)

NF- κ B inducing kinase (NIK)

Non-Hodgkin lymphoma (NHL)

Nuclear factor of activated T-cells (NFAT)

Nuclear localization signal (NLS)

Phosphatase and Tensin homolog (PTEN)

Phosphatidylinositol 4,5-bisphosphate (PIP2)

Phosphatidylinositol 3,4,5-trisphosphate (PIP3)

Phosphoenolpyruvate (PEP)

Phosphoinositide 3-kinase (PI3K)

Phospholipase C γ 2 (PLC γ 2)

Phospholipid hydroperoxide (PLOOH)

Plasma membrane Ca²⁺ ATPase (PMCA)

Polyunsaturated fatty acid (PUFA)

Process of somatic hypermutation (SHM)

Protein kinase C β (PKC β)

Reactive oxygen species (ROS)

Rel-homology domain (RHD)

Sarco/ER Ca²⁺-ATPase (SERCA)

Ser/Thr kinase transforming growth factor β activated kinase 1 (TAK1)

Serine-rich region (SRR)

SH2 domain containing inositol polyphosphate 5-phosphatase 1 (SHIP-1)

SH2 domain containing phosphatase-1 (SHP-1)

Spleen tyrosine kinase (SYK)

SPXX-repeat motifs (SP)

Store operated Ca²⁺ entry (SOCE)

Stromal interaction molecule 1 (STIM1)

TAK1-binding protein 2/3 (TAB2/3)

TNF receptor associated factor 6 (TRAF6)

Toll-like receptor 9 (TLR9)

Transactivation domain (TAD)

Transient receptor potential channel 1 (TRPC1)

Type I phosphatidylinositol 4-phosphate 5-kinase (PIP5K)

List of publications

I) Included publications

- **Targeting chronic NFAT activation with calcineurin inhibitors in diffuse large B-cell lymphoma**

Blood, 2020

Philip Bucher, Tabea Erdmann, Paula Grondona, Wendan Xu, Anja Schmitt, Christoph Schürch, Myroslav Zapukhlyak, Caroline Schönfeld, Edgar Serfling, Daniela Kramer, Michael Grau, Pavel Klener, Claudia Lengerke, Klaus Schulze-Osthoff, Georg Lenz, Stephan Hailfinger

- **Dimethyl fumarate induces ferroptosis and impairs NF- κ B/STAT3 signaling in DLBCL**

Blood, 2021

Anja Schmitt, Wendan Xu, **Philip Bucher**, Melanie Grimm, Martina Konantz, Heike Horn, Myroslav Zapukhlyak, Philipp Berning, Marc Brändle, Mohamed-Ali Jarboui, Caroline Schönfeld, Karsten Boldt, Andreas Rosenwald, German Ott, Michael Grau, Pavel Klener, Petra Vockova, Claudia Lengerke, Georg Lenz, Klaus Schulze-Osthoff, Stephan Hailfinger

II) Accepted publications

- **NF- κ B Activation in Lymphoid Malignancies: Genetics, Signaling, and Targeted Therapy**

Biomedicines, 2018

Paula Grondona, **Philip Bucher**, Klaus Schulze-Osthoff, Stephan Hailfinger, Anja Schmitt

- **Threonine Phosphorylation of I κ B ζ Mediates Inhibition of Selective Proinflammatory Target Genes**

J Invest Dermatol, 2019

Paula Grondona, **Philip Bucher**, Anja Schmitt, Caroline Schönfeld, Barbara Streibl, Anne Müller, Frank Essmann, Sabrina Liberatori, Shabaz Mohammed, André Hennig, Daniela Kramer, Klaus Schulze-Osthoff, Stephan Hailfinger

- **Keratinocyte-derived I κ B ζ drives psoriasis and associated systemic inflammation**

JCI Insight, 2019

Sebastian Lorscheid, Anne Müller, Jessica Löffler, Claudia Resch, **Philip Bucher**, Florian C Kurschus, Ari Waisman, Knut Schäkel, Stephan Hailfinger, Klaus Schulze-Osthoff, Daniela Kramer

1. Introduction

Diffuse large B-cell lymphoma (DLBCL) is the most frequent non-Hodgkin lymphoma (NHL) [1-3]. It is characterized by a very heterogeneous structure, consisting of different cell types. In addition to the malignant B-cells, also T-cells, monocytes/macrophages and natural killer (NK) cells are often present in the lymphoma foci [4]. First line treatment for DLBCLs comprises an anti-CD20 monoclonal antibody (Rituximab) combined with Cyclophosphamide, Hydroxydaunorubicin, Vincristine (Oncovin™) and Prednisone (R-CHOP). While durable remission is achieved in roughly 60% of cases, still over one third of patients is not cured [5, 6]. The severe heterogeneity of DLBCL is a strong therapeutic obstacle since multiple pathways and mutations as well as the tumor environment influence the malignant process. The malignant B-cells themselves frequently harbor hallmarks of germinal center (GC) or of further developed B-cells and exhibit several mutations and translocations and often rely on ongoing B-cell receptor (BCR) signaling [7, 8].

1.1. B-cell receptor signaling

The B-cell development, survival and proliferation is crucially linked to BCR signaling, therefore also malignant B-cells are often dependent on BCR signaling. The BCR can activate different branches of signaling pathways. Tonic BCR signaling is important for B-cell survival and maintenance, whereas antigen-dependent signals after BCR ligation lead to a strong B-cell activation and induces proliferation. BCR ligation by its specific epitope initiates several signaling cascades (Figure 1). Ligand binding results in a conformational change of the BCR, revealing the immunoreceptor tyrosine-based activation motifs (ITAMs) in the cytoplasmic domain of its co-receptors CD79a (Ig α) and CD79b (Ig β) [9, 10]. The tyrosines of the ITAMs are phosphorylated by an initiator kinase, such as Lyn. The phosphorylated ITAMs serve as binding sites for the SH2 domain of the spleen tyrosine kinase (SYK) [11]. After ITAM binding and autophosphorylation, SYK becomes fully activated. Active SYK initiates the formation of a multiprotein complex by phosphorylation of the B-cell linker protein (BLNK). BLNK is a key adaptor protein in BCR mediated signaling and in its phosphorylated form it

provides a docking station for several proteins such as phospholipase C γ 2 (PLC γ 2), Bruton's tyrosine kinase (BTK), and growth factor receptor-bound protein 2 (Grb2) [12, 13]. This allows activated SYK to phosphorylate further effector molecules of this multiprotein complex like BTK. Simultaneously, SYK is responsible for CD19 phosphorylation which results in the activation of the PI3K-PDK1-Akt axis [14]. Meanwhile, phosphorylated BTK activates a second axis via PLC γ 2, which leads to the cleavage of phosphatidylinositol 4,5-bisphosphate (PIP2) into the second messengers inositol 1,4,5-trisphosphate (IP3) and diacylglycerol (DAG). Subsequently, IP3 is released from the membrane and induces Ca²⁺ release from the endoplasmic reticulum (ER) by binding to and opening the ER-resident IP3 receptor (IP3R). In concert with the elevated Ca²⁺ levels, DAG activates protein kinase C β (PKC β), which phosphorylates the scaffold protein caspase recruitment domain-containing protein 11 (CARD11) resulting in active NF- κ B dimers [15] (Figure 1).

1.2. NF- κ B signaling in B-cells

Several B-cell lymphomas are dependent on NF- κ B signaling, but also non-malignant B-cells exhibit NF- κ B activation after different stimulations. Active NF- κ B can be induced by the canonical and the non-canonical pathway. Activation of the canonical NF- κ B pathway in B-cells is initiated for example by BCR ligation, which activates the above described BCR signaling cascade and results in PKC β activation (Figure 1). In unstimulated B-cells, autoinhibition of CARD11 occurs via its inhibitory linker region which keeps CARD11 in an inactive state [16]. After phosphorylation by active PKC β , the inhibitory conformation is released and CARD11 oligomerizes mediated by their coiled-coiled domain [16, 17]. Oligomerized CARD11 provides a binding platform for constitutive associated mucosa-associated lymphoid tissue lymphoma translocation protein 1 (MALT1) and B-cell lymphoma 10 (Bcl-10). Together with CARD11 they form the CBM complex. Subsequently, MALT1 is responsible for recruiting TNF receptor associated factor 6 (TRAF6), which (auto-)polyubiquitinates itself, MALT1 and Bcl-10 [18, 19]. The polyubiquitin chains allow binding of the inhibitor of nuclear factor κ B kinase (IKK) complex consisting of IKK α , IKK β and IKK γ /NEMO. Furthermore, the polyubiquitin chains mediate IKK β phosphorylation by Ser/Thr kinase transforming growth factor β activated kinase 1 (TAK1) which is recruited to the polyubiquitin chains

of the CBM complex by TAK1-binding protein 2/3 (TAB2/3) [20, 21]. In turn, phosphorylated IKK β marks the inhibitor of nuclear factor κ B α (I κ B α) by phosphorylation for proteasomal degradation, thereby releasing transcriptionally active NF- κ B homo- and heterodimers, which translocate to the nucleus [22] (Figure 1). In the nucleus these dimers promote transcription of different genes like *MYC*, *CCND1* (cyclin D1), *BCL2L1* (Bcl-xl), *BCL2*, *IRF4* and *JUN* [23-25]. In B-cells canonical NF- κ B activity is necessary for B-cell activation and proliferation, thus favors survival of malignant B-cells like ABC DLBCLs. Nevertheless, NF- κ B activity not only results in the expression of the already mentioned pro-survival genes, but it also leads to a negative feedback loop by activating gene transcription of *TNFAIP3* and *NFKBIA*, encoding A20 and I κ B α respectively. A20 dampens NF- κ B activity by removing activating ubiquitinations from the CBM complex [26, 27]. I κ B α binds to NF- κ B dimers and covers their nuclear localization signal (NLS), inhibiting their nuclear translocation. Moreover, I κ B α mediates NF- κ B dimer export from the nucleus [28]. Finally, both results in inhibited transcriptional activity of the bound NF- κ B dimers. The NF- κ B dimers can consist of five structurally related transcription factors named RelA/p65, RelB, c-Rel, p52 and p50. Different hetero- and also homodimer combinations of these factors result in various transcriptionally active complexes. NF- κ B dimer formation itself can be initiated either by the canonical pathway described above or by a second pathway termed the non-canonical pathway. The non-canonical NF- κ B pathway is initiated by cell surface receptors like CD40, BAFF-R or RANK [29]. Upon ligation of these receptors a complex containing TRAF2-TRAF3-cIAP1/2 is recruited to the cell membrane and releases NF- κ B inducing kinase (NIK), which is in the steady state constantly marked for degradation by TRAF3 dependent ubiquitination [29]. Subsequent to the recruitment to the cell membrane, the TRAF3 containing complex itself is degraded due to ubiquitination. In turn, released NIK accumulates in the cytoplasm and phosphorylates IKK α [30]. By phosphorylation, active IKK α marks the inhibitory domain of p100 for proteasomal processing which yields in transcriptionally active p52. Accordingly, the non-canonical pathway predominantly results in formation of p52/RelB heterodimers, which can translocate to the nucleus [30]. Contrarily, the canonical pathway rather leads to release of p50/RelA or p50/c-Rel complexes after proteasomal degradation of I κ B α . Next to I κ B α , the classical I κ B family consists of I κ B β and I κ B ϵ sharing the ability to mask the NLS of NF- κ B dimers. The atypical family of I κ Bs including Bcl-3, I κ BNS and I κ B ζ , features a more heterogeneous effect on NF- κ B

dimers. Their gene expression is often induced by transcriptionally active NF- κ B dimers themselves. For I κ B ζ a positive as well as a negative regulation of target genes is reported [31]. In B-cells, especially in DLBCLs, I κ B ζ exhibits a crucial role for cell survival after NF- κ B activation, mainly by activating anti-apoptotic and pro-survival genes [32]. In general, NF- κ B activation upon BCR ligation has a key role in B-cells, thereby supporting non-malignant and malignant cell growth and survival.

1.3. AP-1 family

BCR induced signaling not only activates NF- κ B members but also the heterodimers of the activator protein-1 (AP-1) family [33] (Figure 1). AP-1 transcription factors are subdivided into four subfamilies. The Jun subfamily consists of c-Jun, JunB and JunD. The Fos family (c-Fos, FosB, Fra1, Fra2), the Maf family (c-Maf, MafB, MafA, MafG, Nrl) and the activating transcription factor (ATF) family (ATF2, ATF3, ATF7, BATF, JDP1, JDP2) account for the remaining three subfamilies [34]. BCR induced activation of AP-1 dimers containing c-Fos or c-Jun is mediated by kinases like extracellular signal-regulated kinase (ERK) and c-Jun N-terminal kinase (JNK), which phosphorylate AP-1 family members. Thereby, JNK and ERK regulate their stability and activity [35]. Different AP-1 members influence cell cycle regulators and can positively or negatively impact cell division [36]. Active AP-1 dimers have distinct roles, for example c-Jun containing heterodimers often interact with NFAT members to promote gene expression resulting in survival and proliferation [37]. Downstream of BCR signaling, MALT1 and TAK1 activity were shown to induce expression of AP-1 family members, predominantly ATF2, ATF3, ATF7, c-Jun and JunB, resulting in active AP-1 dimers [24]. Furthermore, AP-1 activity is also necessary for B-cell development which can be counteracted by Bcl-6 expression. This zinc-finger domain containing transcription factor interacts with AP-1 dimers and diminishes their activity on differentiation promoting genes like *PRDM1* (Blimp-1) [38]. In general, AP-1 dimers have a broad mode of action regulating cell division via cyclins, cell survival via Bax and Bcl-2 and also p53 with more distinct roles depending on cell type and dimer composition [39, 40].

1.4. PI3K signaling in B-cells

BCR stimulation and the subsequent activity of SYK results besides BLNK phosphorylation also in the phosphorylation of CD19, another important adaptor protein. Phosphorylated CD19 serves as a docking site for the signal transducing enzyme phosphoinositide 3-kinase (PI3K), which mediates survival and proliferation processes in B lymphocytes (Figure 1). Mainly Class I PI3Ks (i.e. PI3K α , PI3K β , PI3K δ and PI3K γ) are expressed in B-cells. Among these PI3K δ is predominantly found in mature B-cells, whereas PI3K β is the least strongly expressed isoform [41]. Class I PI3Ks catalyze the conversion of PIP2 to phosphatidylinositol 3,4,5-trisphosphates (PIP3s). In turn, accumulated PIP3 acts as a second messenger and recruits PDK-1 and Akt via their pleckstrin homology domains to the cell membrane [41]. PDK-1 phosphorylates Akt at threonine 308, activating its kinase function. Major targets of Akt in B-cells are Foxo transcription factors and mechanistic target of rapamycin (mTOR) which are inhibited and activated, respectively. The phosphatase Phosphatase and Tensin homolog (PTEN) counteracts active PI3K by removing 3-phosphate from PIP3. Similar, SH2 domain containing inositol polyphosphate 5-phosphatase 1 (SHIP-1) antagonizes PI3K activity by dephosphorylating the 5-phosphate of PIP3 [41]. In general, PI3K activity in B-cells possesses an important role for cell survival and proliferation mainly via Akt and/or PDK-1 activation [14, 41]. PI3K and Akt signaling was also reported to be involved in malignant B-cell survival and proliferation [42].

1.5. Ca²⁺ mediated NFAT activation in B-cells

BCR stimulation results in a signaling cascade which activates several important pathways important for B-cell survival and proliferation. Downstream of SYK activation, BLNK phosphorylation leads, next to BTK recruitment and activation, also to PLC γ 2 activity. In turn, active PLC γ 2 converts PIP3 to IP3 and DAG. Subsequently, IP3 binds to IP3 receptors (IP3Rs) residing in the ER membrane. This induces Ca²⁺ influx from the ER to the cytoplasm through the IP3Rs itself. This is potentiated by a process known as store operated Ca²⁺ entry (SOCE). Stromal interaction molecule 1 (STIM1) and STIM2 sense minimal increases of cytosolic Ca²⁺ by binding Ca²⁺ ions followed by

STIM conformational change. Subsequently, STIMs accumulate in parts of the ER membrane localized next to the outer cell membrane. There, STIMs lead to the combination of ORAI molecules in the membrane resulting in Ca^{2+} influx through the assembled Ca^{2+} release activated channels (CRAC). In B-cells, ORAI1 containing CRACs are thought to be the main isoform responsible for BCR mediated Ca^{2+} influx [43]. After activation, CRAC releases Ca^{2+} from the extracellular part into the cytosol, increasing the intracellular Ca^{2+} level. At least one other membrane resident Ca^{2+} channel, TRPC1, was described to be related to BCR induced Ca^{2+} influx [44]. B-cells also show the capacity of BCR independent Ca^{2+} influx, mediated by Erk1/2 activation followed by upregulation of transient receptor potential channel 1 (TRPC1) [45]. If a basal Ca^{2+} concentration threshold is exceeded, calmodulin binds four Ca^{2+} ions [46]. Upon Ca^{2+} binding, calmodulin interacts with the phosphatase calcineurin, releasing its autoinhibition. The main function of active calcineurin is the dephosphorylation of the constitutively phosphorylated Nuclear Factor of activated T-cells (NFAT), thereby revealing its NLS and allowing its translocation to the nucleus. Here, NFAT binds and activates several promoters, supporting transcription of target genes (Figure 1). The NFAT protein family consist of five transcription factors: NFATc1 (also known as NFATc and NFAT2), NFATc2 (NFAT1), NFATc3 (NFAT4), NFATc4 (NFAT3) and the calcineurin independent NFAT5. Additionally, for example NFATc1 is expressed in several isoforms. The spliced variant NFATc1 α A is a strongly active isoform of NFATc1, exhibiting a distinct regulation by NF- κ B [47] and providing a autoregulatory loop [48]. In general, NFATs share next to an amino-terminal transactivation domain (TAD), a NFAT homology region (NHR) and a Rel-homology domain (RHD). The highly conserved RHD mediates DNA binding. Also, the interaction site of NFAT with calcineurin is located in the RHD, consisting of a highly conserved peptide sequence (Pro-X-Ile-X-Ile-Thr) [49]. The NHR domain harbors three SPXX-repeat motifs (SP) and two serine-rich region (SRR) motifs. SRR1, SP2 and SP3 bear 13 constitutive phosphorylation sites which are dephosphorylated by calcineurin resulting in hypophosphorylated NFAT. The NLS is located next to the SP2 motif and is exposed upon dephosphorylation, in turn NFAT can shuttle to the nucleus. This process can be impaired by use of the FDA-approved calcineurin inhibitors Cyclosporin A (CsA) and Tacrolimus/FK506, both broadly used for immunosuppressive treatment. Several constitutively active maintenance kinases ensure NFAT hyperphosphorylation in absence of calcineurin activity. Among these, casein kinase 1, glycogen synthase

kinase 3 and the dual-specificity tyrosine-phosphorylation-regulated kinases are the best studied [50]. Interestingly, active NFATc1 was shown to change NF- κ B dimer formation from p50/p50 homodimers to more active NF- κ B heterodimers, whereas the total expression levels of NF- κ B members were unaffected [47]. Albeit single reports suggest at least interaction of NFAT and NF- κ B on promoter sites [51], the main interaction partners of NFATs are AP-1 dimers [37, 52]. In B lymphocytes the predominant NFAT protein is NFATc1, suggested by a study investigating the effects of *NFATc1*^{-/-} mice, whereas NFATc2 was shown to be dispensable [53]. Furthermore, *NFATc1*^{-/-} mice exhibited a reduced proliferative capacity of B-cells [54]. In cooperation with active NF- κ B and AP-1, Ca²⁺ induced NFAT mediates the signal transduction after BCR stimulation to maintain B-cell survival and to support B-cell proliferation. Moreover, for the B-cell derived chronic lymphocytic leukemia (CLL) active NFAT was reported to be important for cell survival [55].

1.6. B-cell development

B-cells from different maturation stages are reported to develop tumors and numerous originate from B-cells which have undergone immunoglobulin gene rearrangement. B-cells arise from multipotent hematopoietic stem cells (HSCs) which are located in the bone marrow. Various cytokines and stimuli like CXCL12, FLT3 ligand, IL-7 and RANKL tip the balance towards B-cell differentiation of HSCs in specialized niches. Depending on their immunoglobulin gene rearrangement status and surface expression of defined proteins, the B-cell stages can be classified [56]. During B-cell development, the variable (V), joining (J), and diversity (D) loci of the immunoglobulin genes undergo random rearrangement processes in the heavy (H) and light (L) chain. Initiation of gene rearrangement occurs in pre-pro B-cells. The transcription factor EBF1 plays a key role in early B-cell development by promoting D_HJ_H recombination as well as the expression of pre-BCR and the BCR co-receptors CD79a and CD79b. Furthermore, early pro-B-cells initiate the expression of PAX5, determining the fate of the progenitor cell to B-cell differentiation. Accordingly, V_H to D_HJ_H recombination occurs, driving transition to late pro B-cells. After complete V_HD_HJ_H recombination, pre B-cells start surface presentation of pre-BCR and the co-receptors CD79a and CD79b [56]. Subsequently, the proliferating pre B-cells initiate rearrangement of the light

chain, resulting in a fully functional IgM BCR. With IgM surface expression, B-cells enter the immature state. Negative selection deletes immature B-cells expressing IgM with an affinity to self-antigens presented by the bone marrow. The strong BCR signal upon binding of the presented self-antigens results in B-cell apoptosis, a process termed clonal deletion [56]. Alternatively, immature B-cells can reenter the rearrangement process of the light chain, generating an edited IgM BCR. If the self-antigen affinity is low but still present, immature B-cells adopt an anergic state. By downregulation of their proliferative capacity and their BCR signaling, they are blocked in the immature state [56]. Different mechanisms of shutting down BCR signals are known. Mainly, inhibitory receptors and phosphatases like CD22 or FcγRIIB and SHIP-1, SHP-1 or PTEN, respectively, are responsible [43] but also the BCR itself is internalized leading to reduced signaling. Especially compared to IgG-BCRs, IgM containing BCRs are rapidly internalized. IgM dependent internalization is one mechanism suggested to shape the anergic phenotype of immature B-cells [54, 57]. Next to decreased BCR signaling potential, anergic B-cells are characterized by a higher intracellular Ca^{2+} level. However, mice expressing a soluble self-antigen showed that some of these B-cells could escape from the bone marrow to the periphery, still exhibiting an unresponsive, anergic phenotype [58]. Moreover, some reports show a partial reversibility of this anergic state by strong BCR stimulation [59]. Collectively, anergic B-cells seem to be silenced in order to prevent their constitutive activation due to chronic BCR activation. Meanwhile, functional immature B-cells rapidly transit after the maturation process, including affinity selection by clonal deletion, from the bone marrow to the periphery. In the spleen, they differentiate to naïve, follicular or marginal zone B-cells. Marginal zone B-cells seem not to transit the GCs and rather differentiate to short-lived plasma cells independent of T-cell help [57]. Follicular B-cells are in turn T-cell dependent and get activated in the GC through interaction with $CD4^+$ T helper cells. GCs represent a distinct structure in secondary lymphoid organs, comprised by the dark zone (DZ) and the light zone (LZ). In the DZ, B-cells undergo immunoglobulin somatic hypermutation (SHM) after being activated by T-cell dependent antigens in the LZ [60-62]. In this process activation-induced cytidine deaminase (AID) generates point mutations preferably in the variable regions of the immunoglobulin genes. These mutations result in altered immunoglobulin binding affinities and specificity, which are thereafter positively selected in the LZ [63]. Additionally, $CD4^+$ T helper cells support survival and proliferation of GC B-cells by presentation of CD40L [64]. In the LZ, B-cells

differentiate after affinity selection either to memory B-cells or to long-lived plasma cells, which secrete antigen-specific antibodies. Alternatively, they migrate back to the DZ to further mutate their BCR affinity by SHM. Still in the GC, LZ B-cells undergo class-switch recombination (CSR) of IgM to IgA, IgE or IgG by an intrachromosomal recombination in the constant region of the immunoglobulin heavy chain. This process allows altering effector function of immunoglobulins and is initiated by the activation of AID, which relies next to CD40 ligation also on the presence of IL-4 [65]. The selection and SHM process is accompanied by a high proliferative capacity of GC B-cells. Somatic hypermutated immunoglobulin genes are also present in DLBCLs which suggest an origin of DLBCLs from B-cells at least experienced the GC [66]. DNA remodeling occurring during SHM and CSR is most likely responsible for genetic lesions like translocation which are often observed in DLBCLs [67, 68]. Moreover, aberrant somatic hypermutation is thought to occur by the overactivity of AID, causing mutations in proto-oncogenes and thereby driving the malignant process [69]. This strengthens a strong connection of B-cell development accompanied by genetic modifications and the formation of B-cell derived tumors like DLBCLs.

1.7. DLBCL classification and mutations

Based on gene expression profiling (GEP), DLBCLs can be subdivided into two major groups, the germinal center B-cell-like (GCB) and the activated B-cell-like (ABC) DLBCL [70]. Whereas the GCB DLBCLs show hallmarks of GC B-cells itself, the ABC DLBCLs are more poised towards a differentiation to plasma cells, exhibiting a plasmablast like phenotype [70]. In non-malignant GC B-cells the expression of interferon regulatory factor 4 (IRF4) drives Blimp-1 expression, which represses Bcl-6 and downregulates PAX5. Thereby, terminal differentiation to plasma cells or memory B-cells is forced [57, 71]. ABC DLBCLs often show Blimp-1 inactivation [72, 73], arresting ABC DLBCLs in an intermediate state between GC B-cells and plasma cells. Moreover, Spi-B is amplified or overexpressed in ABC DLBCLs and thereby inhibits Blimp-1 expression [74, 75]. With the same consequence as Spi-B overexpression, Bcl-6 translocations occur in ABC DLBCLs [76], preventing Bcl-6 downregulation and thereby blocking Blimp-1 activation. Expression of Bcl-6 in DLBCLs is crucial for repressing several pathways inhibiting cell survival and proliferation like initiation of cell

cycle arrest, response to DNA damage as well as downregulation of anti-apoptotic proteins like Bcl-2 [77]. Next to Bcl-6 activity, Bcl-2 expression is also deregulated by other mechanisms like translocations. In cooperation with aberrant Mcl-1 expression, Bcl-2 overexpression mediates increased resistance to apoptosis in ABC DLBCLs [78, 79]. Besides deregulated cell death mechanisms, gene expression profiling revealed NF- κ B activity as a hallmark of ABC DLBCLs [70, 80-82]. Aberrant NF- κ B signaling in ABC DLBCLs is supported by different mechanisms. Chronic BCR signaling caused by self-antigen reactivity, even among the presented immunoglobulins themselves, drives NF- κ B activity in ABC DLBCLs [7]. Normally, chronic BCR signaling results in anergic B-cells [58] but, for example, in roughly 20% of ABC DLBCLs anergy is prevented by blocking the BCR internalization due to mutations in the CD79 immunoreceptor tyrosine-based activation motifs (ITAMs) thus preventing Lyn-mediated negative regulation [7]. Several other mutations and genetic disorders lead to NF- κ B activity, such as CARD11 mutations [83], *TAK1* mutations [84] and *TNFAIP3/A20* inactivations or deletions [84]. MyD88 mutations provide a second mechanism for activating NF- κ B in ABC DLBCL. Predominantly, the MyD88 L265P mutation is associated with CD79 mutations [85]. The L265P mutation is a gain-of-function mutation causing spontaneous oligomerization and subsequent activation of interleukin-1 receptor-associated kinase 1/4 (IRAK1/4) [85, 86]. Recently, a supercomplex consisting of mutated MyD88, BCR and Toll-like receptor 9 (TLR9) was described in ABC DLBCLs, highlighting the importance of MyD88 mutations alongside with CD79 mutations [87]. This supercomplex was termed My-T-BCR and localizes in endolysosomes, synergistically activating NF- κ B and mTOR. ABC DLBCL exhibiting the My-T-BCR showed to be more responsive to treatment with the BTK inhibitor Ibrutinib than ABC DLBCLs lacking My-T-BCR [87]. Disruption of MyD88 or BCR signaling in ABC DLBCL cell lines was furthermore inhibiting NF- κ B activity and impairing cell survival [85]. A general NF- κ B dependency of ABC DLBCL was shown by overexpression of dominant negative I κ B α or inhibition of IKK γ and IKK β causing severe cytotoxicity in ABC DLBCL cell lines [88, 89]. Nevertheless, systemic use of NF- κ B inhibitors is not feasible due to severe side effects. Therefore, upstream targets promoting NF- κ B activity like BTK or MALT1 are more relevant for therapeutic use, regarding the fact that they are better targetable by small molecule inhibitors with less side effects [90, 91]. Furthermore, some downstream targets of NF- κ B were shown to be crucial for ABC DLBCL viability. One of the most essential ones was I κ B ζ , which

was shown to control NF- κ B target genes by interacting with transcriptionally active NF- κ B dimers. I κ B ζ knock-down in ABC DLBCL cell lines results in severe toxicity [32]. Besides NF- κ B activity, several other pathways are deregulated in ABC DLBCLs, partially based on NF- κ B activity itself. For example, interleukin (IL)-6 and IL-10, are upregulated by NF- κ B, driving the Janus kinase (JAK)-STAT3 pathway by auto- and paracrine stimulation [92]. STAT3 activation supports cell growth as well as resistance to treatment by upregulating e.g. Mcl-1 [78]. Moreover, NF- κ B activity drives AP-1 family member expression and AP-1 activity in ABC DLBCLs. Predominantly, c-Jun, ATF2 and ATF3 were overexpressed in this subtype. Inhibition of NF- κ B signaling as well as knock-down of the mentioned AP-1 members resulted in decreased AP-1 activity and impaired cell survival [24]. Moreover, aberrant c-Jun activity plays a key role in cell migration and evasion of ABC DLBCLs by regulating cell adhesion and motility [33].

In contrast to mutations supporting chronic BCR signaling and NF- κ B activity, GCB DLBCLs more frequently harbor mutations in tumor suppressor genes like *EZH2* or *TP53* [93]. PTEN deletion or downregulation by miR-17-92 results in chronic Akt activation in 30% of the GCB DLBCLs [74]. Moreover, Bcl-2 deregulation based on the t(14:18) translocation is more common for GCB DLBCLs [81]. Similar to ABC DLBCLs, differentiation is often blocked but results in a more GC related phenotype. Therefore, GCB DLBCLs frequently harbor mutations of the Bcl-6 autoregulatory domain [76]. In a subgroup of GCB DLBCL *BCL6* and/or *BCL2* translocation in combination with *MYC* rearrangements result in a more aggressive form termed double- or triple-hit lymphoma [94, 95]. Moreover, GCB DLBCLs exhibit *S1PR2*, *GNA13*, *ARHGEF1* and *P2RY8* mutations, components of a pathway relevant for suppression of cell migration which might cause a disruption of GC architecture with ensuing spread of malignant cells to blood and lymphoid organs [96-98].

Based on new classification strategies [99-101], not only GC related origins of DLBCLs are discussed but also subtypes arising from memory B-cells [102]. In this subgroup *TBL1XR1* mutations play an eminent role in retargeting the SMRT/HDAC3 repressor complex from Bcl6 to BACH2 binding. This results in pre-memory transcriptional reprogramming [103]. This MCD subgroup is in general determined by *MYD88*^{L265P} and *CD79B* mutations. The other redefined genetic subgroups consist of the BN2 type with *BCL6* fusions and *NOTCH2* mutations, a group based on *NOTCH1* mutations

named N1 and the EZB group characterized by *EZH2* mutations and *BCL2* translocations [100]. According to this study a similar classification by Chapuy et al. ordered DLBCLs into five clusters (C1-C5). C5 was predominantly defined by *BCL2* amplification, *MYD88*^{L265P} and *CD79B* mutations often encountering with additional mutations of *ETV6*, *PIM1*, *GRHPR*, *TBL1XR1*, and *BTG1*, whereas C1 showed *BCL6* translocation and *NOTCH2* mutations often accompanied by *BCL10*, *TNFAIP3* (A20) and *FAS* mutations. In general, C1 DLBCLs shared a genetic background with marginal zone lymphomas (MZLs). The C3 DLBCL subgroup was characterized by *BCL2* amplification and mutations in epigenetic regulators like *KMT2D*, *CREBBP* and *EZH2*. Furthermore, C3 DLBCL often exhibited *PTEN* inactivation or loss, representing mainly the GCB DLBCL cases. The C4 subgroup was also predominantly represented by GCB DLBCLs, showing frequent mutations in histone core and histone linker proteins. C2 DLBCLs often harbor mutations affecting cell cycle and chromosomal stability like biallelic *TP53* mutations and *17p* copy loss [101]. Besides the overlap of C5 and MCD also BN2 and EZB correlated with C1 and C3, respectively. Generally, the C5/MCD subgroup consists of ABC DLBCLs with an unfavorable outcome after R-CHOP treatment, whereas the GCB DLBCL with worse outcome comprise mainly the C3/EZB subgroup. Treatment options based on the mutation profile were predicted for these subgroups [104], whereas the predicted therapy for each subgroup were so far not examined nor reanalyzed for response from previous studies. However, some of the suggested inhibitors like Ibrutinib (BTK inhibitor), Venetoclax/ABT-199 (Bcl-2 inhibitor) or the NF-κB targeting bortezomib (proteasome inhibitor) were tested in combination or in addition to R-CHOP therapy without showing superior effects on general outcome of DLBCLs [94, 105]. Even though the new classification might improve outcome of single groups regarding a more targeted therapy, the treatment of DLBCLs remains insufficient and requires further improvement.

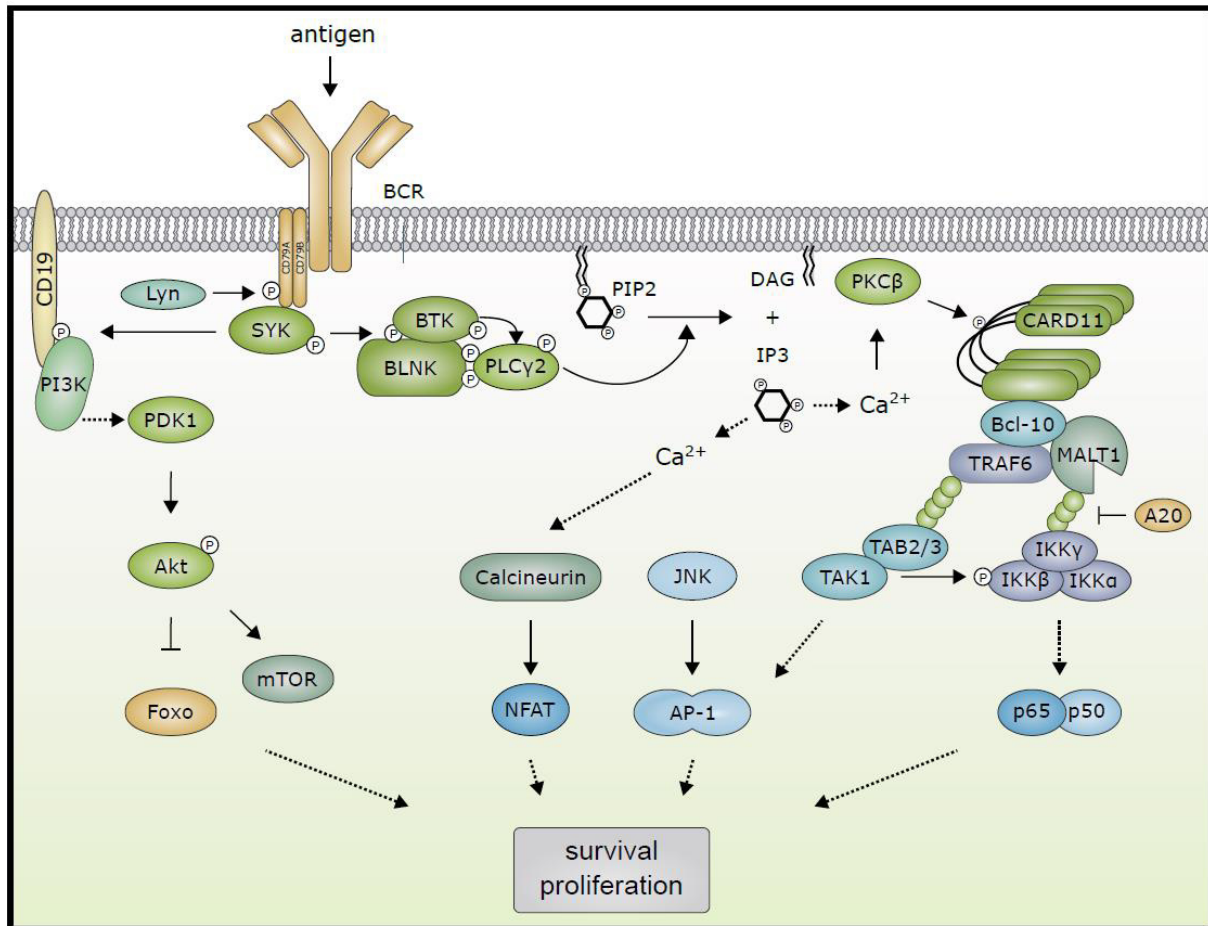


Figure 1: B-cell receptor induced signaling in B lymphocytes. Stimulation of the BCR leads to Lyn mediated phosphorylation of the BCR co-receptors CD79A and CD79B. In turn, SYK binds to phosphorylated CD79 and by further phosphorylations it initiates formation of signaling complexes. Thus, CD19 phosphorylation results in PI3K activity which subsequently results in PDK-1 mediated Akt activity. Akt is responsible for several processes important for B-cell survival and proliferation like Foxo inhibition and mTOR activation. SYK phosphorylated BLNK serves as a docking platform for several proteins like BTK and PLC γ 2. In turn, BTK gets activated, and promotes full activation of PLC γ 2. PLC γ 2 catalyzes the breakdown of PIP2 to DAG and IP3. IP3 leads to subsequent Ca²⁺ influx, which activates, in cooperation with DAG, PKC β . Upon activation PKC β phosphorylates CARD11, thereby initiating the formation of a big signal complex formation, as activated CARD11 provides a scaffold function for proteins like Bcl-10, MALT1 and TRAF6. TRAF6 mediated ubiquitination of this complex results in binding of TAB2/3 and the IKK complex consisting of IKK α , IKK β and IKK γ . By binding of TAK1 to TAB2/3 and the resulting TAK-1 mediated phosphorylation of IKK β , the IKK complex becomes fully activated. This results in I κ B α phosphorylation, which releases NF- κ B heterodimers like p65/p50. Moreover, MALT1 and TAK1 activity mediate AP-1 dimer activation which is supported by kinases like JNK. Furthermore, Ca²⁺ influx activates calcineurin, which dephosphorylates NFAT, which then becomes transcriptional active. Together, Akt activation, NFAT, AP-1 and NF- κ B activity support B-cell growth and survival. Dashed lines indicate indirect effects on respective events.

2. Aims

DLBCLs is a frequently occurring lymphoid malignant disease. GEP analysis suggest a classification into two major subtypes, ABC and GCB DLBCLs. Whereas GCB DLBCLs are more commonly mutated in tumor suppressor genes and harbor translocations leading to aberrant expression of Bcl-2 or c-Myc, ABC DLBCLs seem to be more reliant on chronic BCR signaling including downstream mutations, resulting in a strong NF- κ B dependency. Meanwhile, it has been shed light on several other important pathways in ABC DLBCLs, which are often reported to have a connection to the central NF- κ B signaling in this malignancy. So far, the role of Ca²⁺ signaling in ABC DLBCLs was not specifically investigated. Typically, a signal cascade initiated after BCR ligation results via PLC γ 2 activation in the release of Ca²⁺ from the ER as well as from the extracellular space. Besides NF- κ B activity, the calcineurin-NFAT axis is a central Ca²⁺ dependent pathway in the activation of lymphocytes after antigen-dependent stimulation. Since ABC DLBCL exhibit chronic BCR signaling, our aim was to investigate the hypothesized Ca²⁺ influx in ABC DLBCLs. Subsequently, the role of downstream calcineurin and NFAT activity on gene expression and survival was analyzed. Since the two calcineurin inhibitors Cyclosporin A and Tacrolimus are clinically well established immunosuppressive drugs, repurposing would open new opportunities for ABC DLBCL treatment. Furthermore, we were interested in the relation of NFAT to NF- κ B in ABC DLBCLs as NFAT and NF- κ B are often reported to have related roles in lymphocyte activation. While NF- κ B itself is therapeutically difficult to target. But recent reports showed that the NF- κ B induced atypical I κ B ζ can be targeted by a small drug named DMF. Interestingly, Lenz et al. could show a strong I κ B ζ dependency of ABC DLBCLs. Therefore, DMF would be an interesting compound, not targeting classical NF- κ B itself, but a crucial downstream effector protein of NF- κ B. Consequently, we intended to study the effects of DMF on the survival of ABC DLBCLs. Since several small molecule inhibitors used for DLBCL treatment showed superior effects after combination with a second inhibitor, we further aimed to screen for synergistic combinations with already established inhibitors *in vitro* and *in vivo*.

3. Results and Discussion

3.1. Calcineurin inhibitors impair survival by targeting chronic NFAT activity in ABC DLBCL

This section refers to the publication “Targeting chronic NFAT activation with calcineurin inhibitors in diffuse large B-cell lymphoma”, hereafter cited as “Bucher et al.”.

This research was originally published in *Blood* (2020) 135 (2): 121–132. © the American Society of Hematology.

3.1.1. DLBCL cell lines exhibit high intracellular Ca²⁺ levels

Chronic BCR signaling is a hallmark of ABC DLBCL [7]. Generally, BCR ligation drives a signaling cascade resulting in activation of PLC γ 2, subsequent Ca²⁺ influx and finally in PKC β mediated NF- κ B activity. Ca²⁺ influx in B lymphocytes is crucial for full activation upon BCR stimulation. This is not only due to its ability of PKC β activation in B-cells, but also because Ca²⁺ influx activates several other pathways like the calmodulin-calcineurin-NFAT axis. This pathway was closely studied in lymphocytes, especially in T-cells. In ABC DLBCL it remains elusive except for one report showing nuclear NFAT in DLBCLs by immunohistochemistry staining [106]. Therefore, we analyzed ABC DLBCL cell lines for their intracellular calcium levels by staining with the Ca²⁺ dyes Calbryte-520 AM (Bucher et al., Fig. 2a) and Fura-2 (Bucher et al., supplemental Figure 2A). Surprisingly, not only ABC DLBCL cell lines with chronic BCR signaling, but also GCB-cell lines lacking chronic BCR signaling showed increased Ca²⁺ levels compared to splenic primary mouse B-cells, the Burkitt lymphoma cell line Ramos and the T-cell line Jurkat. Since increased Ca²⁺ levels should result in activation of calcineurin, the observation of NFAT activity in ABC and GCB DLBCL cell lines would support this hypothesis. NFAT activation is controlled (i) by hypophosphorylation and (ii) by nuclear translocation. Both requires phosphatase activity of calcineurin, which induces NLS exposure by NFAT dephosphorylation. Indeed, NFATc1 and

NFATc2 were almost exclusively detected in the nuclear compartment of ABC and GCB DLBCL cell lines analyzed by Western Blot (Bucher et al., Fig. 2g and h), whereas Ramos and Jurkat cell lines showed only weak or no NFATc1 or NFATc2 presence in the nuclear fraction (Bucher et al., Fig. 2i). Moreover, treatment with the calcineurin inhibitors CsA and FK506 removed NFATc1 or NFATc2 from the nuclear fraction and led to NFAT hyperphosphorylation in DLBCL cell lines. NFAT localization and phosphorylation status in DLBCL cell lines after calcineurin inhibition were comparable to those of Ramos and Jurkat cells without treatment (Bucher et al., Fig. 2c-e, supplemental Figure 2F). Of note, in addition to all DLBCL cell lines tested also Mantle cell lymphoma (MCL) cell lines showed nuclear hypophosphorylated NFATc1 and NFATc2 which could be reversed by CsA and FK506 treatment (Bucher et al., supplemental Figure 2d). To ensure that NFAT activity in DLBCLs was not due to an increased calcineurin activity caused by calcineurin overexpression, we compared the calcineurin A and calcineurin B protein levels in DLBCL cell lines, Jurkat and Ramos cells by Western Blot (Bucher et al., supplemental Figure 1). As calcineurin expression was comparable among all analyzed cell lines, we concluded that calcineurin expression was not the cause for active NFATc1 and NFATc2 in DLBCL cell lines. Furthermore, decreased activity of kinases phosphorylating NFAT could be excluded, since inhibition of the phosphatase calcineurin could restore NFAT hyperphosphorylation. Instead, increased Ca^{2+} levels probably accounted for calcineurin activity resulting in NFATc1 and NFATc2 hypophosphorylation and nuclear translocation as increased intracellular Ca^{2+} levels correlated with NFATc1 and NFATc2 activity. To examine this hypothesis, we starved DLBCL cell lines in either Ca^{2+} -free, Fetal Calf Serum (FCS)- free or Ca^{2+} - and FCS-free medium. Analysis by Western Blot revealed that only the combination of Ca^{2+} - and FCS-free medium led to hyperphosphorylation of NFATc1 and NFATc2 (Bucher et al., Figure 2f, supplemental Figure 2e), indicating Ca^{2+} presence also in FCS. By reducing the extracellular Ca^{2+} concentration, we could inhibit calcineurin activity which was confirmed by NFAT hyperphosphorylation observed by Western Blot. The influence of extracellular Ca^{2+} did not seem to be a general bias of cell lines, as the two cell lines Ramos and Jurkat neither exhibit increased intracellular Ca^{2+} levels nor hypophosphorylated NFATc1 or NFATc2 presence in the nucleus in Ca^{2+} -containing medium (Bucher et al., Figure 2e). However, an additional role of FCS in inducing NFAT activity, for example by stimulation of receptors only present in DLBCL cell lines cannot be excluded. In

general, inhibition of Ca^{2+} influx is challenging, therefore calcineurin and NFAT remain as druggable targets for impairing Ca^{2+} mediated signaling in DLBCLs.

3.1.2. Calcineurin inhibitors impair ABC DLBCL cell line survival

DLBCL cell lines exhibited increased intracellular Ca^{2+} levels which resulted in active calcineurin and NFAT. Therefore, it was reasonable to test whether calcineurin inhibitors also had an impact on survival of DLBCL cell lines. Since the two compounds CsA and FK506 are clinically well established, we chose those for testing calcineurin dependency of DLBCL cell lines. Unexpectedly, we only observed cytotoxicity in ABC DLBCL cell lines in response to CsA and FK506 treatment, whereas neither GCB-cell lines nor MCL cell lines showed any response to calcineurin inhibition (Bucher et al., Figure 2b and e), even though both exhibit NFAT activity (Bucher et al., Figure 2a, supplemental Figure 2d). In ABC DLBCL cell lines, calcineurin inhibitors increased the AnnexinV⁺ levels as well as the Caspase 3 activity, indicating that apoptotic cell death was induced by CsA and FK506 treatment (Bucher et al., Figure 1c-d). Interestingly, the ABC DLBCL cell lines harboring a CD79 mutation and/or BCR dependency (i.e. HBL-1, TMD8, OCI-Ly10 and U2932) [7] showed stronger sensitivity towards CsA and FK506 treatment than the BCR independent and CARD11-mutated cell line OCI-Ly3 [7, 83]. Since NFATs are the main target of calcineurin activity, we investigated the importance of NFAT in DLBCL cell lines closer. According to the response of the BCR dependent ABC DLBCL cell lines to CsA and FK506, also shRNA mediated knock-down of NFATc1 exhibited a severe impact on their survival, whereas the CsA and FK506 insensitive GCB DLBCL cell line HT did not show any effect upon NFATc1 silencing (Bucher et al., supplemental Figure 7b-c). The importance of NFATc1 in B-cells is further supported by studies of *NFATc1*^{-/-} mice showing a NFATc1 dependency for normal B-cell development [53].

By use of TMD8 xenograft models in zebrafish, we observed toxicity of CsA and FK506 not only *in vitro* but also *in vivo* (Bucher et al., Figure 6c). Both drugs efficiently inhibited tumor formation in zebrafish, whereby FK506 seemed to be more potent (Bucher et al., Figure 6c-d). Additionally, TMD8 xenograft models in NOD.Cg-Rag1 mice showed significantly reduced tumor volume and tumor weight after a treatment period of nine

days with FK506 (Bucher et al., Figure 6a-b). Superior effects were achieved when CsA was combined with the Bcl-2 inhibitor ABT-199 (Venetoclax) in the TMD8 zebrafish xenograft model. The fraction of zebrafish developing tumors was decreased by roughly 50% compared to single treatment with each of the compounds (Bucher et al., Figure 6c). Not only CsA in combination with ABT-199 but also with the Mcl-1 inhibitor S63845 exhibited synergistic effects in the treatment of ABC DLBCL cell lines (Bucher et al., Figure 6f, supplemental Figure 8b). This effect was only detected in ABC DLBCL cell lines with BCR dependency, whereas the OCI-Ly3 cell line did not show synergistic response to the combination of CsA with the Mcl-1 or the Bcl-2 inhibitor (Bucher et al., supplemental Figure 8a-b). Therefore, BCR dependent cell lines seemed to be susceptible of CsA and FK506 treatments, both *in vitro* and *in vivo*.

3.1.3. NFAT and NF- κ B share target genes relevant for ABC DLBCL survival

Calcineurin inhibitors exhibited a cytotoxic effect on ABC DLBCL cell lines, likely mediated by decreased NFAT activity after treatment. Since neither the increased Ca^{2+} level nor the nuclear location of NFAT could predict the response to calcineurin inhibition, we aimed to understand the underlying mechanism. Therefore, we performed a GEP of untreated and CsA treated DLBCL cell lines (Bucher et al., Figure 4a, supplemental Figure 4a, supplemental Table 3). To assess differently regulated genes which are crucial for cell survival we compared the CsA sensitive ABC DLBCL cell line HBL-1 with the CsA insensitive GCB DLBCL cell line HT (Bucher et al., supplemental Figure 5b). GEP analysis revealed only a small overlap of affected genes in both cell lines, which we excluded from further analysis. Interestingly, numerous genes downregulated after CsA treatment in HBL-1 were associated with NF- κ B activity like *JUN*, *IL10*, *IRF4* or *NFKBIA*. Gene set enrichment analysis highlighted this correlation, since HBL-1 cells exhibited a NF- κ B gene signature after CsA treatment (Bucher et al., supplemental Figure 4b). Surprisingly, a gene signature of ABC DLBCLs treated with the PI3K α/δ inhibitor AZD8835 was also highly enriched (Bucher et al., supplemental Figure 4b). Interestingly, AZD8835 treatment was previously shown to inhibit NF- κ B signaling in ABC DLBCL [42]. Since we could neither detect any NF- κ B deregulation on luciferase-based reporter activity in the ABC DLBCL cell line U2932 (Bucher et al., supplemental Figure 4c) nor deregulated phosphorylation levels of I κ B α

and PLC γ 2 in ABC DLBCL cell lines after CsA treatment (Figure 2), we examined the importance of NFATc1 on the identified target genes from the GEP. Of note, also pAkt levels were unaffected (Figure 2), excluding the possibility of CsA targeting PI3K or Akt.

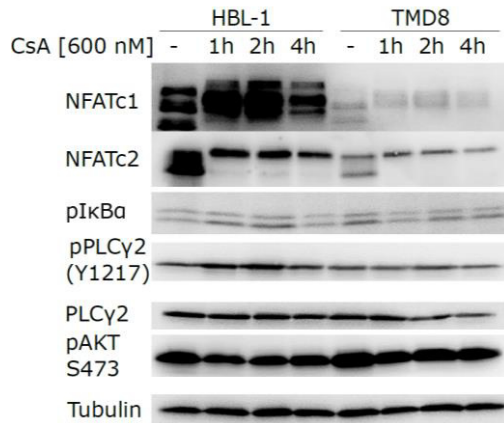


Figure 2: Upstream signaling of NF- κ B was unaffected after calcineurin inhibition in ABC DLBCL cell lines. The ABC DLBCL cell lines HBL-1 and TMD8 were treated with CsA for the indicated time periods. NF- κ B upstream signaling was analyzed by Western Blot by assessing the phosphorylation status of I κ B α , PLC γ 2 and Akt. Tubulin and PLC γ 2 served as loading controls, NFATc1 and NFATc2 hyperphosphorylation confirmed effective CsA treatment.

GEP results were validated by qPCR, showing that *IL10*, *SOCS3*, *STAT3*, *JUN* and *NFKBIA* mRNA levels were downregulated after CsA and FK506 treatment (Bucher et al., Figure 4b-c). Noteworthy, also classical NFAT target genes like Early growth response protein 1 (EGR1), EGR2 and EGR3 were downregulated after CsA treatment, confirming reduced NFAT activity in CsA treated ABC DLBCL cell lines (Bucher et al., supplemental Figure 4d). In contrast to NF- κ B inhibition [24] mRNA levels of other AP-1 members, such as JunB and JunD, were not affected after CsA treatment (Bucher et al., Figure 4c, supplemental Figure 4d). Nevertheless, *JUN* mRNA levels were affected in all tested CsA sensitive ABC DLBCL cell lines (Bucher et al., supplemental Figure 4d), which was confirmed by Western Blot (Bucher et al., Figure 4f). As already reported [33], c-Jun is crucial for the interaction of ABC DLBCLs with the tumor microenvironment. According to this finding, we observed a strong reduction in adhesion to fibronectin coated surfaces of the ABC DLBCL cell line TMD8 after treatment with CsA and FK506 (Bucher et al., Figure 4g). By restoring c-Jun levels with phorbol 12-myristate 13-acetate treatment, the effect of CsA and FK506 on cell adhesion was abrogated (Bucher et al., Figure 4g, supplemental Figure 6c). Moreover, also *IL10* mRNA levels were downregulated in the CsA sensitive ABC DLBCL cell lines HBL-1, TMD8 and OCI-Ly10, (Bucher et al., Figure 4d). This was confirmed by ELISA

from supernatants of ABC DLBCL cell lines treated with CsA and FK506 (Bucher et al., Figure 4e, supplemental Figure 4f). Accordingly, a NFATc1 dependency of IL-10 secretion was recently shown for ABC DLBCL cell lines [107]. Additionally, another important ABC DLBCL cytokine IL-6 [92] was reduced in supernatants of CsA and FK506 treated HBL-1 and TMD8 cells (Bucher et al., Figure 4e, supplemental Figure 4f). Since IL-10 and IL-6 work in an auto- and paracrine manner by activating the JAK-STAT3 pathway via their respective receptors, we expected a concomitant downregulation of STAT3 activity in CsA sensitive ABC DLBCL cell lines. Indeed, diminished IL-10 and IL-6 levels resulted in reduced pSTAT3 levels and in decreased mRNA levels of the STAT3 target *SOCS3* in CsA sensitive ABC DLBCL cell lines (Bucher et al., Figure 4b), whereas the less CsA sensitive ABC DLBCL cell line OCI-Ly3 did not show significantly reduced IL-10, IL-6 or pSTAT3 levels (Bucher et al., Figure 4e-f, supplemental Figure 4f). As phosphorylation of STAT3 is needed for STAT3 dimerization and translocation to the nucleus, diminished pSTAT3 levels caused by reduced IL-10 and IL-6 secretion indicated an impaired transcriptional STAT3 activity which resulted in decreased *SOCS3* transcription. Impaired STAT3 activity likely had a strong impact on the survival of ABC DLBCLs (Figure 3). This has already been described for ABC DLBCLs after JAK inhibition, which also decreased STAT3 activity in DLBCLs [92]. Impaired survival was probably due to decreased *MCL1* and *BCL2* transcription [92] which might explain the increased sensitivity of ABC DLBCLs after calcineurin inhibition towards the Bcl-2 and Mcl-1 inhibitors ABT-199 and S63845, respectively (Bucher et al., Figure 6e-f, supplemental Figure 8a-b) (Figure 3).

Since NF- κ B activity was not impaired after CsA treatment and NFATs are due to their TAD transcriptionally active, a direct role of NFATs in the regulation of *IL10*, *IL6* and *JUN* transcription was conceivable. Therefore, we cloned the *JUN* promoter in a luciferase-based reporter construct to examine its induction by NFAT in the GCB-cell lines BJAB and SU-DHL-4. Like RelA overexpression, also exogenous NFATc1 could indeed enhance *JUN* promoter activity in the two GCB DLBCL cell lines (Bucher et al., Figure 5c). The same hold true for the tested ABC DLBCL cell line U2932 (Bucher et al., Figure 5d). In immune cells, *IL10* transcription is regulated by a proximal and a distal part of the promoter [108]. We tested both parts of the promoter cloned in a luciferase-based reporter construct in HEK293T and U2932 cells. RelA overexpression induced both promoters, whereas NFATc1 only led to a response for the distal promoter (Bucher et al., Figure 5e-f). Both experiments provided evidence for a direct

activation of both, the *JUN* and the *IL10* promoter by NFATc1. However, the *IL6* promoter could neither be activated by NFATc1 nor by NFATc2 (Bucher et al., Figure 5g-h, supplemental Figure 6e). Since NFATc1 was already reported to form transcriptionally active complexes with AP-1 members [37], it was reasonable to test a combination of NFATc1 and the AP-1 member c-Jun for the induction of the *IL6* promoter. Indeed, NFATc1 and c-Jun collectively induced *IL6* promoter activity in HEK293T and U2932 cells as well as a combination of NFATc2 and c-Jun (Bucher et al., Figure 5g-h, supplemental Figure 6e). NFATc1 binding to the *IL6* promoter could be validated by chromatin immunoprecipitation (ChIP) (Bucher et al., Figure 5i). Furthermore, NFATc1 binding to *IL10* and *JUN* promoter sequences was also detected by ChIP in HBL-1 cells. In turn, CsA treatment reduced NFATc1 binding to all three promoters (Bucher et al., Figure 5i). Accordingly, NFATc1 knock-down in the ABC DLBCL cell line HBL-1 resulted in downregulation of *IL10* and *JUN* mRNA levels (Bucher et al., supplemental Figure 7a), (Figure 3).

Since reconstitution with IL-10, IL-6 and c-Jun only partially protected from CsA induced toxicity in ABC DLBCL cell lines but completely restored pSTAT3 and c-Jun protein levels (Bucher et al., Figure 5a-b, supplemental Figure 6d), some other relevant targets remained elusive. As NFATc1 often collaborates with other transcription factors like AP-1 [37] or NF- κ B [51], it is tempting to speculate that some DLBCLs, especially with strong NF- κ B activity like the ABC DLBCL cell line OCI-Ly3, can compensate for the lack of active NFAT (Bucher et al., Figure 1a). Due to the mutation of CARD11, OCI-Ly3 cells exhibit a strong, BCR-independent NF- κ B signal [83]. To test the relevance of mutated CARD11, we overexpressed the hyperactive mutant CARD11^{L244P} in the CsA sensitive ABC DLBCL cell line OCI-Ly10 (Bucher et al., supplemental Figure 7d). This resulted in a significant rescue of cell survival upon CsA treatment (Bucher et al., supplemental Figure 7e), which provided evidence that the CARD11 mutation was indeed responsible for the superior survival of OCI-Ly3 cells. Since active CARD11 results in strong NF- κ B and AP-1 activation, this might provide an explanation for the decreased dependency on NFAT. In this case, BCR induced CARD11 activation must be weaker than the activity of the mutated CARD11. Alternatively, a strong CARD11 mediated and BCR-independent NF- κ B activity might result in a different composition of NF- κ B dimers, although this has not been closely studied so far. As NFATc1 was reported to change NF- κ B dimer formation [47],

NFATc1 might only influence NF- κ B composition of BCR dependent cells and not of CARD11^{L244P} mutated cells.

Furthermore, other genes were found to be deregulated after calcineurin inhibition by GEP. For example, some interesting candidates like cyclin dependent kinase inhibitors 1A and 2C were upregulated in HBL-1 cells after CsA treatment (Bucher et al., supplemental Table 3). This might have an influence on cell growth in ABC DLBCLs without involvement of NF- κ B and would also provide an explanation why CARD11 mutated cells are still partially sensitive to calcineurin inhibition.

3.1.4. BCR signaling is not directly linked to increased intracellular Ca²⁺ levels

According to the literature, activation of the BCR signaling cascade is the central pathway for initiation of Ca²⁺ flux in B-cells. Therefore, we also speculated about the importance of upstream BCR signaling for calcineurin activity. By inhibiting signaling kinases downstream of the BCR complex, we investigated the dependency of the Ca²⁺-calcineurin-NFAT axis towards BCR signaling. Surprisingly, neither NFATc1 and NFATc2 nuclear localization nor their phosphorylation status were changed following inhibition of SYK with GS-9973 or R406 (Bucher et al., Figure 3b, supplemental Figure 3b). To confirm this unexpected outcome, the Src kinase inhibitor Saracatinib, the PI3K α/δ inhibitor AZD8835 and the BTK inhibitor Ibrutinib were tested for their effect on NFATc1 and NFATc2 nuclear localization and their phosphorylation status (Bucher et al., Figure 3f, supplemental Figure d-e). Additionally, knock-down of BCR complex components like CD79A, CD79B or IgM confirmed that NFATc1 and NFATc2 localization and phosphorylation were unaffected by the chronic BCR signal present in most of the ABC DLBCL cell lines (Bucher et al., Figure 3d-e, supplemental Figure 3h-i). Moreover, the capacity of NFATc1 binding to its consensus nucleotide sequence after inhibition of calcineurin and inhibition of upstream BCR signaling was tested in a TransAM assay (Bucher et al., Figure 3c, supplemental Figure 3e). CsA was able to strongly inhibit NFATc1 binding to its consensus nucleotide sequence, whereas Saracatinib did not show any effect on NFATc1 binding activity in the TransAM assay. AZD8835, GS-9973 and Ibrutinib only moderately inhibited NFATc1 binding to its consensus site. Since these inhibitors did not show any effect on NFATc1

regarding nuclear localization or phosphorylation, they might indirectly regulate NFATc1 on gene expression level. Western Blot analysis indeed revealed downregulation of total NFATc1 protein levels after treatment with AZD8835, GS-9973 and Ibrutinib, whereas NFATc2 levels remained unaffected (Bucher et al., Figure 3f). This was in accordance with a recently published report showing a BTK dependency of NFATc1 protein expression in ABC DLBCL cell lines [107]. The same applied to the ABC DLBCL cell line HBL-1 after knock-down of BCR components. siRNA and shRNA mediated knock-down of IgM and CD79A/B, respectively, correlated with the reduction of overall NFATc1 protein levels, whereas NFATc2 levels remained constant (Bucher et al., Figure 3d-e, supplemental Figure 3h-i). This was confirmed on mRNA level, as *NFATC1* but not *NFATC2* transcripts were downregulated after AZD8835, GS-9973 and Ibrutinib treatment in HBL-1 cells (Bucher et al., Figure 3g). Furthermore, *NFATC1* promoter activity was reduced by treatment with AZD8835, Ibrutinib and the IKK inhibitor BMS-345541 in a dual luciferase reporter assay in the ABC DLBCL cell line HBL-1 (Bucher et al., Figure 3h). Considering that all inhibitors resulted in reduced NF- κ B activity and expression of a dominant negative form of I κ B α similarly reduced NFATc1 protein levels (Bucher et al., Figure 3i), it appeared that NF- κ B directly regulates NFATc1 expression. According to previous reports [47], the NF- κ B subunit RelA induced transcription of the distal *NFATC1* promoter (Bucher et al., supplemental Figure 3j). Together, this indicates that chronic BCR signaling and NF- κ B activity induces NFATc1 gene expression but not its activation. Consequently, NF- κ B activity should result in higher NFATc1 protein levels compared to cells with low or absent NF- κ B activity. Indeed, ABC DLBCL cell lines, which are characterized by high NF- κ B activity, showed increased NFATc1 levels compared to all GCB-cell lines tested or the Burkitt lymphoma cell line Ramos which exhibit much lower NF- κ B activity (Bucher et al., supplemental Figure 3g). Together with the fact that NFATc1 knock-down was exclusively toxic for ABC DLBCL cell lines (Bucher et al., supplemental Figure 7b-c), the importance of NFATc1 for ABC DLBCL survival was highlighted. In contrast, GCB DLBCL cell lines also showed increased basal Ca²⁺ levels and resulting NFAT hypophosphorylation but did not rely on NFATc1 activity for cell growth and survival. Since calcineurin was shown to influence upstream T-cell receptor signaling in T lymphocytes [109], we speculated that this might also apply for B lymphocytes. But neither NF- κ B activity nor analyzed upstream signaling was affected in ABC DLBCL cell lines after CsA treatment (Bucher et al., supplemental Figure 4c; Figure 2).

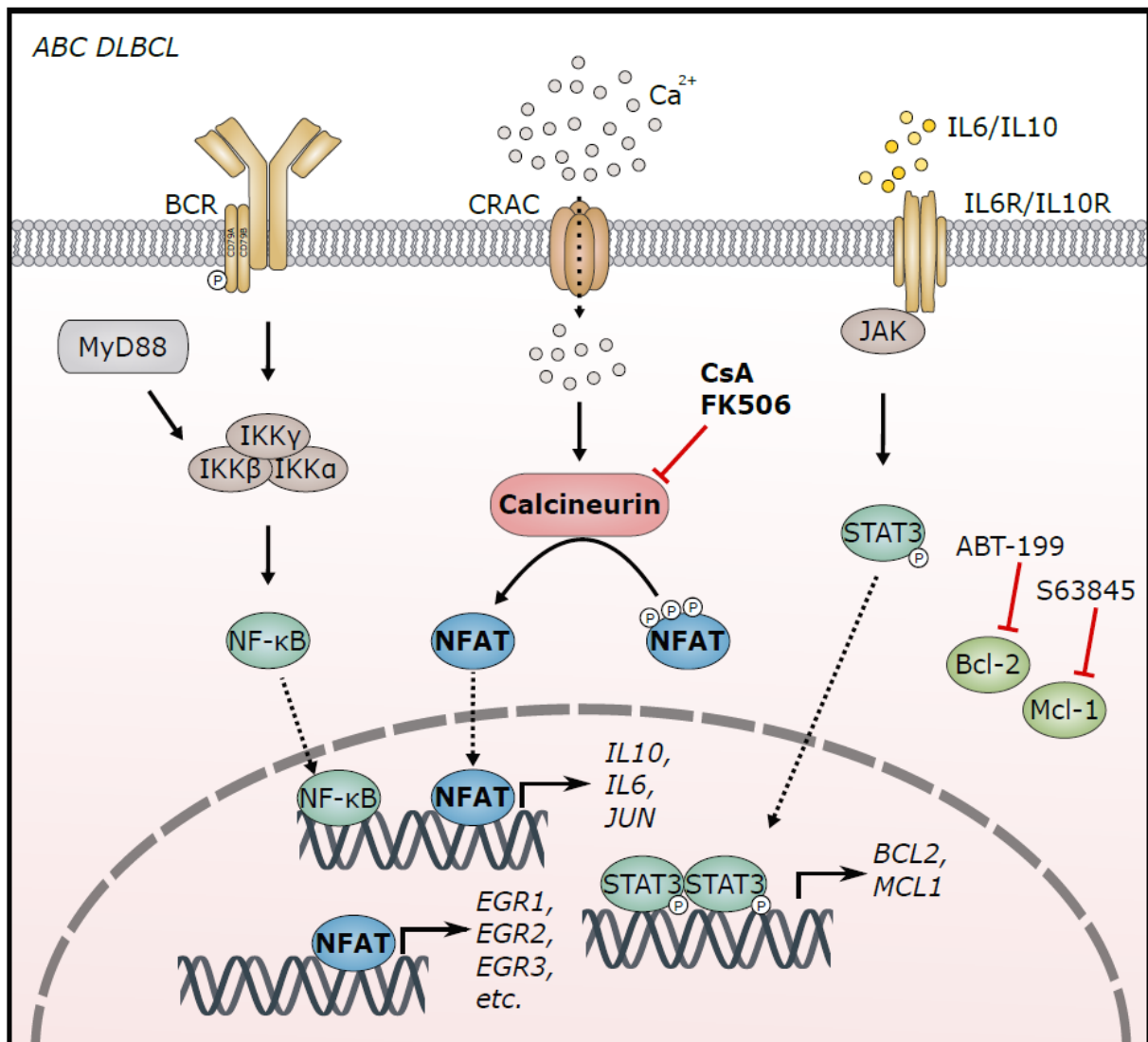


Figure 3: calcineurin mediated NFAT activity drives ABC DLBCL survival. Chronic BCR signaling in ABC DLBCLs results in IKK complex mediated NF-κB activity. MyD88 supports NF-κB activity in cooperation with the BCR. In parallel, extracellular Ca²⁺ influx through open Ca²⁺ channels like CRAC is responsible for elevated intracellular Ca²⁺ resulting in active calcineurin. Hyperphosphorylated NFAT gets dephosphorylated by calcineurin. In turn, hypophosphorylated NFAT translocates to the nucleus where it acts as a transcription factor, e.g. for *EGR1-3*. Moreover, NFAT and NF-κB share target genes like *IL10*, *IL6* and *JUN*. Secretion of IL-10 and IL-6 results in auto- and paracrine stimulation of their cognate receptors. This results in JAK activity which in turn phosphorylates STAT3. Thereby, STAT3 gets transcriptionally active leading to expression of survival supporting genes like *BCL2* and *MCL1*. Bcl-2 and Mcl-1 inhibition by ABT-199 and S63845, respectively, counteract pro-survival effects of their targets. Synergistically with the calcineurin inhibitors CsA and FK506, which inhibit NFAT activity, they mediate cell death of ABC DLBCL cell lines.

Although NFATc1 transcript levels were regulated by downstream effects of BCR signaling, inhibition of chronic BCR signal in ABC DLBCL cell lines did not influence Ca²⁺ levels and calcineurin activity itself, indicated by chronic nuclear localization and hypophosphorylation of NFATc1 and NFATc2. To validate these results, we blocked upstream BCR signaling with a panel of inhibitors targeting calcineurin, Src, BTK, SYK or PI3K. Inhibition of BCR signaling had furthermore no short-term effect on intracellular Ca²⁺ levels in the ABC DLBCL cell lines HBL-1 and TMD8 which was assessed by Calbryte™ 520 AM staining (Bucher et al., Figure 3a). As a positive

control the Ca^{2+} ionophore Ionomycin or BCR stimulation by α -IgM antibodies were used, which indeed rapidly increased intracellular Ca^{2+} levels. In the immunoglobulin negative GCB DLBCL cell line HT neither the blockade of upstream BCR signaling nor α -IgM treatment had any impact on the intracellular Ca^{2+} levels (Bucher et al., Figure 3a). Ionomycin served again as a positive control. For all three cell lines, the cell permeable Ca^{2+} chelator EGTA decreased the intracellular Ca^{2+} levels, demonstrating the functionality of the experimental setup. Additionally, α -IgM induced Ca^{2+} influx could be inhibited by co-treatment with the upstream BCR signaling inhibitors AZD8835, GS-9973 and Ibrutinib, proving their inhibitory effect on BCR signaling (Bucher et al., supplemental Figure 3a). In general, this implies no involvement of the chronic BCR signaling cascade on Ca^{2+} influx and signaling in ABC DLBCL cell lines as basal intracellular Ca^{2+} levels were unaffected after inhibiting upstream BCR signaling. This was in line with the unaffected NFATc1 and NFATc2 nuclear localization and phosphorylation status after inhibiting upstream BCR signaling (Figure 3). As the BCR mediated Ca^{2+} influx is quickly downregulated after IgM stimulation, also negative feedback loops for regulating Ca^{2+} levels after BCR ligation seemed to be intact as well as the ability to induce SYK, BTK and PI3K dependent Ca^{2+} influx after BCR ligation. Of note, the detected increased basal Ca^{2+} levels are not maximal, which was only achieved by additional Ionomycin treatment or IgM stimulation. Apparently, cell lines exhibiting the My-T-BCR supercomplex [87] seemed to be more sensitive towards CsA treatment. Since the BCR is not responsible in activating Ca^{2+} influx and NFATc1 activity, also the My-T-BCR is probably no primary cause for it. Generally, these findings support the idea of BCR independent elevated basal Ca^{2+} levels. This can also be extrapolated to GCB DLBCLs, which are characterized by tonic BCR signaling, triggering mainly the PI3K-Akt pathway [8]. Since inhibiting PI3K in ABC DLBCL cell lines did result neither in altered NFAT localization and phosphorylation nor in reduced intracellular Ca^{2+} levels (Bucher et al., Figure 3a, supplemental Figure 3e), a link between Akt activity and Ca^{2+} influx seems unlikely.

3.1.5. Pathways affecting Ca²⁺ influx in DLBCLs

As discussed above, chronic BCR signaling was not responsible for the elevated Ca²⁺ levels in ABC DLBCLs, therefore the cause for the increased basal Ca²⁺ levels remained elusive. By use of MnCl₂ quenching assays [110] we aimed to determine the source of the Ca²⁺ ions in DLBCL cell lines. Therefore, we stained intracellular Ca²⁺ with Fura-2, a Ca²⁺-specific fluorescent dye. Since Mn²⁺ ions have similar properties than Ca²⁺ ions, they pass the cell membrane via Ca²⁺ channels. In case of open Ca²⁺ channels in the cell membrane, Mn²⁺ ions can enter the cytoplasm. Here, Mn²⁺ ions replace Ca²⁺ ions from Fura-2, thereby quenching the fluorescent signal. We observed this effect in all ABC and GCB DLBCL cell lines tested (Bucher et al., Figure 2b, supplemental Figure 2b). Both cell lines with lower basal Ca²⁺ levels, i.e. Ramos and Jurkat, did not exhibit similar Fura-2 quenching, indicating that ABC and GCB DLBCL cell lines allowed more Mn²⁺ influx compared to the cell lines with lower Ca²⁺ levels. Assuming, that Mn²⁺ ions pass the membrane through the same channels than Ca²⁺ ions, DLBCL cell lines exhibit an increased permeability of Ca²⁺ channels in the cell membrane (Figure 3). This correlates with our finding that DLBCL cell lines exhibit increased Ca²⁺ levels compared to the cell lines Ramos and Jurkat or primary B-cells as well as increased calcineurin activity resulting in hypophosphorylated NFAT (Bucher et al., Figure 2a, supplemental Figure 2a). Taken together, this indicates a role of Ca²⁺ influx via Ca²⁺ channels in the plasma membrane, which are not regulated by BCR signaling.

In previous reports not only BCR signaling was described for inducing Ca²⁺ influx in B lymphocytes, but also CD19 was linked to Ca²⁺ signaling in B-cells [111-114]. Phosphorylated CD19 was shown to bind and activate Vav [115]. Vav1^{-/-}Vav2^{-/-} knock-out in mice has been shown to diminish at least BCR-induced Ca²⁺ influx [116]. Moreover, CD19 ligation without BCR stimulation resulted in increased intracellular Ca²⁺ levels [111]. Therefore, we investigated CD19 in DLBCL cell lines regarding its influence on Ca²⁺ levels and on NFAT phosphorylation. shRNA mediated silencing successfully reduced CD19 surface levels in the ABC DLBCL cell line HBL-1 (Figure 4a). Indeed, CD19 knock-down resulted in decreased intracellular Ca²⁺ (Figure 4b), but not to a level comparable to the basal Ca²⁺ level of Ramos or Jurkat cells (Bucher et al., Figure 2a, supplemental Figure 2a). Additionally, neither NFATc1 nor NFATc2

phosphorylation was altered by CD19 knock-down in the GCB DLBCL cell line HT and in the ABC DLBCL cell line HBL-1 (Figure 4c). Obviously, CD19 accounts partially for the observed Ca^{2+} influx in DLBCLs but is not the unique cause for the elevated Ca^{2+} levels (Figure 5, ①) and is therefore not solely responsible for calcineurin and NFAT activity in DLBCL cell lines.

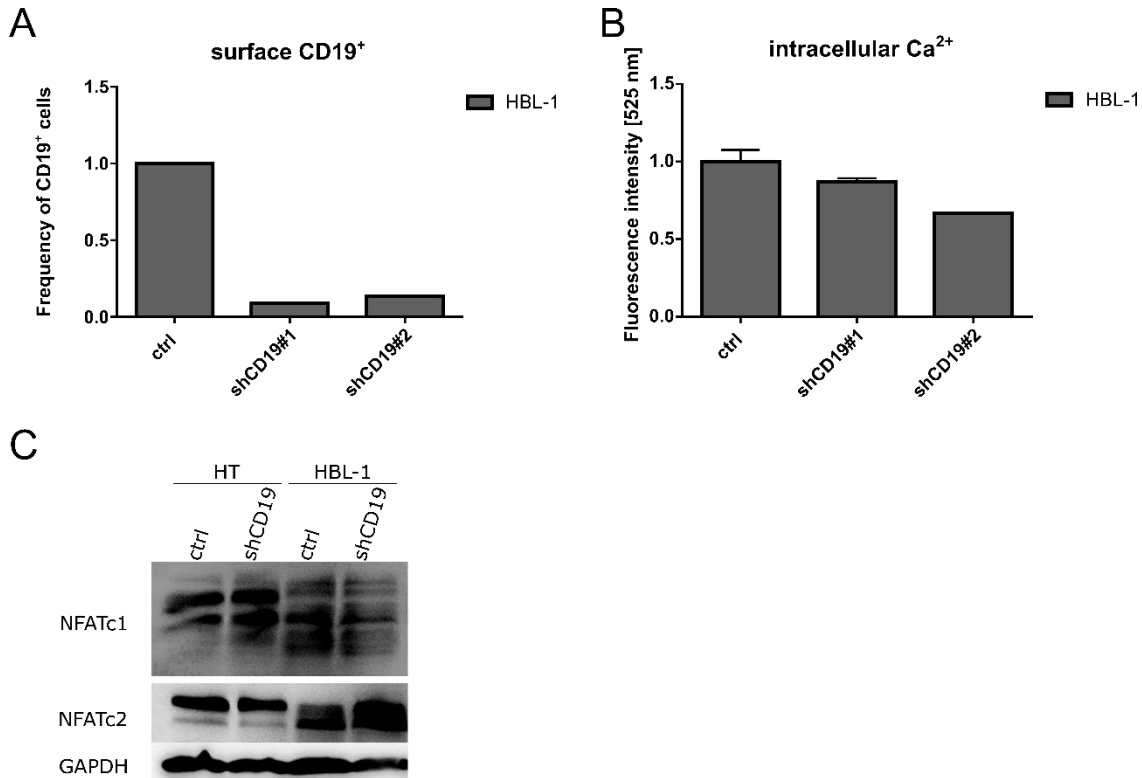


Figure 4: Effect of CD19 silencing on intracellular Ca^{2+} levels and NFAT phosphorylation status. (A) shRNA mediated CD19 knock-down in the ABC DLBCL cell line HBL-1 was validated by analyzing surface CD19 levels by flow cytometry and normalized to control transfected cells. (B) Intracellular Ca^{2+} levels of the control transfected (ctrl) or CD19 silenced HBL-1 cells were measured by analyzing Calbryte 520AM excitation at 525 nm. (C) NFATc1 and NFATc2 protein expression and phosphorylation status were analyzed by Western Blot in the indicated cell lines. GAPDH served as loading control.

This indicates that the elevated basal Ca^{2+} levels in DLBCL compared to other cell lines is the consequence of cooperation between several factors. Some reports showed a positive feedback loop involving PLC γ 2 activation after an initial BCR signal (reviewed in [117]). In turn, active PLC γ 2 steadily converts PIP2 to IP3 and DAG. Exceeding a certain threshold of IP3, ER-stored Ca^{2+} is released and initiates the SOCE process [118]. In case of (i) ongoing PLC γ 2 activity or (ii) a slow reduction of the cytoplasmic IP3 concentration after BCR blockade, intracellular Ca^{2+} could remain elevated after BCR knockdown (Figure 5, ②). Further reports support the idea of ongoing PLC γ 2 activity, showing a BTK independency of its own kinase function in provoking generation of PIP2 by type I phosphatidylinositol 4-phosphate 5-kinase

(PIP5K) [119, 120]. In turn, increased PIP2 levels serve as a substrate for PLC γ 2. In CLL, also a catalytically inactive form of BTK was able to induce PLC γ 2 activity and Ca $^{2+}$ influx [121]. Therefore, even inhibition of BTK by Ibrutinib might result in ongoing Ca $^{2+}$ flux, i.e. if BTK is overexpressed in DLBCL cell lines compared to cell lines with lower basal Ca $^{2+}$ levels (Figure 5, ③). Whether this also applies to ABC DLBCLs remains elusive. Nevertheless, this process must be BCR independent as Ibrutinib inhibited Ca $^{2+}$ influx upon IgM stimulation in HBL-1 cells (Bucher et al., supplemental Figure 3a). This indicates that at least the kinase function of BTK is important for BCR mediated Ca $^{2+}$ flux in ABC DLBCLs.

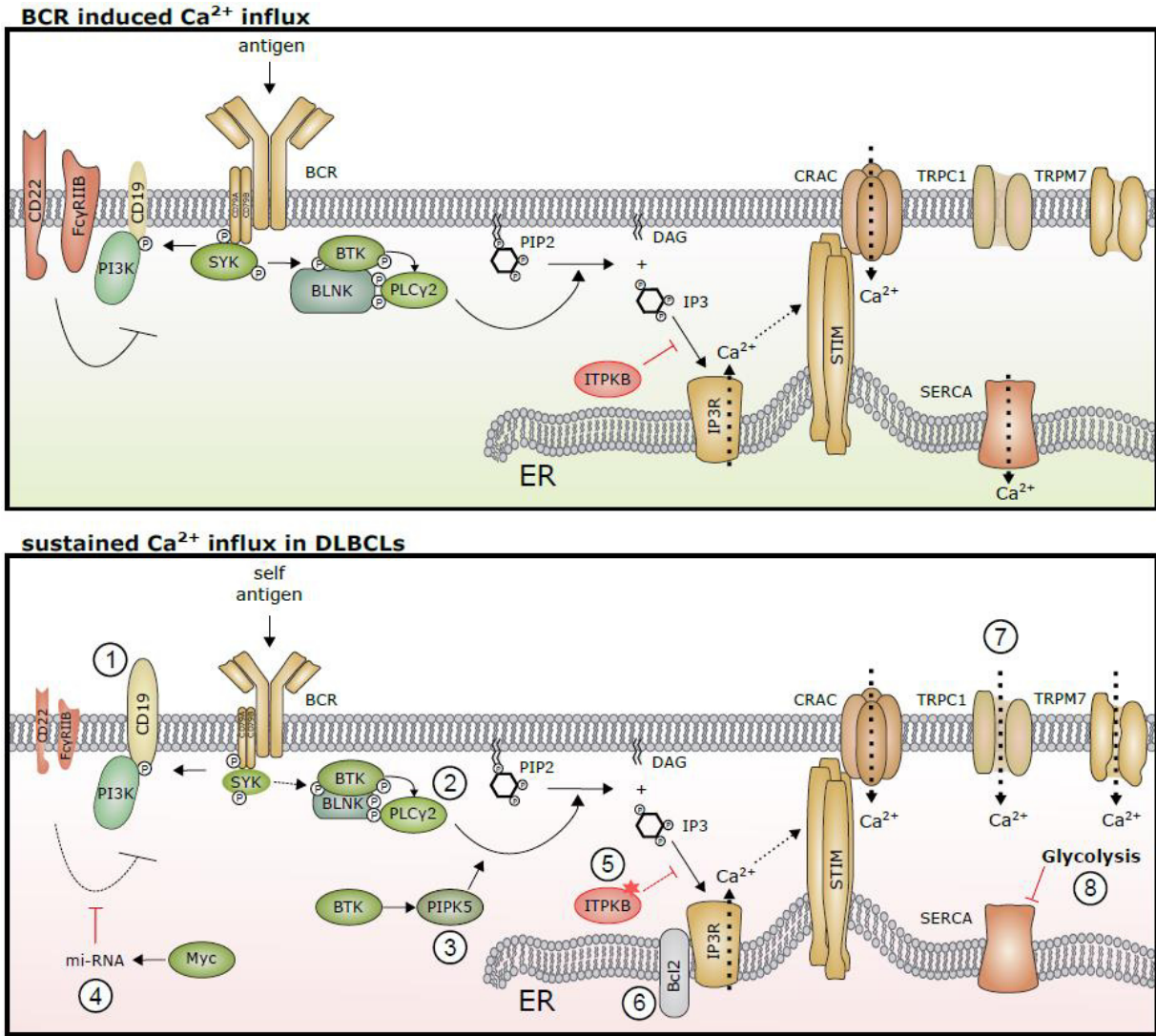


Figure 5: Potential mechanisms resulting in increased basal Ca $^{2+}$ levels in DLBCLs compared to normal BCR induced Ca $^{2+}$ influx. BCR induced Ca $^{2+}$ influx upon stimulation with antigen is mediated by SYK activity. Resulting BLNK phosphorylation serves as a platform for BTK and PLC γ 2 activation. PLC γ 2 cleaves PIP2 to DAG and IP3. In turn, IP3 mediates Ca $^{2+}$ influx from the ER by binding to its cognate receptor in the ER membrane. Increased intracellular Ca $^{2+}$ induces a conformational change of STIM, which subsequently binds to CRAC in the cell membrane, resulting in CRAC activation and Ca $^{2+}$ influx from the extracellular space. To shut off BCR mediated Ca $^{2+}$ flux, negative regulators like CD22 and Fc γ RIIB are activated upon BCR stimulation. Moreover, ITPKB inhibits accumulation of IP3 by further phosphorylating IP3 to IP4. SERCA balances intracellular Ca $^{2+}$ by pumping it to the

ER. Upon BCR activation CD19 is phosphorylated, which mediates Ca^{2+} influx in B-cells (①). PLC γ 2 drives Ca^{2+} influx after BCR ligation supported by a positive feed forward loop (②). Moreover, BTK is capable to support PLC γ 2 activation by activating PIPK5 without being enzymatically active (③). Due to high c-Myc levels, DLBCLs express transcripts of the miR-17~92 cluster, which results in a reduced expression of negative regulators like CD22 and Fc γ RIIB (④). DLBCLs also harbor frequent mutations of ITPKB, resulting in increased IP3 levels. This leads to sustained IP3 binding to its cognate receptor, resulting in sustained Ca^{2+} influx from the ER (⑤). Overexpression or overactivity of Ca^{2+} channels might result in increased intracellular Ca^{2+} levels (⑥). Increased glycolysis results in higher phosphoenolpyruvate levels which inhibits SERCA function, thus preventing reuptake of Ca^{2+} into the ER (⑦). Reduced and increased size of depicted components indicates a minor and major role, respectively, in sustained Ca^{2+} influx in DLBCLs compared to normal BCR induced Ca^{2+} influx.

Besides overexpression of single proteins from the Ca^{2+} influx cascade, also overactivity of single components can be a reason for enhanced Ca^{2+} influx into DLBCL cell lines. Overactivity can be either induced by activating pathways like the BCR signaling cascade or due to missing negative regulation. Since inhibition of BCR signaling does not affect Ca^{2+} levels, rather deletion or silencing of negative regulators seems likely. For example, CD22 and FcγRIIB are described to negatively regulate Ca^{2+} signaling in B-cells, where CD22 for example recruits the phosphatase SH2 domain containing phosphatase-1 (SHP-1) which might lead to the activation of the plasma membrane Ca^{2+} ATPase (PMCA) which shapes CRAC mediated Ca^{2+} influx [43, 117]. CD22 and FcγRIIB were shown to be downregulated in DLBCLs upon c-Myc induced mi-RNA expression from the miR-17~92 cluster [122] (Figure 5, ④). Consequently, c-Myc overexpression could cause increased Ca^{2+} levels. Another important gene involved in the regulation of ongoing Ca^{2+} signaling in DLBCLs might be a frequent occurring deletion or downregulation of *ITPKB* [100, 123], as ITPKB inhibits SOCE via generation of inositol 1,3,4,5-tetrakisphosphate (IP4) from IP3. This was shown in ITPKB deficient cells which had higher intracellular Ca^{2+} levels after BCR stimulation [124]. Lacking the expression of ITPKB, DLBCLs might sustain Ca^{2+} influx even after inhibited upstream BCR signaling due to missing negative regulation of IP3 generation, resulting in ongoing Ca^{2+} depletion from the ER, which would drive the SOCE process (Figure 5, ⑤). Moreover, *Itpkb*^{-/-} B-cells were described to exhibit an unresponsive state similar to anergic B-cells. Anergic B-cells were shown to have increased basal Ca^{2+} levels due to chronic BCR signaling and concomitant decreased response to BCR stimulation [43]. While ABC DLBCLs exhibit chronic BCR signaling [7] they could probably escape anergy due to oncogenic mutations [125]. Accordingly, anergic cells exhibit NFAT activity [126]. Similar to DLBCLs, a subgroup of CLL, termed non-responding CLL, is also characterized by elevated basal Ca^{2+} levels and an anergic phenotype. Blockade of NFAT activity in CLL was shown to induce the escape of this anergic-like state and to elicit cell death [127]. Since CLL and ABC DLBCL share malignant hallmarks like BCR and BTK dependency and a transformation of CLL to DLBCL termed Richter syndrome has been described [128], a similar behavior in regard to NFAT signaling and anergy could be considered. One escape mechanism of NFAT induced apoptosis in DLBCLs might be the characteristic overexpression of anti-apoptotic proteins like Bcl-2 and Mcl-1. Due to a STAT3 dependency of Bcl-2 and Mcl-1 expression [92], calcineurin inhibition and subsequently reduced STAT3 activity

might explain the observed synergism between calcineurin inhibitors and Bcl-2 or Mcl-1 inhibitors (Bucher et al., Figure 6e-f, supplemental Figure 8a-b). Bcl-2 and Mcl-1 were reported to exhibit redundant effects in preventing apoptosis, which explains the survival of cells treated with either a Bcl-2 or a Mcl-1 inhibitor alone [129]. Therefore, reduced STAT3 activity after calcineurin inhibition could also increase the response to single inhibition of Bcl-2 or Mcl-1, as total expression level of both might be reduced and thus potentiate the effect of Bcl-2 or Mcl-1 inhibition.

Alternative explanations for increased Ca^{2+} levels with or without BCR stimulation might be upregulation of single components in the cascade leading to SOCE or of additional Ca^{2+} channels (Figure 5, ©). Some factors like IP3R subunits, the central CRAC members ORAI1-3, STIM1 and STIM2 are crucial for SOCE mediated Ca^{2+} entry. Unfortunately, we could not detect upregulation of any of these genes on mRNA level in DLBCL cell lines compared to the Burkitt lymphoma cell lines Ramos and Raji which are characterized by lower intracellular Ca^{2+} levels (Figure 6a-c). Furthermore, a published CRISPR/Cas9 screen in DLBCL cell lines [87] did not show a dependency on genes involved in the SOCE (Table 1). Noteworthy, ORAIs and STIMs are redundant in their function, which could mask the knock-out effect of single components.

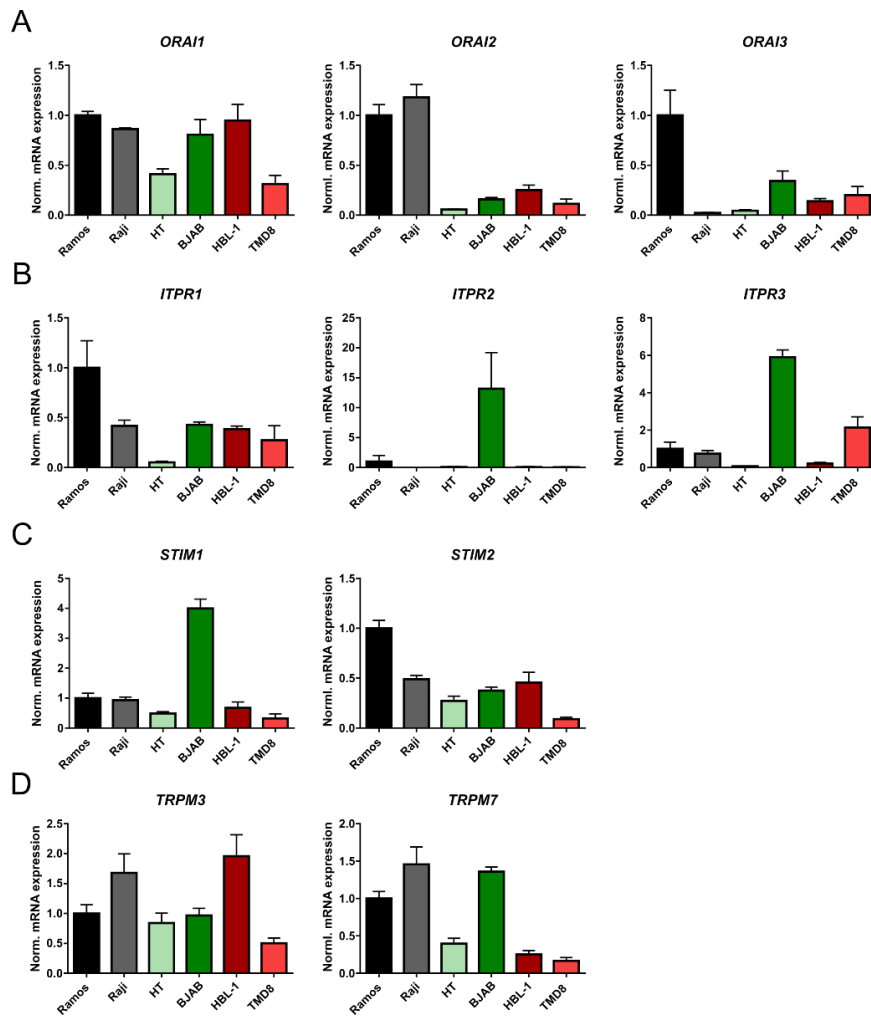


Figure 6: mRNA levels of central components involved in Ca^{2+} influx were not deregulated in DLBCL cell lines. Transcripts of (A) the central CRAC compartments *ORAI1*, *ORAI2* and *ORAI3*, (B) of the IP3R isoforms *ITPR1*, *ITPR2* and *ITPR3*, (C) of *STIM1* and *STIM2* and (D) of *TRPM3* and *TRPM7* were measured by qPCR and normalized to a housekeeper gene. Transcripts of cell lines with lower intracellular Ca^{2+} levels Ramos and Raji were compared to DLBCL cell lines HT, BJAB, HBL-1 and TMD8 with increased intracellular Ca^{2+} levels. Relative mRNA levels were normalized to the Ramos cells.

Besides the classical members involved in SOCE, also other factors were suggested to influence Ca^{2+} entry. TRPM7 is a Ca^{2+} and Mg^{2+} channel reported to show basal activity and lead to spontaneous Ca^{2+} influx [130]. TRPM7 plays a central role in B lymphocytes by mediating and sustaining Ca^{2+} levels after BCR ligation [131]. Although knock-out of this Ca^{2+} channel resulted in decreased cell survival in the CRISPR/Cas9 screen (Table 1), the mRNA expression levels themselves were not deregulated in DLBCLs compared to cell lines with lower basal Ca^{2+} levels (Figure 6). Also *TRPM3* transcripts, a Ca^{2+} channel expressed in B lymphocytes [132], were not increased in DLBCLs (Figure 6). In B-cells some other Ca^{2+} channels have been described to have influence on Ca^{2+} signaling. One of these Ca^{2+} channels is TRPC1 which has been shown to affect Ca^{2+} signaling independently of BCR mediated signaling in B-cells [44]. Finally, in the recently published CRISPR/Cas9 screen ([87],

Table 1) none of these Ca²⁺ channels lead to decreased cell survival. However, redundancy of two or more channels in sustaining Ca²⁺ levels in DLBCLs cannot be excluded.

Table 1: Impact on cell survival of genes potentially involved in Ca²⁺ signaling in DLBCLs. Selected data of a published CRISPR/Cas9 screen [87] with four ABC DLBCL cell lines (HBL-1, TMD8, U2932, HLY1), four GCB DLBCL cell lines (DOHH2, SU-DHL4, SU-DHL5, WSUDLCL2), two multiple myeloma cell lines (ARP1C and KMS11) and one Anaplastic large-cell lymphoma T-cell line (DEL). Genes were highlighted with green and red colors depending on better or worse survival, respectively, after individual gene knock-out. Depicted genes were selected according to their ability to influence Ca²⁺ influx.

Gene Symbol	HBL-1	TMD8	U2932	HLY1	DOHH2	SU-DHL-4	SU-DHL-5	WSUDLCL2	ARP1C	KMS11	DEL
Orai1	0.13	0.05	0.20	0.51	0.11	-0.24	0.10	0.27	0.72	0.16	0.43
Orai2	0.49	0.21	0.27	-0.44	-1.06	-0.38	-0.25	-0.30	-0.12	-0.08	0.13
Orai3	0.19	0.19	0.27	0.73	0.24	-0.08	0.39	0.57	-0.18	0.12	0.44
STIM1	-0.44	-0.74	-0.23	0.09	0.37	-0.40	0.53	0.38	-0.60	0.01	0.22
STIM2	-0.02	0.02	-0.28	0.49	0.49	0.69	0.48	0.50	0.04	0.54	0.68
ITPR1	0.04	0.76	0.19	0.61	0.18	0.26	0.36	-0.05	-0.64	0.05	-0.13
ITPR2	0.36	-0.32	0.88	0.12	0.41	-0.17	0.17	0.29	-0.42	0.10	0.83
ITPR3	0.63	-0.20	0.07	0.36	0.11	-0.32	0.29	-0.04	0.92	-0.08	-0.25
PLCG1	0.33	0.67	0.40	0.56	0.51	0.36	0.53	0.38	-0.42	0.41	0.67
PLCG2	-4.71	-2.92	-0.92	0.40	0.04	0.09	-0.24	-0.10	0.02	-0.30	-0.23
TRPC1	-0.04	0.42	0.19	0.48	0.28	-0.10	0.04	0.40	-0.43	0.55	0.08
TRPC3	0.05	0.35	0.25	0.42	0.10	0.39	0.27	0.13	-0.04	-0.46	0.39
TRPC4	0.35	0.39	0.64	0.10	0.16	-0.13	0.08	0.20	-1.19	0.43	-0.38
TRPC4AP	0.53	0.54	0.71	0.38	0.16	-0.46	0.06	0.00	0.05	-0.15	0.42
TRPC5	0.38	0.16	0.41	0.48	0.43	0.53	0.55	0.71	0.86	0.73	0.18
TRPC5OS	0.65	0.13	0.85	0.64	0.77	0.21	0.59	0.39	0.86	0.86	-0.16
TRPC6	0.14	0.57	0.46	0.38	0.46	0.20	0.36	0.37	0.50	0.52	-0.06
TRPC7	0.42	0.58	-0.33	0.40	0.16	0.09	0.28	0.34	-1.29	-0.02	-0.39
TRPM1	0.13	0.47	0.45	0.34	0.51	-0.61	-0.10	0.19	0.05	0.11	0.44
TRPM2	-0.04	0.32	1.82	0.31	0.48	0.47	-0.06	0.17	-0.32	-0.13	0.27
TRPM3	-0.11	-0.11	-0.19	0.19	0.16	-0.18	0.31	0.53	0.67	-0.07	0.30
TRPM4	-0.05	-0.75	-0.15	0.02	-0.23	0.30	-0.25	0.00	-0.18	0.32	0.19
TRPM5	0.70	0.03	0.19	0.85	-0.03	-0.48	0.51	0.02	0.83	0.63	0.50
TRPM6	0.52	0.27	0.49	0.42	0.44	0.05	0.53	0.23	0.48	0.35	0.21
TRPM7	-4.37	-0.99	-3.94	-3.79	-3.26	-3.67	-3.70	-3.81	-1.45	-3.39	-3.20
P2RX1	1.14	-0.15	0.13	0.04	-0.59	-0.62	-0.48	-0.98	0.19	-1.01	0.42
P2RX2	0.50	0.58	0.57	0.35	0.17	-0.20	-0.05	0.09	-1.09	-0.29	-0.10
P2RX3	0.33	0.25	0.24	0.46	0.45	-0.55	0.16	0.25	-0.17	0.02	0.29
P2RX4	-0.57	0.25	0.29	0.42	0.30	-0.45	0.09	0.16	-0.02	0.31	-0.05
P2RX5	0.38	0.48	0.58	0.07	-0.31	0.67	0.57	1.05	0.62	1.29	0.97
P2RX6	0.42	-0.27	0.40	0.81	0.37	0.05	0.60	0.19	0.50	1.13	0.37
P2RX7	-0.27	0.22	-0.33	-0.05	-1.27	-0.42	-0.07	-0.43	-0.41	-0.33	0.32
TRPV1	0.43	0.48	0.15	0.45	0.22	-0.33	0.26	-0.03	1.02	-0.03	-0.06
TRPV2	-0.02	0.43	-0.03	0.14	0.36	0.33	0.32	0.12	-0.27	-0.02	0.44
TRPV3	0.18	0.19	0.08	0.65	-0.02	-0.29	0.29	0.27	0.69	0.45	0.34
TRPV4	0.39	0.21	0.37	0.47	0.27	0.04	-0.14	0.32	-0.09	0.95	0.54
TRPV5	0.47	0.09	0.39	0.54	0.37	0.59	0.79	0.63	-0.13	0.35	0.97
TRPV6	0.09	0.36	-0.23	-0.51	-0.40	-0.34	0.32	0.66	-0.19	0.08	0.29

Besides deregulated gene expression and genetic mutations, also metabolites can influence basal Ca²⁺ levels. A high proliferative capacity of oncogenic cells is often linked to increased glycolysis, resulting in the accumulation of phosphoenolpyruvate (PEP). In T lymphocytes increased PEP levels inhibit Ca²⁺ reuptake from the cytosol to the ER via sarco/ER Ca²⁺-ATPase (SERCA), resulting in increased basal Ca²⁺ levels [133]. Studies in DLBCLs suggest an increased glucose consumption [134], supporting a potential link between glycolysis and Ca²⁺ level in DLBCLs (Figure 5, ⊙). Since GC derived cells exhibit a high proliferative capacity [62], increased basal Ca²⁺ levels could

also be a hallmark of GC derived malignancies. Similar to the GCB DLBCL subtype, also Burkitt lymphomas are thought to arise from GC derived B-cells [66]. This disfavors a developmental related upregulation of intracellular Ca^{2+} levels.

Nevertheless, targeting the as yet unknown cause to inhibit Ca^{2+} influx in DLBCL cell lines would probably result in decreased cell survival, as DLBCL cell lines exhibited reduced cell growth already after 6 h in absence of Ca^{2+} (Figure 7). Unfortunately, this was only achieved by reducing FCS in the medium, as FCS supplementation led to calcineurin activity even in Ca^{2+} -free medium (Bucher et al., Figure 2f, supplemental Figure 2e). Since FCS is crucial for long-term survival of cell lines in culture, long-term starving in FCS-free medium to deplete Ca^{2+} is challenging. However, withdraw of Ca^{2+} decreases specifically DLBCL survival as the control cell lines Ramos and Jurkat were not affected. Furthermore, this correlated nicely with the observation that both, Ramos and Jurkat cells exhibited lower basal Ca^{2+} levels than all DLBCL cell lines tested (Bucher et al., Fig. 2a, supplemental Figure 2A).

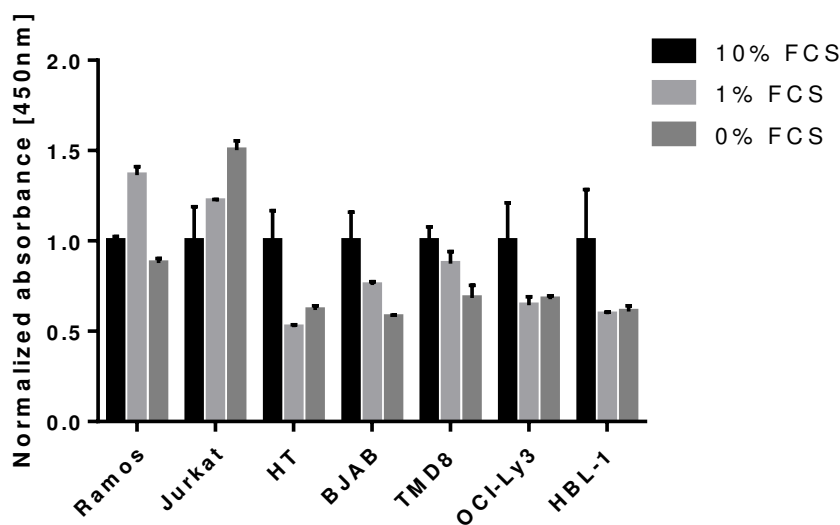


Figure 7: Impact of Ca^{2+} starvation on DLBCL cell line survival. Cell survival analyzed by MTS assay was compared between the two cell lines with lower intracellular Ca^{2+} levels, Ramos and Jurkat, and the DLBCL cell lines HT, BJAB, TMD8, OCI-Ly3 and HBL-1 after 6 h incubation in Ca^{2+} free medium and either 10% FCS, 1% FCS or 0% FCS.

Regarding the effect of Ca^{2+} starvation on all DLBCL cell lines, an inhibition of Ca^{2+} influx or of Ca^{2+} mediated signaling would not only be effective against ABC DLBCL cell lines but also against GCB DLBCL cell lines. Therefore, deeper analysis of deregulated Ca^{2+} influx and signaling on molecular basis might result in new treatment options for DLBCLs. Nevertheless, the calcineurin inhibitors CsA and FK506 already exhibit a strong effect on ABC DLBCL survival, highlighting the important role of the

Ca²⁺-calcineurin-NFAT axis in this malignancy. Furthermore, CsA and FK506 are clinically well-established and FDA-approved drugs, used for immunosuppression in autoimmune diseases and for suppression of immune mediated transplant rejection. Despite the potential of repurposing CsA and FK506 for DLBCL treatment, their efficacy in for DLBCL treatment must be further evaluated. Beyond that, it must be considered that calcineurin inhibitors are also directly targeting activity of T-cells. Therefore, a combination with immunotherapies like chimeric antigen receptor (CAR) T-cells or immune checkpoint inhibitors might lower the efficacy of the two latter approaches. On the other hand, a recent report could show an upregulation of the immunosuppressive PD-L1 by NFATc1 mediated IL-10 expression in ABC DLBCLs, suggesting also a role for calcineurin inhibition in reducing immune evasion of ABC DLBCLs [107]. Collectively, a combination of calcineurin inhibitors with immunotherapies should at least be sequentially applied. A common characteristic of DLBCLs is the increased expression of Bcl-2 and Mcl-1 which reduces the sensitivity towards chemotherapeutic and immunotherapeutic treatment [78, 79, 129, 135-137]. The Bcl-2 inhibitor ABT-199 was therefore already combined with R-CHOP [138] and suggested for Ibrutinib treatment [139]. As we could further show synergistic effects of calcineurin inhibitors with ABT-199 and S6384, a combination of calcineurin inhibitors with either the Bcl-2 inhibitor ABT-199 or the Mcl-1 inhibitor S6384 seems therefore to be a plausible and promising approach for ABC DLBCL treatment.

3.2. Dimethyl fumarate inhibits ABC and GCB DLBCL survival via targeting NF- κ B/STAT3 and inducing ferroptosis, respectively

This section refers to the publication “Dimethyl fumarate induces ferroptosis and impairs NF- κ B/STAT3 signaling in DLBCL”, hereafter cited as “Schmitt et al.”.

This research was originally published in *Blood* (2021) 138 (10): 871–884. © the American Society of Hematology.

3.2.1. DMF is toxic for DLBCL cell lines

ABC DLBCLs were shown to be crucially dependent on NF- κ B activity. Some of the NF- κ B regulated genes like Bcl-2 and I κ B ζ exhibit major roles in DLBCL survival. In ABC DLBCL cell lines, I κ B ζ mediates survival by co-regulating many NF- κ B target genes predominantly by interacting with p50 and p52 subunits [32]. Unfortunately, neither NF- κ B itself nor I κ B ζ is easily targetable clinically by small molecule inhibitors. Recently, the two electrophilic substances dimethyl fumarate (DMF) and dimethyl itaconate (DI) were shown to target I κ B ζ by affecting its mRNA stability [140, 141]. Therefore, it was reasonable to test whether DMF induces cytotoxicity in ABC DLBCLs. Indeed, treatment of ABC DLBCL cell lines with DMF over 10 days resulted in a significant decrease in cell counts (Schmitt et al., Figure 1b, supplemental Figure 1b, d). Surprisingly, GCB DLBCL cell lines exhibited an even greater toxicity upon DMF treatment (Schmitt et al., Figure 1a, supplemental Figure 1a, c). Especially, the GCB DLBCL cell lines DOHH2 and OCI-Ly7 showed with doses as low as 5 μ M DMF a strong cytotoxic effect within a few days (Schmitt et al., supplemental Figure 1c). Not only DLBCL cell lines but also MCL cell lines exhibited impaired cell survival after DMF treatment (Schmitt et al., Figure 2a), whereas other cell lines from myeloid origin, carcinoma or melanoma cell lines were unaffected by treatment with 20 μ M DMF (Schmitt et al., Figure 1c, supplemental Figure 2b). Since both GCB DLBCL and MCL cell lines are independent of I κ B ζ [32], the effect of DMF on I κ B ζ did not serve as explanation for the observed toxicity, at least in these lymphoma subtypes.

3.2.2. DMF induces ferroptosis in GCB DLBCLs

Since DMF has electrophilic properties, we considered this for mediating toxicity. The DMF-related, non-electrophilic compounds dimethyl succinate and monomethyl fumarate showed no effect on DLBCL cell survival, whereas treatment with the electrophilic DI had a similar outcome as DMF treatment. Consequently, the observed effect seemed to be based on with the electrophilic properties of both substances. As glutathione (GSH) serves as a cellular antioxidant to trap electrophilic substances, we evaluated the effect of DMF on GSH levels, which were indeed reduced after DMF treatment. Moreover, by GSH depletion DMF interfered with GSH-dependent processes on like the detoxification of phospholipid hydroperoxides (PLOOHs), a lipid form of reactive oxygen species (ROS), which is mediated by Glutathione peroxidase 4 (GPX4). The increased lipid peroxidation in response to DMF treatment was illustrated by the oxidation sensitive lipophilic probe BODIPY C11 in DLBCL cell lines. Again, GCB DLBCL cell lines proved to be more sensitive to lower concentrations of DMF regarding the level of lipid oxidation. Similar to DMF treatment, accumulation of PLOOHs by RSL3 mediated GPX4 inhibition [142] resulted in increased lipid oxidation. Also, decreased GSH synthesis by blocking cysteine import with erastin-1 led to increased lipid peroxidation in DLBCL cell lines. Both, RSL3 and erastin-1 are established inhibitors to induce ferroptosis. Therefore we speculated that the ferroptosis inhibitors ferrostatin-1, α -tocopherol and deferoxamine [142] could inhibit DMF induced lipid peroxidation. For example, deferoxamine can inhibit ferroptosis by chelating iron, thereby preventing the oxidization process of polyunsaturated fatty acids (PUFAs). α -tocopherol scavenges lipid peroxy radicals, thereby inhibiting the ferroptosis process. Ferroptosis is a non-apoptotic form of cell death and is characterized by excessive lipid peroxidation. Finally, accumulated PLOOHs results in ruptured membranes of organelles and of the cell membrane [142, 143]. Since we observed similar effects with DMF treatment as evoked by ferroptosis inducing agents in GCB DLBCLs and the effects of DMF were reversed by ferroptosis inhibitors, we suggest that DMF treatment resulted in ferroptosis in GCB DLBCL cell lines.

3.2.3. DMF directly targets IKK β and JAK1 thus inhibiting NF- κ B and STAT3 activity

Since the NF- κ B dependent ABC DLBCL cell lines were not as susceptible to undergo ferroptosis after DMF treatment as GCB DLBCLs, we speculated that NF- κ B was capable of inhibiting ferroptosis. Indeed, overexpression of the NF- κ B subunit RelA in GCB DLBCL cell lines reduced lipid peroxidation and increased survival of DMF treated cells. Nevertheless, ABC DLBCL cell lines were also affected by low concentrations of DMF. RNAseq experiments revealed a strong reduction in NF- κ B target gene expression after treatment with DMF, implying NF- κ B inhibition. Next to *NFKBIZ*, also other NF- κ B target genes like *NFKBIA*, *TNFAIP3*, *BIRC3* and *CFLAR* were downregulated upon DMF treatment. I κ B α phosphorylation levels were rapidly reduced upon DMF treatment as well as RelA activity in a TransAM assay and RelA nuclear localization. Since I κ B α phosphorylation is dependent on IKK activity and neither CBM complex formation nor other upstream signaling events were affected, we focused on the activity of the IKK complex. Intriguingly, biotin-coupled iodoacetamide (IA) pull-down of IKK β was reduced after DMF treatment which indicates a decreased availability to reactive cysteine residues. Moreover, mass spectrometric analysis of HBL-1 cells revealed a succination of IKK β at several cysteine residues after DMF treatment. The detected modification resulted in decreased kinase activity, explaining the decreased I κ B α phosphorylation and reduced NF- κ B activity.

Next to NF- κ B inhibition, also STAT3 signaling was immediately impaired after DMF treatment. Therefore, we analyzed Janus kinase family members for reduced IA pull-down after DMF treatment. Indeed, reactive cysteine accessibility was decreased for all Janus kinases. As for IKK β , DMF-induced succination of JAK1 was detected by mass spectrometry. The identified succination sites were responsible for reduced interaction of JAK1 with cytokine receptors like IL10R, providing an explanation for the fast reduction of JAK-STAT3 signaling in ABC DLBCL cell lines after DMF treatment. Overall, STAT3 and NF- κ B activity were inhibited after DMF treatment in ABC DLBCLs accounting predominantly for the decreased cell survival in this subtype.

3.2.4. BCR signaling counteracts ferroptosis sensitivity in ABC DLBCLs

Unlike ABC DLBCLs, GCB DLBCLs are not dependent on NF- κ B signaling. Therefore, antioxidant proteins may not be expressed to a similar extent as in ABC DLBCLs [144]. GPX4 was one protein higher expression in ABC than in GCB DLBCLs, possibly explaining decreased lipid peroxidation upon DMF treatment, since GPX4 is responsible for reducing oxidized lipids and preventing ferroptosis. Contrarily, expression of the enzyme arachidonate 5-lipoxygenase (5-LOX, *ALOX5*) was only abundant in sensitive GCB DLBCL cell lines but absent in ABC DLBCL cell lines. This correlation was confirmed by immunohistochemistry staining of DLBCL biopsies. Reversely, inhibition of BCR signaling and thereby reduced NF- κ B activity increased *ALOX5* transcript levels in ABC DLBCLs. Moreover, in GCB DLBCL cell lines 5-LOX contributed to reduced GSH levels and inhibition of 5-LOX partially reversed DMF-mediated cytotoxicity, whereas induction of BCR signaling in GCB DLBCL cell lines led to reduced *ALOX5* transcription.

3.2.5. DMF treatment synergizes with FSP1 and Bcl-2 inhibition

DMF treatment in DLBCL cell lines was highly efficient *in vitro*. To validate these results, we examined DMF effects *in vivo*. Tumor formation of the GCB DLBCL cell lines SU-DHL-6 and DOHH2 was reduced by 50% and 70%, respectively, in a zebrafish xenograft model. Moreover, concurrent inhibition of the GSH independent ferroptosis suppressor protein 1 (FSP1) together with DMF synergistically enhanced cytotoxicity in GCB DLBCL cell lines (Schmitt et al., Figure 6c, supplemental Figure 18a). Like CsA treatment, the Bcl-2 inhibitor ABT-199 showed synergistic effects with DMF in ABC DLBCL cell lines, whereas other inhibitors like AZD8835 or vincristine had no combinatorial benefit (Schmitt et al., Figure 6d, supplemental Figure 18b, 19a-b). The combinatorial effect of ABT-199 treatment together with DMF was further validated in HBL-1 and patient-derived (VFN-D1) xenograft mouse models. The synergistic effect of Bcl-2 and DMF might stem from the reduced STAT3 activity upon DMF treatment. Similar, also calcineurin inhibitors led to reduced STAT3 activity and also synergized with the Bcl-2 inhibitor. Reduced STAT3 activity may result in decreased

protein expression of Bcl-2 and Mcl-1 [92], thereby sensitizing ABC DLBCL cell lines for Bcl-2 inhibition.

3.2.6. Cytokine treatment sensitizes DLBCLs for DMF induced ferroptosis

Ferroptosis susceptibility is strongly linked to GSH levels, whose synthesis is dependent on intracellular cysteine levels. Therefore, reduced intracellular cysteine levels result in a cell fate more sensitive towards ferroptosis. Downregulation of subunits of the system x_c^- , a cysteine-glutamate antiporter in the cell membrane, leads to the reduction of intracellular cysteine levels. For example, IFN γ , secreted by T-cells, increased ferroptosis susceptibility in cell lines of solid tumors by decreasing the expression of SLC3A2 and SLC7A11, the two subunits of the system x_c^- [145]. DLBCLs are often exposed to T-cells in the DLBCL tumor microenvironment. T-cells and other cell types like natural killer cells are capable of secreting cytokines. In a physiological setting, DLBCLs are therefore exposed to a variety of cytokines and stimuli which can modulate cell fate. Therefore, we investigated further cytokines and other stimuli for their effect on ferroptosis susceptibility in DLBCL cell lines. We tested a broad panel of immunomodulators which theoretically are suited to manipulate cell fate of DLBCL cell lines (Figure 8).

Intriguingly, IFN γ did not elicit an enhanced ferroptosis sensitivity upon combinatorial treatment with DMF in the GCB DLBCL cell line DOHH2 (Figure 8). Co-treatment with IFN γ even tended to result in a reduced sensitivity towards DMF treatment, indicated by decreased levels of oxidized BODIPY C11 compared to DMF single treatment. Similarly, TGF β 2 decreased the capability of DOHH2 cells to undergo ferroptosis. In contrast to TGF β 2, TGF β 1 and especially TGF β 3 could enhance DOHH2 susceptibility to DMF induced ferroptosis as both cytokines increased oxidized BODIPY C11 levels together with DMF compared to treatment with DMF alone (Figure 8). IL-37 accounted for another candidate which increased the susceptibility of DOHH2 cells to undergo DMF mediated ferroptosis as indicated by increased oxidation of BODIPY C11 after combinatorial treatment of IL-37 and DMF (Figure 8).

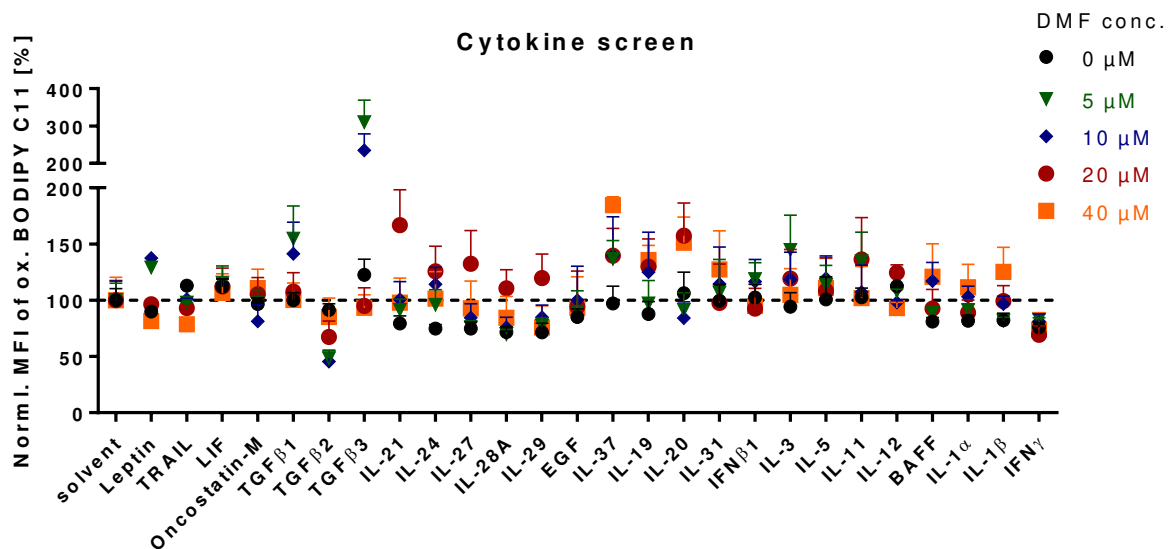


Figure 8: Combinatorial cytokine screen with DMF to enhance ferroptosis induction. Various cytokines and receptor stimulating peptides were screened to evaluate their capability to enhance DMF induced ferroptosis in the GCB DLBCL cell line DOHH2. Cytokines and peptides were treated with and without increasing concentrations of DMF in the range of 5 to 40 μM, as indicated. Mean fluorescence intensity of oxidized BODIPY C11 was normalized to untreated control or to the respective DMF concentration, displaying only the additional effect of the agent compared to the corresponding DMF treatment. All components were finally concentrated to 10 ng/ml, except Leptin (50 ng/ml), TRAIL (125 ng/ml), EGF (100 ng/ml) and BAFF (100 ng/ml). DMF was added for the last 2h, cytokines and peptides for 24h.

Furthermore, IL-3, IL-20 and IL-19 enhanced DMF induced effects on the oxidation status of BODIPY C11. Nevertheless, these cytokines did not exhibit effects as prominent effects as observed for TGFβ1, TGFβ2, TGFβ3, IL-21 and IL-37. Moreover, we tested CD40 stimulation of DOHH2 cells, as CD40 was reported to play an important role in B-cell development as well as malignancy [64, 146]. To this end, DOHH2 cells were exposed to a CD40 stimulus by coating either CD40 ligand or an α-CD40 antibody (Figure 9). Upon treatment with DMF, DOHH2 cells exhibited reduced levels of oxidized BODIPY C11, indicating a protective effect of CD40 stimulation on cells regarding ferroptosis sensitivity. CD40 stimulation was reported to enhance resistance of ABC DLBCLs and MCLs towards Ibrutinib by activating the non-canonical NF-κB pathway [146, 147]. Activation of non-canonical NF-κB by CD40 stimulation might also explain the reduced sensitivity of the GCB DLBCL cell line DOHH2 in terms of DMF induced ferroptosis, since we showed that NF-κB activity in ABC DLBCLs counteracted ferroptosis.

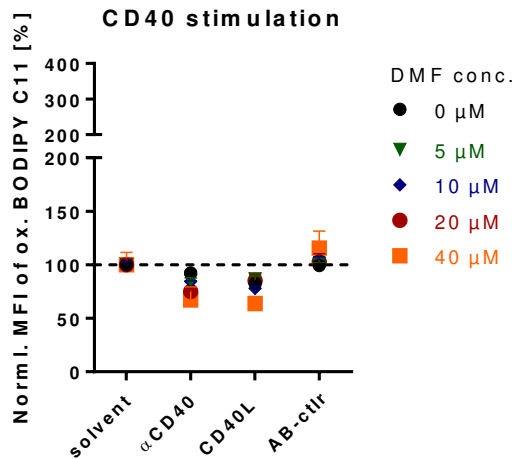


Figure 9: Effect of CD40 stimulation on DMF induced ferroptosis. CD40 stimulation achieved by a coated α -CD40 antibody or a coated peptide corresponding to the sequence of CD40 ligand was tested for its potential to induce oxidation of BODIPY C11 alone or in combination with increasing concentrations of DMF compared to the respective controls in the GCB DLBCL cell line DOHH2. CD40L was coated at 100 μ g/ml, α -CD40 of 10 μ g/ml. Mean fluorescence intensity of oxidized BODIPY C11 was normalized to the untreated control or to the respective DMF concentration, displaying only the additional effect of the agent compared to the corresponding DMF treatment. DMF was added for the last 2h, CD40 was triggered for 48h.

The effect of the cytokines IL-21, IL-37, TGF β 1, TGF β 2 and TGF β 3 were validated in further cell lines. The GCB DLBCL cell line WSU-DLCL2 as well as the ABC DLBCL cell lines HBL-1 and U2932 exhibited increased oxidization of BODIPY C11 upon cytokine treatment in combination with DMF compared to sole DMF treatment (Figure 10). In general, HBL-1 cells showed only moderate effects of cytokines on oxidized BODIPY C11 compared to the other cell lines, although the tendency was similar to U2932 cells. Both ABC DLBCL cell lines exhibited increased ferroptosis upon co-treatment of IL-21 and TGF β 1 with DMF, indicated by increased oxidization of BODIPY C11. Similarly, IL-21 and DMF co-treatment induced oxidation of BODIPY C11 in the GBC DLBCL cell lines WSU-DLCL2, whereas the effect of TGF β 1 was not as strong as the effect of TGF β 3 co-treatment with DMF. This was already observed for the GCB DLBCL cell line DOHH2 (Figure 8). Besides, sensitivity to IL-37 treatment was stronger for the GCB DLBCL cell lines WSU-DLCL2 and DOHH2, whereas ABC DLBCL cell lines were almost unaffected by IL-37 co-treatment. Unlike in DOHH2 cells, the effect of TGF β 2 on oxidized BODIPY C11 upon DMF treatment was almost absent in all further cell lines tested (Figure 10).

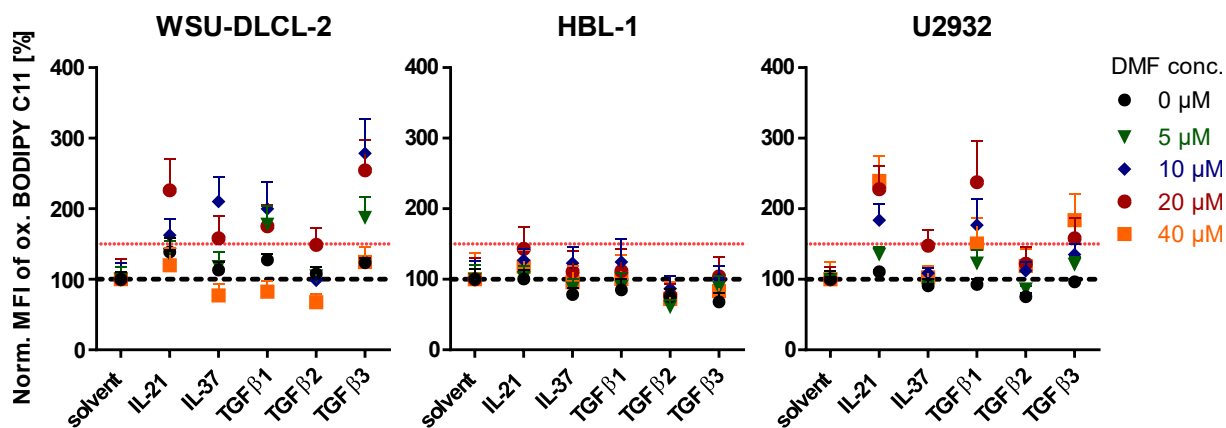


Figure 10: Potential of selected cytokines to enhance DMF induced ferroptosis in DLBCL cell lines. IL-21, IL-37, TGF β 1, TGF β 2 and TGF β 3 were validated for their ability to enhance DMF induced ferroptosis in the GCB DLBCL cell line WSU-DLCL2 and the ABC DLBCL cell lines HBL-1 and U2932. Selected cytokines were used in combination with and without increasing concentrations of DMF in the range of 5 to 40 μ M, as indicated. Mean fluorescence intensity of oxidized BODIPY C11 was normalized to untreated control or to the respective DMF concentration, displaying only the additional effect of the agent compared to the corresponding DMF treatment. All cytokines were used at 10 ng/ml. DMF was added for the last 2h, cytokines and peptides for 24h.


TGF β 1 has already been reported to enhance ferroptosis in hepatocellular carcinoma cells and in kidney tubular cells by reducing the expression of SLC7A11 [148] and of GPX4 and the whole system x_c^- [149]. TGF β 1 activates, after binding to its cognate TGF β receptor, Smad proteins, which translocate to the nucleus where they interact with other transcription factors to regulate gene expression [150]. TGF β signaling is in general reported to suppress cell growth [150] and also for B-cell lymphoma a TGF β mediated growth inhibition is suggested [151], whereas especially for DLBCL this has not been investigated in detail. IL-37 has so far not been reported to be implicated in ferroptosis induction. It has an anti-inflammatory role and is expressed primarily by B-cells, plasma cells and macrophages. Extracellular IL-37 binds to IL-18 receptor α and IL-1 receptor 8, thus activating MyD88 and IRAKs. IL-37 can also act intracellularly, where it binds to Smad3 and thereby translocates to the nucleus, regulating gene expression [152]. Interestingly, both TGF β and IL-37 induce Smad3 activity [152], stressing its important role in regulation of ferroptosis induction. Since IL-37 was almost ineffective in ABC DLBCL cell lines, this suggests that this DLBCL subtype either (i) already expresses IL-37, lacks (ii) the ability to import IL-37 or (iii) the expression of Smad3. Since ABC DLBCLs respond to TGF β treatment (Figure 10), which is most likely Smad dependent, a potential absence of Smad3 might be compensated by expression of other Smad proteins. At last, IL-21 enhanced DMF induced ferroptosis in ABC as well as GCB DLBCL cell lines. IL-21 is physiologically expressed by natural killer T-cells, by CD8 $^+$ T-cells and primarily by CD4 $^+$ T-cells. IL-21 has already been reported to have different roles in DLBCLs. Whereas EBV positive

DLBCL cells exhibited superior survival upon IL-21 stimulation due to increased STAT3 signaling [153], studies in classical DLBCL cell lines suggest increased cell death after IL-21 stimulation [154]. Stimulation with IL-21 results in the activation of STAT1, STAT3 and STAT5. Surprisingly, knock-down of STAT3 and c-Myc rescued IL-21 induced apoptosis in these cell lines. Since these transcription factors normally drive DLBCL survival and proliferation, the collaboration of STAT3 or c-Myc with the additionally active STAT1 and STAT5 could cause cell death, although this has to be evaluated further. Nevertheless, IL-21 treatment might provide a new possibility to enhance DMF induced ferroptosis in DLBCL cell lines. Considering that in average 24% of all tumor infiltrating lymphocytes of the DLBCL tumor microenvironment represent CD4⁺ T-cells [155], it would be interesting to induce IL-21 production in these cells, which would probably enhance DMF treatment although this needs closer investigation.

Nevertheless, we could show that single treatment of DMF is already highly effective against DLBCL *in vitro* and *in vivo*. It is approved for the treatment of moderate-to-severe psoriasis and multiple sclerosis. Therefore, DMF repurposing for treatment in DLBCLs would be feasible. Furthermore, we showed that DMF exhibited the potential to induce ferroptosis in lymphoid tumors, suggesting its application also in other lymphoid malignancies. As Bcl-2 and FSP1 inhibitors were shown to act synergistically with DMF in DLBCLs, we would suggest a combination of DMF with these compounds. Especially, combination of DMF with FSP1 inhibitors would constitute a new approach for DLBCL treatment by inducing ferroptosis. Moreover, IL-21 secretion, for example by activated CD4⁺ T-cells, may enhance the ferroptosis induction in DLBCLs. In general, DMF treatment promises a great therapeutical potential, which can be further boosted by immune responses and combinatorial treatment.

4. References

1. Beham-Schmid, C., *Aggressive lymphoma 2016: revision of the WHO classification*. memo - Magazine of European Medical Oncology, 2017. **10**(4): p. 248-254.
2. *A Clinical Evaluation of the International Lymphoma Study Group Classification of Non-Hodgkin's Lymphoma*. Blood, 1997. **89**(11): p. 3909-3918.
3. Swerdlow, S.H., et al., *The 2016 revision of the World Health Organization classification of lymphoid neoplasms*. Blood, 2016. **127**(20): p. 2375-90.
4. Opinto, G., et al., *The Tumor Microenvironment of DLBCL in the Computational Era*. Frontiers in Oncology, 2020. **10**: p. 351.
5. Vaidya, R. and T.E. Witzig, *Prognostic factors for diffuse large B-cell lymphoma in the R(X)CHOP era*. Annals of Oncology, 2014. **25**(11): p. 2124-2133.
6. Gisselbrecht, C., et al., *Salvage regimens with autologous transplantation for relapsed large B-cell lymphoma in the rituximab era*. J Clin Oncol, 2010. **28**(27): p. 4184-90.
7. Davis, R.E., et al., *Chronic active B-cell-receptor signalling in diffuse large B-cell lymphoma*. Nature, 2010. **463**(7277): p. 88-92.
8. Havranek, O., et al., *Tonic B-cell receptor signaling in diffuse large B-cell lymphoma*. Blood, 2017. **130**(8): p. 995.
9. Reth, M., *Antigen Receptors on B Lymphocytes*. Annual Review of Immunology, 1992. **10**(1): p. 97-121.
10. Wienands, J. and N. Engels, *Multitasking of Ig-alpha and Ig-beta to regulate B cell antigen receptor function*. Int Rev Immunol, 2001. **20**(6): p. 379-696.
11. Johnson, S.A., et al., *Phosphorylated immunoreceptor signaling motifs (ITAMs) exhibit unique abilities to bind and activate Lyn and Syk tyrosine kinases*. The Journal of Immunology, 1995. **155**(10): p. 4596.
12. Fu, C., et al., *BLNK: a Central Linker Protein in B Cell Activation*. Immunity, 1998. **9**(1): p. 93-103.
13. Watanabe, D., et al., *Four tyrosine residues in phospholipase C-gamma 2, identified as Btk-dependent phosphorylation sites, are required for B cell antigen receptor-coupled calcium signaling*. J Biol Chem, 2001. **276**(0021-9258 (Print)): p. 38595-38601.
14. Lien, E.C., C.C. Dibble, and A. Toker, *PI3K signaling in cancer: beyond AKT*. Current Opinion in Cell Biology, 2017. **45**: p. 62-71.
15. Thome, M., et al., *Antigen receptor signaling to NF-kappaB via CARMA1, BCL10, and MALT1*. Cold Spring Harb Perspect Biol, 2010. **2**(9): p. a003004.
16. Sommer, K., et al., *Phosphorylation of the CARMA1 Linker Controls NF-kB Activation*. Immunity, 2005. **23**(6): p. 561-574.
17. David, L., et al., *Assembly mechanism of the CARMA1-BCL10-MALT1-TRAF6 signalosome*. Proceedings of the National Academy of Sciences, 2018. **115**(7): p. 1499.
18. Qiao, Q., et al., *Structural Architecture of the CARMA1/Bcl10/MALT1 Signalosome: Nucleation-Induced Filamentous Assembly*. Molecular Cell, 2013. **51**(6): p. 766-779.
19. Gaide, O., et al., *Carma1, a CARD-containing binding partner of Bcl10, induces Bcl10 phosphorylation and NF-kB activation1*. FEBS Letters, 2001. **496**(2-3): p. 121-127.
20. Wang, C., et al., *TAK1 is a ubiquitin-dependent kinase of MKK and IKK*. Nature, 2001. **412**(6844): p. 346-351.
21. Adhikari, A., M. Xu, and Z.J. Chen, *Ubiquitin-mediated activation of TAK1 and IKK*. Oncogene, 2007. **26**(22): p. 3214-3226.
22. Oeckinghaus, A. and S. Ghosh, *The NF-kB Family of Transcription Factors and Its Regulation*. Cold Spring Harbor Perspectives in Biology, 2009. **1**(4).
23. Dolcet, X., et al., *NF-kB in development and progression of human cancer*. Virchows Archiv, 2005. **446**(5): p. 475-482.
24. Juilland, M., et al., *CARMA1- and MyD88-dependent activation of Jun/ATF-type AP-1 complexes is a hallmark of ABC diffuse large B-cell lymphomas*. Blood, 2016. **127**(14): p. 1780-9.

25. Zhang, B., et al., *An Oncogenic Role for Alternative NF- κ B Signaling in DLBCL Revealed upon Deregulated BCL6 Expression*. Cell Reports, 2015. **11**(5): p. 715-726.
26. Grondona, P., et al., *NF-kappaB Activation in Lymphoid Malignancies: Genetics, Signaling, and Targeted Therapy*. Biomedicines, 2018. **6**(2): p. 38.
27. Abbasi, A., K. Forsberg, and F. Bischof, *The role of the ubiquitin-editing enzyme A20 in diseases of the central nervous system and other pathological processes*. Frontiers in Molecular Neuroscience, 2015. **8**: p. 21.
28. Hoesel, B. and J.A. Schmid, *The complexity of NF- κ B signaling in inflammation and cancer*. Molecular Cancer, 2013. **12**(1): p. 86.
29. Sun, S.-C., *Non-canonical NF- κ B signaling pathway*. Cell Research, 2011. **21**(1): p. 71-85.
30. Senftleben, U., et al., *Activation by IKK α of a Second, Evolutionary Conserved, NF- κ B Signaling Pathway*. Science, 2001. **293**(5534): p. 1495.
31. Annemann, M., et al., *Atypical I κ B proteins in immune cell differentiation and function*. Immunology Letters, 2016. **171**: p. 26-35.
32. Nogai, H., et al., *I κ B- ζ controls the constitutive NF- κ B target gene network and survival of ABC DLBCL*. Blood, 2013. **122**(13): p. 2242-2250.
33. Blonska, M., et al., *Jun-regulated genes promote interaction of diffuse large B-cell lymphoma with the microenvironment*. Blood, 2015. **125**(6): p. 981-91.
34. Atsaves, V., et al., *AP-1 Transcription Factors as Regulators of Immune Responses in Cancer*. Cancers, 2019. **11**(7).
35. Eferl, R. and E.F. Wagner, *AP-1: a double-edged sword in tumorigenesis*. Nature Reviews Cancer, 2003. **3**(11): p. 859-868.
36. Shaulian, E., *AP-1 — The Jun proteins: Oncogenes or tumor suppressors in disguise?* Cellular Signalling, 2010. **22**(6): p. 894-899.
37. Macian, F., C. Lopez-Rodriguez, and A. Rao, *Partners in transcription: NFAT and AP-1*. Oncogene, 2001. **20**(19): p. 2476-89.
38. Vasanwala, F.H., et al., *Repression of AP-1 Function: A Mechanism for the Regulation of Blimp-1 Expression and B Lymphocyte Differentiation by the B Cell Lymphoma-6 Protooncogene*. The Journal of Immunology, 2002. **169**(4): p. 1922.
39. Papoudou-Bai, A., et al., *Expression patterns of the activator protein-1 (AP-1) family members in lymphoid neoplasms*. Clinical and Experimental Medicine, 2017. **17**(3): p. 291-304.
40. Meng, Q. and Y. Xia, *c-Jun, at the crossroad of the signaling network*. Protein & Cell, 2011. **2**(11): p. 889-898.
41. Okkenhaug, K. and J.A. Burger, *PI3K Signaling in Normal B Cells and Chronic Lymphocytic Leukemia (CLL)*, in *B Cell Receptor Signaling*, T. Kurosaki and J. Wienands, Editors. 2016, Springer International Publishing: Cham. p. 123-142.
42. Erdmann, T., et al., *Sensitivity to PI3K and AKT inhibitors is mediated by divergent molecular mechanisms in subtypes of DLBCL*. Blood, 2017. **130**(3): p. 310-322.
43. Hemon, P., et al., *Calcium Signaling: From Normal B Cell Development to Tolerance Breakdown and Autoimmunity*. Clinical Reviews in Allergy & Immunology, 2017. **53**(2): p. 141-165.
44. Mori, Y., et al., *Transient Receptor Potential 1 Regulates Capacitative Ca²⁺ Entry and Ca²⁺ Release from Endoplasmic Reticulum in B Lymphocytes* . Journal of Experimental Medicine, 2002. **195**(6): p. 673-681.
45. Garaud, S., et al., *CD5 expression promotes IL-10 production through activation of the MAPK/Erk pathway and upregulation of TRPC1 channels in B lymphocytes*. Cellular & Molecular Immunology, 2016. **15**: p. 158.
46. Persechini, A. and B. Cronk, *The Relationship between the Free Concentrations of Ca²⁺ and Ca²⁺-calmodulin in Intact Cells*. Journal of Biological Chemistry, 1999. **274**(11): p. 6827-6830.
47. Muhammad, K., et al., *NF-kappaB factors control the induction of NFATc1 in B lymphocytes*. Eur J Immunol, 2014. **44**(11): p. 3392-402.
48. Serfling, E., et al., *NFATc1 autoregulation: a crucial step for cell-fate determination*. Trends in Immunology, 2006. **27**(10): p. 461-469.

49. Li, H., A. Rao, and P.G. Hogan, *Interaction of calcineurin with substrates and targeting proteins*. Trends in cell biology, 2011. **21**(2): p. 91-103.
50. Muller, M.R. and A. Rao, *NFAT, immunity and cancer: a transcription factor comes of age*. Nat Rev Immunol, 2010. **10**(9): p. 645-56.
51. Pham, L.V., et al., *Constitutive NF-kappaB and NFAT activation in aggressive B-cell lymphomas synergistically activates the CD154 gene and maintains lymphoma cell survival*. Blood, 2005. **106**(12): p. 3940-7.
52. Chen, L., et al., *Structure of the DNA-binding domains from NFAT, Fos and Jun bound specifically to DNA*. Nature, 1998. **392**(6671): p. 42-8.
53. Berland, R. and H.H. Wortis, *Normal B-1a cell development requires B cell-intrinsic NFATc1 activity*. Proceedings of the National Academy of Sciences, 2003. **100**(23): p. 13459.
54. Yoshida, H., et al., *The Transcription Factor NF-ATc1 Regulates Lymphocyte Proliferation and Th2 Cytokine Production*. Immunity, 1998. **8**(1): p. 115-124.
55. Le Roy, C., et al., *The degree of BCR and NFAT activation predicts clinical outcomes in chronic lymphocytic leukemia*. Blood, 2012. **120**(2): p. 356.
56. Wang, Y., et al., *B Cell Development and Maturation*, in *B Cells in Immunity and Tolerance*, J.-Y. Wang, Editor. 2020, Springer Singapore: Singapore. p. 1-22.
57. Pieper, K., B. Grimbacher, and H. Eibel, *B-cell biology and development*. Journal of Allergy and Clinical Immunology, 2013. **131**(4): p. 959-971.
58. Cyster, J.G., S.B. Hartley, and C.C. Goodnow, *Competition for follicular niches excludes self-reactive cells from the recirculating B-cell repertoire*. Nature, 1994. **371**(6496): p. 389-395.
59. Cambier, J.C., et al., *B-cell anergy: from transgenic models to naturally occurring anergic B cells?* Nature Reviews Immunology, 2007. **7**(8): p. 633-643.
60. Klien, U., et al., *Somatic hypermutation in normal and transformed human B cells*. Immunological Reviews, 1998. **162**(1): p. 261-280.
61. Mesin, L., J. Ersching, and Gabriel D. Victora, *Germinal Center B Cell Dynamics*. Immunity, 2016. **45**(3): p. 471-482.
62. De Silva, N.S. and U. Klein, *Dynamics of B cells in germinal centres*. Nature Reviews Immunology, 2015. **15**(3): p. 137-148.
63. Gatto, D. and R. Brink, *The germinal center reaction*. Journal of Allergy and Clinical Immunology, 2010. **126**(5): p. 898-907.
64. Foy, T.M., et al., *gp39-CD40 interactions are essential for germinal center formation and the development of B cell memory*. Journal of Experimental Medicine, 1994. **180**(1): p. 157-163.
65. Stavnezer, J., J.E.J. Guikema, and C.E. Schrader, *Mechanism and Regulation of Class Switch Recombination*. Annual Review of Immunology, 2008. **26**(1): p. 261-292.
66. Küppers, R., et al., *Cellular Origin of Human B-Cell Lymphomas*. New England Journal of Medicine, 1999. **341**(20): p. 1520-1529.
67. Küppers, R. and R. Dalla-Favera, *Mechanisms of chromosomal translocations in B cell lymphomas*. Oncogene, 2001. **20**(40): p. 5580-5594.
68. Victora, G.D., et al., *Identification of human germinal center light and dark zone cells and their relationship to human B-cell lymphomas*. Blood, 2012. **120**(11): p. 2240-2248.
69. Pasqualucci, L., et al., *Hypermutation of multiple proto-oncogenes in B-cell diffuse large-cell lymphomas*. Nature, 2001. **412**(6844): p. 341-346.
70. Alizadeh, A.A., et al., *Distinct types of diffuse large B-cell lymphoma identified by gene expression profiling*. Nature, 2000. **403**(6769): p. 503-11.
71. Lenz, G. and L.M. Staudt, *Aggressive lymphomas*. N Engl J Med, 2010. **362**(15): p. 1417-29.
72. Mandelbaum, J., et al., *BLIMP1 Is a Tumor Suppressor Gene Frequently Disrupted in Activated B Cell-like Diffuse Large B Cell Lymphoma*. Cancer Cell, 2010. **18**(6): p. 568-579.
73. Pasqualucci, L., et al., *Inactivation of the PRDM1/BLIMP1 gene in diffuse large B cell lymphoma*. Journal of Experimental Medicine, 2006. **203**(2): p. 311-317.
74. Lenz, G., et al., *Molecular subtypes of diffuse large B-cell lymphoma arise by distinct genetic pathways*. Proceedings of the National Academy of Sciences, 2008. **105**(36): p. 13520.

75. Schmidlin, H., et al., *Spi-B inhibits human plasma cell differentiation by repressing BLIMP1 and XBP-1 expression*. *Blood*, 2008. **112**(5): p. 1804-1812.
76. Iqbal, J., et al., *Distinctive patterns of BCL6 molecular alterations and their functional consequences in different subgroups of diffuse large B-cell lymphoma*. *Leukemia*, 2007. **21**(11): p. 2332-2343.
77. Pasqualucci, L. and R. Dalla-Favera, *Genetics of diffuse large B-cell lymphoma*. *Blood*, 2018. **131**(21): p. 2307-2319.
78. Wenzel, S.S., et al., *MCL1 is deregulated in subgroups of diffuse large B-cell lymphoma*. *Leukemia*, 2013. **27**(6): p. 1381-90.
79. Hu, S., et al., *MYC/BCL2 protein coexpression contributes to the inferior survival of activated B-cell subtype of diffuse large B-cell lymphoma and demonstrates high-risk gene expression signatures: a report from The International DLBCL Rituximab-CHOP Consortium Program*. *Blood*, 2013. **121**(20): p. 4021-31; quiz 4250.
80. Lenz, G., et al., *Stromal gene signatures in large-B-cell lymphomas*. *N Engl J Med*, 2008. **359**(22): p. 2313-23.
81. Rosenwald, A., et al., *The use of molecular profiling to predict survival after chemotherapy for diffuse large-B-cell lymphoma*. *N Engl J Med*, 2002. **346**(25): p. 1937-47.
82. Wright, G., et al., *A gene expression-based method to diagnose clinically distinct subgroups of diffuse large B cell lymphoma*. *Proc Natl Acad Sci U S A*, 2003. **100**(17): p. 9991-6.
83. Lenz, G., et al., *Oncogenic CARD11 mutations in human diffuse large B cell lymphoma*. *Science*, 2008. **319**(5870): p. 1676-9.
84. Compagno, M., et al., *Mutations of multiple genes cause deregulation of NF-kappaB in diffuse large B-cell lymphoma*. *Nature*, 2009. **459**(7247): p. 717-21.
85. Ngo, V.N., et al., *Oncogenically active MYD88 mutations in human lymphoma*. *Nature*, 2011. **470**(7332): p. 115-9.
86. Avbelj, M., et al., *Activation of lymphoma-associated MyD88 mutations via allosterically-induced TIR-domain oligomerization*. *Blood*, 2014. **124**(26): p. 3896-3904.
87. Phelan, J.D., et al., *A multiprotein supercomplex controlling oncogenic signalling in lymphoma*. *Nature*, 2018. **560**(7718): p. 387-391.
88. Davis, R.E., et al., *Constitutive nuclear factor kappaB activity is required for survival of activated B cell-like diffuse large B cell lymphoma cells*. *J Exp Med*, 2001. **194**(12): p. 1861-74.
89. Lam, L.T., et al., *Small molecule inhibitors of IkappaB kinase are selectively toxic for subgroups of diffuse large B-cell lymphoma defined by gene expression profiling*. *Clin Cancer Res*, 2005. **11**(1): p. 28-40.
90. Fontán, L., et al., *Specific covalent inhibition of MALT1 paracaspase suppresses B cell lymphoma growth*. *The Journal of Clinical Investigation*, 2018. **128**(10): p. 4397-4412.
91. Younes, A., et al., *Randomized Phase III Trial of Ibrutinib and Rituximab Plus Cyclophosphamide, Doxorubicin, Vincristine, and Prednisone in Non-Germinal Center B-Cell Diffuse Large B-Cell Lymphoma*. *Journal of Clinical Oncology*, 2019. **37**(15): p. 1285-1295.
92. Lam, L.T., et al., *Cooperative signaling through the signal transducer and activator of transcription 3 and nuclear factor-kappaB pathways in subtypes of diffuse large B-cell lymphoma*. *Blood*, 2008. **111**(7): p. 3701-13.
93. Nogai, H., B. Dorken, and G. Lenz, *Pathogenesis of non-Hodgkin's lymphoma*. *J Clin Oncol*, 2011. **29**(14): p. 1803-11.
94. Walewski, J., *Aggressive B-cell lymphoma: chasing the target*. *Journal of Investigative Medicine*, 2020. **68**(2): p. 331.
95. Rosenthal, A. and A. Younes, *High grade B-cell lymphoma with rearrangements of MYC and BCL2 and/or BCL6: Double hit and triple hit lymphomas and double expressing lymphoma*. *Blood Reviews*, 2017. **31**(2): p. 37-42.
96. Green, J.A. and J.G. Cyster, *S1PR2 links germinal center confinement and growth regulation*. *Immunological Reviews*, 2012. **247**(1): p. 36-51.

97. Muppidi, J.R., et al., *Loss of signalling via Gα13 in germinal centre B-cell-derived lymphoma*. Nature, 2014. **516**(7530): p. 254-258.
98. Cattoretti, G., et al., *Targeted Disruption of the Sphingosine 1-Phosphate Receptor Gene Leads to Diffuse Large B-Cell Lymphoma Formation*. Cancer Research, 2009. **69**(22): p. 8686.
99. Wright, G.W., et al., *A Probabilistic Classification Tool for Genetic Subtypes of Diffuse Large B Cell Lymphoma with Therapeutic Implications*. Cancer Cell, 2020. **37**(4): p. 551-568.e14.
100. Schmitz, R., et al., *Genetics and Pathogenesis of Diffuse Large B-Cell Lymphoma*. N Engl J Med, 2018. **378**(15): p. 1396-1407.
101. Chapuy, B., et al., *Molecular subtypes of diffuse large B cell lymphoma are associated with distinct pathogenic mechanisms and outcomes*. Nat Med, 2018. **24**(5): p. 679-690.
102. Venturutti, L. and A.M. Melnick, *The dangers of déjà vu: memory B cells as the cells of origin of ABC-DLBCLs*. Blood, 2020. **136**(20): p. 2263-2274.
103. Venturutti, L., et al., *TBL1XR1 Mutations Drive Extranodal Lymphoma by Inducing a Pro-tumorigenic Memory Fate*. Cell, 2020. **182**(2): p. 297-316.e27.
104. Landsburg, D.J. and B.S. Kahl, *Can We Exploit the Molecular Heterogeneity of Aggressive B Cell Lymphomas Into Effective New Therapies?* Clinical Lymphoma Myeloma and Leukemia, 2019. **19**(2): p. 65-67.
105. Klanova, M. and P. Klener, *BCL-2 Proteins in Pathogenesis and Therapy of B-Cell Non-Hodgkin Lymphomas*. Cancers, 2020. **12**(4): p. 938.
106. Marafioti, T., et al., *The NFATc1 transcription factor is widely expressed in white cells and translocates from the cytoplasm to the nucleus in a subset of human lymphomas*. Br J Haematol, 2005. **128**(3): p. 333-42.
107. Li, L., et al., *B-cell receptor-mediated NFATc1 activation induces IL-10/STAT3/PD-L1 signaling in diffuse large B-cell lymphoma*. Blood, 2018. **132**(17): p. 1805-1817.
108. Saraiva, M. and A. O'Garra, *The regulation of IL-10 production by immune cells*. Nat Rev Immunol, 2010. **10**(3): p. 170-81.
109. Dutta, D., et al., *Recruitment of calcineurin to the TCR positively regulates T cell activation*. Nature Immunology, 2017. **18**(2): p. 196-204.
110. Pan, Z., S. Choi, and Y. Luo, *Mn(2+) Quenching Assay for Store-Operated Calcium Entry*. Methods Mol Biol, 2018. **1843**: p. 55-62.
111. Fujimoto, M., et al., *CD19 Amplification of B Lymphocyte Ca²⁺ Responses: A role for Lyn sequestration in extinguishing negative regulation*. Journal of Biological Chemistry, 2001. **276**(48): p. 44820-44827.
112. Bradbury, L.E., V.S. Goldmacher, and T.F. Tedder, *The CD19 signal transduction complex of B lymphocytes. Deletion of the CD19 cytoplasmic domain alters signal transduction but not complex formation with TAPA-1 and Leu 13*. The Journal of Immunology, 1993. **151**(6): p. 2915.
113. Sato, S., et al., *Regulation of B lymphocyte development and activation by the CD19/CD21/CD81/Leu 13 complex requires the cytoplasmic domain of CD19*. The Journal of Immunology, 1997. **159**(7): p. 3278.
114. Carter, R.H. and R.A. Barrington, *Signaling by the CD19/CD21 Complex on B Cells*. Current Directions in Autoimmunity, 2004. **7**: p. 4-32.
115. Li, X., et al., *Role of CD19 tyrosine 391 in synergistic activation of B lymphocytes by coligation of CD19 and membrane Ig*. The Journal of Immunology, 1997. **158**(12): p. 5649.
116. Tedford, K., et al., *Compensation between Vav-1 and Vav-2 in B cell development and antigen receptor signaling*. Nature Immunology, 2001. **2**(6): p. 548-555.
117. Scharenberg, A.M., L.A. Humphries, and D.J. Rawlings, *Calcium signalling and cell-fate choice in B cells*. Nature reviews. Immunology, 2007. **7**(10): p. 778-789.
118. Parekh, A.B., A. Fleig, and R. Penner, *The Store-Operated Calcium Current ICRAC: Nonlinear Activation by InsP3 and Dissociation from Calcium Release*. Cell, 1997. **89**(6): p. 973-980.
119. Tomlinson, M.G., et al., *A conditional form of Bruton's tyrosine kinase is sufficient to activate multiple downstream signaling pathways via PLC Gamma 2 in B cells*. BMC Immunology, 2001. **2**(1): p. 4.

120. Saito, K., et al., *BTK Regulates PtdIns-4,5-P2 Synthesis: Importance for Calcium Signaling and PI3K Activity*. *Immunity*, 2003. **19**(5): p. 669-677.
121. Wist, M., et al., *Noncatalytic Bruton's tyrosine kinase activates PLC γ 2 variants mediating ibrutinib resistance in human chronic lymphocytic leukemia cells*. *Journal of Biological Chemistry*, 2020. **295**(17): p. 5717-5736.
122. Psathas, J.N., et al., *The Myc-miR-17-92 axis amplifies B-cell receptor signaling via inhibition of ITIM proteins: a novel lymphomagenic feed-forward loop*. *Blood*, 2013. **122**(26): p. 4220-4229.
123. Sauer, K., et al., *IP3 3-Kinase B Suppresses B Cell Lymphoma by Antagonizing PI3K/mTOR in B cells*. *The Journal of Immunology*, 2016. **196**(1 Supplement): p. 142.2.
124. Miller, A.T., et al., *Production of Ins(1,3,4,5)P4 mediated by the kinase Itpkb inhibits store-operated calcium channels and regulates B cell selection and activation*. *Nature Immunology*, 2007. **8**(5): p. 514-521.
125. Young, R.M., et al., *B-Cell Receptor Signaling in Diffuse Large B-Cell lymphoma*. *Seminars in Hematology*, 2015. **52**(2): p. 77-85.
126. Healy, J.I., et al., *Different Nuclear Signals Are Activated by the B Cell Receptor during Positive Versus Negative Signaling*. *Immunity*, 1997. **6**(4): p. 419-428.
127. Apollonio, B., et al., *Targeting B-cell anergy in chronic lymphocytic leukemia*. *Blood*, 2013. **121**(19): p. 3879-3888.
128. Rossi, D., V. Spina, and G. Gaidano, *Biology and treatment of Richter syndrome*. *Blood*, 2018. **131**(25): p. 2761-2772.
129. Li, L., et al., *Synergistic induction of apoptosis in high-risk DLBCL by BCL2 inhibition with ABT-199 combined with pharmacologic loss of MCL1*. *Leukemia*, 2015. **29**(8): p. 1702-12.
130. Takahashi, K., et al., *TRPM7-mediated spontaneous Ca²⁺ entry regulates the proliferation and differentiation of human leukemia cell line K562*. *Physiological Reports*, 2018. **6**(14): p. e13796.
131. Krishnamoorthy, M., et al., *The channel-kinase TRPM7 regulates antigen gathering and internalization in B cells*. *Science Signaling*, 2018. **11**(533): p. eaah6692.
132. Nguyen, T., et al., *Novel identification and characterisation of Transient receptor potential melastatin 3 ion channels on Natural Killer cells and B lymphocytes: effects on cell signalling in Chronic fatigue syndrome/Myalgic encephalomyelitis patients*. *Biological Research*, 2016. **49**(1): p. 27.
133. Ho, P.-C., et al., *Phosphoenolpyruvate Is a Metabolic Checkpoint of Anti-tumor T Cell Responses*. *Cell*, 2015. **162**(6): p. 1217-1228.
134. Bhalla, K., et al., *Role of hypoxia in Diffuse Large B-cell Lymphoma: Metabolic repression and selective translation of HK2 facilitates development of DLBCL*. *Scientific Reports*, 2018. **8**(1): p. 744.
135. Green, T.M., et al., *Immunohistochemical double-hit score is a strong predictor of outcome in patients with diffuse large B-cell lymphoma treated with rituximab plus cyclophosphamide, doxorubicin, vincristine, and prednisone*. *J Clin Oncol*, 2012. **30**(28): p. 3460-7.
136. Johnson, N.A., et al., *Concurrent expression of MYC and BCL2 in diffuse large B-cell lymphoma treated with rituximab plus cyclophosphamide, doxorubicin, vincristine, and prednisone*. *J Clin Oncol*, 2012. **30**(28): p. 3452-9.
137. Tsuyama, N., et al., *BCL2 expression in DLBCL: reappraisal of immunohistochemistry with new criteria for therapeutic biomarker evaluation*. *Blood*, 2017. **130**(4): p. 489-500.
138. Morschhauser, F., et al., *A phase 2 study of venetoclax plus R-CHOP as first-line treatment for patients with diffuse large B-cell lymphoma*. *Blood*, 2021. **137**(5): p. 600-609.
139. Kuo, H.-P., et al., *Combination of Ibrutinib and ABT-199 in Diffuse Large B-Cell Lymphoma and Follicular Lymphoma*. *Molecular Cancer Therapeutics*, 2017. **16**(7): p. 1246.
140. Bambouskova, M., et al., *Electrophilic properties of itaconate and derivatives regulate the I κ B ζ -ATF3 inflammatory axis*. *Nature*, 2018. **556**(7702): p. 501-504.
141. Ohgakiuchi, Y., et al., *Dimethyl fumarate dampens IL-17-ACT1-TBK1 axis-mediated phosphorylation of Regnase-1 and suppresses IL-17-induced I κ B- ζ expression*. *Biochemical and Biophysical Research Communications*, 2020. **521**(4): p. 957-963.

142. Jiang, X., B.R. Stockwell, and M. Conrad, *Ferroptosis: mechanisms, biology and role in disease*. Nature Reviews Molecular Cell Biology, 2021. **22**(4): p. 266-282.
143. Dixon, S.J., et al., *Ferroptosis: an iron-dependent form of nonapoptotic cell death*. Cell, 2012. **149**(5): p. 1060-72.
144. Lingappan, K., *NF-kappaB in Oxidative Stress*. Curr Opin Toxicol, 2018. **7**: p. 81-86.
145. Wang, W., et al., *CD8+ T cells regulate tumour ferroptosis during cancer immunotherapy*. Nature, 2019. **569**(7755): p. 270-274.
146. Rauert-Wunderlich, H., et al., *CD40L mediated alternative NFkB-signaling induces resistance to BCR-inhibitors in patients with mantle cell lymphoma*. Cell Death & Disease, 2018. **9**(2): p. 86.
147. Sun, Z. and L. Luo, *Abstract 1298: CD40L-CD40 signaling on B-cell lymphoma response to BTK inhibitors*. Cancer Research, 2016. **76**(14 Supplement): p. 1298.
148. Kim, D.H., et al., *TGF-β1-mediated repression of SLC7A11 drives vulnerability to GPX4 inhibition in hepatocellular carcinoma cells*. Cell Death & Disease, 2020. **11**(5): p. 406.
149. Kim, S., et al., *Characterization of ferroptosis in kidney tubular cell death under diabetic conditions*. Cell Death & Disease, 2021. **12**(2): p. 160.
150. Syed, V., *TGF-β Signaling in Cancer*. Journal of Cellular Biochemistry, 2016. **117**(6): p. 1279-1287.
151. Bakkebo, M., et al., *TGF-β-induced growth inhibition in B-cell lymphoma correlates with Smad1/5 signalling and constitutively active p38 MAPK*. BMC Immunology, 2010. **11**(1): p. 57.
152. Cavalli, G. and C.A. Dinarello, *Suppression of inflammation and acquired immunity by IL-37*. Immunological Reviews, 2018. **281**(1): p. 179-190.
153. Wang, Y., et al., *IL-21 Stimulates the expression and activation of cell cycle regulators and promotes cell proliferation in EBV-positive diffuse large B cell lymphoma*. Scientific Reports, 2020. **10**(1): p. 12326.
154. Sarosiek, K.A., et al., *Novel IL-21 signaling pathway up-regulates c-Myc and induces apoptosis of diffuse large B-cell lymphomas*. Blood, 2010. **115**(3): p. 570-580.
155. Keane, C., et al., *CD4+ Tumor infiltrating lymphocytes are prognostic and independent of R-IP1 in patients with DLBCL receiving R-CHOP chemo-immunotherapy*. American Journal of Hematology, 2013. **88**(4): p. 273-276.

LYMPHOID NEOPLASIA

Targeting chronic NFAT activation with calcineurin inhibitors in diffuse large B-cell lymphoma

Philip Bucher,¹ Tabea Erdmann,² Paula Grondona,¹ Wendan Xu,² Anja Schmitt,¹ Christoph Schürch,³ Myroslav Zapukhlyak,² Caroline Schönfeld,¹ Edgar Serfling,⁴ Daniela Kramer,¹ Michael Grau,² Pavel Klener,^{5,6} Claudia Lengerke,^{3,7} Klaus Schulze-Osthoff,^{1,8-10} Georg Lenz,² and Stephan Hailfinger^{1,10}

¹Interfaculty Institute for Biochemistry, Eberhard Karls University, Tübingen, Germany; ²Department of Medicine A, Hematology, Oncology, and Pneumology, University Hospital Münster, Münster, Germany; ³Department of Biomedicine, University Hospital and University of Basel, Basel, Switzerland; ⁴Department of Molecular Pathology, University of Würzburg, Würzburg, Germany; ⁵Institute of Pathological Physiology, First Faculty of Medicine, and ⁶Department of Hematology, Charles University General Hospital Prague, Prague, Czech Republic; ⁷Division of Hematology, University Hospital Basel, Basel, Switzerland; ⁸German Cancer Consortium (DKTK), Heidelberg, Germany; ⁹German Cancer Research Center (DKFZ), Heidelberg, Germany; and ¹⁰Cluster of Excellence iFIT (EXC 2180) "Image-Guided and Functionally Instructed Tumor Therapies," University of Tübingen, Tübingen, Germany

KEY POINTS

- DLBCL cell lines exhibit chronic NFAT activation, which is independent of B-cell receptor-mediated signals.
- Long-term treatment of ABC DLBCL with calcineurin inhibitors induces cytotoxicity and synergizes with BCL-2 and MCL-1 inhibition.

Diffuse large B-cell lymphoma (DLBCL) represents the most common adult lymphoma and can be divided into 2 major molecular subtypes: the germinal center B-cell-like and the aggressive activated B-cell-like (ABC) DLBCL. Previous studies suggested that chronic B-cell receptor signaling and increased NF- κ B activation contribute to ABC DLBCL survival. Here we show that the activity of the transcription factor NFAT is chronically elevated in both DLBCL subtypes. Surprisingly, NFAT activation is independent of B-cell receptor signaling, but mediated by an increased calcium flux and calcineurin-mediated dephosphorylation of NFAT. Intriguingly, although NFAT is activated in both DLBCL subtypes, long-term calcineurin inhibition with cyclosporin A or FK506, both clinically approved drugs, triggers potent cytotoxicity specifically in ABC DLBCL cells. The antitumor effects of calcineurin inhibitors are associated with the reduced expression of *c-Jun*, *interleukin-6*, and *interleukin-10*, which were identified as NFAT target genes that are particularly important for the survival of ABC DLBCL. Furthermore, calcineurin blockade synergized with BCL-2 and MCL-1 inhibitors in killing ABC DLBCL cells. Collectively, these findings identify constitutive NFAT signaling as a

crucial functional driver of ABC DLBCL and highlight calcineurin inhibition as a novel strategy for the treatment of this aggressive lymphoma subtype. (*Blood*. 2020;135(2):121-132)

Introduction

Diffuse large B-cell lymphoma (DLBCL) is the most common type of malignant lymphoma in adults and represents a heterogeneous entity with respect to morphology, biology, and clinical presentation.^{1,2} Roughly 65% of affected patients can be cured by cyclophosphamide, doxorubicin hydrochloride, vincristine sulfate, and prednisone chemotherapy combined with the anti-CD20 antibody rituximab. However, in the remaining cases, either no response to first-line therapy or relapse after an initial response are documented and associated with adverse prognosis.³ Gene expression profiling of DLBCL allows the discrimination of 2 major subtypes, termed activated B-cell-like (ABC) and germinal center B-cell-like (GCB) DLBCL.⁴⁻⁷ GCB DLBCLs frequently carry alterations in tumor suppressor genes, such as *PTEN*, *ING1*, or *TP53*, and tonic B-cell receptor (BCR) signaling promotes cell survival.^{8,9} In contrast, constitutive activation of the transcription factor NF- κ B driven by different mutations in genes encoding regulators of immune receptor signaling is a hallmark of the ABC DLBCL subgroup.¹⁰⁻¹² Chronic BCR signaling caused

by either self-antigens or abnormal expression of key components of the BCR pathway, such as CD79, CARD11, or A20, activates NF- κ B and thus promotes the outgrowth of ABC DLBCL.^{10,11,13-15} However, therapeutic intervention in humans is challenging because of the high toxicity of pan-NF- κ B inhibitors.

Recently, it became evident that not only NF- κ B, but also transcription factors of the activator protein-1 (AP-1) family are deregulated in ABC DLBCL.^{16,17} Members of the Jun, Fos, ATF, and MAF families form various hetero- and homodimeric AP-1 complexes regulating genes essential for cell growth, differentiation, and survival.^{16,18,19} Furthermore, the Jun family was shown to be important for the interaction of the DLBCL cells with the microenvironment and associated with in vivo lymphoma dissemination.²⁰

Besides NF- κ B and AP-1, the transcription factor NFAT has been implicated in DLBCL pathogenesis.²¹⁻²⁵ Four of 5 NFAT proteins (NFATc1-4) are activated by calcium and calcineurin, whereas

the activity of NFAT5 is induced by osmotic stress.^{26,27} Several kinases can phosphorylate NFAT, including GSK3, CK1, and DYRK1/2, thus keeping the transcription factor in an inactive state. Dephosphorylation of several amino acid residues in the N terminus of NFAT by the phosphatase calcineurin exposes its nuclear localization sequence, leading to the nuclear translocation of NFAT and target gene expression. Calcineurin itself is activated by calcium through binding to the calcium-sensor calmodulin.²⁷ Calcium mobilization can be induced by antigen receptors, which promote the activation of phospholipase C γ leading to inositol 1,4,5-trisphosphate production.²⁷ Inositol 1,4,5-trisphosphate induces the release of calcium from endoplasmic reticulum stores, which is recognized by stromal interaction molecule. Upon interaction with ORAI proteins, stromal interaction molecule stimulates the permeability of the calcium release-activated channel in the plasma membrane, a process referred to as store-operated calcium entry.²⁷

In this study, we demonstrate a constitutive NFAT activation in DLBCL cells. Long-term inhibition of calcineurin by cyclosporin A or FK506 was selectively cytotoxic for ABC but not for GCB DLBCLs. Calcineurin blockade further synergized with BCL-2 and MCL-1 inhibitors in killing ABC DLBCL cells, suggesting inhibition of the NFAT-calcineurin axis as a novel strategy for the treatment of ABC DLBCL.

Material and methods

Cell culture, lentiviral and retroviral transduction, survival assay

Protocols are available in the supplemental Materials and methods, available on the *Blood* Web site.

Antibodies

Immunoblot protocols and a list of primary antibodies are available in the supplemental Materials and methods.

ELISA

Secreted interleukin-6 (IL-6) and IL-10 were quantified using human IL-6 and IL-10 Ready-SET-Go enzyme-linked immunosorbent assay (ELISA) kits (eBioscience).

Gene expression profiling, gene set enrichment analysis, and dual luciferase reporter assay

Protocols are available in the supplemental Materials and methods.

Cell death analysis, calcium measurement and quenching assay, quantitative polymerase chain reaction, adhesion assay, and nuclear fractionation

Protocols are available in the supplemental Materials and methods.

DNA-binding of NFAT (TransAM)

NFATc1 TransAM (ActiveMotif) was performed according to the manufacturer's protocol after incubation with the indicated inhibitors for 24 hours.

Xenograft mouse model, zebrafish husbandry, and yolk sac transplantation

Protocols are available in the supplemental Materials and methods.

Results

Treatment with calcineurin inhibitors induces selective cytotoxicity in ABC DLBCL

To investigate whether calcineurin activity is important for the survival of DLBCL, we treated cell lines of the ABC or GCB subtypes with the calcineurin inhibitors cyclosporin A (CsA) or tacrolimus (FK506) for 12 days. Intriguingly, cell numbers were markedly decreased in several ABC DLBCL cell lines (Figure 1A), whereas all GCB DLBCLs tested exhibited unimpaired growth in the presence of calcineurin inhibitors (Figure 1B). This differential response of the DLBCL subtypes to calcineurin inhibition did not appear to correlate to the levels of calcineurin protein expression (supplemental Figure 1). The largest decrease in cell numbers in ABC DLBCL models occurred between days 4 and 6 after initiation of treatment with the calcineurin inhibitors (Figure 1A), which is slower than reported effects of small-molecule inhibitors targeting BCR or NF- κ B signaling or other cytotoxic drugs. This delayed cytotoxicity might be reason why calcineurin inhibitors have so far not been reported as anti-proliferative agents in ABC DLBCL. Calcineurin inhibition also led to increased numbers of annexin V-positive cells and elevated caspase activity in various ABC DLBCL cell lines, but not in the GCB DLBCL models HT and BJAB (Figure 1C-D), indicating that calcineurin inhibition induced apoptotic cell death of ABC DLBCL. Mantle cell lymphoma (MCL) also depend on BCR signaling for their survival.²⁸ Therefore, we next tested the influence of calcineurin inhibition on the growth of various MCL cell lines. Neither the MCL cell lines depending on canonical (Mino, Rec-1) nor those relying on alternative (JVM2, Z138) NF- κ B signaling showed any sensitivity toward CsA (Figure 1E). Thus, sensitivity toward calcineurin inhibition is unique for ABC DLBCL.

Chronic activation of the calcineurin-NFAT pathway in DLBCL cells

The selective sensitivity of ABC DLBCL cells toward calcineurin inhibitors indicates an involvement of the calcium-calcineurin-NFAT pathway in the survival of this subgroup. To visualize the activity of this pathway in DLBCL, we investigated 4 hallmarks of NFAT activation: (1) the increase of intracellular calcium; (2) the permeability of calcium channels; (3) the phosphorylation status of NFAT; and (4) its nuclear translocation. First, we determined the frequency of cells with increased intracellular calcium by flow cytometry using a fluorescent sensor. Surprisingly, not only ABC DLBCL, but all investigated DLBCL cell lines exhibited increased intracellular calcium levels compared with primary B cells, the Burkitt lymphoma cell line Ramos or the T-cell line Jurkat (Figure 2A; supplemental Figure 2A). Using an Mn²⁺ quenching approach, we demonstrated that all DLBCL cell lines exhibit a higher cation influx compared with the control cell lines Ramos or Jurkat, indicating an increased permeability of calcium channels in the plasma membrane (Figure 2B; supplemental Figure 2B).²⁹ Because increased intracellular calcium levels result in the activation of the phosphatase calcineurin and dephosphorylation of NFAT,²⁷ we visualized NFAT phosphorylation by immunoblotting. We focused on NFATc1 and NFATc2 because these are the most abundant NFAT proteins in lymphocytes.³⁰ Several NFAT isoforms were expressed in the investigated B-cell lines, so we treated the cells either with CsA, FK506, or solvent control to discriminate the hyperphosphorylated from the hypophosphorylated NFAT species. Whereas the control cell lines Ramos or Jurkat showed neither NFATc1 nor NFATc2 hypophosphorylation in an unstimulated

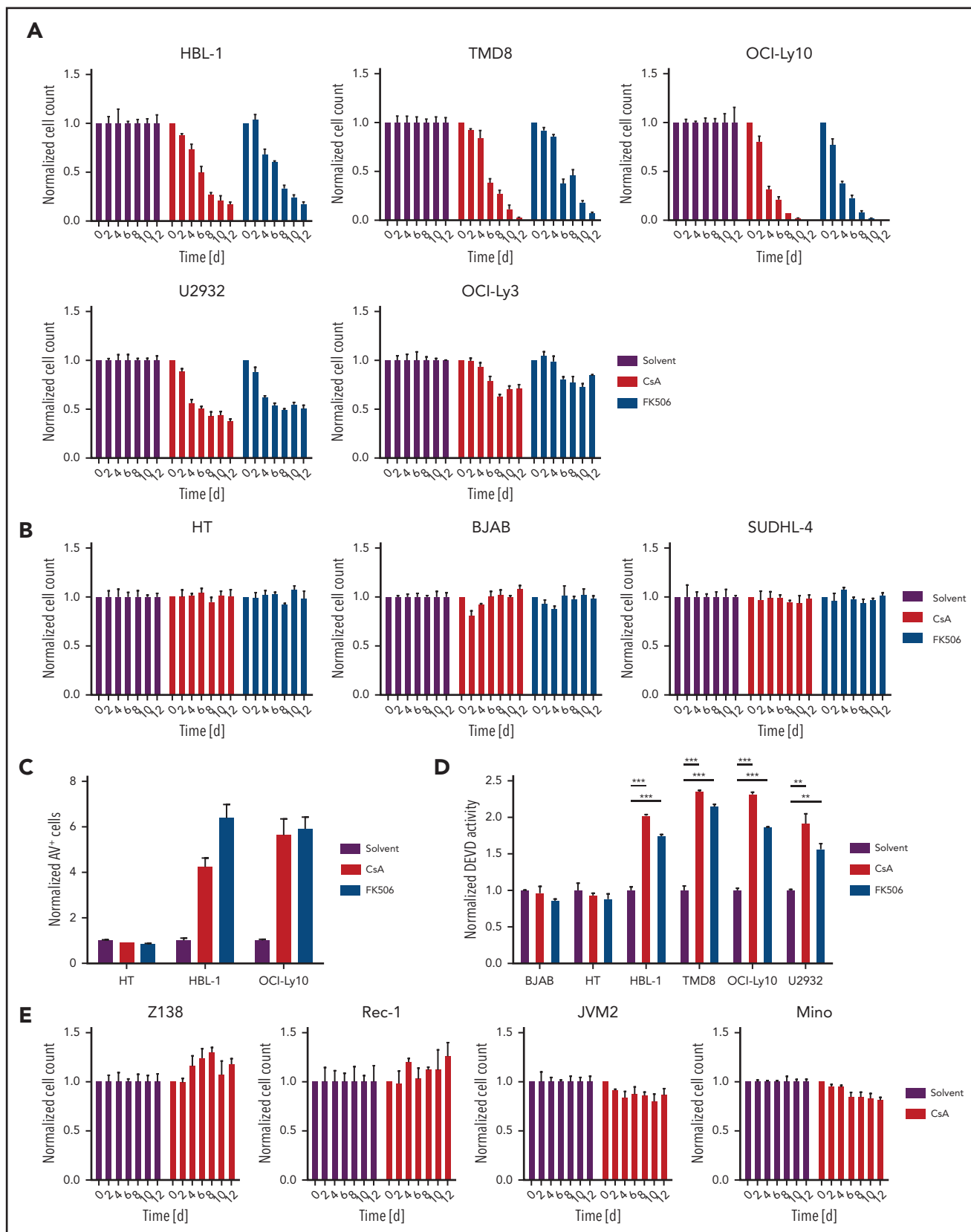


Figure 1. Calcineurin inhibition triggers cytotoxicity in ABC DLBCL. (A) ABC DLBCL or (B) GCB DLBCL cells lines were treated with DMSO, 300 nM CsA, or 300 nM FK506, and cell numbers were counted every second day as indicated. (C) Annexin V-positive cells were measured by flow cytometry after 4 days of DMSO, CsA, or FK506 treatment. (D) GCB (BJAB and HT) and ABC (HBL-1, TMD8, OCI-Ly10, U2932) DLBCL cell lines were treated with DMSO, CsA, or FK506 for 4 days and caspase activity was determined using DEVD-AMC as substrate. (E) Cell count of MCL cell lines treated with either DMSO or 300 nM CsA as indicated. (A-E) Cell counts, frequency of cells, or caspase activity were normalized to the solvent control. Error bars correspond to the mean \pm SD. Statistical significance was calculated using Student t test ($*P < .05$, $**P < .01$, $***P < .001$). Data are representative of at least 3 (A-C,E) or 2 (D) independent experiments. d, days; DMSO, dimethyl sulfoxide; SD, standard deviation.

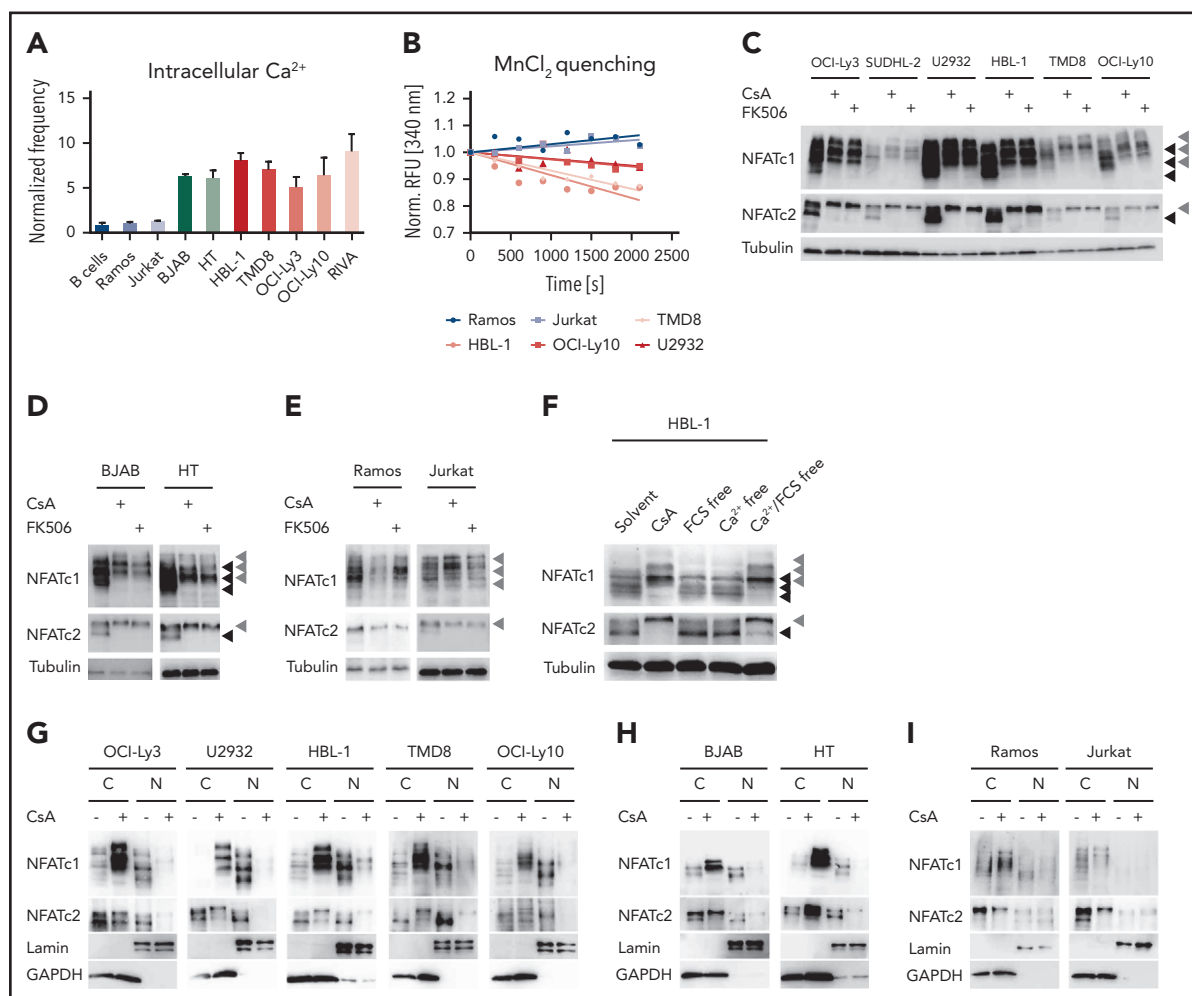


Figure 2. Calcium-mediated NFAT activation is deregulated in DLBCL cell lines. (A) Intracellular calcium levels of splenic primary mouse B cells or of the indicated cell lines measured by flow cytometry. Frequencies of positive cells were normalized to the control cell line Ramos. (B) To measure the permeability of cation channels at the plasma membrane, $MnCl_2$ was added to the medium and Fura-2 quenching was assessed by flow cytometry over time. Fura-2 excitation was normalized to the fluorescence of each individual cell line before $MnCl_2$ was added. Immunoblot analysis of (C) ABC DLBCL, (D) GCB DLBCL, or (E) control cell lines Ramos and Jurkat, which were either treated with solvent, 600 nM CsA, or 600 nM FK506 for 4 hours to assess the phosphorylation status of NFATc1 and NFATc2. Tubulin served as loading control. (F) To investigate the importance of extracellular calcium, HBL-1 cells were kept for 4 hours in calcium-free and/or in fetal calf serum-free medium as indicated and analyzed for NFATc1/2 phosphorylation status by immunoblotting. Subcellular localization of NFATc1/2 in cytoplasmic and nuclear fractions of (G) solvent- or CsA-treated ABC DLBCL, (H) GCB DLBCL, or (I) control cell lines. Lamin A/C and GAPDH served as markers for N or C fractions, respectively. Data in panels A-E and G-I are representative of at least 3 independent experiments, in panel F of 2 independent experiments. (C-E) Black arrowheads mark hypophosphorylated and hence activated NFAT isoforms, whereas gray arrowheads indicate the hyperphosphorylated forms of the transcription factors. C, cytoplasmic; N, nuclear.

condition, all NFATc1/2 isoforms were hypophosphorylated and hence activated in both GCB and ABC DLBCL cells, which could be reversed by CsA or FK506 treatment (Figure 2C-E; supplemental Figure 2C). Similar to the DLBCL cells, MCL cell lines also showed constitutive NFATc1/2 hypophosphorylation (supplemental Figure 2D), even though GCB DLBCL and MCL cell lines were not sensitive toward calcineurin inhibitors. To assess whether the observed increased permeability of cation channels was responsible for NFATc1/2 dephosphorylation, we cultured DLBCL cells in calcium-free medium. Under these conditions, the lack of external calcium rapidly reduced NFATc1/2 dephosphorylation, suggesting that open calcium channels at the plasma membrane are essential for NFATc1/2 activation in DLBCLs (Figure 2F; supplemental Figure 2E).

NFAT dephosphorylation by calcineurin is important for the unmasking of the nuclear localization sequence and thus for its

rapid transport to the nucleus.²⁷ To check whether the detected dephosphorylated NFATc1/2 species in DLBCL indeed undergo nuclear translocation, we purified cytoplasmic and nuclear fractions from DLBCL and control cell lines and visualized NFATc1/2 localization by immunoblotting. In ABC and GCB DLBCL cell lines, NFATc1/2 was clearly detected in the nuclear fraction and treatment with CsA or FK506 resulted in the export of NFATc1/2 (Figure 2G-I; supplemental Figure 2F). Collectively, an increased intracellular calcium level, an enhanced permeability of cation channels, as well as dephosphorylation and nuclear translocation of NFATc1/2 indicate a chronic activation of the calcineurin-NFATc1/2 pathway in DLBCL cells.

Increased NFAT activity in DLBCL does not derive from BCR signaling

Because autoreactive BCRs, CD79 mutations, and chronic BCR signaling were suggested to drive the growth of ABC

DLBCLs,^{8,10,11,14} we speculated that the activation of the calcium-calcineurin-NFAT axis might be triggered by antigen receptor signaling. We therefore treated ABC and GCB DLBCL cell lines with small-molecule kinase inhibitors targeting Src, BTK, SYK, or phosphatidylinositol 3-kinase (PI3K) to block upstream BCR signaling and measured intracellular calcium levels over time. Surprisingly, none of the upstream kinase inhibitors was able to reduce calcium flux in DLBCL cells (Figure 3A). To validate the reliability of the fluorescent calcium probe used, we either added the calcium chelator EGTA, which indeed lowered the fluorescence intensity of the calcium sensor over time, or induced calcium flux with the ionophore ionomycin or an agonistic anti-immunoglobulin M (IgM) antibody (Figure 3A). Both ionomycin and anti-IgM induced a transient increase in calcium flux in all cells except for the GCB DLBCL cell line HT, which did not react to anti-IgM stimulation because of its lack of IgM surface expression (Figure 3A).⁸ Both the SYK inhibitor GS-9973 and the BTK inhibitor ibrutinib efficiently blocked anti-IgM-induced calcium flux in HBL-1 cells, but did not affect the increased steady-state calcium levels (Figure 3A; supplemental Figure 3A).

To confirm that the increased calcium flux does not originate from a BCR-induced signal, we treated several DLBCL cell lines with the SYK inhibitors GS-9973 or R406 and assessed the nuclear pool of NFATc1. Whereas CsA profoundly reduced the nuclear localization of NFATc1 (Figure 2G), both SYK inhibitors had only a mild impact on the localization of NFATc1 in DLBCL cells (Figure 3B; supplemental Figure 3B-C). Accordingly, neither Src, BTK, nor PI3K inhibitors altered NFATc1/2 phosphorylation and only mildly affected NFATc1 DNA binding (Figure 3C; supplemental Figure 3D-E). Silencing of IgM, CD79A, or CD79B in the ABC DLBCL cell line HBL-1 also confirmed that neither phosphorylation nor nuclear localization of NFATc1/2 were controlled by BCR-derived signals (Figure 3D-E).

Increased NFATc1 expression is regulated by NF- κ B

Interestingly, we and others noticed that ABC DLBCLs on average express higher levels of NFATc1 compared with GCB DLBCLs and that silencing of IgM, CD79A, or CD79B for 48 hours as well as inhibition of BCR upstream signaling by SYK, BTK, or PI3K inhibitors for 24 hours lowered the protein levels of NFATc1, but not of NFATc2 (Figure 3D-F; supplemental Figure 3F-I).²² The reduction of NFATc1 expression was apparently the result of impaired transcription because messenger RNA (mRNA) levels of *NFATC1*, but not of *NFATC2*, were decreased by SYK, BTK, or PI3K inhibitor treatment (Figure 3G). One of the main factors driving NFATc1 expression is the transcription factor NF- κ B.³¹ To test if NF- κ B was involved in the expression of NFATc1 in DLBCL, we transfected an NFATc1 reporter into HBL-1 cells and blocked NF- κ B activity with an IKK inhibitor. Indeed, inhibition of IKK, but also of PI3K or BTK, strongly reduced the NFATc1 reporter activity (Figure 3H).³² Accordingly, expression of a dominant-negative mutant of I κ B α (DN-I κ B α) to block canonical NF- κ B activity strongly interfered with NFATc1 expression in various ABC DLBCL cell lines (Figure 3I). In line with a previous report, NF- κ B induced *NFATC1* expression by activating the distal, but not the proximal promoter in DLBCL cells (supplemental Figure 3J).³¹ Collectively, these results suggest that the increased intracellular calcium levels, the calcineurin-mediated dephosphorylation, and nuclear translocation of NFAT are independent of signals from the BCR, whereas the strong

expression of NFATc1 in ABC DLBCL cells is driven by a BCR-mediated activation of NF- κ B. In line with this hypothesis, we were unable to block NFATc1 expression with inhibitors targeting BCR signaling in OCI-Ly3 cells, which harbor a CARD11 mutation that promotes NF- κ B activity independently of the BCR (Figure 3F).¹⁵ In contrast, NF- κ B inhibition downstream of CARD11, through the expression of DN-I κ B α , efficiently reduced NFATc1 in the OCI-Ly3 cell line (Figure 3I).

Calcineurin inhibition impairs IL-6, IL-10, and c-Jun expression

To better understand the mechanism underlying the toxicity of calcineurin inhibition in ABC DLBCL, we analyzed the global gene expression profiles of the ABC DLBCL cell line HBL-1 after 12, 24, 36, and 48 hours of CsA treatment (Figure 4A; supplemental Figure 4A; supplemental Table 3). Gene set enrichment analysis revealed that calcineurin inhibition affected numerous NF- κ B target genes as well as genes regulated by the PI3K inhibitor AZD8835 (supplemental Figure 4B; supplemental Table 4). Because PI3K inhibition impairs NF- κ B activity in DLBCLs, but luciferase-based reporter assay analysis did not reveal any reduction in NF- κ B activity by CsA or FK506 (supplemental Figure 4C), we speculated that NFAT and NF- κ B regulate common target genes in B cells.³³ Indeed, in addition to typical NFAT target genes such as *EGR2*, we identified *IL10*, *NFKBIA*, and *JUN*, previously described as NF- κ B target genes in DLBCL, as genes that are also regulated by NFAT (Figure 4B-D; supplemental Figure 4D-E).^{34,35} This is in agreement with recent findings that NFATc1 regulates *IL10* and thus PD-L1 expression.²² Additionally, we detected decreased mRNA expression of *STAT3* and *SOCS3*, which might result from reduced IL-10 production (Figure 4B; supplemental Figure 4D).^{35,36} Interestingly, only the expression of *JUN*, but not of *JUNB* or *JUND*, was affected by calcineurin inhibition (Figure 4C; supplemental Figure 4D). CsA treatment of the GCB DLBCL cell line HT did not affect *JUN*, *SOCS3*, or *IL10* expression, indicating that NFAT regulates a different subset of target genes in the 2 DLBCL subtypes (supplemental Figure 5A-B; supplemental Table 5).

The observed reduction in *IL10* mRNA levels in CsA-treated HBL-1 cells correlated with a decreased secretion of IL-10 in the supernatants of the ABC DLBCL cell lines HBL-1 and TMD8 upon CsA or FK506 treatment (Figure 4E; supplemental Figure 4F). The cytokines IL-10 and IL-6 stimulate the growth of ABC DLBCL in an auto- and paracrine manner via the JAK/STAT3 pathway.³⁵ Therefore, we next investigated whether the calcineurin inhibitor-mediated downregulation of IL-10 affected STAT3 phosphorylation. Strikingly, P-STAT3 levels were strongly reduced after CsA or FK506 treatment in the majority of ABC DLBCL cell lines, indicating that secretion of IL-10 and possibly also of IL-6 might be affected by calcineurin inhibition (Figure 4F; supplemental Figure 6A). Indeed, secretion of both, IL-10 and IL-6, was dependent on NFAT activity, explaining the strong reduction in STAT3 phosphorylation (Figure 4E-F; supplemental Figure 4F). Thus, the CsA-mediated cytotoxicity observed for ABC DLBCL cell lines likely results from the inhibition of the NFAT-dependent production of these growth-promoting cytokines.

The transcription factor c-Jun was strongly downregulated at both the mRNA and protein level upon calcineurin inhibition in most ABC DLBCL cell lines (Figure 4C-D,F; supplemental

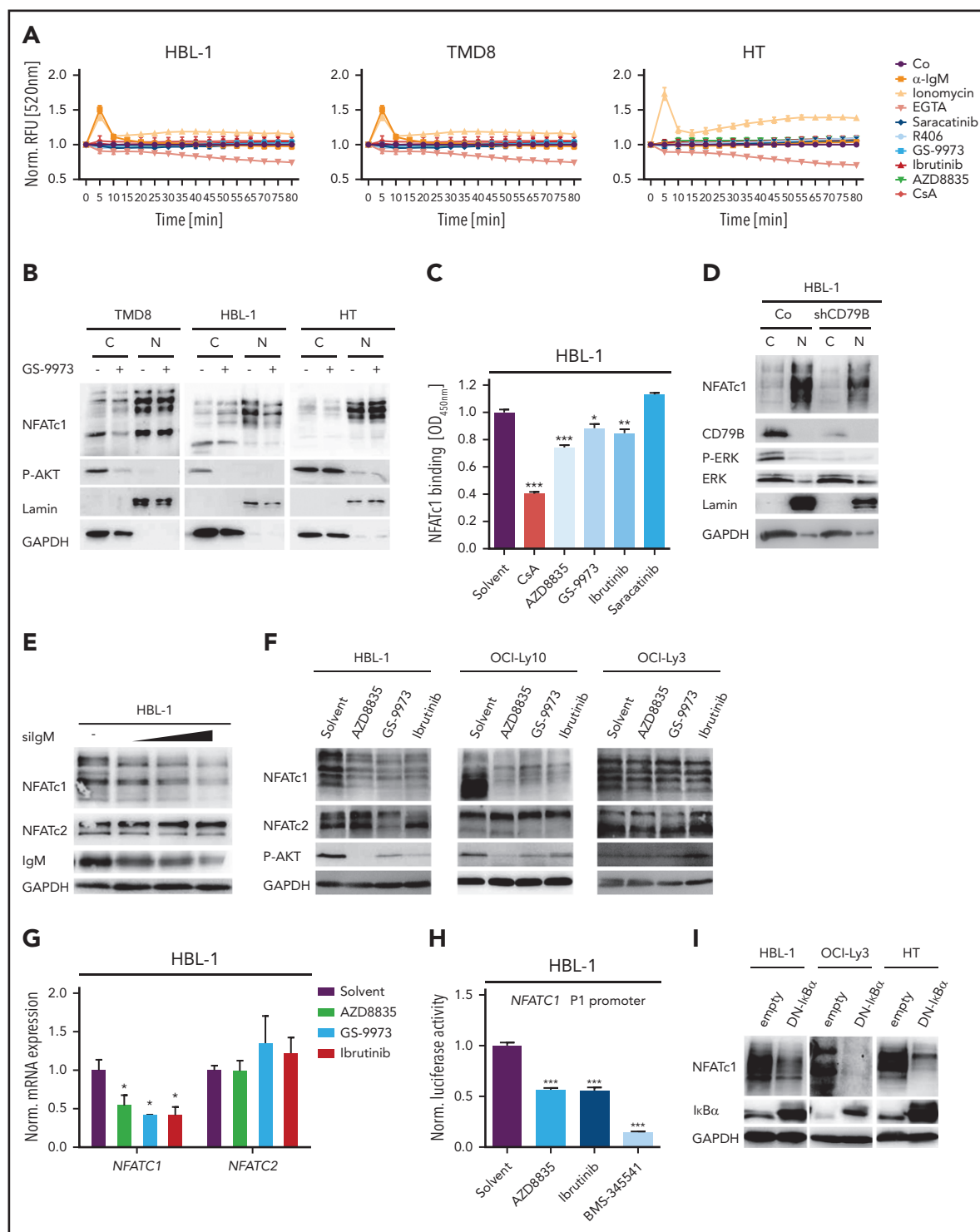


Figure 3. NFAT dephosphorylation and nuclear translocation are not driven by BCR signaling. (A) Measurement of intracellular calcium levels in the presence of either agonistic anti-IgM antibodies, the ionophore ionomycin, the Ca²⁺ chelator EGTA, the Src kinase inhibitor saracatinib, the SYK inhibitors GS-9973 and R406, the BTK inhibitor ibrutinib, or the PI3K inhibitor AZD8835. The intensity of the calcium sensor Calbryte 520 was measured over time by flow cytometry. (B) Cytoplasmic and nuclear fractions of DLBCL cell lines treated with solvent or the SYK inhibitor GS-9973 for 4 hours. NFATc1 localization was visualized by immunoblotting. P-AKT was used to control the efficacy of SYK inhibition in the ABC DLBCL cell lines TMD8 and HBL-1. Lamin A/C and GAPDH served as nuclear and cytoplasmic markers, respectively. (C) HBL-1 cells were treated with either solvent or the indicated inhibitors for 4 hours before quantification of NFATc1 binding to its consensus nucleotide sequence by TransAM assay. (D) Localization of NFATc1 in control or CD79B-silenced HBL-1 cells visualized by immunoblot analysis. (E) HBL-1 cells were transfected with scrambled or with increasing amounts of small interfering RNA targeting IgM. NFATc1/2 expression was analyzed by immunoblotting. (F) The ABC DLBCL cell lines were treated with solvent or the indicated inhibitors for 24 hours, before NFATc1/2 levels were measured by immunoblotting. (G) HBL-1 cells were treated with inhibitors targeting PI3K, SYK, or BTK and NFATc1/2 mRNA levels were quantified by qPCR. All samples were normalized to the solvent control. (H) The NFATc1 P1 luciferase-based reporter construct was transfected into HBL-1 cells, which were subsequently treated with inhibitors targeting PI3K, BTK, or IKK for 24 hours. Luciferase signals were normalized to the DMSO-treated sample. (I) The ABC DLBCL cell lines HBL-1 and OCI-Ly3 as well as the GCB cell line HT were lentivirally transduced with a DN-IκBα expression

Figure 6B). c-Jun plays at least 2 important roles in DLBCL tumor biology. First, c-Jun regulates the interaction of tumor cells with the microenvironment and is required for efficient metastasis.²⁰ This might be due to a Jun-mediated control of adhesion to extracellular matrix proteins, such as fibronectin. Because calcineurin inhibitors reduce c-Jun expression in ABC DLBCL cells, we tested whether CsA or FK506 treatment affects the adhesion of lymphoma cells to fibronectin. Indeed, both calcineurin inhibitors decreased the capability of the ABC DLBCL cell line TMD8 to adhere to fibronectin-coated plates (Figure 4G). The reduction of adhesion was not caused by cytotoxicity of the calcineurin inhibitors because phorbol 12-myristate 13-acetate treatment restored c-Jun protein levels and adhesion to fibronectin (Figure 4G; supplemental Figure 6C). Another important role of c-Jun, as a constituent of the heterodimeric transcription factor AP-1, is to regulate the expression of IL-6, IL-10, and other pro-survival factors.^{16,20} To investigate whether c-Jun deficiency or the reduced IL-6/IL-10 expression contributes to the cytotoxic effects of calcineurin inhibitors, we transduced OCI-Ly10 cells with a c-Jun expression vector or reconstituted IL-6/IL-10 in the culture medium and assessed cell growth upon calcineurin inhibition. c-Jun expression and IL-6/IL-10 supplementation partially rescued the impaired survival caused by calcineurin inhibition, whereas the combination of both c-Jun and IL-6/IL-10 had no further significant effect (Figure 5A-B; supplemental Figure 6D). Thus, CsA-mediated reduction of c-Jun levels not only affects the adhesiveness of ABC DLBCL cells, but also controls the growth and survival together with other NFAT targets like IL-6 and IL-10.

Molecular mechanism of NFAT-mediated *JUN*, *IL6*, and *IL10* expression

To assess if *JUN*, *IL6*, and *IL10* are direct NFAT target genes, we generated luciferase-based reporter constructs comprising their promoters. Coexpression of the *JUN* reporter with RelA or NFATc1 in the ABC cell line U2932 or the GCB cell lines BJAB and SUDHL-4 showed that *JUN* transcription can be induced not only by NF- κ B but also by NFATc1 (Figure 5C-D). Based on published chromatin immunoprecipitation (ChIP) data and in silico analyses, a proximal and a distal region of the *IL10* promoter might be responsible for the control of *IL10* expression.³⁷ Although the reporter containing the proximal *IL10* promoter was only responsive to RelA, the distal promoter was activated by both RelA and NFATc1 (Figure 5E-F).

In contrast to the *JUN* and *IL10* promoters, simple coexpression of NFATc1 or NFATc2 was not sufficient to drive *IL6* reporter gene activity (Figure 5G-H; supplemental Figure 6E). Interestingly, several reports suggested that NFAT can form complexes with AP-1 to regulate a unique set of genes.³⁸ Indeed, although NFATc1 or c-Jun expression alone was unable to activate the *IL6* promoter, coexpression of both proteins induced *IL6* reporter gene activity in a dose-dependent manner (Figure 5G-H; supplemental Figure 6E). NFATc1 ChIP analyses confirmed that NFATc1 is constitutively bound to the *JUN*, *IL6*, and the distal *IL10* promoters in the ABC DLBCL cell line HBL-1 and that CsA treatment reduces DNA binding to these sites (Figure 5I).

In accordance to the *JUN* and *IL10* reporter gene assay, silencing of NFATc1 led to reduced expression of *IL10* and *JUN* mRNA in the ABC DLBCL cell line HBL-1 (supplemental Figure 7A). Interestingly, NFATc1 silencing by 2 independent short hairpin RNAs impaired the growth of the ABC DLBCL cell lines HBL-1, TMD8 and U2932, but not of the GCB cell line HT (supplemental Figure 7B-C), suggesting that calcineurin inhibitors mediate its cytotoxic effects in ABC DLBCL via NFATc1 inhibition. Collectively, we propose that *JUN*, *IL10*, and *IL6* are direct NFATc1 target genes in ABC DLBCLs and that their expression is regulated by an interplay of NFATc1 with other transcription factors, such as NF- κ B and AP-1.

Several NFATc1/2 target genes are also controlled by NF- κ B. We therefore hypothesized that DLBCL cells with an activating CARD11 mutation, leading to constitutive NF- κ B activation,¹⁵ should be less sensitive toward calcineurin inhibitors. We noticed that neither IL-6/IL-10 nor P-STAT3 or c-Jun levels were affected by CsA or FK506 in OCI-Ly3 cells, which express the activating CARD11 mutation L244P (Figure 4E-F; supplemental Figure 4F).¹⁵ To confirm that activating *CARD11* mutations indeed weaken the toxicity of calcineurin inhibitors, we transduced OCI-Ly10 cells with *CARD11*^{L244P} and treated those cells with CsA and FK506. Indeed, *CARD11*^{L244P}-expressing cells not only showed improved survival upon CsA and FK506 treatment, but also exhibited enhanced c-Jun and P-STAT3 levels compared with control cells (supplemental Figure 7D-E).

Inhibition of BCL-2 or MCL-1 synergizes with calcineurin blockade in ABC DLBCL

To investigate the potential of calcineurin inhibitors *in vivo*, we used a TMD8 xenograft mouse model, administered FK506 for 5 consecutive days and quantified tumor growth over time. FK506 treatment reduced both tumor volume and weight significantly (Figure 6A-B). To screen for combinatorial effects of calcineurin inhibitors with drugs previously described to be active in patients with B-cell lymphomas *in vivo*, we transplanted the ABC DLBCL cell line TMD8 into the yolk of zebrafish embryos that were subsequently cultured in solvent- or inhibitor-supplemented medium. Whereas the solvent control group developed tumors in ~60% of animals after 3 days, CsA and FK506 treatment impaired tumor formation (Figure 6C-D). Interestingly, we noticed that combination of the BCL-2 inhibitor ABT-199 with CsA prevented tumor formation in more than two-thirds of the animals. The BCL-2 inhibitor ABT-199 (venetoclax), a BH3 mimetic, which exhibited a partial efficacy in a phase 1 first-in-human study and in a recent trial combined with rituximab, cyclophosphamide, doxorubicin hydrochloride, vincristine sulfate, and prednisone,^{39,40} was further characterized in combination with CsA in several DLBCL cell lines. Whereas ABT-199 only weakly interfered with the survival of ABC DLBCL at low concentrations, calcineurin inhibitors strongly sensitized the cells to BCL-2 inhibition (Figure 6E; supplemental Figure 8A). Because the BCL-2 member MCL-1 is frequently overexpressed in DLBCL and also fulfills an antiapoptotic function,^{41,42} we tested an MCL-1 inhibitor, S63845, for its potential to synergize with calcineurin inhibitors. Comparable to ABT-199, S63845

Figure 3 (continued) construct and NFATc1 levels were visualized by immunoblotting. (A-I) Data are representative of at least 3 independent experiments. Error bars correspond to the mean \pm SD. Statistical significance was calculated using Student t test (* P < .05, ** P < .01, *** P < .001). GAPDH, glyceraldehyde-3-phosphate dehydrogenase; qPCR, quantitative polymerase chain reaction.

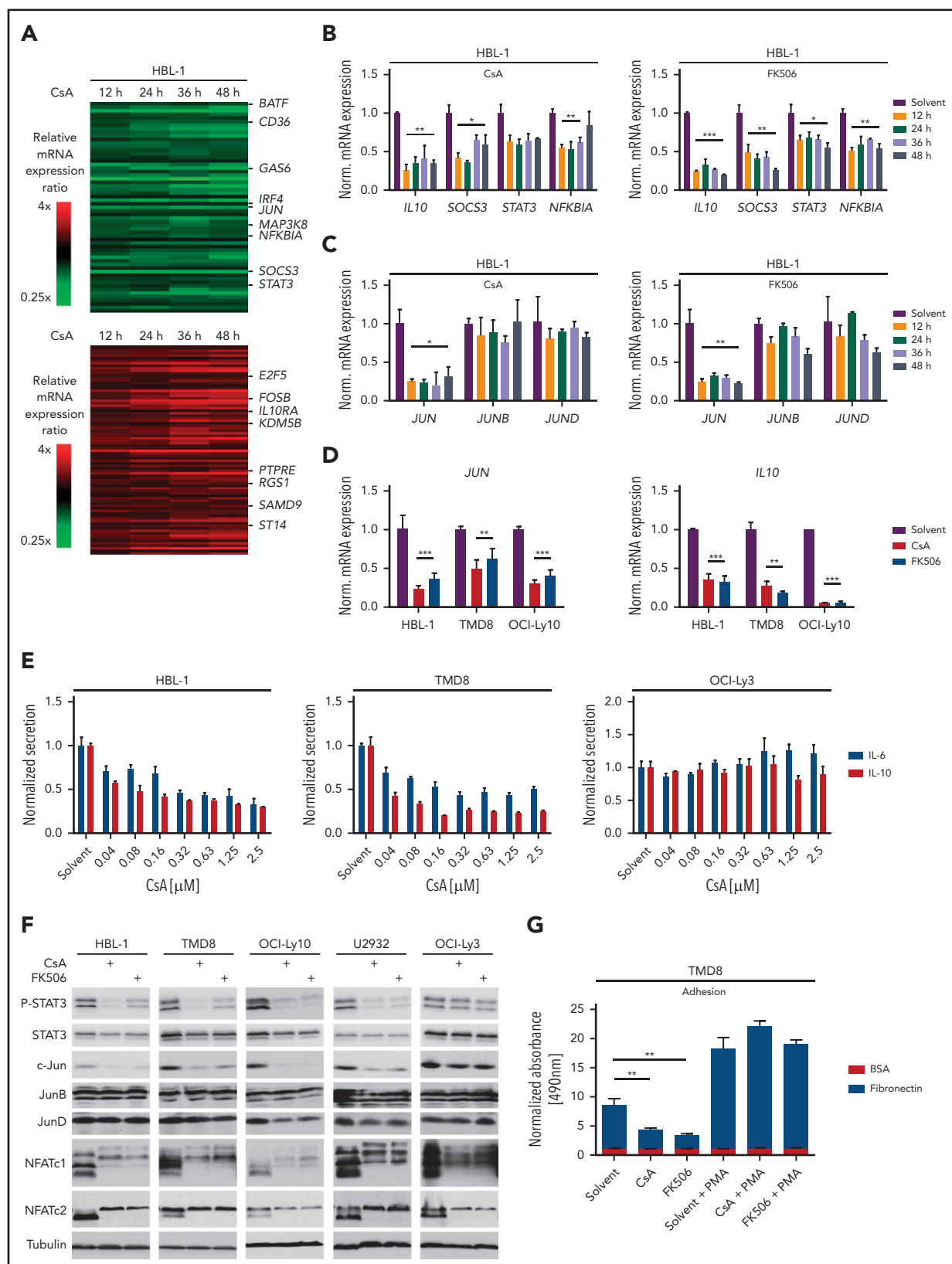


Figure 4. NFAT controls the expression of IL-6, IL-10, and c-Jun. (A) Heatmaps of differentially expressed genes in HBL-1 treated for 12, 24, 36, and 48 hours with CsA compared with the solvent control. Gene expression changes are depicted according to the color scale. (B,C) HBL-1 cells were treated with solvent, CsA, or FK506; mRNA levels of the indicated genes were quantified by qPCR analysis. (D) *JUN* and *IL10* mRNA expression were measured by qPCR in the indicated ABC DLBCL cell lines. (E) IL-6 and IL-10 protein levels were quantified in the medium of solvent- or CsA-treated ABC DLBCL cell lines by ELISA and normalized to the DMSO control. (F) The indicated ABC DLBCL cell lines were treated for 48 hours with solvent, CsA or FK506 and cell lysates were analyzed by western blotting. (G) TMD8 cells were treated with solvent or the calcineurin inhibitors for 48 hours and part of the cells were incubated with PMA for 6 hours subsequently. Adhesion to BSA- or fibronectin-coated plates was measured by an

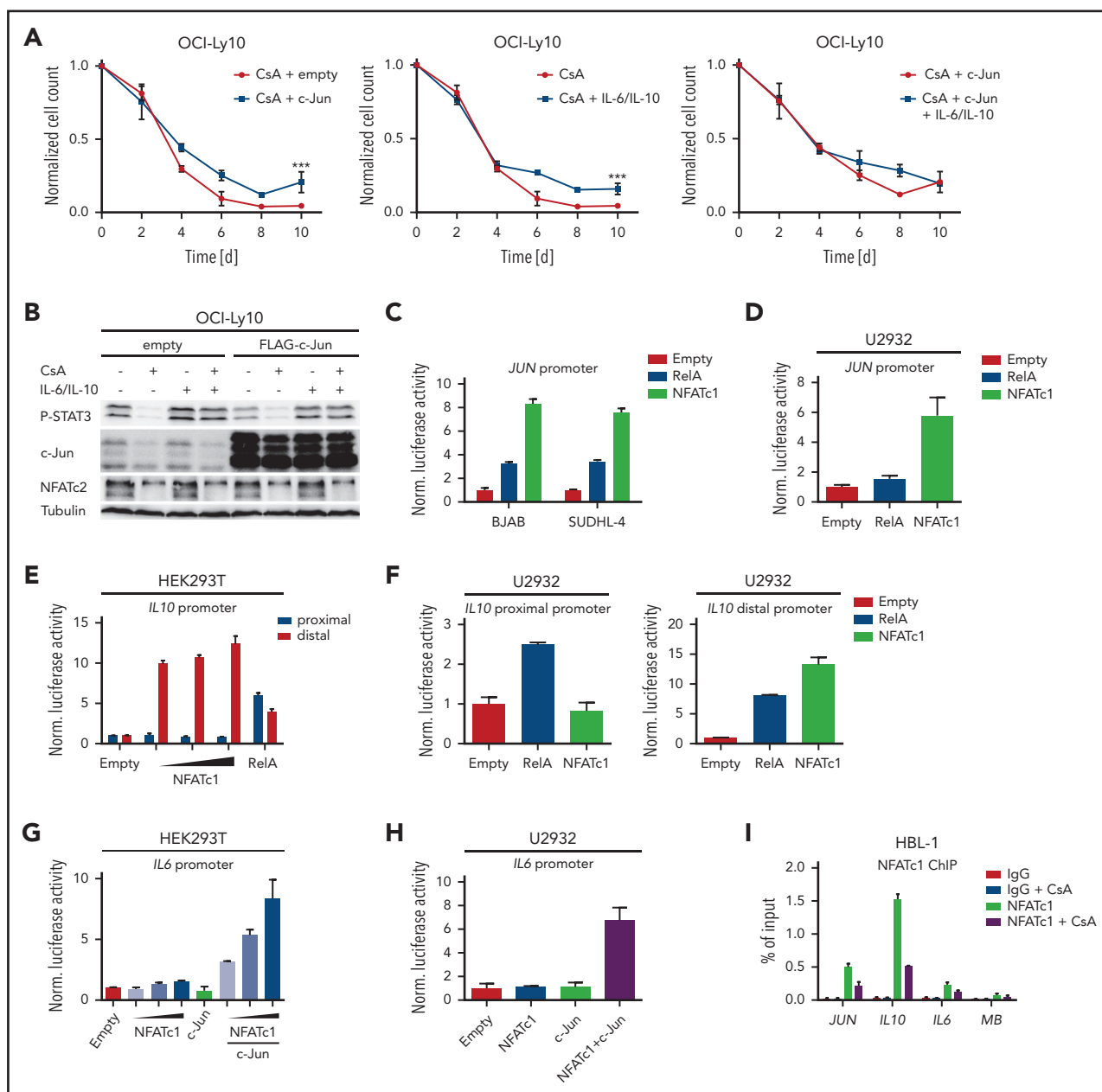


Figure 5. *IL6*, *IL10*, and *JUN* expression is directly regulated by NFAT. (A) c-Jun overexpressing or control OCI-Ly10 cells were treated every second day with CsA and/or IL-6/IL-10 as indicated. Treated cells were counted and normalized to the solvent controls. (B) OCI-Ly10 cells, which had been transfected with either a c-Jun or an empty expression vector, were treated for 48 hours with solvent, CsA, and/or IL-6/IL-10 as indicated. P-STAT3 and c-Jun protein levels were assessed by immunoblotting. A JUN reporter construct was cotransfected with either empty vector control, RelA, or NFATc1/ α A in the indicated (C) GCB DLBCL cell lines or (D) in U2932. Luciferase activity was measured (C) 48 or (D) 36 hours after transfection and normalized to the empty vector control. (E,G) HEK293T cells were transfected with IL-6 or IL-10 reporter constructs in combination with RelA, c-Jun, and NFATc1/ α A as indicated. Luciferase activity was measured 24 hours after transfection and normalized to the empty vector control. (F,H) The ABC DLBCL cell line U2932 was electroporated with either a proximal/distal *IL10* or an *IL6* reporter construct. Expression vectors containing RelA, NFATc1/ α A, or c-Jun were cotransfected as indicated. Thirty-six hours after transfection, luciferase activity was quantified and normalized to the empty vector control. (I) ChIP analysis from CsA- or solvent-treated (4 hours) HBL-1 cells. NFATc1 binding to the *JUN*, *IL10*, *IL6*, and myoglobin (*MB*) promoters was compared with the IgG control. The data are representative of (A-H) at least 3 or (I) 2 independent experiments. Error bars correspond to the mean \pm SD. Statistical significance was calculated using Student t test (* P < .05, ** P < .01, *** P < .001).

synergized with CsA in the killing of various ABC DLBCL cell lines (Figure 6F; supplemental Figure 8B). Collectively, our data suggest that the use of calcineurin inhibitors in combination

with BH3 mimetics targeting BCL-2 or MCL-1 might represent a promising novel strategy in targeting the survival of ABC DLBCL cells.

Figure 4 (continued) MTS assay. Adhesion was normalized to solvent-treated cells bound to BSA-coated plates. (A-G) Data are representative of at least 3 independent experiments. Error bars correspond to the mean \pm SD. Statistical significance was calculated using Student t test (* P < .05, ** P < .01, *** P < .001). PMA, phorbol 12-myristate 13-acetate.

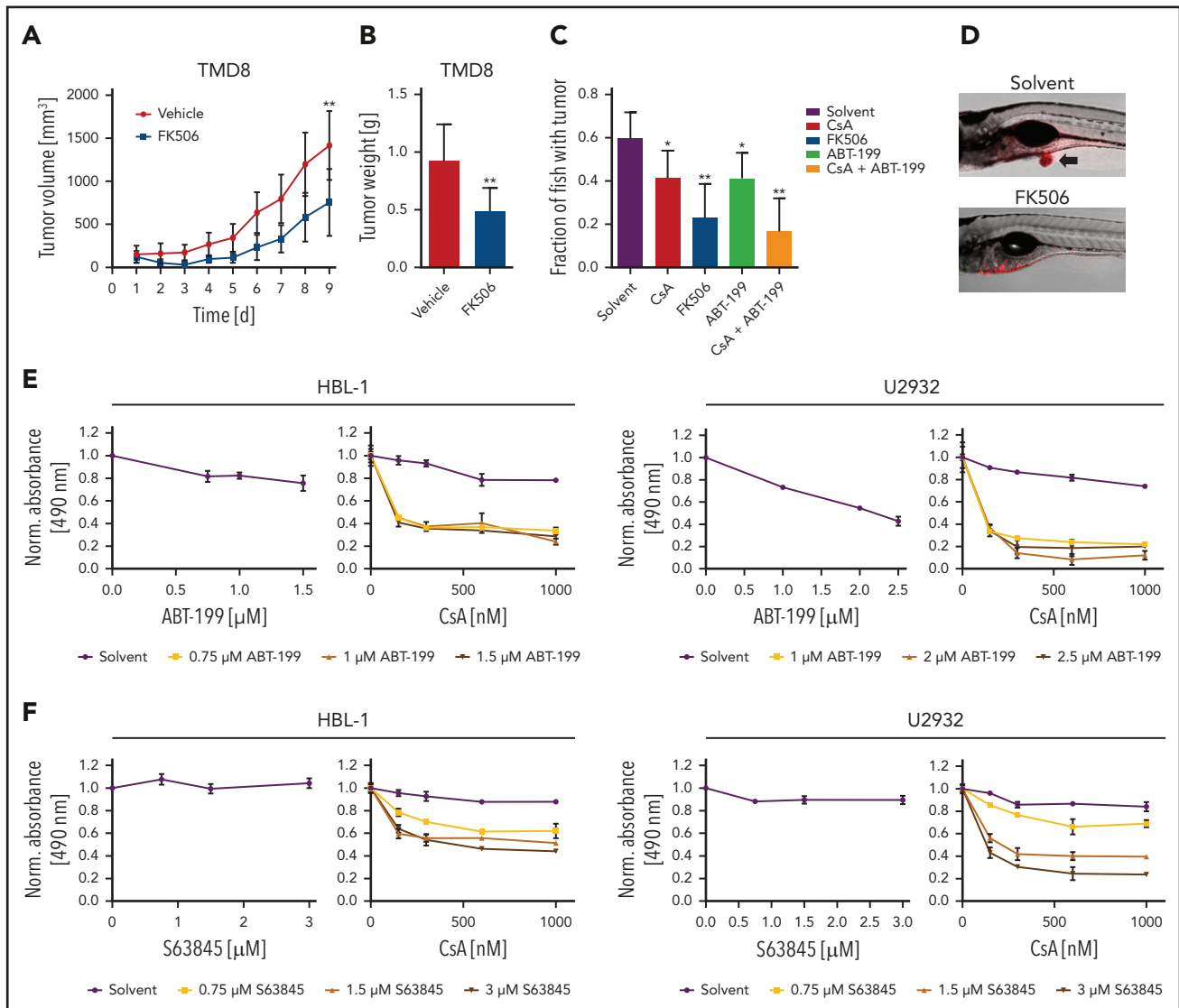


Figure 6. BCL-2 or MCL-1 inhibition synergizes with calcineurin blockade. (A) TMD8 xenograft mice were treated for 5 consecutive days with vehicle ($n = 7$) or 4 mg/kg FK506 ($n = 6$) and tumor volume was quantified by caliper measurements. FK506 significantly reduces tumor growth ($P = .0093$). (B) Average tumor weight of TMD8 xenograft mice after treatment of 9 days with vehicle ($n = 7$) or FK506 ($n = 6$). FK506 significantly reduces tumor mass ($P = .0058$). (C) TMD8 cells were transplanted in zebrafish embryos and tumor formation of treated animals was counted after 3 days by microscopy ($n \geq 20$). (D) Representative images of transplanted zebrafish embryos after solvent or FK506 treatment. Arrow indicates the formation of a tumor. The ABC DLBCL cell lines HBL-1 or U2932 were treated with either (E) ABT-199 or (F) the MCL-1 inhibitor S63845 in the absence (left) or presence of CsA (right). Cell survival was quantified by an MTS assay. The combination index for CsA and ABT-199 in HBL-1 and U2932 is ≤ 0.17 and ≤ 0.34 , respectively. For CsA and S63845, the combination index is ≤ 0.19 for HBL-1 and ≤ 0.23 for U2932. The data are representative of (E-F) at least 3 independent experiments. Error bars correspond to the mean \pm SD. Statistical significance was calculated using Student *t* test (* $P < .05$, ** $P < .01$, *** $P < .001$).

Discussion

Here we provide several lines of evidence that NFAT signaling is chronically activated in DLBCL and controls biological key processes, such as cell survival and interaction with the tumor environment. Unlike the GCB subtype, ABC DLBCL cells were particularly sensitive to inhibition of the NFAT pathway, identifying calcineurin inhibitors as a promising therapeutic approach for these aggressive tumors. Because the survival of ABC DLBCL cells critically depends on chronic BCR signaling, which originates from autoreactive BCRs or mutations in BCR proximal signaling components (eg, CD79), it has been assumed that the BCR-derived signal might represent the molecular basis for the nuclear localization of NFAT found in human biopsies.²² Intriguingly, our work clearly reveals that neither silencing of IgM

or CD79 nor inhibition of BCR associated kinases, such as BTK, SYK, or Src kinase family members, affected NFATc1/2 phosphorylation or localization to the nucleus. Accordingly, whereas SYK and Src kinase inhibitors efficiently abrogated the anti-IgM-induced calcium flux, they did not alter the increased basal calcium levels observed in DLBCL cell lines. These surprising findings suggest that NFAT is not activated by BCR signaling in DLBCL, and that future efforts are required to elucidate the molecular mechanism underlying constitutive NFAT activation. Interestingly, even though DLBCLs show only a moderate increase in intracellular calcium concentrations, this is sufficient to trigger a substantial translocation of NFATc1/2 to the nucleus. Although chronic BCR activation in DLBCL is not responsible for the increased calcium levels or NFATc1/2 dephosphorylation, it

still promotes NFAT signaling indirectly, by inducing transcription of *NFATC1*, but not *NFATC2*. *NFATC1* induction is driven by NF- κ B because an IKK inhibitor or expression of the I κ B super-repressor interfered with *NFATC1* expression.

We propose a model in which calcineurin inhibitors induce cytotoxicity in ABC DLBCL by preventing the NFAT-mediated expression of critical genes, including the STAT3 activators IL-6 and IL-10 and the AP-1 member c-Jun, which are crucial for the survival of ABC but not of GCB DLBCL cells.^{16,35} Reporter gene analyses revealed that NFATc1 can directly control the transcription of *IL10* and *JUN*, whereas *IL6* expression relied on the activity of both NFATc1 and c-Jun, suggesting that a previously described AP-1:NFAT complex is able to activate *IL6* transcription.^{38,43} Interestingly, our global gene expression profiling and gene set enrichment analysis suggested that expression of NF- κ B target genes, such as *IL10* and *JUN*, was particularly affected by calcineurin inhibition. This indicates that NFATc1/2 and NF- κ B synergize on the promoter of these pro-survival genes and thus orchestrate their expression in ABC DLBCL. Whereas general NF- κ B inhibitors have not made their way into clinical application because of their high toxicity, therapeutic inhibition of NFAT by calcineurin inhibitors has proven to be beneficial and comparably safe over the past decades. Both CsA and FK506 are potent immunosuppressive drugs that have been extensively used in patients receiving allogeneic transplants as well as in autoimmune diseases.⁴⁴ Repurposing of calcineurin inhibitors might represent therefore a promising strategy for ABC DLBCL treatment. It should not be ignored however that in simultaneous combination regimens immunosuppressive effects of calcineurin inhibitors might weaken the efficacy of immunotherapies with, for example, T-cell engagers or checkpoint inhibitors. Further studies are therefore needed to evaluate the therapeutic potential of sequential treatment regimes.

Roughly 40% to 80% of primary DLBCL samples exhibit high levels of BCL-2 expression, identifying this pro-survival protein as another promising target for the treatment of DLBCL patients.⁴⁵⁻⁴⁸ The BCL-2 inhibitor ABT-199 is highly selective and has shown very promising results in chronic lymphocytic leukemia.^{19,49} MCL-1, which is also overrepresented especially in the ABC DLBCL subtype, can overcome BCL-2 inhibition. Therefore, targeting of both proteins might represent an approach superior to monotherapy.^{41,42} Our data reveal that calcineurin inhibitors synergize with both the BCL-2 inhibitor ABT-199 and the MCL-1 inhibitor S63845, resulting in improved targeting of cells from the ABC DLBCL subtype. In conclusion, our results suggest that a combination of these drugs with calcineurin inhibitors could provide a promising therapeutic strategy for ABC DLBCL treatment.

REFERENCES

1. Nogai H, Dörken B, Lenz G. Pathogenesis of non-Hodgkin's lymphoma. *J Clin Oncol*. 2011; 29(14):1803-1811.
2. Swerdlow SH, Campo E, Pileri SA, et al. The 2016 revision of the World Health Organization classification of lymphoid neoplasms. *Blood*. 2016;127(20):2375-2390.
3. Gisselbrecht C, Glass B, Mounier N, et al. Salvage regimens with autologous transplantation for relapsed large B-cell lymphoma

in the rituximab era. *J Clin Oncol*. 2010;28(27): 4184-4190.

4. Alizadeh AA, Eisen MB, Davis RE, et al. Distinct types of diffuse large B-cell lymphoma identified by gene expression profiling. *Nature*. 2000;403(6769):503-511.
5. Lenz G, Wright G, Dave SS, et al; Lymphoma/Leukemia Molecular Profiling Project. Stromal gene signatures in large-B-cell lymphomas. *N Engl J Med*. 2008;359(22): 2313-2323.

6. Rosenwald A, Wright G, Chan WC, et al; Lymphoma/Leukemia Molecular Profiling Project. The use of molecular profiling to predict survival after chemotherapy for diffuse large-B-cell lymphoma. *N Engl J Med*. 2002; 346(25):1937-1947.

7. Wright G, Tan B, Rosenwald A, Hurt EH, Wiestner A, Staudt LM. A gene expression-based method to diagnose clinically distinct subgroups of diffuse large B cell lymphoma. *Proc Natl Acad Sci USA*. 2003;100(17): 9991-9996.

Acknowledgments

The authors thank Margot Thome for critical reading of the manuscript and for reagents.

This work was supported by the Collaborative Research Center Transregio SFB/TR 156 (S.H. and D.K.), SFB/TR 209 (K.S.-O. and S.H.), the Emmy-Noether program of the DFG and the DFG under Germany's Excellence Strategy EXC2180 (S.H.), the Deutsche Krebshilfe (G.L. and S.H.), the Ministry of Health of the Czech Republic (grant NV19-08-00144) (P.K.), and the Charles University Center of Excellence (UNCE/MED/016) (P.K.).

Authorship

Contribution: P.B., T.E., C.S., P.G., W.X., A.S., P.K., and C.S. performed experiments; P.B., T.E., E.S., D.K., M.Z., M.G., K.S.-O., C.L., P.K., G.L., and S.H. analyzed data; P.B., G.L., and S.H. wrote the manuscript, which all other authors commented on; and G.L. and S.H. conceived and coordinated the study.

Conflict-of-interest disclosure: G.L. has received honoraria from Bayer, AstraZeneca, NanoString, Celgene, Gilead, Janssen, and Roche; has participated in a consulting or advisory role for AstraZeneca, Bayer, Celgene, Gilead, Janssen, NanoString, and Roche; has been on a speaker's bureau for Bayer, Celgene, Gilead, Janssen, and Roche; has received research funding from AQUINOX, AstraZeneca, Bayer, Celgene, Gilead, Janssen, and Roche; and has had travel, accommodation, and expenses reimbursed by Bayer, Celgene, Gilead, Janssen, Roche, and Verastem. The remaining authors declare no competing financial interests.

ORCID profiles: P.B., 0000-0001-7951-1580; P.G., 0000-0002-2938-9975; A.S., 0000-0003-0219-4454; D.K., 0000-0002-3451-6182; P.K., 0000-0001-7786-9378; C.L., 0000-0001-5442-2805; S.H., 0000-0003-0276-2263.

Correspondence: Stephan Hailfinger, Interfaculty Institute for Biochemistry, University of Tübingen, Hoppe-Seyler-Str 4, D-72076 Tübingen, Germany; e-mail: stephan.hailfinger@uni-tuebingen.de.

Footnotes

Submitted 3 June 2019; accepted 7 November 2019. Prepublished online as *Blood* First Edition paper, 3 December 2019; DOI 10.1182/blood.2019001866.

The gene expression data are available from the Gene Expression Omnibus of the National Center for Biotechnology Information (www.ncbi.nlm.nih.gov/geo) through GEO accession number GSE140882.

The online version of this article contains a data supplement.

There is a *Blood* Commentary on this article in this issue.

The publication costs of this article were defrayed in part by page charge payment. Therefore, and solely to indicate this fact, this article is hereby marked "advertisement" in accordance with 18 USC section 1734.

8. Havranek O, Xu J, Köhrer S, et al. Tonic B-cell receptor signaling in diffuse large B-cell lymphoma. *Blood*. 2017;130(8):995-1006.
9. Lenz G, Staudt LM. Aggressive lymphomas. *N Engl J Med*. 2010;362(15):1417-1429.
10. Grondona P, Bucher P, Schulze-Osthoff K, Hailfinger S, Schmitt A. NF- κ B activation in lymphoid malignancies: genetics, signaling, and targeted therapy. *Biomedicines*. 2018; 6(2):E38.
11. Young RM, Wu T, Schmitz R, et al. Survival of human lymphoma cells requires B-cell receptor engagement by self-antigens. *Proc Natl Acad Sci USA*. 2015;112(44): 13447-13454.
12. Davis RE, Brown KD, Siebenlist U, Staudt LM. Constitutive nuclear factor kappaB activity is required for survival of activated B cell-like diffuse large B cell lymphoma cells. *J Exp Med*. 2001;194(12):1861-1874.
13. Compagno M, Lim WK, Grunn A, et al. Mutations of multiple genes cause deregulation of NF-kappaB in diffuse large B-cell lymphoma. *Nature*. 2009;459(7247):717-721.
14. Davis RE, Ngo VN, Lenz G, et al. Chronic active B-cell-receptor signalling in diffuse large B-cell lymphoma. *Nature*. 2010; 463(7277):88-92.
15. Lenz G, Davis RE, Ngo VN, et al. Oncogenic CARD11 mutations in human diffuse large B cell lymphoma. *Science*. 2008;319(5870): 1676-1679.
16. Juillard M, Gonzalez M, Erdmann T, et al. CARMA1- and MyD88-dependent activation of Jun/ATF-type AP-1 complexes is a hallmark of ABC diffuse large B-cell lymphomas. *Blood*. 2016;127(14):1780-1789.
17. Knies N, Alankus B, Weilemann A, et al. Lymphomagenic CARD11/BCL10/MALT1 signaling drives malignant B-cell proliferation via cooperative NF- κ B and JNK activation. *Proc Natl Acad Sci USA*. 2015;112(52): E7230-E7238.
18. Lopez-Bergami P, Lau E, Ronai Z. Emerging roles of ATF2 and the dynamic AP1 network in cancer [published correction appears in *Nat Rev Cancer*. 2010;10(5):379]. *Nat Rev Cancer*. 2010;10(1):65-76.
19. Souers AJ, Levenson JD, Boghaert ER, et al. ABT-199, a potent and selective BCL-2 inhibitor, achieves antitumor activity while sparing platelets. *Nat Med*. 2013;19(2): 202-208.
20. Blonska M, Zhu Y, Chuang HH, et al. Jun-regulated genes promote interaction of diffuse large B-cell lymphoma with the micro-environment. *Blood*. 2015;125(6):981-991.
21. Fu L, Lin-Lee YC, Pham LV, Tamayo A, Yoshimura L, Ford RJ. Constitutive NF-kappaB and NFAT activation leads to stimulation of the BLYS survival pathway in aggressive B-cell lymphomas. *Blood*. 2006;107(11):4540-4548.
22. Li L, Zhang J, Chen J, et al. B-cell receptor-mediated NFATc1 activation induces IL-10/STAT3/PD-L1 signaling in diffuse large B-cell lymphoma. *Blood*. 2018;132(17):1805-1817.
23. Marafioti T, Pozzobon M, Hansmann ML, et al. The NFATc1 transcription factor is widely expressed in white cells and translocates from the cytoplasm to the nucleus in a subset of human lymphomas. *Br J Haematol*. 2005; 128(3):333-342.
24. Pham LV, Tamayo AT, Li C, Bueso-Ramos C, Ford RJ. An epigenetic chromatin remodeling role for NFATc1 in transcriptional regulation of growth and survival genes in diffuse large B-cell lymphomas. *Blood*. 2010;116(19): 3899-3906.
25. Pham LV, Tamayo AT, Yoshimura LC, Lin-Lee YC, Ford RJ. Constitutive NF-kappaB and NFAT activation in aggressive B-cell lymphomas synergistically activates the CD154 gene and maintains lymphoma cell survival. *Blood*. 2005;106(12):3940-3947.
26. Mancini M, Toker A. NFAT proteins: emerging roles in cancer progression. *Nat Rev Cancer*. 2009;9(11):810-820.
27. Müller MR, Rao A. NFAT, immunity and cancer: a transcription factor comes of age. *Nat Rev Immunol*. 2010;10(9):645-656.
28. Rahal R, Frick M, Romero R, et al. Pharmacological and genomic profiling identifies NF- κ B-targeted treatment strategies for mantle cell lymphoma. *Nat Med*. 2014;20(1):87-92.
29. Pan Z, Choi S, Luo Y. Mn²⁺ quenching assay for store-operated calcium entry. *Methods Mol Biol*. 2018;1843:55-62.
30. Rao A, Luo C, Hogan PG. Transcription factors of the NFAT family: regulation and function. *Annu Rev Immunol*. 1997;15(1):707-747.
31. Muhammad K, Alrefai H, Marienfeld R, et al. NF- κ B factors control the induction of NFATc1 in B lymphocytes. *Eur J Immunol*. 2014;44(11): 3392-3402.
32. Chuvpilo S, Jankevics E, Tyrns D, et al. Autoregulation of NFATc1/A expression facilitates effector T cells to escape from rapid apoptosis. *Immunity*. 2002;16(6):881-895.
33. Erdmann T, Klener P, Lynch JT, et al. Sensitivity to PI3K and AKT inhibitors is mediated by divergent molecular mechanisms in subtypes of DLBCL. *Blood*. 2017;130(3): 310-322.
34. Lam LT, Davis RE, Pierce J, et al. Small molecule inhibitors of I κ B kinase are selectively toxic for subgroups of diffuse large B-cell lymphoma defined by gene expression profiling. *Clin Cancer Res*. 2005;11(1):28-40.
35. Lam LT, Wright G, Davis RE, et al. Cooperative signaling through the signal transducer and activator of transcription 3 and nuclear factor-kappaB pathways in subtypes of diffuse large B-cell lymphoma. *Blood*. 2008;111(7): 3701-3713.
36. Nicholson SE, Hilton DJ. The SOCS proteins: a new family of negative regulators of signal transduction. *J Leukoc Biol*. 1998;63(6): 665-668.
37. Saraiva M, O'Garra A. The regulation of IL-10 production by immune cells. *Nat Rev Immunol*. 2010;10(3):170-181.
38. Macián F, López-Rodríguez C, Rao A. Partners in transcription: NFAT and AP-1. *Oncogene*. 2001;20(19):2476-2489.
39. Davids MS, Roberts AW, Seymour JF, et al. Phase I first-in-human study of venetoclax in patients with relapsed or refractory non-Hodgkin lymphoma. *J Clin Oncol*. 2017;35(8): 826-833.
40. Zelenetz AD, Salles G, Mason KD, et al. Venetoclax plus R- or G-CHOP in non-Hodgkin lymphoma: results from the CAVALLI phase 1b trial. *Blood*. 2019;133(18): 1964-1976.
41. Wenzel SS, Grau M, Mavis C, et al. MCL1 is deregulated in subgroups of diffuse large B-cell lymphoma. *Leukemia*. 2013;27(6): 1381-1390.
42. Li L, Pongtompipat P, Titaan T, et al. Synergistic induction of apoptosis in high-risk DLBCL by BCL2 inhibition with ABT-199 combined with pharmacologic loss of MCL1. *Leukemia*. 2015;29(8):1702-1712.
43. Chen L, Glover JN, Hogan PG, Rao A, Harrison SC. Structure of the DNA-binding domains from NFAT, Fos and Jun bound specifically to DNA. *Nature*. 1998;392(6671):42-48.
44. Azzi JR, Sayegh MH, Mallat SG. Calcineurin inhibitors: 40 years later, can't live without. *J Immunol*. 2013;191(12):5785-5791.
45. Green TM, Young KH, Visco C, et al. Immunohistochemical double-hit score is a strong predictor of outcome in patients with diffuse large B-cell lymphoma treated with rituximab plus cyclophosphamide, doxorubicin, vincristine, and prednisone. *J Clin Oncol*. 2012;30(28):3460-3467.
46. Hu S, Xu-Monette ZY, Tzankov A, et al. MYC/BCL2 protein coexpression contributes to the inferior survival of activated B-cell subtype of diffuse large B-cell lymphoma and demonstrates high-risk gene expression signatures: a report from The International DLBCL Rituximab-CHOP Consortium Program. *Blood*. 2013;121(20):4021-4031, quiz 4250.
47. Johnson NA, Slack GW, Savage KJ, et al. Concurrent expression of MYC and BCL2 in diffuse large B-cell lymphoma treated with rituximab plus cyclophosphamide, doxorubicin, vincristine, and prednisone. *J Clin Oncol*. 2012;30(28):3452-3459.
48. Tsuyama N, Sakata S, Baba S, et al. BCL2 expression in DLBCL: reappraisal of immunohistochemistry with new criteria for therapeutic biomarker evaluation. *Blood*. 2017; 130(4):489-500.
49. Roberts AW, Davids MS, Pagel JM, et al. Targeting BCL2 with venetoclax in relapsed chronic lymphocytic leukemia. *N Engl J Med*. 2016;374(4):311-322.

Targeting chronic NFAT activation with calcineurin inhibitors in diffuse large B-cell lymphoma

Supplemental Material and Methods

Cell culture, lentiviral and retroviral transduction, survival assay

GCB and ABC DLBCL cell lines were cultured in RPMI-1640 supplemented with 10 % and 20 % fetal calf serum (FCS), respectively. OCI-Ly10 cells were cultured in Iscove's modified Dulbecco's medium supplemented with 20 % human plasma. Ramos and Jurkat cell lines were cultured in RPMI-1640 supplemented with 10 % FCS. HEK293T cells were cultured in DMEM and 10 % FCS. All cells were maintained at 37°C and 5 % CO₂. Inhibitors were used at the following concentrations if not otherwise indicated: AZD8835 (4 μM; Selleckchem), BMS-345541 (10 μM; Selleckchem), CsA (600 nM; Selleckchem), EGTA (1 mM; Merck), FK506 (600 nM; Selleckchem), GS-9973 (4 μM; Selleckchem), ibrutinib (1 μM; Selleckchem), R406 (4 μM; Selleckchem), saracatinib (4 μM; Selleckchem). DLBCL cell lines were stimulated with anti-IgM (20 μg/ml; Invitrogen), rhIL-6 (10 ng/ml; R&D Systems), rhIL-10 (10 ng/ml; Immunotools), PMA (10 ng/ml; Merck) or ionomycin (0.5 μM; Cayman). ABT-199 and S63845 were purchased from Cayman Chemicals or Selleckchem, respectively.

Retroviral transduction and subsequent determination of cytotoxicity in the transduced cells were performed as previously described.¹⁻⁵ GCB and ABC DLBCL cell lines were lentivirally transduced for shRNA mediated knock-down. The clone IDs of the pLKO.1 plasmids including the respective shRNA sequences are listed in Supplemental Table 1 and were obtained from BCCM/GeneCorner DNA libraries. Electroporation of ON-TARGETplus siRNA was performed with the Neon® Transfection System (Thermo

Fisher Scientific) according to the supplied protocol. Non-targeting control siRNAs were used as control. The DN-I κ B α expression construct was kindly provided by Margot Thome (University of Lausanne, Switzerland).

For survival assays, cells were seeded with 200.000 cells/ml. Every second day cells were counted, split and treated again with inhibitors or solvent control. Synergism was obtained by five-day treatment with the respective inhibitor combination for 5000 cells/well, cell quantification was performed via MTS assay (Promega). The Combination Index (CI) was calculated with the CompuSyn software.⁶

Nuclear fractionation

Nuclear fractionation was performed using the Nuclear Extract Kit from Active Motive according to the supplied protocol. Lamin A/C and GAPDH were used as nuclear and cytosolic markers, respectively.

Gene expression profiling and GSEA

Gene expression profiling was performed in HBL-1 cells after 12, 24, 36 and 48 h treatment with 600 nM CsA cells as described.^{1,2} Briefly, total RNA was isolated using the NucleoSpin RNA II Kit (Macherey & Nagel) following the manufacturer's protocol. RNA was amplified and labeled with the TotalPrep RNA Amplification Kit (Thermo Fisher Scientific) and labeled samples were hybridized on HumanHT-12 v4 Expression BeadChips (Illumina) according to the manufacturer's protocol. A one-tailed paired t-test was used over all time points to calculate p-values for every gene based on all microarray pairs. To analyze in an unbiased fashion which biological processes were affected by CsA, we performed gene set enrichment analysis (GSEA) [A] using an integrated database of 17.315 gene expression signatures, comprised of signatures

with at least 5 genes from the Molecular Signatures Database v5.1, the GeneSigDB v4, HGCN gene families and the Staudt laboratory library [B-E]. GSEA p-values were computed by permutation tests and FDRs were computed relative to respective signature families. The gene expression data are available from the Gene Expression Omnibus of the National Center for Biotechnology Information (www.ncbi.nlm.nih.gov/geo) through GEO accession number GSE140882.

Dual Luciferase Reporter Assay

Dual Luciferase was performed as described in Dual-Glo® Luciferase Assay System Kit provided by Promega. The NF- κ B, NFAT and *IL6* reporter constructs were kindly provided by Margot Thome (University of Lausanne, Switzerland), Edgar Serfling (University of Würzburg, Germany) and the BCCM (LMBP 4495), respectively. The distal and proximal IL10 promoters were amplified using standard PCR and cloned into the pGL3-basic reporter plasmid (Promega).

Cell death analysis

Cells were incubated with AnnexinV-FITC (Biolegend) for 15 min in the dark followed by flow cytometric analysis. Quantification of cell death was performed using the Caspase-Glo 3/7 Assay Kit (Promega) according to manufacturer's instructions.

Calcium measurement and quenching assay

Calcium levels were measured with the fluorophore Calbryte™ 520 AM (2.5 ng/ μ l, AAT Bioquest). Cells were incubated for one hour with the dye and measured using flow cytometry (BD LSRII) or a fluorescence plate reader (Tecan Infinity 200). Calcium quenching assay was performed using the calcium sensor Fura-2 AM (Invitrogen) as

described.^{7,8} Briefly, 50.000 cells/well were seeded and stained for 30 min with 5 ng/ μ l Fura-2. After removing the dye, cells rested for 30 min at 37°C. For Fura-2 quenching, 10 mM MnCl₂ was added to the medium and Fura-2 emission was measured at 340 nm over time.

Quantitative RT-PCR

Whole-cell RNA was isolated using the Qiagen RNA mini kit according to manufacturer's instructions. Reverse transcription was performed the Biozym cDNA Synthesis Kit with random hexamers primers. RT-PCR was performed using SYBR Fast qPCR master mix (Genaxxon). Relative mRNA levels were normalized to the reference gene SDHA using the $2^{-\Delta\Delta CT}$ method.

Adhesion assay

Cells were grown in RPMI-1640 supplemented with 30% FCS three days prior to the experiments.⁹ 96-well plates were coated for 90 min at RT with 40 μ g/ml fibronectin (Merck) diluted in PBS followed by 60 min blocking with 1% BSA in PBS at RT. Cells were seeded after treatment for 2 h in the plates and non-adherent cells were washed off afterwards. Cell quantification was performed via MTS assay. For negative control fibronectin was replaced by BSA.

In vivo xenograft mouse studies

For *in vivo* testing of TMD8 xenograft mouse models, NOD.Cg-Rag1 mice were used. TMD8 cells (1×10^7 cells in PBS mixed 50:50 with Matrigel™ (BD)) were implanted subcutaneously into the flank of the mice. Once tumors reached approximately 150-200 mm³, animals were randomized into control or FK506 treated groups. Mice were treated i.p. for five consecutive days with 4 mg/kg FK506 (MedChemExpress) solved

in DMSO/corn oil (Sigma-Aldrich) or solvent. The tumor volume was measured daily with a caliper and calculated with $V = 1/2 \times (\text{length} \times \text{width}^2)$. The animal experiment was approved by the institutional Animal Welfare Committee (Czech Republic, Approval MSMT-32441/2018-5). Significance was calculated with a one-tailed two-sample t-test.

Chromatin Immunoprecipitation (ChIP).

ChIP was basically performed as already described.¹⁰ In brief, HBL-1 cells were treated for 4 h with CsA, before cells were crosslinked with 1% PFA for 10 min. After sonication for 2 x 10 min using the Bioruptor (Diagenode), chromatin from approx. 3.6×10^7 cells was incubated with protein G-coupled Dynabeads and 4 μg NFATc1 antibody (A303-508A, Bethyl) or IgG as control (PP64B, EMD Millipore) overnight at 4°C. After intensive washing, decrosslinking and purification, ChIP samples were analyzed using the Maxima Mastermix (K0221, Thermo Fisher) and the following self-designed primers. The promoter region of *MYOD* served as an internal negative control.

ChIP hIL10_F	TTGAGGTTGCAGTTTCGTTG
ChIP hIL10_R	ACCAAGTGGAGGCTCTTCTG
ChIP hJUN_F	GGCTGAGAATCCAAGTACGC
ChIP hJUN_R	CTTGACCGAGATGCAAACCTTC
ChIP hIL6_F	AAATGCCCAACAGAGGTCAC
ChIP hIL6_R	AAACCAGACCCTTGCACAAC
ChIP hMyoD_F	CTCTGCTCCTTTGCCACAAC
ChIP hMyoD_R	GAGTGCTCTTCGGGTTTCAG

Zebrafish husbandry and yolk sac transplantation

Zebrafish from the Tuebingen strain were maintained as described by Nüsslein-Volhard and Dahm¹¹ in accordance with the guidelines of the veterinary office of the city of Basel (“Kantonales Veterinäramt Basel-Stadt”).

TMD8 cells were stained using CellTracker™ CM-Dil Dye according to the manufacturer’s protocol (Thermo Fisher Scientific) and transplanted into the yolk of wild-type embryos 2 days post fertilization (100 cells per embryo). One hour post transplantation, embryos were screened for fluorescence to identify successfully transplanted animals, which were then transferred to E3-medium containing FK506 (1 μ M), CsA (1 μ M), ABT-199 (1 μ M) or CsA + ABT-199, respectively. After three days of incubation at 33°C, TMD8 tumor formation was assessed by fluorescent confocal microscopy (SP5-II-MATRIX, 10x objective, Leica Microsystems). Fiji package of ImageJ was used for image analysis.¹²

Western blotting and antibodies

Primary antibodies are summarized in Supplemental Table 2. Western Blots were developed as previously described.¹³

References

1. Dai B, Grau M, Juilland M, et al. B-cell receptor-driven MALT1 activity regulates MYC signaling in mantle cell lymphoma. *Blood*. 2017;129(3):333-346.
2. Erdmann T, Klener P, Lynch JT, et al. Sensitivity to PI3K and AKT inhibitors is mediated by divergent molecular mechanisms in subtypes of DLBCL. *Blood*. 2017;130(3):310-322.
3. Ngo VN, Davis RE, Lamy L, et al. A loss-of-function RNA interference screen for molecular targets in cancer. *Nature*. 2006;441(7089):106-110.
4. Nogai H, Wenzel SS, Hailfinger S, et al. IkappaB-zeta controls the constitutive NF-kappaB target gene network and survival of ABC DLBCL. *Blood*. 2013;122(13):2242-2250.
5. Pfeifer M, Grau M, Lenze D, et al. PTEN loss defines a PI3K/AKT pathway-dependent germinal center subtype of diffuse large B-cell lymphoma. *Proc Natl Acad Sci U S A*. 2013;110(30):12420-12425.
6. Chou TC. Theoretical basis, experimental design, and computerized simulation of synergism and antagonism in drug combination studies. *Pharmacol Rev*. 2006;58(3):621-681.
7. Hallam TJ, Rink TJ. Agonists stimulate divalent cation channels in the plasma membrane of human platelets. *FEBS Lett*. 1985;186(2):175-179.
8. Merritt JE, Jacob R, Hallam TJ. Use of manganese to discriminate between calcium influx and mobilization from internal stores in stimulated human neutrophils. *J Biol Chem*. 1989;264(3):1522-1527.
9. Blonska M, Zhu Y, Chuang HH, et al. Jun-regulated genes promote interaction of diffuse large B-cell lymphoma with the microenvironment. *Blood*. 2015;125(6):981-991.
10. Nemajerova A, Kramer D, Siller SS, et al. TAp73 is a central transcriptional regulator of airway multiciliogenesis. *Genes Dev*. 2016;30(11):1300-1312.
11. Nüsslein-Volhard C, Dahm R. Zebrafish : a practical approach (ed 1st). Oxford: Oxford University Press; 2002.
12. Schindelin J, Arganda-Carreras I, Frise E, et al. Fiji: an open-source platform for biological-image analysis. *Nat Methods*. 2012;9(7):676-682.
13. Schmitt A, Grondona P, Maier T, et al. MALT1 Protease Activity Controls the Expression of Inflammatory Genes in Keratinocytes upon Zymosan Stimulation. *J Invest Dermatol*. 2016;136(4):788-797.

Supplemental Figures

Supplemental Figure 1. Calcineurin expression in DLBCL.

The protein expression levels of phosphorylated STAT3, c-Jun, the catalytic (CnA) and the regulatory (CnB) calcineurin subunit in various DLBCL cell lines were visualized by Western blot analysis. Tubulin serves as loading control.

Supplemental Figure 2. NFAT is constitutively activated in DLBCL.

A) Intracellular calcium levels of the indicated cell lines were visualized with Calbryte 520AM and measured using a plate reader. **B)** The permeability of cation channels at the plasma membrane was analyzed by a Fura-2 quenching assay. Fura-2 excitation was normalized to the fluorescence of each individual cell line before $MnCl_2$ was added. **C, D)** The GCB DLBCL cell lines OCI-Ly7 and OCI-Ly19 (**C**) or the indicated MCL cell lines (**D**) were treated with solvent, CsA or FK506 to assess the phosphorylation status of NFATc1 and NFATc2 by Western blotting. **E)** The indicated ABC DLBCL cell lines were kept for 4 h in calcium-free and/or in FCS-free medium as indicated. NFATc1/2 phosphorylation status was visualized by Western blot analysis. **F)** Cytosolic (C) and nuclear (N) fractions were prepared from solvent- or FK506-treated DLBCL cell lines and analyzed nuclear translocation of NFATc1/2 by Western blotting. Lamin A/C or GAPDH serve as markers for the nuclear or cytoplasmic fractions, respectively.

Supplemental Figure 3. BCR-mediated signals are not responsible for NFAT activation.

A) Quantification of intracellular calcium levels in the presence of the PI3K inhibitor AZD8835, the SYK inhibitor GS-9973 or the BTK inhibitor ibrutinib. HBL-1 cells were

stimulated with an agonistic anti-IgM antibody, prior to analyzing the intensity of the calcium sensor Calbryte 520 by flow cytometry over time. **B,C**) Cytoplasmic (C) and nuclear (N) fractions were prepared from ABC DLBCL (**B**) or GCB DLBCL (**C**) cell lines treated with solvent or the SYK inhibitor R406. NFATc1/2 localization was visualized by Western blotting. Lamin A/C and GAPDH serve as nuclear and cytoplasmic markers, respectively. **D**) Localization of NFATc1/2 in solvent- or saracatinib-treated DLBCL cell lines was visualized by Western blot analysis. Decrease of P-PLC γ in ABC DLBCL cells confirmed efficacy of the Src inhibitor. **E**) HBL-1 were treated with solvent or the indicated inhibitors for 24 h and NFATc1/2 localization was assessed by immunoblotting. **F**) Densitometric quantification refers to Figure 3F. The ABC DLBCL cell lines were treated with solvent or the indicated inhibitors for 24 h, before NFATc1/2 levels were visualized by immunoblotting. The intensity of NFATc1 signals of three independent experiments were quantified with ImageJ and normalized to GAPDH. **G**) Total NFATc1 protein expression levels were analyzed by Western blotting in the indicated cell lines. **H**) HBL-1 cells were transfected with scrambled or siRNA targeting IgM. NFATc1/2 expression was analyzed 48 h after transfection by immunoblotting. **I**) Control or CD79A-targeting shRNA were lentivirally transduced in HBL-1 cells and NFATc1 protein levels were visualized by Western blot analysis. **J**) BJAB cells were electroporated with a RelA expression construct or empty vector control, together with luciferase-based reporter plasmids containing the distal (P1) or the proximal (P2) *NFATC1* promoter. Luciferase activity was measured 36 h after transfection and normalized to the empty vector control.

Supplemental Figure 4. Identification and validation of NFAT target genes in ABC DLBCL.

A) HBL-1 cells were treated for the indicated times with CsA or FK506 and analyzed for changes in their global gene expression. Immunoblot analysis validated the efficacy of the calcineurin inhibitors. **B)** Gene set enrichment analysis identified an AZD8835 and an NF- κ B gene set regulated upon calcineurin inhibition. **C)** U2932 were transfected with a RelA expression construct or empty vector control together with an NF- κ B reporter plasmid. 24 h after transfection, cells were treated with CsA, FK506 or the solvent DMSO. Luciferase activity was quantified after 8 h of treatment and normalized to the solvent control. **D)** *EGR2*, *SOCS3* and *JUNB* mRNA expression were measured by qPCR in the indicated ABC DLBCL cell lines. **E)** HBL-1 cells were treated with solvent, CsA or FK506 and mRNA levels of the indicated genes was quantified by qPCR analysis. **F)** IL-6 and IL-10 protein levels were quantified in the medium of solvent- or FK506-treated ABC DLBCL cell lines by ELISA and normalized to the DMSO control. Statistical significance was calculated using t-test (* $p < 0.05$, ** $p < 0.01$, *** $p < 0.001$).

Supplemental Figure 5. Overlap of NFAT target genes between ABC and GCB DLBCL.

A) HT cells were treated for the indicated times with CsA and analyzed for changes in their global gene expression. Immunoblot analysis validated the efficacy of the calcineurin inhibitor. **B)** Overlap of the top-regulated genes upon CsA treatment between the ABC DLBCL cell line HBL-1 and the GCB DLBCL cell line HT.

Supplemental Figure 6. Regulation of IL-6, IL-10 and c-Jun by NFAT.

A,B) Densitometric quantification referring to Figure 4F. The indicated ABC DLBCL cell lines were treated for 48 h with solvent, CsA or FK506 and cell lysates were analyzed by immunoblotting. The P-STAT3 (**A**) or c-Jun (**B**) protein levels of three independent experiments were quantified with ImageJ and normalized to Tubulin. **C)** TMD8 cells were treated with solvent or the calcineurin inhibitors for 48 h and subsequently incubated with phorbol 12-myristate 13-acetate (PMA) for 6 h. c-Jun levels were assessed by immunoblotting. **D)** The ABC DLBCL cell lines TMD8 and HBL-1 were treated every second day with CsA and/or IL-6/IL-10 as indicated. Treated cells were counted and normalized to the solvent controls. **E)** HEK293T cells were transfected with an *IL6* reporter constructs in combination with c-Jun and NFATc2 as indicated. Luciferase activity was measured 24 h after transfection and normalized to the empty vector control. Statistical significance was calculated using t-test (* $p < 0.05$, ** $p < 0.01$, *** $p < 0.001$).

Supplemental Figure 7. NFATc1 silencing is toxic for calcineurin inhibitor sensitive ABC DLBCL cells.

A) *IL10* and *JUN* mRNA expression of control, NFATc1- or NFATc2-silenced HBL-1 cells was quantified by qPCR. **B)** Visualization of the efficacy of NFATc1 silencing using two independent NFATc1-specific shRNAs by immunoblotting. **C)** After transduction of non-targeting (Co) or NFATc1-specific shRNAs, the growth of the indicated DLBCL cell lines was quantified and normalized to the controls. **D,E)** The effect of CARD11^{L244P} expression on the sensitivity of OCI-Ly10 towards CsA and FK506 was investigated. c-Jun and P-STAT3 levels were analyzed by immunoblotting (**D**), the survival of the CsA or FK506 treated cells is depicted in a diagram (**E**). Statistical significance was calculated using t-test (* $p < 0.05$, ** $p < 0.01$, *** $p < 0.001$).

Supplemental Figure 8. BCL-2 or MCL-1 inhibition synergizes with calcineurin blockade.

A) The ABC DLBCL cell lines TMD8 or OCI-Ly3 were treated either with ABT-199 alone (left) or together with CsA (right) as indicated. **B)** TMD8 or OCI-Ly3 cells were incubated either with the MCL-1 inhibitor S63845 alone (left) or together with CsA (right) as indicated. Cells were treated once with the respective inhibitors and survival was quantified by an MTS assay. Data represent the mean \pm SD from at least three independent experiments.

Supplemental Table 1: Sequences of utilized shRNAs or siRNA.

Target protein	Sequence	Type	Clone ID
NFATc1#1	CGGAATCCTGAAACTCAGAAA	shRNA	TRCN0000017337
NFATc1#2	CGTCAGTTTCTACGTCTGCAA	shRNA	TRCN0000017335
NFATc2	GTGAACTTCTACGTCATCAAT	shRNA	TRCN0000016147
c-Jun	CCAGCGTATCTATATGGAATT	shRNA	TRCN0000039588
CD79A	ACTTCCAATGCCCGCACAATA	shRNA	TRCN0000057514
CD79B	ACAGCCACCTATGAGGACATA	shRNA	TRCN0000057651
IgM	ACCAGAGAGAGGAACUCAAG	siRNA	

Supplemental Table 2: Western blot antibodies.

Antibody	Source	Provider	Order No.
Calcineurin A	Rabbit polyclonal	Cell Signaling	#2614
Calcineurin B	Rabbit polyclonal	Abcam	ab154650
c-JUN	Rabbit monoclonal	Cell Signaling	#9165
ERK-1/2	Mouse monoclonal	Santa Cruz	sc-514302
Flag	Mouse monoclonal	Sigma	F3165
GAPDH	Rabbit monoclonal	Cell Signaling	#2118
IgM	Mouse monoclonal	Santa Cruz	sc-53347
IκBα	Mouse monoclonal	Cell Signaling	#4814
JunB	Rabbit monoclonal	Cell Signaling	#3753
JunD	Rabbit monoclonal	Cell Signaling	#5000
Lamin A/C	Rabbit polyclonal	Cell Signaling	#2032
NFATc1	Mouse monoclonal	Santa Cruz	sc-7294
NFATc2	Mouse monoclonal	Santa Cruz	sc-7296
P-AKT (Ser473)	Rabbit monoclonal	Cell Signaling	#4060
P-BLNK (Tyr96)	Rabbit polyclonal	Cell Signaling	#3601
P-ERK1/2	Mouse monoclonal	Santa Cruz	sc-7383
P-PLCγ2 (Tyr1217)	Rabbit monoclonal	Cell Signaling	#3871
P-STAT3 (Tyr705)	Rabbit polyclonal	Cell Signaling	#9145
STAT3	Mouse monoclonal	Cell Signaling	#9139
Tubulin	Mouse monoclonal	Sigma	T9026

Supplemental Table 3: Down- and upregulated genes following CsA treatment in HBL-1 cells.

Signature name	Gene symbol	Gene ID	Gene description
Down ($\alpha=0.001$)	ABTB2	25841	ankyrin repeat and BTB domain containing 2
Down ($\alpha=0.001$)	ACPP	55	acid phosphatase, prostate
Down ($\alpha=0.001$)	ADAP2	55803	ArfGAP with dual PH domains 2
Down ($\alpha=0.001$)	ANKRD16	54522	ankyrin repeat domain 16
Down ($\alpha=0.001$)	ARL4A	10124	ADP ribosylation factor like GTPase 4A
Down ($\alpha=0.001$)	BATF	10538	basic leucine zipper ATF-like transcription factor
Down ($\alpha=0.001$)	BSPRY	54836	B-box and SPRY domain containing
Down ($\alpha=0.001$)	C10orf10	11067	chromosome 10 open reading frame 10
Down ($\alpha=0.001$)	C15orf59	388135	chromosome 15 open reading frame 59
Down ($\alpha=0.001$)	C1orf186	440712	chromosome 1 open reading frame 186
Down ($\alpha=0.001$)	CCDC155	147872	coiled-coil domain containing 155
Down ($\alpha=0.001$)	CCHCR1	54535	coiled-coil alpha-helical rod protein 1
Down ($\alpha=0.001$)	CCL4L1	9560	C-C motif chemokine ligand 4 like 2
Down ($\alpha=0.001$)	CCL4L2	388372	C-C motif chemokine ligand 4 like 1
Down ($\alpha=0.001$)	CD36	948	CD36 molecule
Down ($\alpha=0.001$)	CDK5R1	8851	cyclin dependent kinase 5 regulatory subunit 1
Down ($\alpha=0.001$)	CKB	1152	creatine kinase B
Down ($\alpha=0.001$)	CLDN23	137075	claudin 23
Down ($\alpha=0.001$)	CLEC17A	388512	C-type lectin domain family 17 member A
Down ($\alpha=0.001$)	COL9A3	1299	collagen type IX alpha 3 chain
Down ($\alpha=0.001$)	CTSL2	1515	cathepsin V
Down ($\alpha=0.001$)	DACT3	147906	dishevelled binding antagonist of beta catenin 3
Down ($\alpha=0.001$)	DDX49	54555	DEAD-box helicase 49
Down ($\alpha=0.001$)	DHRS3	9249	dehydrogenase/reductase 3
Down ($\alpha=0.001$)	DLX2	1746	distal-less homeobox 2
Down ($\alpha=0.001$)	EPHB1	2047	EPH receptor B1
Down ($\alpha=0.001$)	ERCC6L2	375748	ERCC excision repair 6 like 2
Down ($\alpha=0.001$)	EVI2A	2123	ecotropic viral integration site 2A
Down ($\alpha=0.001$)	FABP5	2171	fatty acid binding protein 5
Down ($\alpha=0.001$)	FAM136BP	387071	family with sequence similarity 136, member B, pseudogene
Down ($\alpha=0.001$)	FEN1	2237	flap structure-specific endonuclease 1
Down ($\alpha=0.001$)	FMOD	2331	fibromodulin
Down ($\alpha=0.001$)	GAS6	2621	growth arrest specific 6
Down ($\alpha=0.001$)	GATM	2628	glycine amidinotransferase
Down ($\alpha=0.001$)	GCSH	2653	glycine cleavage system protein H
Down ($\alpha=0.001$)	GNG10	2790	G protein subunit gamma 10
Down ($\alpha=0.001$)	GNG8	94235	G protein subunit gamma 8
Down ($\alpha=0.001$)	GPRC5C	55890	G protein-coupled receptor class C group 5 member C
Down ($\alpha=0.001$)	GPRIN1	114787	G protein regulated inducer of neurite outgrowth 1
Down ($\alpha=0.001$)	GZMB	3002	granzyme B
Down ($\alpha=0.001$)	GZMH	2999	granzyme H
Down ($\alpha=0.001$)	H3F3C	440093	H3 histone, family 3C
Down ($\alpha=0.001$)	HES6	55502	hes family bHLH transcription factor 6
Down ($\alpha=0.001$)	HIST2H3C	126961	histone cluster 2, H3c
Down ($\alpha=0.001$)	HLF	3131	HLF, PAR bZIP transcription factor
Down ($\alpha=0.001$)	IDO1	3620	indoleamine 2,3-dioxygenase 1
Down ($\alpha=0.001$)	IER5	51278	immediate early response 5

Down ($\alpha=0.001$)	IL411	259307	interleukin 4 induced 1
Down ($\alpha=0.001$)	IRF4	3662	interferon regulatory factor 4
Down ($\alpha=0.001$)	ITM2C	81618	integral membrane protein 2C
Down ($\alpha=0.001$)	JUN	3725	Jun proto-oncogene, AP-1 transcription factor subunit
Down ($\alpha=0.001$)	LBH	81606	limb bud and heart development
Down ($\alpha=0.001$)	LETM1	3954	leucine zipper and EF-hand containing transmembrane protein 1
Down ($\alpha=0.001$)	LILRA5	353514	leukocyte immunoglobulin like receptor A5
Down ($\alpha=0.001$)	LILRB4	11006	leukocyte immunoglobulin like receptor B4
Down ($\alpha=0.001$)	LINC00487	400941	long intergenic non-protein coding RNA 487
Down ($\alpha=0.001$)	LOC732360	732360	
Down ($\alpha=0.001$)	LSM11	134353	LSM11, U7 small nuclear RNA associated
Down ($\alpha=0.001$)	LYSMD2	256586	LysM domain containing 2
Down ($\alpha=0.001$)	MAP3K8	1326	mitogen-activated protein kinase kinase kinase 8
Down ($\alpha=0.001$)	MCM6	4175	minichromosome maintenance complex component 6
Down ($\alpha=0.001$)	MIR320C1	100302135	microRNA 320c-1
Down ($\alpha=0.001$)	MOCOS	55034	molybdenum cofactor sulfurase
Down ($\alpha=0.001$)	MT3	4504	metallothionein 3
Down ($\alpha=0.001$)	MUC1	4582	mucin 1, cell surface associated
Down ($\alpha=0.001$)	MVP	9961	major vault protein
Down ($\alpha=0.001$)	NFKBIA	4792	NFKB inhibitor alpha
Down ($\alpha=0.001$)	NXT1	29107	nuclear transport factor 2 like export factor 1
Down ($\alpha=0.001$)	P2RX1	5023	purinergic receptor P2X 1
Down ($\alpha=0.001$)	PAX9	5083	paired box 9
Down ($\alpha=0.001$)	POLD3	10714	DNA polymerase delta 3, accessory subunit
Down ($\alpha=0.001$)	POLR3B	55703	RNA polymerase III subunit B
Down ($\alpha=0.001$)	POLR3G	10622	RNA polymerase III subunit G
Down ($\alpha=0.001$)	PPAN	56342	peter pan homolog (Drosophila)
Down ($\alpha=0.001$)	PRF1	5551	perforin 1
Down ($\alpha=0.001$)	PTGER4	5734	prostaglandin E receptor 4
Down ($\alpha=0.001$)	RAB11FIP5	26056	RAB11 family interacting protein 5
Down ($\alpha=0.001$)	RASSF4	83937	Ras association domain family member 4
Down ($\alpha=0.001$)	RB1	5925	RB transcriptional corepressor 1
Down ($\alpha=0.001$)	RND1	27289	Rho family GTPase 1
Down ($\alpha=0.001$)	RNF183	138065	ring finger protein 183
Down ($\alpha=0.001$)	SLC12A8	84561	solute carrier family 12 member 8
Down ($\alpha=0.001$)	SLC39A6	25800	solute carrier family 39 member 6
Down ($\alpha=0.001$)	SOCS3	9021	suppressor of cytokine signaling 3
Down ($\alpha=0.001$)	SOD2	6648	superoxide dismutase 2, mitochondrial
Down ($\alpha=0.001$)	SPR	6697	sepiapterin reductase (7,8-dihydrobiopterin:NADP+ oxidoreductase)
Down ($\alpha=0.001$)	SRGN	5552	serglycin
Down ($\alpha=0.001$)	STAT3	6774	signal transducer and activator of transcription 3
Down ($\alpha=0.001$)	TFRC	7037	transferrin receptor
Down ($\alpha=0.001$)	TIAM1	7074	T-cell lymphoma invasion and metastasis 1
Down ($\alpha=0.001$)	TMEM184B	25829	transmembrane protein 184B
Down ($\alpha=0.001$)	TMEM54	113452	transmembrane protein 54
Down ($\alpha=0.001$)	TUBAP2	399942	tubulin alpha pseudogene 2
Down ($\alpha=0.001$)	TUBB6	84617	tubulin beta 6 class V
Down ($\alpha=0.001$)	TUBB7P	56604	tubulin beta 7 pseudogene
Down ($\alpha=0.001$)	TYMP	1890	thymidine phosphorylase
Down ($\alpha=0.001$)	UPK3A	7380	uroplakin 3A
Down ($\alpha=0.001$)	VASH2	79805	vasohibin 2
Down ($\alpha=0.001$)	WARS	7453	tryptophanyl-tRNA synthetase

Down ($\alpha=0.001$)	WBSCR16	81554	RCC1 like
Down ($\alpha=0.001$)	ZBTB32	27033	zinc finger and BTB domain containing 32
Down ($\alpha=0.001$)	ZC3H12A	80149	zinc finger CCCH-type containing 12A
Down ($\alpha=0.001$)	ZFP36	7538	ZFP36 ring finger protein
Up ($\alpha=0.001$)	ABHD3	171586	abhydrolase domain containing 3
Up ($\alpha=0.001$)	ACADM	34	acyl-CoA dehydrogenase, C-4 to C-12 straight chain
Up ($\alpha=0.001$)	ACSF3	197322	acyl-CoA synthetase family member 3
Up ($\alpha=0.001$)	ACSL3	2181	acyl-CoA synthetase long-chain family member 3
Up ($\alpha=0.001$)	ADAM19	8728	ADAM metallopeptidase domain 19
Up ($\alpha=0.001$)	ADCYAP1	116	adenylate cyclase activating polypeptide 1
Up ($\alpha=0.001$)	ADM2	79924	adrenomedullin 2
Up ($\alpha=0.001$)	ADPRHL1	113622	ADP-ribosylhydrolase like 1
Up ($\alpha=0.001$)	AGPAT4	56895	1-acylglycerol-3-phosphate O-acyltransferase 4
Up ($\alpha=0.001$)	ANGEL2	90806	angel homolog 2
Up ($\alpha=0.001$)	ATP13A2	23400	ATPase 13A2
Up ($\alpha=0.001$)	ATP2A3	489	ATPase sarcoplasmic/endoplasmic reticulum Ca ²⁺ transporting 3
Up ($\alpha=0.001$)	ATP9A	10079	ATPase phospholipid transporting 9A (putative)
Up ($\alpha=0.001$)	BTK	695	Bruton tyrosine kinase
Up ($\alpha=0.001$)	C22orf29	79680	chromosome 22 open reading frame 29
Up ($\alpha=0.001$)	CAPN14	440854	calpain 14
Up ($\alpha=0.001$)	CBY1	25776	chibby family member 1, beta catenin antagonist
Up ($\alpha=0.001$)	CCPG1	9236	cell cycle progression 1
Up ($\alpha=0.001$)	CDC40	51362	cell division cycle 40
Up ($\alpha=0.001$)	CDKN1A	1026	cyclin dependent kinase inhibitor 1A
Up ($\alpha=0.001$)	CDKN2C	1031	cyclin dependent kinase inhibitor 2C
Up ($\alpha=0.001$)	CEACAM1	634	carcinoembryonic antigen related cell adhesion molecule 1
Up ($\alpha=0.001$)	CHST4	10164	carbohydrate sulfotransferase 4
Up ($\alpha=0.001$)	CISD2	493856	CDGSH iron sulfur domain 2
Up ($\alpha=0.001$)	CLIP3	25999	CAP-Gly domain containing linker protein 3
Up ($\alpha=0.001$)	CREB3L2	64764	cAMP responsive element binding protein 3 like 2
Up ($\alpha=0.001$)	CRYM	1428	crystallin mu
Up ($\alpha=0.001$)	CUEDC1	404093	CUE domain containing 1
Up ($\alpha=0.001$)	CYP2C8	1558	cytochrome P450 family 2 subfamily C member 8
Up ($\alpha=0.001$)	D4S234E	27065	neuron specific gene family member 1
Up ($\alpha=0.001$)	DDIT3	1649	DNA damage inducible transcript 3
Up ($\alpha=0.001$)	DGKA	1606	diacylglycerol kinase alpha
Up ($\alpha=0.001$)	DNAH1	25981	dynein axonemal heavy chain 1
Up ($\alpha=0.001$)	DNAJB9	4189	DnaJ heat shock protein family (Hsp40) member B9
Up ($\alpha=0.001$)	DNMT3B	1789	DNA methyltransferase 3 beta
Up ($\alpha=0.001$)	DRAM2	128338	DNA damage regulated autophagy modulator 2
Up ($\alpha=0.001$)	DTX1	1840	deltex E3 ubiquitin ligase 1
Up ($\alpha=0.001$)	E2F5	1875	E2F transcription factor 5
Up ($\alpha=0.001$)	ELL3	80237	elongation factor for RNA polymerase II 3
Up ($\alpha=0.001$)	EML6	400954	echinoderm microtubule associated protein like 6
Up ($\alpha=0.001$)	EPST11	94240	epithelial stromal interaction 1 (breast)
Up ($\alpha=0.001$)	ERP27	121506	endoplasmic reticulum protein 27
Up ($\alpha=0.001$)	ESPNL	339768	espin-like
Up ($\alpha=0.001$)	ESR2	2100	estrogen receptor 2
Up ($\alpha=0.001$)	EXTL2	2135	exostosin like glycosyltransferase 2
Up ($\alpha=0.001$)	FAM102A	399665	family with sequence similarity 102 member A
Up ($\alpha=0.001$)	FAM13B	51306	family with sequence similarity 13 member B
Up ($\alpha=0.001$)	FAM214A	56204	family with sequence similarity 214 member A
Up ($\alpha=0.001$)	FAM43A	131583	family with sequence similarity 43 member A
Up ($\alpha=0.001$)	FAM81A	145773	family with sequence similarity 81 member A
Up ($\alpha=0.001$)	FCRL2	79368	Fc receptor like 2

Up ($\alpha=0.001$)	FCRL3	115352	Fc receptor like 3
Up ($\alpha=0.001$)	FGD3	89846	FYVE, RhoGEF and PH domain containing 3
Up ($\alpha=0.001$)	FOSB	2354	FosB proto-oncogene, AP-1 transcription factor subunit
Up ($\alpha=0.001$)	FST	10468	folliculin
Up ($\alpha=0.001$)	FXYD6	53826	FXYD domain containing ion transport regulator 6
Up ($\alpha=0.001$)	GBP1	2633	guanylate binding protein 1
Up ($\alpha=0.001$)	GH1	2688	growth hormone 1
Up ($\alpha=0.001$)	GNB3	2784	G protein subunit beta 3
Up ($\alpha=0.001$)	GPER	2852	G protein-coupled estrogen receptor 1
Up ($\alpha=0.001$)	GRAP	10750	GRB2-related adaptor protein
Up ($\alpha=0.001$)	GUCY2C	2984	guanylate cyclase 2C
Up ($\alpha=0.001$)	GYLTL1B	120071	LARGE xylosyl- and glucuronyltransferase 2
Up ($\alpha=0.001$)	HCAR1	27198	hydroxycarboxylic acid receptor 1
Up ($\alpha=0.001$)	HES1	3280	hes family bHLH transcription factor 1
Up ($\alpha=0.001$)	HHEX	3087	hematopoietically expressed homeobox
Up ($\alpha=0.001$)	HLA-DMB	3109	major histocompatibility complex, class II, DM beta
Up ($\alpha=0.001$)	IBA57	200205	IBA57 homolog, iron-sulfur cluster assembly
Up ($\alpha=0.001$)	IL10RA	3587	interleukin 10 receptor subunit alpha
Up ($\alpha=0.001$)	IL16	3603	interleukin 16
Up ($\alpha=0.001$)	IL28RA	163702	interferon lambda receptor 1
Up ($\alpha=0.001$)	ITGAL	3683	integrin subunit alpha L
Up ($\alpha=0.001$)	ITGB7	3695	integrin subunit beta 7
Up ($\alpha=0.001$)	JARID2	3720	jumonji and AT-rich interaction domain containing 2
Up ($\alpha=0.001$)	KCNK12	56660	potassium two pore domain channel subfamily K member 12
Up ($\alpha=0.001$)	KDM5B	10765	lysine demethylase 5B
Up ($\alpha=0.001$)	KIAA0247	9766	sushi domain containing 6
Up ($\alpha=0.001$)	KLHDC5	57542	kelch like family member 42
Up ($\alpha=0.001$)	KLHL24	54800	kelch like family member 24
Up ($\alpha=0.001$)	KLHL5	51088	kelch like family member 5
Up ($\alpha=0.001$)	LAMA5	3911	laminin subunit alpha 5
Up ($\alpha=0.001$)	LEPREL2	10536	prolyl 3-hydroxylase 3
Up ($\alpha=0.001$)	LGALS8	3964	galectin 8
Up ($\alpha=0.001$)	LHX3	8022	LIM homeobox 3
Up ($\alpha=0.001$)	LOC100129034	100129034	uncharacterized LOC100129034
Up ($\alpha=0.001$)	LOC285359	285359	phosducin-like 3 pseudogene 4
Up ($\alpha=0.001$)	LOC389641	389641	uncharacterized LOC389641
Up ($\alpha=0.001$)	LTB	4050	lymphotoxin beta
Up ($\alpha=0.001$)	LY9	4063	lymphocyte antigen 9
Up ($\alpha=0.001$)	METRNL	284207	meteorin like, glial cell differentiation regulator
Up ($\alpha=0.001$)	METTL7A	25840	methyltransferase like 7A
Up ($\alpha=0.001$)	MKRN1	23608	makorin ring finger protein 1
Up ($\alpha=0.001$)	MSMP	692094	microseminoprotein, prostate associated
Up ($\alpha=0.001$)	MTA3	57504	metastasis associated 1 family member 3
Up ($\alpha=0.001$)	MTHFR	4524	methylenetetrahydrofolate reductase
Up ($\alpha=0.001$)	MYADM	91663	myeloid associated differentiation marker
Up ($\alpha=0.001$)	MYLIP	29116	myosin regulatory light chain interacting protein
Up ($\alpha=0.001$)	MYO18A	399687	myosin XVIIIa
Up ($\alpha=0.001$)	MYPOP	339344	Myb related transcription factor, partner of profilin
Up ($\alpha=0.001$)	MZB1	51237	marginal zone B and B1 cell specific protein
Up ($\alpha=0.001$)	NCF1C	654817	neutrophil cytosolic factor 1C pseudogene
Up ($\alpha=0.001$)	NLRP7	199713	NLR family pyrin domain containing 7
Up ($\alpha=0.001$)	NUAK2	81788	NUAK family kinase 2
Up ($\alpha=0.001$)	OMA1	115209	OMA1 zinc metallopeptidase
Up ($\alpha=0.001$)	OSBPL10	114884	oxysterol binding protein like 10
Up ($\alpha=0.001$)	OSBPL2	9885	oxysterol binding protein like 2
Up ($\alpha=0.001$)	PALD1	27143	phosphatase domain containing, paladin 1
Up ($\alpha=0.001$)	PALM	5064	paralemmin
Up ($\alpha=0.001$)	PARVG	64098	parvin gamma
Up ($\alpha=0.001$)	PDCD4	27250	programmed cell death 4 (neoplastic transformation inhibitor)
Up ($\alpha=0.001$)	PECAM1	5175	platelet and endothelial cell adhesion molecule 1

Up ($\alpha=0.001$)	PHF21A	51317	PHD finger protein 21A
Up ($\alpha=0.001$)	PHYHD1	254295	phytanoyl-CoA dioxygenase domain containing 1
Up ($\alpha=0.001$)	PIK3IP1	113791	phosphoinositide-3-kinase interacting protein 1
Up ($\alpha=0.001$)	PLEKHA2	59339	pleckstrin homology domain containing A2
Up ($\alpha=0.001$)	PODXL	5420	podocalyxin like
Up ($\alpha=0.001$)	PPAPDC1B	84513	phospholipid phosphatase 5
Up ($\alpha=0.001$)	PRCP	5547	prolylcarboxypeptidase
Up ($\alpha=0.001$)	PRKAB2	5565	protein kinase AMP-activated non-catalytic subunit beta 2
Up ($\alpha=0.001$)	PTH LH	5744	parathyroid hormone like hormone
Up ($\alpha=0.001$)	PTPRE	5791	protein tyrosine phosphatase, receptor type E
Up ($\alpha=0.001$)	PTPRG	5793	protein tyrosine phosphatase, receptor type G
Up ($\alpha=0.001$)	PVRIG	79037	poliovirus receptor related immunoglobulin domain containing
Up ($\alpha=0.001$)	QSOX2	169714	quiescin sulfhydryl oxidase 2
Up ($\alpha=0.001$)	RASAL1	8437	RAS protein activator like 1
Up ($\alpha=0.001$)	RASGRP3	25780	RAS guanyl releasing protein 3
Up ($\alpha=0.001$)	RBM20	282996	RNA binding motif protein 20
Up ($\alpha=0.001$)	RBM38	55544	RNA binding motif protein 38
Up ($\alpha=0.001$)	RCSD1	92241	RCSD domain containing 1
Up ($\alpha=0.001$)	RGS1	5996	regulator of G-protein signaling 1
Up ($\alpha=0.001$)	RHBDD1	84236	rhomboid domain containing 1
Up ($\alpha=0.001$)	RHBDF2	79651	rhomboid 5 homolog 2
Up ($\alpha=0.001$)	RHOBTB2	23221	Rho related BTB domain containing 2
Up ($\alpha=0.001$)	RHOQP3	284988	ras homolog family member Q pseudogene 3
Up ($\alpha=0.001$)	RIMS3	9783	regulating synaptic membrane exocytosis 3
Up ($\alpha=0.001$)	RNF144B	255488	ring finger protein 144B
Up ($\alpha=0.001$)	RNF170	81790	ring finger protein 170
Up ($\alpha=0.001$)	RPL15	6138	ribosomal protein L15
Up ($\alpha=0.001$)	RSPH3	83861	radial spoke 3 homolog
Up ($\alpha=0.001$)	S1PR1	1901	sphingosine-1-phosphate receptor 1
Up ($\alpha=0.001$)	SALL2	6297	spalt like transcription factor 2
Up ($\alpha=0.001$)	SAMD7	344658	sterile alpha motif domain containing 7
Up ($\alpha=0.001$)	SAMD9	54809	sterile alpha motif domain containing 9
Up ($\alpha=0.001$)	SEL1L3	23231	SEL1L family member 3
Up ($\alpha=0.001$)	SEMA4A	64218	semaphorin 4A
Up ($\alpha=0.001$)	SETDB2	83852	SET domain bifurcated 2
Up ($\alpha=0.001$)	SH2B2	10603	SH2B adaptor protein 2
Up ($\alpha=0.001$)	SIDT1	54847	SID1 transmembrane family member 1
Up ($\alpha=0.001$)	SIGLEC10	89790	sialic acid binding Ig like lectin 10
Up ($\alpha=0.001$)	SLAMF7	57823	SLAM family member 7
Up ($\alpha=0.001$)	SLC15A4	121260	solute carrier family 15 member 4
Up ($\alpha=0.001$)	SLC1A4	6509	solute carrier family 1 member 4
Up ($\alpha=0.001$)	SLC25A34	284723	solute carrier family 25 member 34
Up ($\alpha=0.001$)	SLC6A16	28968	solute carrier family 6 member 16
Up ($\alpha=0.001$)	SNX29	92017	sorting nexin 29
Up ($\alpha=0.001$)	SORT1	6272	sortilin 1
Up ($\alpha=0.001$)	SPAG9	9043	sperm associated antigen 9
Up ($\alpha=0.001$)	ST14	6768	suppression of tumorigenicity 14
Up ($\alpha=0.001$)	STARD5	80765	StAR related lipid transfer domain containing 5
Up ($\alpha=0.001$)	SUSD3	203328	sushi domain containing 3
Up ($\alpha=0.001$)	SYT11	23208	synaptotagmin 11
Up ($\alpha=0.001$)	SYTL3	94120	synaptotagmin like 3
Up ($\alpha=0.001$)	TAGAP	117289	T-cell activation RhoGTPase activating protein
Up ($\alpha=0.001$)	TEAD2	8463	TEA domain transcription factor 2
Up ($\alpha=0.001$)	TGFBR2	7048	transforming growth factor beta receptor 2
Up ($\alpha=0.001$)	TIAF1	9220	TGFB1-induced anti-apoptotic factor 1
Up ($\alpha=0.001$)	TM4SF19	116211	transmembrane 4 L six family member 19
Up ($\alpha=0.001$)	TMEM129	92305	transmembrane protein 129
Up ($\alpha=0.001$)	TMEM132A	54972	transmembrane protein 132A
Up ($\alpha=0.001$)	TNFRSF17	608	TNF receptor superfamily member 17
Up ($\alpha=0.001$)	TRAF5	7188	TNF receptor associated factor 5

Up ($\alpha=0.001$)	TRAM2	9697	translocation associated membrane protein 2
Up ($\alpha=0.001$)	TRAPPC2	6399	trafficking protein particle complex 2
Up ($\alpha=0.001$)	TRIM8	81603	tripartite motif containing 8
Up ($\alpha=0.001$)	TSC22D3	1831	TSC22 domain family member 3
Up ($\alpha=0.001$)	TXNIP	10628	thioredoxin interacting protein
Up ($\alpha=0.001$)	VEZF1	7716	vascular endothelial zinc finger 1
Up ($\alpha=0.001$)	VPREB3	29802	pre-B lymphocyte 3
Up ($\alpha=0.001$)	YPEL3	83719	yippee like 3
Up ($\alpha=0.001$)	ZBP1	81030	Z-DNA binding protein 1
Up ($\alpha=0.001$)	ZHX2	22882	zinc fingers and homeoboxes 2

Supplemental Table 4: Top gene signatures that are significantly enriched with top regulated genes in HBL1 cells following CsA treatment.
(All signatures are shown that had at least 5 measured genes and an enrichment score of at least 0.7.)

Signatures DB	Category	Sub Category	Signature name	Signature links	Measured genes	Enrichment score	p [GSEA] (by permutation test)
MolSigDBv5_1_dMay2016	c2: curated gene sets	Chemical and genetic perturbations	KALMA_E2F1_TARGETS	http://www.broadinstitute.org/gsea/msigdb/cards/KALMA_E2F1_TARGETS	11	0.888	0.0010
MolSigDBv5_1_dMay2016	c2: curated gene sets	Chemical and genetic perturbations	DER_INFI_ALPHA_RESPONSE_DN	http://www.broadinstitute.org/gsea/msigdb/cards/DER_INFI_ALPHA_RESPONSE_DN	5	0.833	0.0185
MolSigDBv5_1_dMay2016	c2: curated gene sets	Chemical and genetic perturbations	WIEHMANN_TELOMERE_SHORTENING_AND_CHRONIC_LIVER_DAMA	http://www.broadinstitute.org/gsea/msigdb/cards/WIEHMANN_TELOMERE_SHORTENING_AND_CHRONIC_LIVER_DAMA	6	0.833	0.0056
GeneSigDB_v4_Sept2011	Human	Leukemia	Leukemia_Flth007_15genes	http://www.genesigdb.org/genesigdb/signaturedetail.jsp?signatureid=17456722-Table1	14	0.843	0.0010
StaudtSigDB_dNov2012	Cellular process	Proliferation	G2_M_phase	http://lymphochip.nih.gov/cgi-bin/Signatures/signature_eb0b_DisplayGenes.cgi?signatureid=47	6	0.823	0.0129
GeneSigDB_v4_Sept2011	Human	Prostate	Prostate_Wing09_20genes	http://www.genesigdb.org/genesigdb/signaturedetail.jsp?signatureid=13996289-Table3	20	0.818	0.0010
GeneSigDB_v4_Sept2011	Human	Breast	Breast_Owmid0_8genes	http://www.genesigdb.org/genesigdb/signaturedetail.jsp?signatureid=15387888-Table1a	8	0.817	0.0038
MolSigDBv5_1_dMay2016	c2: curated gene sets	Canonical pathways	BIOCARTA_RNAMS_PATHWAY	http://www.broadinstitute.org/gsea/msigdb/cards/BIOCARTA_RNAMS_PATHWAY	10	0.811	0.0010
MolSigDBv5_1_dMay2016	c2: curated gene sets	Canonical pathways	ST_TUMOR_NECROSIS_FACTOR_PATHWAY	http://www.broadinstitute.org/gsea/msigdb/cards/ST_TUMOR_NECROSIS_FACTOR_PATHWAY	29	0.809	0.0010
MolSigDBv5_1_dMay2016	c2: curated gene sets	Chemical and genetic perturbations	PHESE_TARGETS_OF_APC_AND_MBD2_DN	http://www.broadinstitute.org/gsea/msigdb/cards/PHESE_TARGETS_OF_APC_AND_MBD2_DN	12	0.809	0.0010
GeneSigDB_v4_Sept2011	Human	Leukemia	Leukemia_Gctard007_09genes	http://www.genesigdb.org/genesigdb/signaturedetail.jsp?signatureid=17456564-Table2	9	0.806	0.0019
GeneSigDB_v4_Sept2011	Human	Brain	Brain_Kat5e08_10genes	http://www.genesigdb.org/genesigdb/signaturedetail.jsp?signatureid=18322470-Table6	7	0.806	0.0114
MolSigDBv5_1_dMay2016	c2: curated gene sets	Chemical and genetic perturbations	GOUYER_TAT1_TARGETS_UP	http://www.broadinstitute.org/gsea/msigdb/cards/GOUYER_TAT1_TARGETS_UP	10	0.806	0.0018
LensSigDB	from published papers	PMID=28202458; title="Sensitivity to PI3K	Supplemental Table 7: Downregulated genes (alpha4p=0.0001) follow	http://www.ncbi.nlm.nih.gov/pubmed/28202458	53	0.804	0.0010
MolSigDBv5_1_dMay2016	c2: curated gene sets	Chemical and genetic perturbations	OHASHI_AURKB_TARGETS	http://www.broadinstitute.org/gsea/msigdb/cards/OHASHI_AURKB_TARGETS	9	0.803	0.0070
GeneSigDB_v4_Sept2011	Human	Breast	Breast_Finet08_16genes	http://www.genesigdb.org/genesigdb/signaturedetail.jsp?signatureid=18245477-Table1	16	0.800	0.0010
MolSigDBv5_1_dMay2016	c2: curated gene sets	Chemical and genetic perturbations	FINETTI_BREAST_CANCER_KINOME_RED	http://www.broadinstitute.org/gsea/msigdb/cards/FINETTI_BREAST_CANCER_KINOME_RED	16	0.800	0.0010
MolSigDBv5_1_dMay2016	c2: curated gene sets	Chemical and genetic perturbations	MONTERO_THYROID_CANCER_POOR_SURVIVAL_UP	http://www.broadinstitute.org/gsea/msigdb/cards/MONTERO_THYROID_CANCER_POOR_SURVIVAL_UP	12	0.800	0.0018
MolSigDBv5_1_dMay2016	c2: curated gene sets	Canonical pathways	BIOCARTA_DNA_REPLICATION_PATHWAY	http://www.broadinstitute.org/gsea/msigdb/cards/BIOCARTA_DNA_REPLICATION_PATHWAY	10	0.797	0.0010
GeneSigDB_v4_Sept2011	Mouse	Uterine	homolog(Uterine_Gashiwa08_8genes; from Mus musculus; to Homo	http://www.genesigdb.org/genesigdb/signaturedetail.jsp?signatureid=18661203-Table3	7	0.797	0.0173
MolSigDBv5_1_dMay2016	c4: computational gene sets	cancer gene neighborhoods	GNF2_ESP1	http://www.broadinstitute.org/gsea/msigdb/cards/GNF2_ESP1	35	0.797	0.0010
MolSigDBv5_1_dMay2016	c2: curated gene sets	Chemical and genetic perturbations	KUMAMOTO_RESPONSE_TO_NUTLIN_3A_DN	http://www.broadinstitute.org/gsea/msigdb/cards/KUMAMOTO_RESPONSE_TO_NUTLIN_3A_DN	10	0.795	0.0025
GeneSigDB_v4_Sept2011	Human	StemCell	StemCell_Kumamoto08_10genes_Downregulated	http://www.genesigdb.org/genesigdb/signaturedetail.jsp?signatureid=18451145-Table1b	10	0.795	0.0030
MolSigDBv5_1_dMay2016	c4: computational gene sets	cancer gene neighborhoods	GNF2_BUB1	http://www.broadinstitute.org/gsea/msigdb/cards/GNF2_BUB1	26	0.794	0.0010
GeneSigDB_v4_Sept2011	Human	Glioblastoma	Glioblastoma_Morand08_33genes	http://www.genesigdb.org/genesigdb/signaturedetail.jsp?signatureid=18694480-Table2	23	0.794	0.0010
GeneSigDB_v4_Sept2011	Human	Prostate	Prostate_ChoVega05_20genes	http://www.genesigdb.org/genesigdb/signaturedetail.jsp?signatureid=15529182-Table3	7	0.792	0.0110
MolSigDBv5_1_dMay2016	c3: motif gene sets	transcription factor targets	VSEF1_C	http://www.broadinstitute.org/gsea/msigdb/cards/VSEF1_C	6	0.791	0.0019
GeneSigDB_v4_Sept2011	Human	Leukemia	Leukemia_Bal05_07genes	http://www.genesigdb.org/genesigdb/signaturedetail.jsp?signatureid=15896717-Table4	7	0.786	0.0194
GeneSigDB_v4_Sept2011	Human	Lymphoma	Lymphoma_Blenk08_16genes	http://www.genesigdb.org/genesigdb/signaturedetail.jsp?signatureid=18416826-Table2	11	0.785	0.0019
MolSigDBv5_1_dMay2016	c2: curated gene sets	Chemical and genetic perturbations	OHASHI_AURKB_TARGETS	http://www.broadinstitute.org/gsea/msigdb/cards/OHASHI_AURKB_TARGETS	6	0.782	0.0345
MolSigDBv5_1_dMay2016	c4: computational gene sets	cancer gene neighborhoods	GNF2_MK67	http://www.broadinstitute.org/gsea/msigdb/cards/GNF2_MK67	28	0.775	0.0010
MolSigDBv5_1_dMay2016	c5: gene ontology (GO) gene sets	biological processes	RNA_PROCESSING	http://www.broadinstitute.org/gsea/msigdb/cards/RNA_PROCESSING	15	0.774	0.0010
MolSigDBv5_1_dMay2016	c4: computational gene sets	cancer modules	MODULE_388	http://www.broadinstitute.org/gsea/msigdb/cards/MODULE_388	17	0.774	0.0010
GeneSigDB_v4_Sept2011	Human	Lymphoma	Lymphoma_Lam01_23genes	http://www.genesigdb.org/genesigdb/signaturedetail.jsp?signatureid=11597333-Supp Tables	14	0.774	0.0010
MolSigDBv5_1_dMay2016	c2: curated gene sets	Chemical and genetic perturbations	CROSBY_E2F4_TARGETS	http://www.broadinstitute.org/gsea/msigdb/cards/CROSBY_E2F4_TARGETS	6	0.772	0.0369
GeneSigDB_v4_Sept2011	Mouse	Prostate	homolog(Prostate_Haram08_13genes; from Mus musculus; to Homo	http://www.genesigdb.org/genesigdb/signaturedetail.jsp?signatureid=18688517-table2	14	0.771	0.0010
GeneSigDB_v4_Sept2011	Rat	Breast	homolog(Breast_Leung03_10genes; from Rattus norvegicus; to Homo	http://www.genesigdb.org/genesigdb/signaturedetail.jsp?signatureid=12602904-Table1	6	0.770	0.0430
MolSigDBv5_1_dMay2016	c4: computational gene sets	cancer gene neighborhoods	GNF2_HMMR	http://www.broadinstitute.org/gsea/msigdb/cards/GNF2_HMMR	47	0.769	0.0010
GeneSigDB_v4_Sept2011	Human	Breast	Breast_Lud08_28genes	http://www.genesigdb.org/genesigdb/signaturedetail.jsp?signatureid=18786252-Table4	26	0.766	0.0010
StaudtSigDB_dNov2012	Cancer differential	Mantle cell lymphoma	MCL_proliferation_survival	http://lymphochip.nih.gov/cgi-bin/Signatures/signature_eb0b_DisplayGenes.cgi?signatureid=46	17	0.764	0.0010
GeneSigDB_v4_Sept2011	Human	Breast	Breast_Cher09_16genes	http://www.genesigdb.org/genesigdb/signaturedetail.jsp?signatureid=19266279-Table1	15	0.763	0.0019
GeneSigDB_v4_Sept2011	Human	Breast	Breast_Cher09_30genes	http://www.genesigdb.org/genesigdb/signaturedetail.jsp?signatureid=19266279-5T2	30	0.763	0.0010
MolSigDBv5_1_dMay2016	c2: curated gene sets	Chemical and genetic perturbations	IKEDA_MIRL_TARGETS_DN	http://www.broadinstitute.org/gsea/msigdb/cards/IKEDA_MIRL_TARGETS_DN	7	0.763	0.0272
GeneSigDB_v4_Sept2011	Human	StemCell	StemCell_Medjlan04_23genes	http://www.genesigdb.org/genesigdb/signaturedetail.jsp?signatureid=15150093-Table1	21	0.762	0.0010
MolSigDBv5_1_dMay2016	c2: curated gene sets	Chemical and genetic perturbations	OXFORD_RALA_TARGETS_UP	http://www.broadinstitute.org/gsea/msigdb/cards/OXFORD_RALA_TARGETS_UP	9	0.760	0.0119
MolSigDBv5_1_dMay2016	c2: curated gene sets	Chemical and genetic perturbations	BUSA_SAM68_TARGETS_DN	http://www.broadinstitute.org/gsea/msigdb/cards/BUSA_SAM68_TARGETS_DN	6	0.759	0.0574
GeneSigDB_v4_Sept2011	Human	Bone	Bone_Dring04_8genes_MeanDiffBFunction	http://www.genesigdb.org/genesigdb/signaturedetail.jsp?signatureid=15355895-Table2c	7	0.759	0.0206
GeneSigDB_v4_Sept2011	Human	Stomach	Stomach_Lee04_16genes	http://www.genesigdb.org/genesigdb/signaturedetail.jsp?signatureid=15467184-Table1b	16	0.758	0.0010
GeneSigDB_v4_Sept2011	Human	Breast	Breast_Ma02_28genes_IDOVDCS_up	http://www.genesigdb.org/genesigdb/signaturedetail.jsp?signatureid=12714683-Table6	27	0.758	0.0009
GeneSigDB_v4_Sept2011	Human	Breast	Breast_Mareld09_11genes_GeneCodingProtein	http://www.genesigdb.org/genesigdb/signaturedetail.jsp?signatureid=19584277-Table3	10	0.757	0.0091
HGNCSigDB_dMay2014	gene families	HAUS augmin-like complex subunits	HAUS augmin-like complex subunits	http://www.genenames.org/gene/families/HAUS	8	0.757	0.0209
MolSigDBv5_1_dMay2016	c4: computational gene sets	cancer gene neighborhoods	GNF2_RRM2	http://www.broadinstitute.org/gsea/msigdb/cards/GNF2_RRM2	40	0.756	0.0010
GeneSigDB_v4_Sept2011	c5: gene ontology (GO) gene sets	biological processes	RNA_METABOLIC_PROCESS	http://www.broadinstitute.org/gsea/msigdb/cards/RNA_METABOLIC_PROCESS	16	0.754	0.0015
MolSigDBv5_1_dMay2016	c2: curated gene sets	Canonical pathways	BIOCARTA_P35ALZHEIMERS_PATHWAY	http://www.broadinstitute.org/gsea/msigdb/cards/BIOCARTA_P35ALZHEIMERS_PATHWAY	11	0.754	0.0015
MolSigDBv5_1_dMay2016	c4: computational gene sets	cancer gene neighborhoods	GNF2_BUB1B	http://www.broadinstitute.org/gsea/msigdb/cards/GNF2_BUB1B	49	0.753	0.0010
MolSigDBv5_1_dMay2016	c5: gene ontology (GO) gene sets	molecular functions	MAP_KINASE_KINASE_KINASE_ACTIVITY	http://www.broadinstitute.org/gsea/msigdb/cards/MAP_KINASE_KINASE_KINASE_ACTIVITY	10	0.751	0.0143
MolSigDBv5_1_dMay2016	c2: curated gene sets	Chemical and genetic perturbations	EGUCHI_CELL_CYCLE_RBL_TARGETS	http://www.broadinstitute.org/gsea/msigdb/cards/EGUCHI_CELL_CYCLE_RBL_TARGETS	23	0.750	0.0009

Upregulated signatures:

Signatures DB	Category	Sub Category	Signature name	Signature links	Measured genes	Enrichment score	p [GSEA] (by permutation test)
GeneSigDB_v4_Sept2011	Mouse	Lymphoma	homolog(Lymphoma_Par05_10genes_b_from Mus musculus, to Homo sapiens)	http://www.genesigdb.org/genesigdb/signaturedetail.jsp?signatureid=16140930-Table1b	8	-0.923	0.0010
StaudtSigDB_dNov2012	Cancer differential	Diffuse large B cell lymphoma	MHC_classII_DUBCL	http://lymphochip.nih.gov/cgi-bin/signatureweb/signaturedb_DisplayGenes.cgi?signatureid=9	8	-0.906	0.0010
GeneSigDB_v4_Sept2011	Human	Lymphoma	Lymphoma_Tome05_27genes	http://www.genesigdb.org/genesigdb/signaturedetail.jsp?signatureid=16081886-Supp-Table3	8	-0.906	0.0010
StaudtSigDB_dNov2012	Cellular process	MHC class II	MHC_classII_Node528	http://lymphochip.nih.gov/cgi-bin/signatureweb/signaturedb_DisplayGenes.cgi?signatureid=205	7	-0.906	0.0018
MolsigDB_v4_dMay2016	c2: curated gene sets	chemical and genetic perturbations	KOBAYASHI_EGFR_SIGNALING_GHR_UP	http://www.broadinstitute.org/gsea/msigdb/cards/KOBAYASHI_EGFR_SIGNALING_GHR_UP	7	-0.879	0.0019
GeneSigDB_v4_Sept2011	Human	Lung	Lung_Kobayashi06_07genes	http://www.genesigdb.org/genesigdb/signaturedetail.jsp?signatureid=1745885-Table1a	7	-0.879	0.0019
MolsigDB_v4_dMay2016	c2: curated gene sets	chemical and genetic perturbations	ANUMISON_DNA_DAMAGE_RESPONSE_TP53	http://www.broadinstitute.org/gsea/msigdb/cards/ANUMISON_DNA_DAMAGE_RESPONSE_TP53	16	-0.859	0.0010
MolsigDB_v4_dMay2016	c2: curated gene sets	chemical and genetic perturbations	KUMAMOTO_RESPONSE_TO_NUTLIN_3A_UP	http://www.broadinstitute.org/gsea/msigdb/cards/KUMAMOTO_RESPONSE_TO_NUTLIN_3A_UP	9	-0.847	0.0018
GeneSigDB_v4_Sept2011	Human	StemCell	StemCell_Kumamoto08_10genes_Upreregulated	http://www.genesigdb.org/genesigdb/signaturedetail.jsp?signatureid=18451145-Table1a	9	-0.847	0.0019
StaudtSigDB_dNov2012	Cellular differentiation	B cell	B_cell_Node1500	http://lymphochip.nih.gov/cgi-bin/signatureweb/signaturedb_DisplayGenes.cgi?signatureid=94	8	-0.844	0.0031
GeneSigDB_v4_Sept2011	Human	Leukemia	Leukemia_L07_12genes_Anti-apoptosis	http://www.genesigdb.org/genesigdb/signaturedetail.jsp?signatureid=17313671-Supp-Table1a	11	-0.843	0.0010
GeneSigDB_v4_Sept2011	Human	Viral	Viral_Uchimura07_7genes	http://www.genesigdb.org/genesigdb/signaturedetail.jsp?signatureid=17970077-Table2	7	-0.840	0.0042
MolsigDB_v4_dMay2016	c1: positional gene sets	all	chr11p	http://www.broadinstitute.org/gsea/msigdb/cards/chr11p	5	-0.820	0.0338
GeneSigDB	from published papers	PMID=28202458, title="Sensitivity to PI3K inhibition in human breast cancer cell lines"	Supplemental Table 7: Upregulated genes (alpha=0.0001) following PI3K inhibition	http://www.ncbi.nlm.nih.gov/pubmed/28202458	59	-0.807	0.0010
MolsigDB_v4_dMay2016	c2: curated gene sets	chemical and genetic perturbations	DER_FFN_BETA_RESPONSE_DN	http://www.broadinstitute.org/gsea/msigdb/cards/DER_FFN_BETA_RESPONSE_DN	7	-0.801	0.0180
MolsigDB_v4_dMay2016	c2: curated gene sets	canonical pathways	REACTION_ENDOSOMAL_VACUOLAR_PATHWAY	http://www.broadinstitute.org/gsea/msigdb/cards/REACTION_ENDOSOMAL_VACUOLAR_PATHWAY	8	-0.799	0.0074
MolsigDB_v4_dMay2016	c5: gene ontology (GO) gene sets	molecular functions	MANNOSE6P_TRANSCRIPTION_ACTIVATION	http://www.broadinstitute.org/gsea/msigdb/cards/MANNOSE6P_TRANSCRIPTION_ACTIVATION	10	-0.797	0.0052
StaudtSigDB_dNov2012	Cellular differentiation	Non-hematopoietic	Pituitary_Lung_Node1582	http://lymphochip.nih.gov/cgi-bin/signatureweb/signaturedb_DisplayGenes.cgi?signatureid=109	6	-0.794	0.0279
GeneSigDB_v4_Sept2011	Mouse	Leukemia	homolog(Leukemia_Sipe07_12genes, from Mus musculus, to Homo sapiens)	http://www.genesigdb.org/genesigdb/signaturedetail.jsp?signatureid=17377591-Table2	7	-0.792	0.0198
HGNCSigDB_dMay2014	gene families	Histocompatibility complex	Histocompatibility complex	http://www.geneid.com/families/HLA	24	-0.791	0.0010
MolsigDB_v4_dMay2016	c5: gene ontology (GO) gene sets	cellular components	OUGSACCHARYL_TRANSFERASE_COMPLEX	http://www.broadinstitute.org/gsea/msigdb/cards/OUGSACCHARYL_TRANSFERASE_COMPLEX	10	-0.791	0.0020
GeneSigDB_v4_Sept2011	Mouse	Pancreas	homolog(Pancreas_Thakur08_17genes, from Mus musculus, to Homo sapiens)	http://www.genesigdb.org/genesigdb/signaturedetail.jsp?signatureid=18218118-Table4	11	-0.791	0.0026
GeneSigDB_v4_Sept2011	Mouse	Leukemia	homolog(Leukemia_Dalig003_15genes, from Mus musculus, to Homo sapiens)	http://www.genesigdb.org/genesigdb/signaturedetail.jsp?signatureid=12831403-Table1	11	-0.786	0.0013
MolsigDB_v4_dMay2016	c4: computational gene sets	cancer modules	MODULE_293	http://www.broadinstitute.org/gsea/msigdb/cards/MODULE_293	12	-0.784	0.0031
MolsigDB_v4_dMay2016	c2: curated gene sets	chemical and genetic perturbations	IGARASHI_ATA4_TARGETS_LIP	http://www.broadinstitute.org/gsea/msigdb/cards/IGARASHI_ATA4_TARGETS_LIP	6	-0.782	0.0301
MolsigDB_v4_dMay2016	c2: curated gene sets	chemical and genetic perturbations	MOTAMED_RESPONSE_TO_ANDROGEN_DN	http://www.broadinstitute.org/gsea/msigdb/cards/MOTAMED_RESPONSE_TO_ANDROGEN_DN	6	-0.781	0.0417
HGNCSigDB_dMay2014	gene families	Serine	Serine/threonine phosphatases / protein phosphatase 6, regulatory subunit 1	http://www.geneid.com/families/PPP-PPM-CTDPPRPR	6	-0.779	0.0520
MolsigDB_v4_dMay2016	c2: curated gene sets	chemical and genetic perturbations	YAMANAKA_GLOBULASTOMA_SURVIVAL_DN	http://www.broadinstitute.org/gsea/msigdb/cards/YAMANAKA_GLOBULASTOMA_SURVIVAL_DN	9	-0.772	0.0103
MolsigDB_v4_dMay2016	c2: curated gene sets	chemical and genetic perturbations	YANG_BCL3_TARGETS_DN	http://www.broadinstitute.org/gsea/msigdb/cards/YANG_BCL3_TARGETS_DN	8	-0.765	0.0188
MolsigDB_v4_dMay2016	c4: computational gene sets	cancer modules	MODULE_143	http://www.broadinstitute.org/gsea/msigdb/cards/MODULE_143	14	-0.763	0.0010
MolsigDB_v4_dMay2016	c4: computational gene sets	cancer modules	MODULE_211	http://www.broadinstitute.org/gsea/msigdb/cards/MODULE_211	11	-0.762	0.0042
MolsigDB_v4_dMay2016	c2: curated gene sets	chemical and genetic perturbations	MIZUKAMI_HYPONIA_UP	http://www.broadinstitute.org/gsea/msigdb/cards/MIZUKAMI_HYPONIA_UP	12	-0.759	0.0037
GeneSigDB_v4_Sept2011	Human	Breast	Breast_Tangir04_13genes_Dexamethasone	http://www.genesigdb.org/genesigdb/signaturedetail.jsp?signatureid=15679945-Table1	6	-0.751	0.0822

Supplemental Table 5: Down- and upregulated genes following CsA treatment in the GCB DLBCL cell line HT.

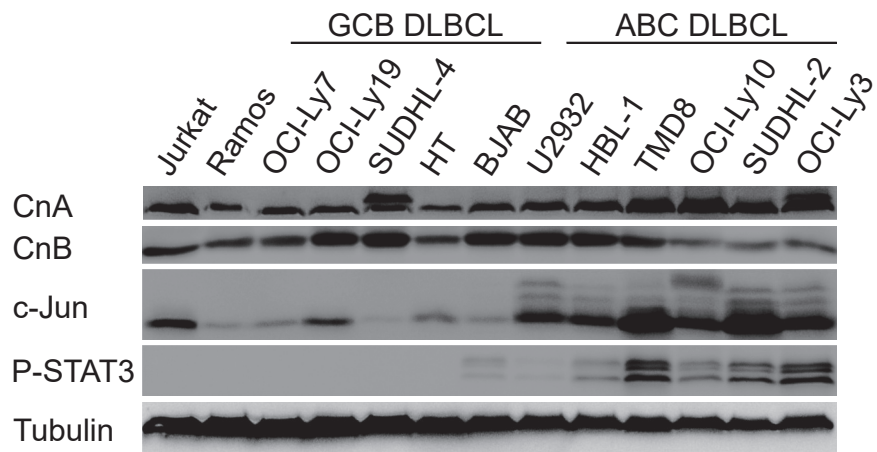
Signature name	Gene symbol	Gene ID	Gene description
Down (alpha=0.005)	ACOT7	11332	acyl-CoA thioesterase 7
Down (alpha=0.005)	ACPL2	92370	2-phosphoxylose phosphatase 1
Down (alpha=0.005)	ACVRL1	94	activin A receptor like type 1
Down (alpha=0.005)	AGT	183	angiotensinogen
Down (alpha=0.005)	AHSP	51327	alpha hemoglobin stabilizing protein
Down (alpha=0.005)	AK8	158067	adenylate kinase 8
Down (alpha=0.005)	ARHGAP11A	9824	Rho GTPase activating protein 11A
Down (alpha=0.005)	ASXL2	55252	ASXL transcriptional regulator 2
Down (alpha=0.005)	ATAD5	79915	ATPase family AAA domain containing 5
Down (alpha=0.005)	ATPAF2	91647	ATP synthase mitochondrial F1 complex assembly factor 2
Down (alpha=0.005)	AXDND1	126859	axonemal dynein light chain domain containing 1
Down (alpha=0.005)	B3GNT3	10331	UDP-GlcNAc:betaGal beta-1,3-N-acetylglucosaminyltransferase 3
Down (alpha=0.005)	B3GNTL1	146712	UDP-GlcNAc:betaGal beta-1,3-N-acetylglucosaminyltransferase like 1
Down (alpha=0.005)	BAP1	8314	BRCA1 associated protein 1
Down (alpha=0.005)	BCAN	63827	brevican
Down (alpha=0.005)	BIK	638	BCL2 interacting killer
Down (alpha=0.005)	BIRC7	79444	baculoviral IAP repeat containing 7
Down (alpha=0.005)	CACHD1	57685	cache domain containing 1
Down (alpha=0.005)	CAPSL	133690	calciphosine like
Down (alpha=0.005)	CARD10	29775	caspase recruitment domain family member 10
Down (alpha=0.005)	CARS2	79587	cysteinyl-tRNA synthetase 2, mitochondrial
Down (alpha=0.005)	CCDC102A	92922	coiled-coil domain containing 102A
Down (alpha=0.005)	CCNF	899	cyclin F
Down (alpha=0.005)	CDK19	23097	cyclin dependent kinase 19
Down (alpha=0.005)	CERK	64781	ceramide kinase
Down (alpha=0.005)	CGN	57530	cingulin
Down (alpha=0.005)	CNNM3	26505	cyclin and CBS domain divalent metal cation transport mediator 3
Down (alpha=0.005)	CPSF1	29894	cleavage and polyadenylation specific factor 1
Down (alpha=0.005)	CSNK1G2	1455	casein kinase 1 gamma 2
Down (alpha=0.005)	CTRL	1506	chymotrypsin like
Down (alpha=0.005)	CTXN1	404217	cortexin 1
Down (alpha=0.005)	DIXDC1	85458	DIX domain containing 1
Down (alpha=0.005)	DUX4L12	440014	double homeobox 4 like 12 (pseudogene)
Down (alpha=0.005)	EIF3C	8663	eukaryotic translation initiation factor 3 subunit C
Down (alpha=0.005)	ELAC1	55520	elaC ribonuclease Z 1
Down (alpha=0.005)	EZH1	2145	enhancer of zeste 1 polycomb repressive complex 2 subunit
Down (alpha=0.005)	EZR	7430	ezrin
Down (alpha=0.005)	FAM108A5P	729495	abhydrolase domain containing 17A pseudogene P4
Down (alpha=0.005)	FAM131B	9715	family with sequence similarity 131 member B
Down (alpha=0.005)	FAM182B	728882	family with sequence similarity 182 member B
Down (alpha=0.005)	FAM188B	84182	MINDY lysine 48 deubiquitinase 4
Down (alpha=0.005)	FAM203B	728071	
Down (alpha=0.005)	FAM207A	85395	family with sequence similarity 207 member A
Down (alpha=0.005)	FAM59B	150946	GRB2 associated regulator of MAPK1 subtype 2
Down (alpha=0.005)	FAM75A6	389730	SPATA31 subfamily A member 6
Down (alpha=0.005)	FANCC	2176	FA complementation group C

Down (alpha=0.005)	FHL3	2275	four and a half LIM domains 3
Down (alpha=0.005)	FLJ40194	124871	uncharacterized FLJ40194
Down (alpha=0.005)	G6PD	2539	glucose-6-phosphate dehydrogenase
Down (alpha=0.005)	GBP2	2634	guanylate binding protein 2
Down (alpha=0.005)	GOLGA6D	653643	golgin A6 family member D
Down (alpha=0.005)	GPATCH8	23131	G-patch domain containing 8
Down (alpha=0.005)	GTPBP3	84705	GTP binding protein 3, mitochondrial
Down (alpha=0.005)	HADHA	3030	hydroxyacyl-CoA dehydrogenase trifunctional multienzyme complex subunit alpha
Down (alpha=0.005)	HAR1B	768097	highly accelerated region 1B
Down (alpha=0.005)	HMBOX1	79618	homeobox containing 1
Down (alpha=0.005)	HNRNPD	3184	heterogeneous nuclear ribonucleoprotein D
Down (alpha=0.005)	HVCN1	84329	hydrogen voltage gated channel 1
Down (alpha=0.005)	IFITM3	10410	interferon induced transmembrane protein 3
Down (alpha=0.005)	INF2	64423	inverted formin, FH2 and WH2 domain containing
Down (alpha=0.005)	INTS1	26173	integrator complex subunit 1
Down (alpha=0.005)	IRAK1	3654	interleukin 1 receptor associated kinase 1
Down (alpha=0.005)	ITGA3	3675	integrin subunit alpha 3
Down (alpha=0.005)	KCNQ1	3784	potassium voltage-gated channel subfamily Q member 1
Down (alpha=0.005)	KHDRBS1	10657	KH RNA binding domain containing, signal transduction associated 1
Down (alpha=0.005)	KIAA0040	9674	KIAA0040
Down (alpha=0.005)	KIAA0100	9703	KIAA0100
Down (alpha=0.005)	KIDINS220	57498	kinase D interacting substrate 220
Down (alpha=0.005)	KLB	152831	klotho beta
Down (alpha=0.005)	KNCN	148930	kinocilin
Down (alpha=0.005)	LEPREL2	10536	prolyl 3-hydroxylase 3
Down (alpha=0.005)	LGALS12	85329	galectin 12
Down (alpha=0.005)	LOC401010	401010	NOC2 like nucleolar associated transcriptional repressor pseudogene 2
Down (alpha=0.005)	LOC440905	440905	fatty acyl-CoA reductase 2 pseudogene 1
Down (alpha=0.005)	LOC643308	643308	ribosomal protein L7 pseudogene 59
Down (alpha=0.005)	LOC644766	644766	
Down (alpha=0.005)	LOC645434	645434	long intergenic non-protein coding RNA 1625
Down (alpha=0.005)	LOC653375	653375	
Down (alpha=0.005)	LOC653602	653602	
Down (alpha=0.005)	LOC727967	727967	
Down (alpha=0.005)	LRFN3	79414	leucine rich repeat and fibronectin type III domain containing 3
Down (alpha=0.005)	LRRRC45	201255	leucine rich repeat containing 45
Down (alpha=0.005)	LRRRC59	55379	leucine rich repeat containing 59
Down (alpha=0.005)	LTB	4050	lymphotoxin beta
Down (alpha=0.005)	MAGED2	10916	MAGE family member D2
Down (alpha=0.005)	MALT1	10892	MALT1 paracaspase
Down (alpha=0.005)	MAN1C1	57134	mannosidase alpha class 1C member 1
Down (alpha=0.005)	MCM7	4176	minichromosome maintenance complex component 7
Down (alpha=0.005)	MED25	81857	mediator complex subunit 25
Down (alpha=0.005)	METTL13	51603	eEF1A lysine and N-terminal methyltransferase
Down (alpha=0.005)	MEX3D	399664	mex-3 RNA binding family member D
Down (alpha=0.005)	MID1IP1	58526	MID1 interacting protein 1
Down (alpha=0.005)	MIR1253	100302208	microRNA 1253
Down (alpha=0.005)	MIR204	406987	microRNA 204
Down (alpha=0.005)	MMP25	64386	matrix metalloproteinase 25
Down (alpha=0.005)	MXRA5	25878	matrix remodeling associated 5
Down (alpha=0.005)	MYOZ1	58529	myozenin 1

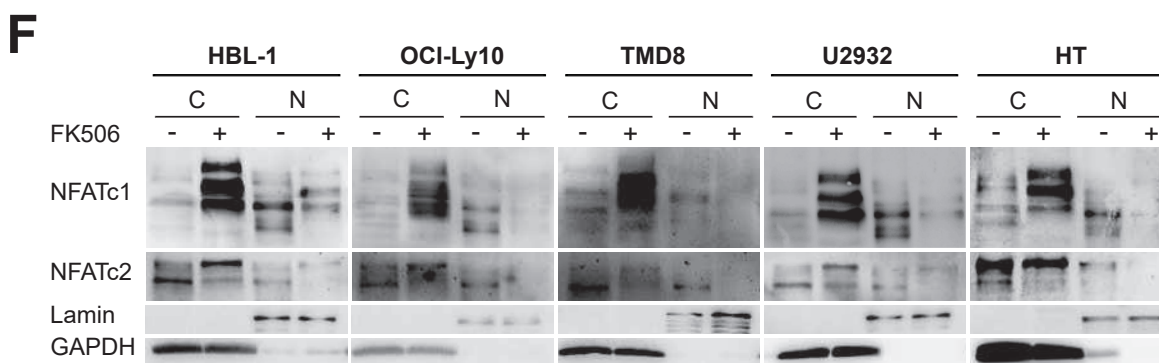
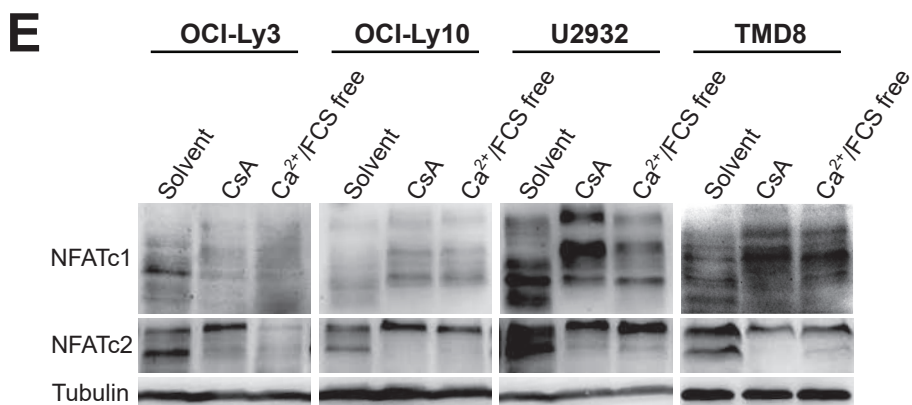
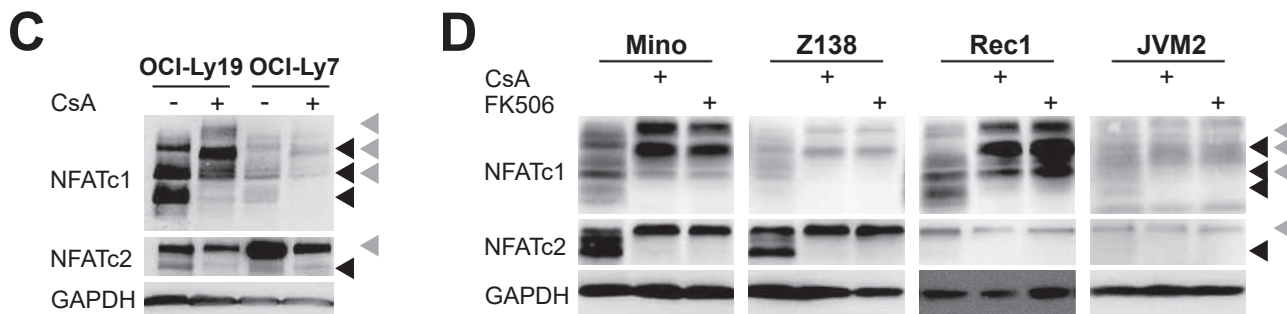
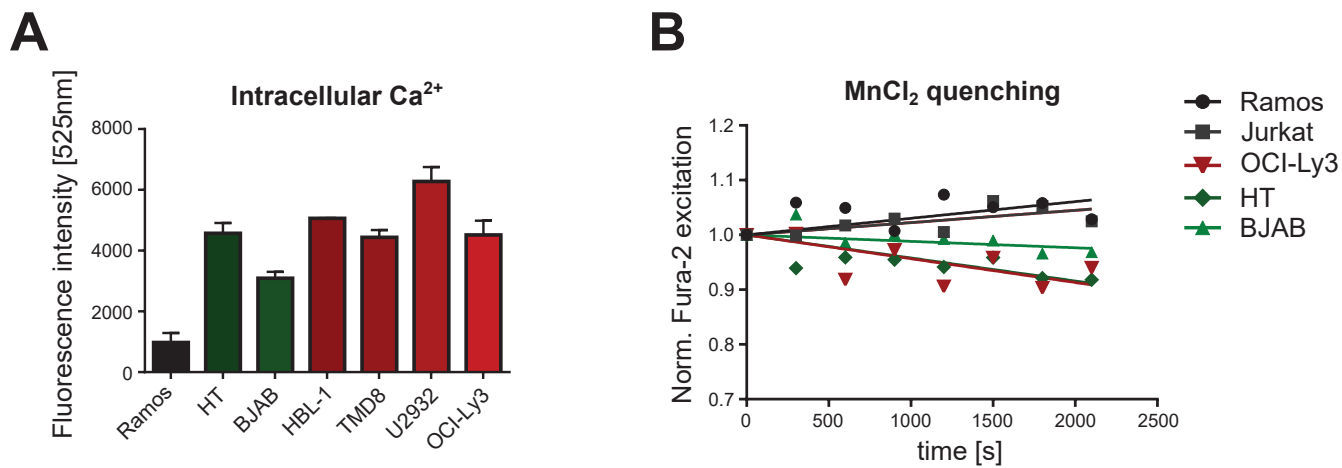
Down (alpha=0.005)	NCAPD3	23310	non-SMC condensin II complex subunit D3
Down (alpha=0.005)	NFAM1	150372	NFAT activating protein with ITAM motif 1
Down (alpha=0.005)	NOXO1	124056	NADPH oxidase organizer 1
Down (alpha=0.005)	OAS1	4938	2'-5'-oligoadenylate synthetase 1
Down (alpha=0.005)	OPA3	80207	outer mitochondrial membrane lipid metabolism regulator OPA3
Down (alpha=0.005)	OR1G1	8390	olfactory receptor family 1 subfamily G member 1
Down (alpha=0.005)	OR2A20P	401428	olfactory receptor family 2 subfamily A member 20 pseudogene
Down (alpha=0.005)	OR52K1	390036	olfactory receptor family 52 subfamily K member 1
Down (alpha=0.005)	PABPC1P4	341315	poly(A) binding protein cytoplasmic 1 pseudogene 4
Down (alpha=0.005)	PCGF2	7703	polycomb group ring finger 2
Down (alpha=0.005)	PLEKHF1	79156	pleckstrin homology and FYVE domain containing 1
Down (alpha=0.005)	POU2AF1	5450	POU class 2 homeobox associating factor 1
Down (alpha=0.005)	PRR15L	79170	proline rich 15 like
Down (alpha=0.005)	PRR19	284338	proline rich 19
Down (alpha=0.005)	RAB34	83871	RAB34, member RAS oncogene family
Down (alpha=0.005)	RANBP1	5902	RAN binding protein 1
Down (alpha=0.005)	RASA2	5922	RAS p21 protein activator 2
Down (alpha=0.005)	RBM14	10432	RNA binding motif protein 14
Down (alpha=0.005)	RGS12	6002	regulator of G protein signaling 12
Down (alpha=0.005)	RHBDL1	9028	rhomboid like 1
Down (alpha=0.005)	RIPK3	11035	receptor interacting serine/threonine kinase 3
Down (alpha=0.005)	RPL26P35	100128115	ribosomal protein L26 pseudogene 35
Down (alpha=0.005)	RPS6KB2	6199	ribosomal protein S6 kinase B2
Down (alpha=0.005)	SACS	26278	sacsin molecular chaperone
Down (alpha=0.005)	SASH3	54440	SAM and SH3 domain containing 3
Down (alpha=0.005)	SCAMP4	113178	secretory carrier membrane protein 4
Down (alpha=0.005)	SETP4	642869	SET pseudogene 4
Down (alpha=0.005)	SF1	7536	splicing factor 1
Down (alpha=0.005)	SHPK	23729	sedoheptulokinase
Down (alpha=0.005)	SLC25A39	51629	solute carrier family 25 member 39
Down (alpha=0.005)	SLC9A3R1	9368	SLC9A3 regulator 1
Down (alpha=0.005)	SNORD32B	692092	small nucleolar RNA, C/D box 32B
Down (alpha=0.005)	SNORD33	26818	small nucleolar RNA, C/D box 33
Down (alpha=0.005)	SPATA2L	124044	spermatogenesis associated 2 like
Down (alpha=0.005)	SPEF2	79925	sperm flagellar 2
Down (alpha=0.005)	SPOCK2	9806	SPARC (osteonectin), cwcv and kazal like domains proteoglycan 2
Down (alpha=0.005)	SPRR4	163778	small proline rich protein 4
Down (alpha=0.005)	STK25	10494	serine/threonine kinase 25
Down (alpha=0.005)	STK32A	202374	serine/threonine kinase 32A
Down (alpha=0.005)	SURF2	6835	surfeit 2
Down (alpha=0.005)	TCF25	22980	transcription factor 25
Down (alpha=0.005)	TMIE	259236	transmembrane inner ear
Down (alpha=0.005)	TNFAIP8L1	126282	TNF alpha induced protein 8 like 1
Down (alpha=0.005)	TPP2	7174	tripeptidyl peptidase 2
Down (alpha=0.005)	TRAF6	7189	TNF receptor associated factor 6
Down (alpha=0.005)	TRIM58	25893	tripartite motif containing 58
Down (alpha=0.005)	TRIM61	391712	tripartite motif containing 61
Down (alpha=0.005)	TSPAN4	7106	tetraspanin 4
Down (alpha=0.005)	TTL	150465	tubulin tyrosine ligase
Down (alpha=0.005)	TUBB	203068	tubulin beta class I
Down (alpha=0.005)	TUFM	7284	Tu translation elongation factor, mitochondrial
Down (alpha=0.005)	UTP18	51096	UTP18 small subunit processome component

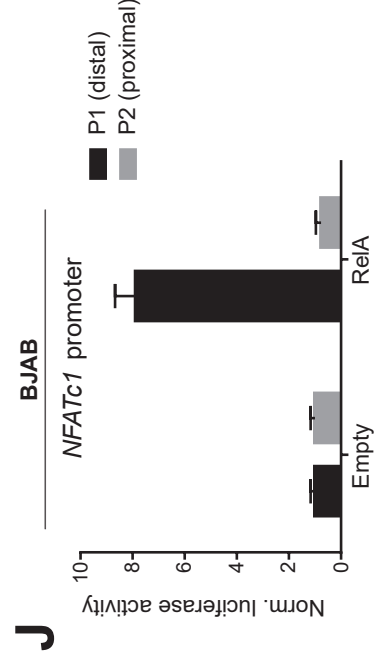
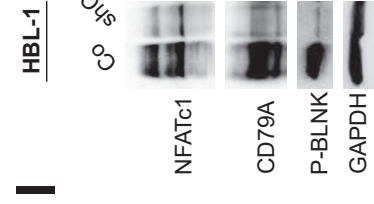
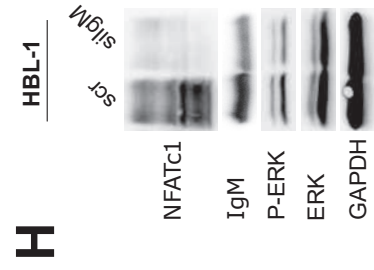
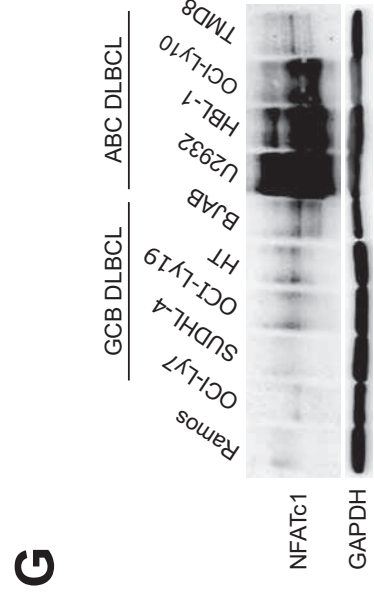
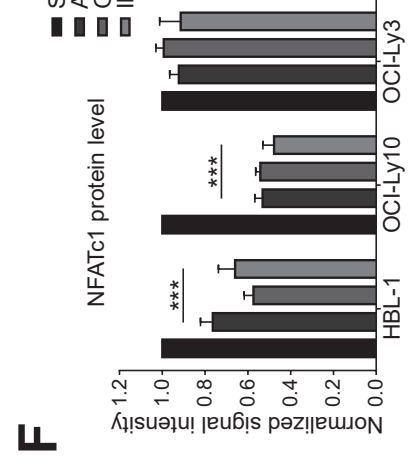
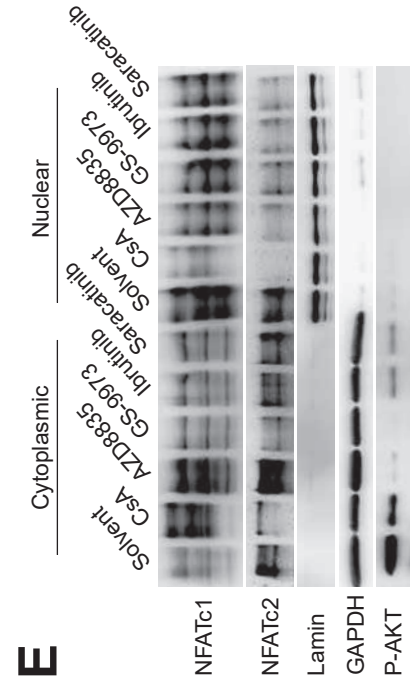
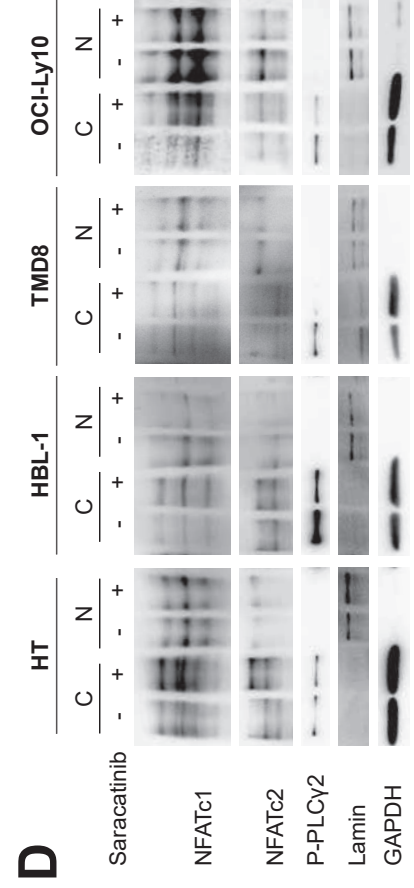
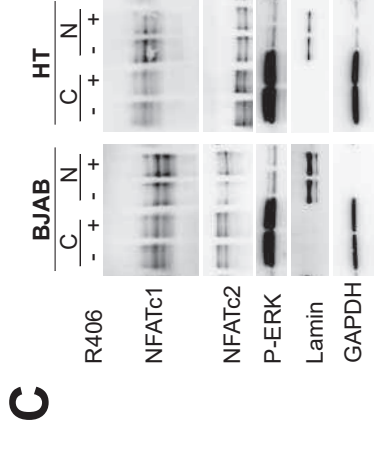
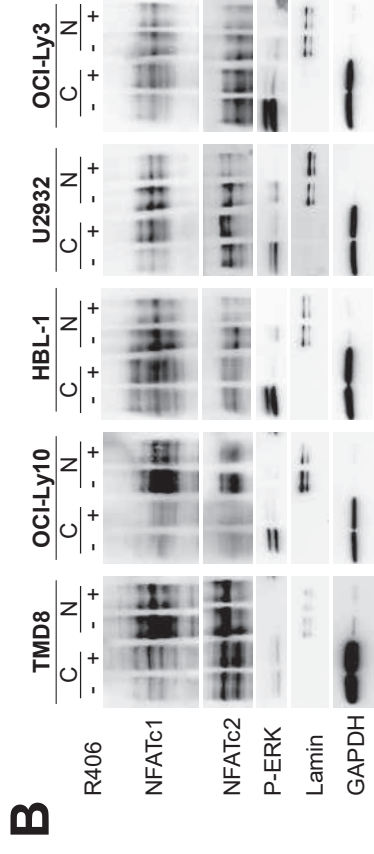
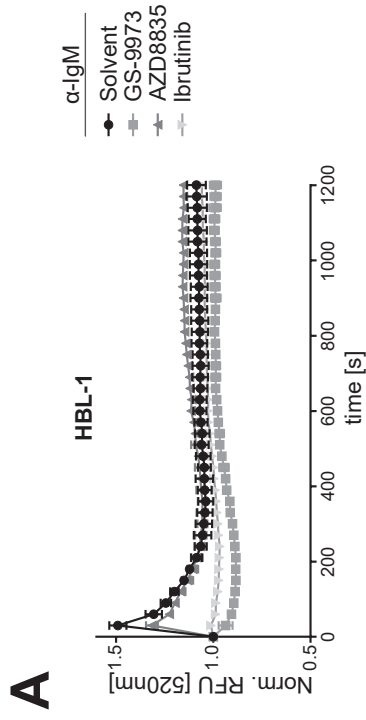
Down (alpha=0.005)	VARS	7407	valyl-tRNA synthetase
Down (alpha=0.005)	WHSC1L1	54904	nuclear receptor binding SET domain protein 3
Down (alpha=0.005)	XAF1	54739	XIAP associated factor 1
Down (alpha=0.005)	XXYL1	152002	xyloside xylosyltransferase 1
Down (alpha=0.005)	YSK4	80122	mitogen-activated protein kinase kinase kinase 19
Down (alpha=0.005)	ZAP70	7535	zeta chain of T cell receptor associated protein kinase 70
Down (alpha=0.005)	ZBTB45	84878	zinc finger and BTB domain containing 45
Down (alpha=0.005)	ZC3H10	84872	zinc finger CCCH-type containing 10
Down (alpha=0.005)	ZDHC12	84885	zinc finger DHHC-type containing 12
Down (alpha=0.005)	ZNF579	163033	zinc finger protein 579
Up (alpha=0.005)	ANXA2	302	annexin A2
Up (alpha=0.005)	ANXA5	308	annexin A5
Up (alpha=0.005)	APLF	200558	aprataxin and PNKP like factor
Up (alpha=0.005)	APOC1	341	apolipoprotein C1
Up (alpha=0.005)	ARMC9	80210	armadillo repeat containing 9
Up (alpha=0.005)	ATG12	9140	autophagy related 12
Up (alpha=0.005)	ATP5G2	517	ATP synthase membrane subunit c locus 2
Up (alpha=0.005)	BAX	581	BCL2 associated X, apoptosis regulator
Up (alpha=0.005)	BET1	10282	Bet1 golgi vesicular membrane trafficking protein
Up (alpha=0.005)	BLOC1S6	26258	biogenesis of lysosomal organelles complex 1 subunit 6
Up (alpha=0.005)	BTF3L4	91408	basic transcription factor 3 like 4
Up (alpha=0.005)	C17orf79	55352	coordinator of PRMT5 and differentiation stimulator
Up (alpha=0.005)	C19orf10	56005	myeloid derived growth factor
Up (alpha=0.005)	CBY1	25776	chibby family member 1, beta catenin antagonist
Up (alpha=0.005)	CCDC90B	60492	coiled-coil domain containing 90B
Up (alpha=0.005)	CDK2AP2	10263	cyclin dependent kinase 2 associated protein 2
Up (alpha=0.005)	CNPY3	10695	canopy FGF signaling regulator 3
Up (alpha=0.005)	CYB5R4	51167	cytochrome b5 reductase 4
Up (alpha=0.005)	DCTN5	84516	dynactin subunit 5
Up (alpha=0.005)	DGUOK	1716	deoxyguanosine kinase
Up (alpha=0.005)	DHX40	79665	DEAH-box helicase 40
Up (alpha=0.005)	DNAJB9	4189	DnaJ heat shock protein family (Hsp40) member B9
Up (alpha=0.005)	DNAJC15	29103	DnaJ heat shock protein family (Hsp40) member C15
Up (alpha=0.005)	EIF6	3692	eukaryotic translation initiation factor 6
Up (alpha=0.005)	EVI2B	2124	ecotropic viral integration site 2B
Up (alpha=0.005)	FAM48A	55578	SPT20 homolog, SAGA complex component
Up (alpha=0.005)	GEMIN2	8487	gem nuclear organelle associated protein 2
Up (alpha=0.005)	GFER	2671	growth factor, augments liver regeneration
Up (alpha=0.005)	GPNMB	10457	glycoprotein nmb
Up (alpha=0.005)	HERPUD1	9709	homocysteine inducible ER protein with ubiquitin like domain 1
Up (alpha=0.005)	KIF26A	26153	kinesin family member 26A
Up (alpha=0.005)	KLHL5	51088	kelch like family member 5
Up (alpha=0.005)	KRCC1	51315	lysine rich coiled-coil 1
Up (alpha=0.005)	LAMA5	3911	laminin subunit alpha 5
Up (alpha=0.005)	LARP7	51574	La ribonucleoprotein domain family member 7
Up (alpha=0.005)	LOC100132240	100132240	
Up (alpha=0.005)	LOC648691	648691	uncharacterized LOC648691
Up (alpha=0.005)	LOC731157	731157	uncharacterized LOC731157
Up (alpha=0.005)	LY96	23643	lymphocyte antigen 96
Up (alpha=0.005)	LYRM5	144363	electron transfer flavoprotein regulatory factor 1
Up (alpha=0.005)	NEU1	4758	neuraminidase 1

Up (alpha=0.005)	OR2AG2	338755	olfactory receptor family 2 subfamily AG member 2
Up (alpha=0.005)	OSTCP2	646567	oligosaccharyltransferase complex subunit pseudogene 2
Up (alpha=0.005)	PLA2G16	11145	phospholipase A and acyltransferase 3
Up (alpha=0.005)	PPAPDC1B	84513	phospholipid phosphatase 5
Up (alpha=0.005)	PRDX5	25824	peroxiredoxin 5
Up (alpha=0.005)	PSMB2	5690	proteasome subunit beta 2
Up (alpha=0.005)	RGS13	6003	regulator of G protein signaling 13
Up (alpha=0.005)	RGS8	85397	regulator of G protein signaling 8
Up (alpha=0.005)	RHBDL3	162494	rhomboid like 3
Up (alpha=0.005)	RNF144B	255488	ring finger protein 144B
Up (alpha=0.005)	RPL23AP42	647099	ribosomal protein L23a pseudogene 42
Up (alpha=0.005)	RPS15AP19	646819	ribosomal protein S15a pseudogene 19
Up (alpha=0.005)	RPS3	6188	ribosomal protein S3
Up (alpha=0.005)	SDHC	6391	succinate dehydrogenase complex subunit C
Up (alpha=0.005)	SFT2D1	113402	SFT2 domain containing 1
Up (alpha=0.005)	SNORA84	100124534	small nucleolar RNA, H/ACA box 84
Up (alpha=0.005)	SNX2	6643	sorting nexin 2
Up (alpha=0.005)	STARD3NL	83930	STARD3 N-terminal like
Up (alpha=0.005)	STK19	8859	serine/threonine kinase 19
Up (alpha=0.005)	THAP9	79725	THAP domain containing 9
Up (alpha=0.005)	TIPRL	261726	TOR signaling pathway regulator
Up (alpha=0.005)	TMEM38B	55151	transmembrane protein 38B
Up (alpha=0.005)	TMEM50B	757	transmembrane protein 50B
Up (alpha=0.005)	TMEM59	9528	transmembrane protein 59
Up (alpha=0.005)	TNFRSF17	608	TNF receptor superfamily member 17
Up (alpha=0.005)	VEZT	55591	vezatin, adherens junctions transmembrane protein
Up (alpha=0.005)	YIPF6	286451	Yip1 domain family member 6

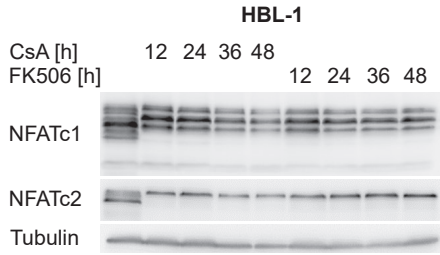
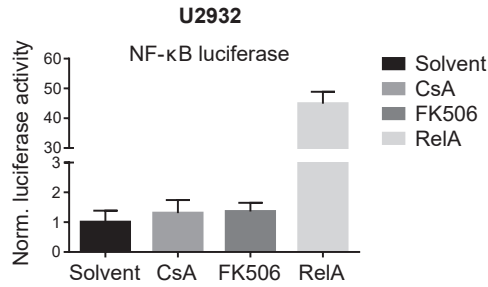
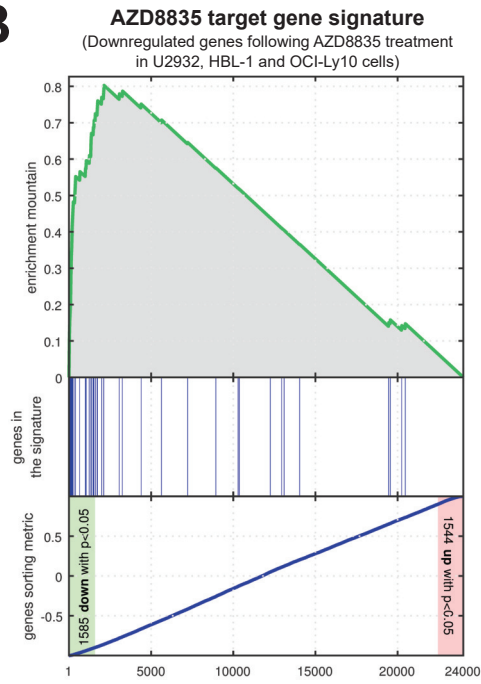
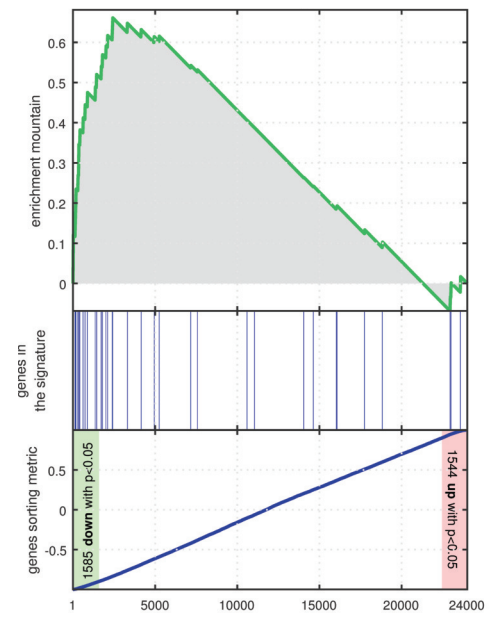
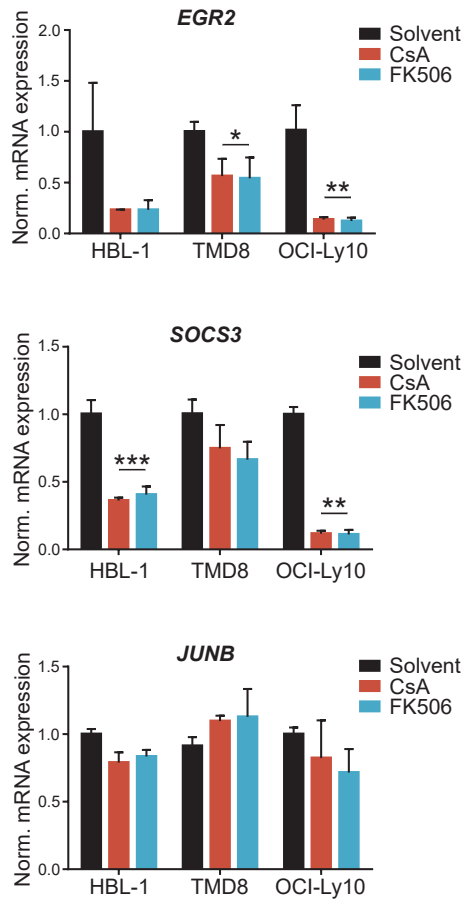
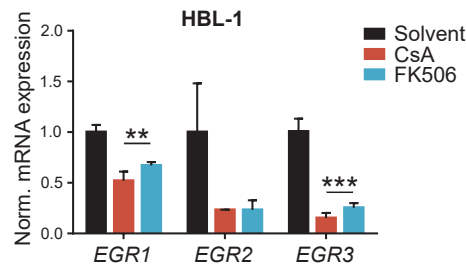
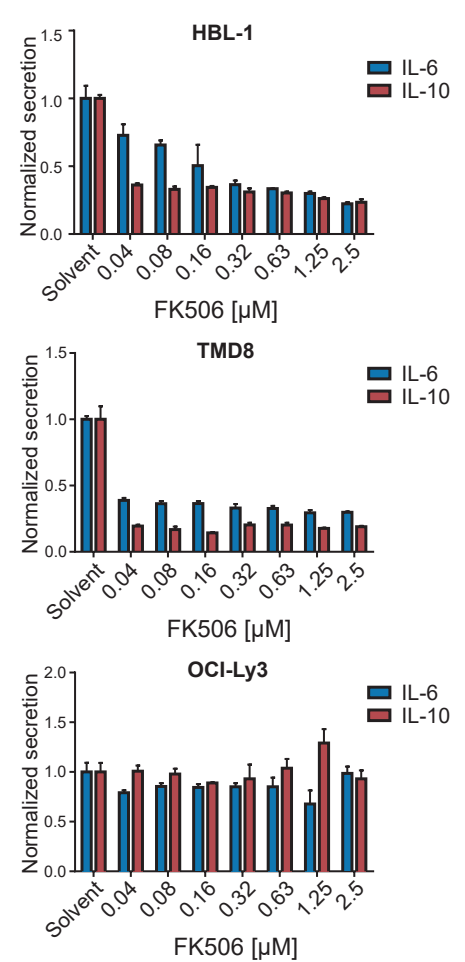


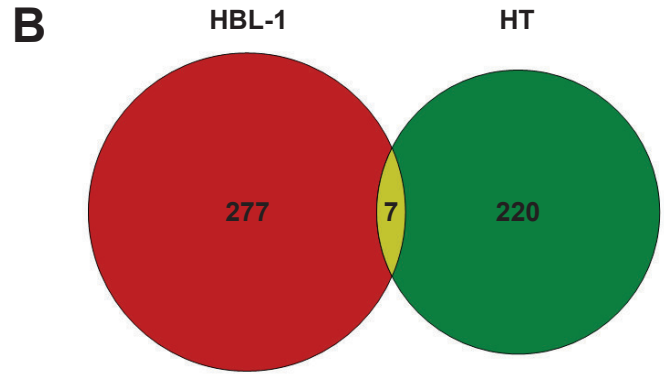
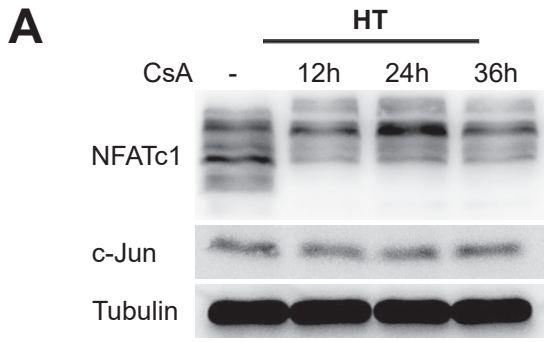
Supplemental Figure 1



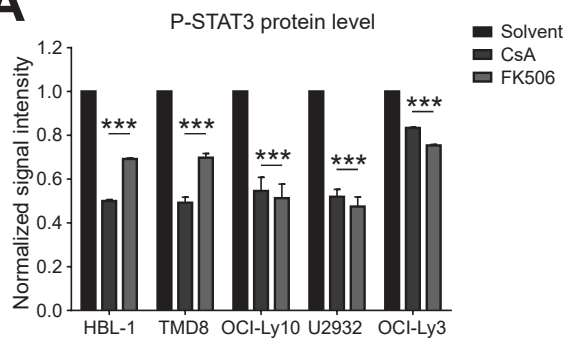
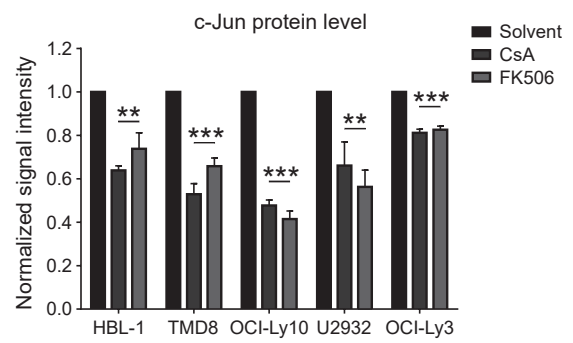
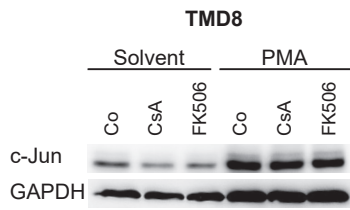
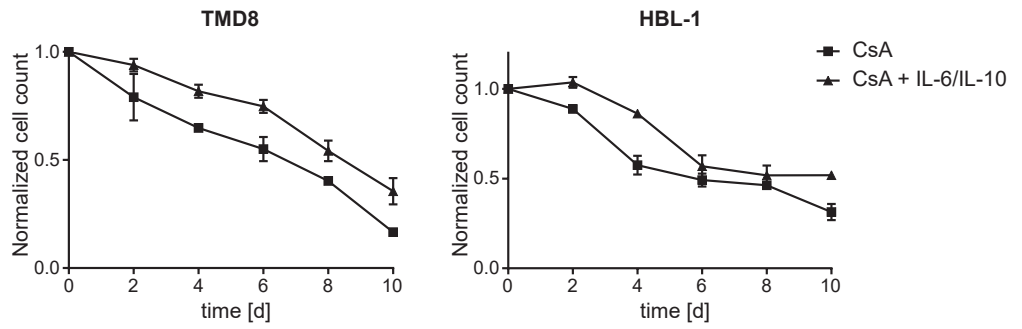
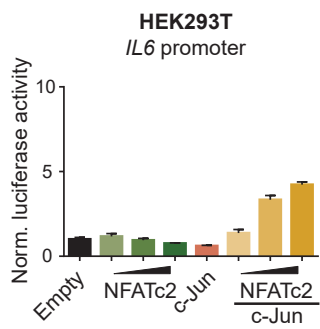


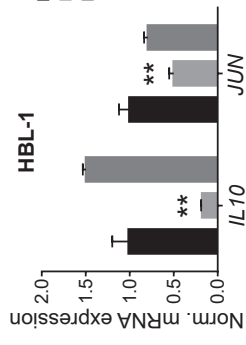
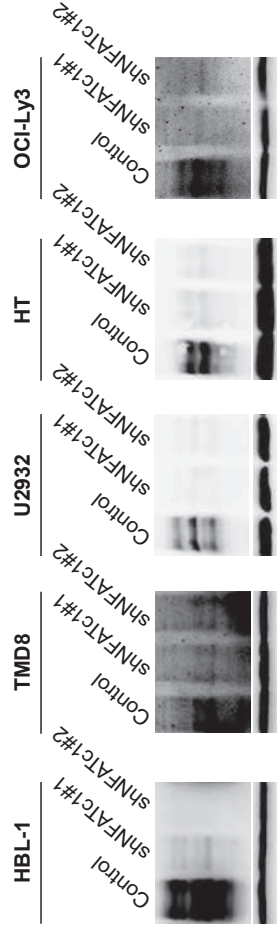
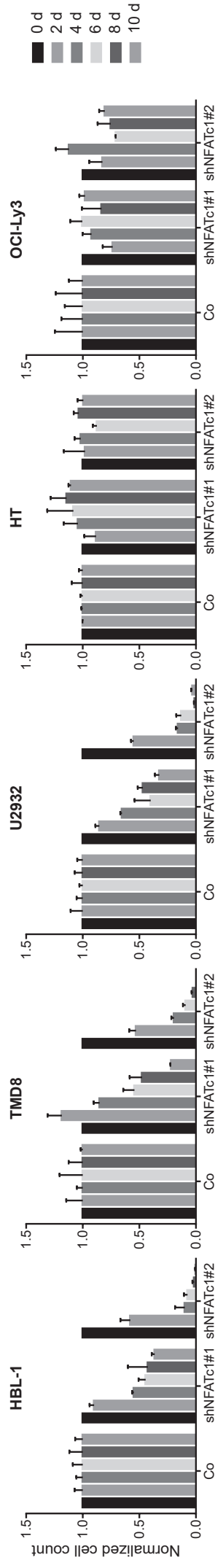
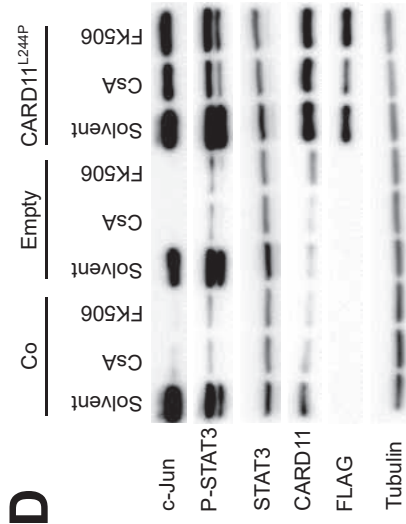
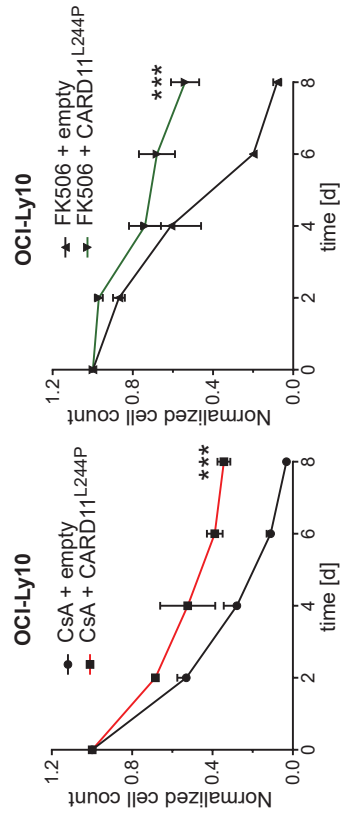
Supplemental Figure 3

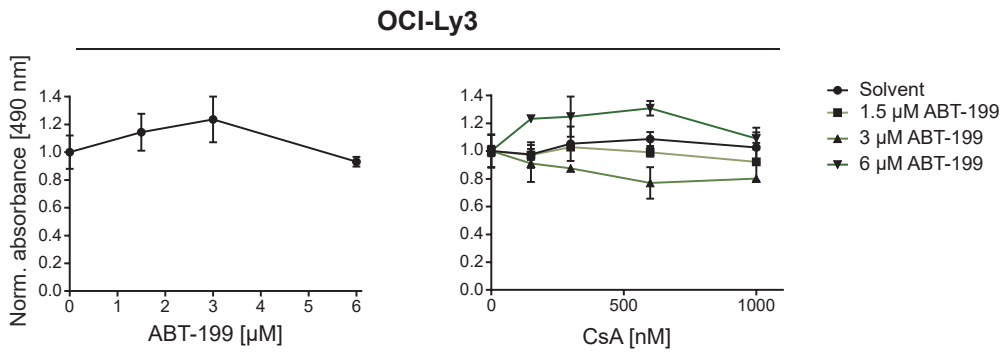
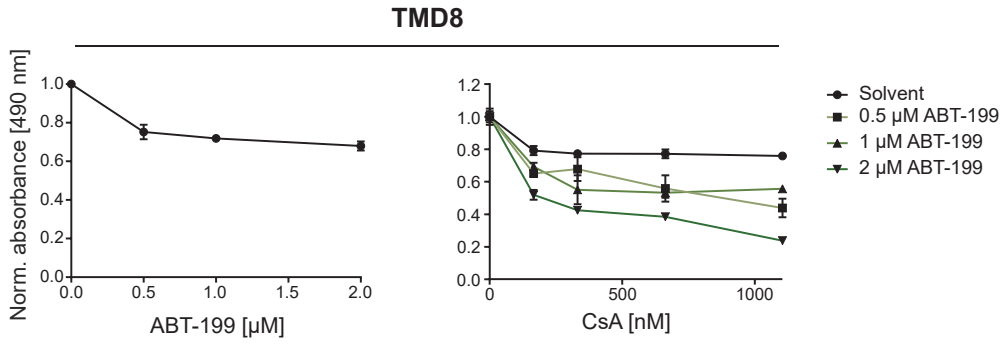
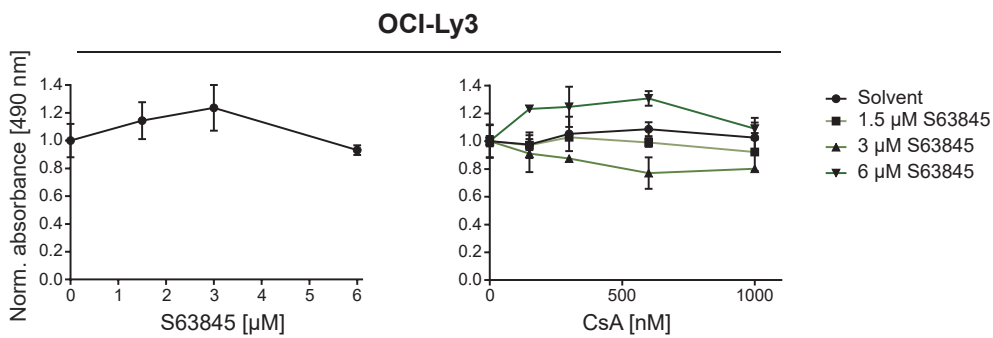
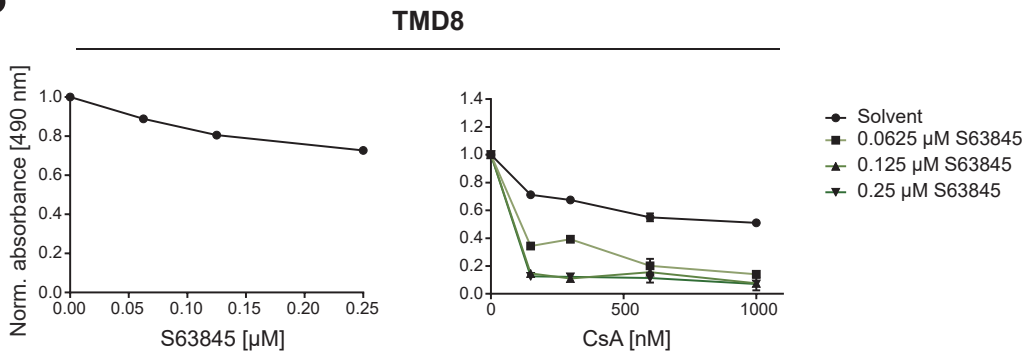
A**C****B****NF- κ B target gene signature**
(NF κ B_Up_bothOCIly3andLy10)**D****E****F**



Supplemental Figure 5

A**B****C****D****E**

A**B****C****D****E**

A**B**

Dimethyl fumarate induces ferroptosis and impairs NF- κ B/STAT3 signaling in DLBCL

Anja Schmitt¹, Wendan Xu², Philip Bucher¹, Melanie Grimm¹, Martina Konantz³, Heike Horn^{4,5}, Myroslav Zapukhlyak², Philipp Berning², Marc Brändle¹, Mohamed-Ali Jarbouï⁶, Caroline Schönfeld¹, Karsten Boldt⁶, Andreas Rosenwald⁷, German Ott⁵, Michael Grau², Pavel Klener^{8,9}, Petra Vockova^{8,9}, Claudia Lengerke^{3,10}, Georg Lenz², Klaus Schulze-Osthoff^{1,11,12}, Stephan Hailfinger^{1,2,12}

¹ Interfaculty Institute of Biochemistry, University of Tübingen, Tübingen, Germany

² Department of Medicine A, Hematology, Oncology and Pneumology, University Hospital Münster, Münster, Germany

³ Department of Biomedicine, University Hospital and University of Basel, Basel, Switzerland

⁴ Dr. Margarete Fischer-Bosch-Institute of Clinical Pharmacology and University of Tübingen, Stuttgart, Germany

⁵ Department of Clinical Pathology, Robert-Bosch-Krankenhaus, Stuttgart, Germany

⁶ Institute for Ophthalmic Research, University of Tübingen, Tübingen, Germany

⁷ Institute of Pathology, Universität Würzburg and Comprehensive Cancer Center Mainfranken (CCCMF), Würzburg, Germany

⁸ Institute of Pathological Physiology, First Faculty of Medicine, Charles University Prague, Prague, Czech Republic

⁹ First Department of Medicine, Hematology, University General Hospital and First Faculty of Medicine, Charles University Prague, Prague, Czech Republic

¹⁰ Internal Medicine II, Hematology, Oncology, Clinical Immunology and Rheumatology, Department for Internal Medicine, University Hospital Tübingen, Tübingen, Germany

¹¹ German Cancer Consortium (DKTK) and German Cancer Research Center (DKFZ),

Heidelberg, Germany

¹² Cluster of Excellence iFIT (EXC 2180) “Image-Guided and Functionally Instructed Tumor Therapies”, University of Tübingen, Tübingen, Germany

Address correspondence to Stephan Hailfinger

Dr. Stephan Hailfinger
Interfaculty Institute of Biochemistry
University of Tübingen
Auf der Morgenstelle 34
72076 Tübingen
Germany

Phone: +49-7071-29-74175

Email: Stephan.Hailfinger@uni-tuebingen.de

Key Points

- Due to low glutathione and GPX4 levels in concert with high 5-LOX expression, DMF potently induces ferroptosis in GCB DLBCL.
- In ABC DLBCL, DMF induces succination of the kinases IKK2 and JAK1, thus inhibiting NF- κ B and JAK/STAT survival signaling.

Abstract

Despite the development of novel targeted drugs, the molecular heterogeneity of diffuse large B-cell lymphoma (DLBCL) still poses a major therapeutic challenge. DLBCL can be classified into at least two major subtypes, i.e. germinal center B-cell-like (GCB) and the aggressive activated B-cell-like (ABC) DLBCL, each characterized by specific gene expression profiles and mutation patterns. Here we demonstrate a broad anti-tumor effect of dimethyl fumarate (DMF) on both DLBCL subtypes, which is mediated by the induction of ferroptosis, a form of cell death driven by the peroxidation of phospholipids. Due to high expression of arachidonate 5-lipoxygenase in concert with low glutathione and glutathione peroxidase 4 levels, DMF induces lipid peroxidation and thus ferroptosis particularly in GCB DLBCL. In ABC DLBCL cells, which are addicted to NF- κ B and STAT3 survival signaling, DMF treatment efficiently inhibits the activity of the IKK complex and JAK kinases. Interestingly, the BCL-2 specific BH3 mimetic ABT-199 and an inhibitor of ferroptosis suppressor protein 1 synergize with DMF in inducing cell death in DLBCL. Collectively, our findings identify the clinically approved drug DMF as a promising novel therapeutic option in the treatment of both GCB and ABC DLBCL.

Introduction

Diffuse large B-cell lymphoma (DLBCL) represents with approximately 30-40% of cases the most frequent malignant lymphoma in adults and is characterized by an aggressive clinical course.^{1,2} With the standard-of-care first-line multi-agent chemotherapy about 2/3 of patients show a durable response, while the remaining patients are either refractory to this first-line therapy or relapse after an initial response.³⁻⁵ Although DLBCL constitutes a clinically heterogeneous group, gene expression profiling has led to the identification of two major subtypes, termed germinal center B-cell-like (GCB) and activated B-cell-like (ABC) DLBCL.⁶⁻⁹ Whereas mutations, e.g. of *CD79*, *CARD11*, *MYD88* or *TNFAIP3*, leading to constitutive NF- κ B activation are enriched in the ABC DLBCL subtype, GCB DLBCLs frequently harbor alterations in genes, such as *EZH2*, *CREBBP* or *SGK1*, as well as *BCL2* translocations.¹⁰⁻¹⁶ Due to chronic NF- κ B activity, ABC DLBCL cells constitutively produce cytokines, such as interleukin (IL)-6 and IL-10, which promote the activation of signal transducer and activator of transcription (STAT) 3 in an auto- or paracrine manner.¹⁷ STAT3 activation is mediated by Janus kinases (JAKs), which phosphorylate STAT3 at tyrosine residues, resulting in its dimerization, nuclear translocation, DNA binding and eventually in the expression of pro-survival target genes.^{17,18}

Ferroptosis is a non-apoptotic form of cell death characterized by the accumulation of phospholipid peroxides and specific changes in cellular morphology including mitochondrial shrinkage.¹⁹⁻²¹ As the name implies, the transition metal iron plays an essential role in the initiation and execution of ferroptosis, which involve the oxidation of polyunsaturated fatty acids (PUFAs). Consequently, iron-chelating agents, such as deferoxamine (DFX), can be experimentally used in certain concentrations to impair ferroptosis. In addition to iron-dependent auto-oxidation of lipids, lipoxygenases

(LOXs), which catalyze the peroxidation of PUFAs during leukotriene biosynthesis, potentially modulate ferroptosis susceptibility, although their precise role in ferroptosis is under debate.²²⁻²⁶ Lipid peroxides can be detoxified in a glutathione (GSH)-consuming manner by the selenoprotein glutathione peroxidase 4 (GPX4), the only enzyme capable of reducing lipid peroxides in membranes.^{27,28} Well-established ferroptosis inducers either inhibit GPX4 activity directly, such as RAS-selective lethal 3 (RSL3), or indirectly (e.g. erastin) by blocking cystine import via the system x_c^- antiporter and thus decreasing glutathione synthesis.^{19,20} Even if GPX4 is inhibited, lipophilic antioxidants, such as ferrostatin-1 (Fer-1) or α -tocopherol, can prevent lipid peroxidation and hence ferroptosis induction.^{21,28}

Dimethyl fumarate (DMF) is an FDA-approved drug used as first-line treatment for relapsing-remitting multiple sclerosis (RRMS) or as a systemic medication of moderate-to-severe psoriasis. On a molecular level, the beneficial pharmacological effects of the electrophile DMF are not well understood, but several modes of action have been proposed. On the one hand, DMF is assumed to exert a neuroprotective effect by activating the nuclear factor erythroid 2-related factor 2 (Nrf2) pathway, which promotes the expression of several antioxidant proteins and thus protects against reactive oxygen species (ROS) generated during injury and inflammation.²⁹⁻³¹ On the other hand, DMF reacts directly and irreversibly with accessible cysteines of a variety of proteins involved in redox regulation, glycolysis, NF- κ B and HIF-1 α signaling.^{30,32-36}

In this study, we demonstrate a robust anti-lymphoma effect of DMF on both major DLBCL subtypes. While DMF inhibited NF- κ B and JAK/STAT3 survival signaling in ABC DLBCL, it efficiently induced ferroptotic cell death in GCB DLBCL cells. Combination of DMF treatment with inhibitors of the ferroptosis suppressor protein 1

or with BH3 mimetics synergistically induced cell death in DLBCL cells, highlighting the promising therapeutic potential of DMF in the treatment of this malignancy.

Materials and Methods

Cell culture, transfection, lentiviral and retroviral transduction, survival assays

Protocols are provided in the Supplemental Materials and Methods section.

Quantification of cellular glutathione levels

Levels of reduced (GSH) and oxidized (GSSG) glutathione in cellular lysates were quantified using the GSH/GSSG-Glo Assay (Promega) according to the manufacturer's protocol.

Analysis of lipid peroxidation

To monitor ferroptosis induction, cells were stained with the lipid peroxidation sensor BODIPY 581/591 undecanoic acid (BODIPY C11, ThermoFisher). In brief, cells were stained with 2 μ M BODIPY C11 in HBSS for 15 min at 37°C. After washing, dead cells were stained using SYTOX Blue dead cell stain (ThermoFisher). The mean fluorescence intensity (MFI) of oxidized BODIPY C11 was quantified by flow cytometry (BD LSRII) and normalized to the MFI of the reduced probe.

Cell lysis, nuclear fractionation, immunoprecipitation, mass spectrometry and immunoblotting

Protocols are provided in the Supplemental Materials and Methods section.

Gene expression profiling, GSEA and quantitative real-time PCR

Protocols are provided in the Supplemental Materials and Methods section.

Analysis of ALOX5 promoter methylation, DNA-binding of NF- κ B (TransAM) and IHC

Protocols are provided in the Supplemental Materials and Methods section.

Xenograft mouse models, zebrafish husbandry and yolk sac transplantation

Protocols are provided in the Supplemental Materials and Methods section.

Results

DMF treatment impairs DLBCL growth

Since DMF has been shown to inhibit lymphocyte activation and proliferation in multiple sclerosis or psoriasis patients, we tested its potential to impair the growth of various human lymphoma cell lines. Strikingly, the survival of most DLBCL cell lines was markedly reduced by treatment with 20 μ M of DMF (**Figure 1A-B** and **Suppl. Figure 1A-B**). DMF treatment was cytotoxic for both major DLBCL subtypes, GCB DLBCL (**Figure 1A** and **Suppl. Figure 1A, C**) and ABC DLBCL (**Figure 1B** and **Suppl. Figure 1B, D**). While mantle cell lymphoma (MCL) cell lines exhibited a similar sensitivity towards DMF (**Suppl. Figure 2A**), the growth of myeloid cell lines derived from lymphoma/leukemia patients and of various carcinoma/melanoma cell lines was not affected by treatment with 20 μ M DMF (**Figure 1C** and **Suppl. Figure 2B**). These results indicate that B-cell lymphomas, such as DLBCL and MCL, exhibit an increased DMF sensitivity.

DMF induces ferroptosis in DLBCL

To gain insights into the molecular mechanism of DMF-dependent cytotoxicity in DLBCL, we investigated the importance of the electrophilic properties of DMF for its anti-lymphoma activity. Indeed, the structural analog dimethyl succinate (DMS), which lacks the electrophilic carbon-carbon double bond of DMF, was unable to impair the growth of DLBCL cell lines (**Suppl. Figure 3A-B**). Similarly, the DMF metabolite monomethyl fumarate (MMF), which has been described as a potent agonist of the hydroxycarboxylic acid receptor 2 (HCA₂), did not interfere with the survival of DLBCL cells (**Suppl. Figure 3A-B**).^{30,37-40} In contrast, the electrophile dimethyl itaconate (DI) inhibited the growth of GCB and ABC DLBCL cell lines, when applied in concentrations that induced a similar extent of Nrf2 stabilization as 20 μ M DMF (**Suppl. Figure 3C-E**).

Next, we assessed the capacity of DMF to deplete reduced glutathione (GSH), which constitutes a major cellular antioxidant.³¹ Interestingly, we noticed that GCB DLBCL on average exhibited lower GSH levels than ABC DLBCL cell lines and that DMF very efficiently diminished the GSH pool, especially in GCB DLBCL cell lines (**Figure 2A-B**). Similar to the well-established inhibitors of GSH synthesis γ -glutamyl-cysteine synthetase inhibitor buthionine sulfoximine (BSO) and the cystine-glutamate antiporter (system x_c^-) inhibitor erastin, DMF treatment resulted in a rapid depletion of the GSH pool (**Suppl. Figure 4A**). The detoxification of lipid peroxides by GPX4 critically requires reduced glutathione. We therefore quantified lipid peroxidation using the oxidation-sensitive lipophilic probe BODIPY C11 in several DMF-treated DLBCL cell lines. Strikingly, low doses of DMF were already sufficient to induce massive lipid peroxidation in GCB DLBCL cell lines, whereas induction of lipid peroxidation in ABC DLBCL cells required higher DMF concentrations (**Figure 2C** and **Suppl. Figure 4B**). Additionally, various MCL cell lines also exhibited strong lipid peroxidation after DMF treatment, while in myeloid cell lines DMF only slightly reduced GSH levels and failed to induce lipid peroxidation (**Figure 2B** and **Suppl. Figure 4C-D**).

As lipid peroxidation constitutes a hallmark of the non-apoptotic form of cell death termed ferroptosis, we assessed the impact of iron chelators (deferrioxamine; DFX) and lipophilic antioxidants (α -tocopherol and ferrostatin-1; Fer-1) on DMF-induced lipid peroxidation and cell death. Similar to the GPX4 inhibitor RSL3, DMF induced strong lipid peroxidation, which was almost completely abolished by co-treatment with Fer-1, DFX or α -tocopherol (**Suppl. Figure 5A**). At DMF doses of 20 μ M, Fer-1 prevented the induction of cell death in GCB but not in ABC DLBCL cell lines, indicating that the GCB subtype is particularly sensitive towards DMF-dependent ferroptosis (**Figure 2D-E** and **Suppl. Figure 5B-C**). Additionally, the ferroptosis inhibitors DFX, N-acetyl-L-cysteine

(NAC) and α -tocopherol but not the broad-spectrum caspase inhibitor Q-VD protected GCB DLBCL cells from DMF-induced toxicity (**Figure 2F** and **Suppl. Figure 5D**). To understand why ABC DLBCL cells are less susceptible to DMF-induced ferroptotic cell death than GCB DLBCLs, we investigated a potential involvement of the transcription factor NF- κ B, which is constitutively activated in ABC DLBCL.⁴¹ Strikingly, overexpression of the NF- κ B member RelA in two GCB DLBCL cell lines partially reduced lipid peroxidation and cytotoxicity after DMF treatment (**Figure 2G-I** and **Suppl. Figure 6A-B**). This might be due to NF- κ B-mediated induction of various antioxidant proteins, such as thioredoxin, NAD(P)H dehydrogenase [quinone] 1, heme oxygenase-1, manganese superoxide dismutase and ferritin heavy chain.⁴² In conclusion, we could demonstrate that DMF treatment efficiently depleted the already low GSH levels in GCB DLBCL cells and induced lipid peroxidation which resulted in ferroptotic cell death.

High 5-LOX expression in GCB DLBCL correlates with ferroptosis susceptibility

To gain further insights into the molecular basis of the increased susceptibility of GCB DLBCLs to DMF-induced ferroptosis, we screened for ferroptosis-associated genes that are differentially expressed in the two major DLBCL subtypes. While we did not detect any differences in the expression of long-chain-fatty-acid-CoA ligase 4 (ACSL4), ferroptosis suppressor protein 1 (FSP1) or the system x_c^- subunit SLC7A11, ABC DLBCL cell lines exhibited increased GPX4 levels compared to their GCB counterparts (**Figure 3A** and **Suppl. Figure 7A-C**). However, the most prominent difference between the DLBCL subtypes was observed for the *ALOX5* gene, which encodes the enzyme arachidonate 5-lipoxygenase (5-LOX) (**Figure 3A-B**). Immunohistochemistry of human DLBCL biopsies revealed a strong perinuclear/nuclear staining for 5-LOX in approx. 50% of GCB DLBCLs. In contrast, nuclear localization of 5-LOX was absent in

germinal center B cells of reactive lymph nodes and only rarely observed in ABC DLBCL biopsies (**Figure 3C-D** and **Suppl. Figure 7D**).^{43,44} Similar to human biopsies, nuclear 5-LOX was also detected in GCB DLBCL cell lines (**Suppl. Figure 7E**). To shed light on the molecular basis underlying the different *ALOX5* expression patterns observed in DLBCL, we investigated the DNA methylation status of the GC-rich region surrounding the transcription start site in the *ALOX5* promoter, which also includes binding sites of the transcription factor Sp1.⁴⁵ However, we did not detect differences in the methylation status between the DLBCL subtypes (**Suppl. Figure 7F**). In contrast, three out of five GCB DLBCL cell lines exhibited reduced 5-LOX expression in response to treatment with the Sp1 inhibitor mithramycin A (**Suppl. Figure 7G**). Since there is so far no evidence for differences in Sp1 activity between the DLBCL subtypes, we investigated whether B-cell receptor (BCR) signaling, which is deregulated in ABC DLBCL, might influence 5-LOX expression. Indeed, inhibition of chronic active BCR signaling in ABC DLBCL with Src, BTK, SYK and PKC inhibitors or by *CD79A*-silencing not only reduced the expression of the NF- κ B target gene *TNFAIP3*, but also significantly increased *ALOX5* levels (**Figure 3E** and **Suppl. Figure 8A-C**). In contrast, activation of GCB DLBCL cells by BCR-crosslinking or stimulation with phorbol 12-myristate 13-acetate (PMA) and ionomycin increased *TNFAIP3* but reduced *ALOX5* expression (**Figure 3F** and **Suppl. Figure 8D-E**), suggesting that chronic active BCR signaling is involved in the suppression of 5-LOX expression in ABC DLBCL.

5-LOX promotes ferroptosis induction by DMF

To investigate the importance of 5-LOX in DMF-induced ferroptosis, we inhibited its activity with the LOX inhibitor nordihydroguaiaretic acid (NDGA) or the 5-LOX specific inhibitor zileuton. Both NDGA and zileuton efficiently protected GCB DLBCL cell lines from DMF-induced lipid peroxidation and cytotoxicity (**Suppl. Figure 9A-D**).

Unexpectedly, shRNA-mediated silencing of 5-LOX expression only slightly alleviated DMF-induced toxicity, indicating that the antioxidant properties of NDGA and zileuton rather than LOX inhibition mediate their protective role against DMF (**Suppl. Figure 9E**).²⁶ Co-treatment with 5-LOX inhibitors which lack this radical-trapping activity (i.e. CJ-13610 and CAY10649) or with an inhibitor targeting the 5-LOX-activating protein (i.e. MK-886) resulted in a partial but not complete rescue from DMF-mediated cytotoxicity (**Figure 3G** and **Suppl. Figure 9F**). Interestingly, *ALOX5* silencing increased the relative amount of GSH in DLBCL cells and reduced DMF-induced lipid peroxidation (**Figure 3H** and **Suppl. Figure 9G-H**). Moreover, cells surviving repetitive treatments with DMF exhibited reduced 5-LOX protein expression, suggesting that even though 5-LOX is not essential for DMF-induced ferroptosis, it might contribute to the general oxidative milieu within the cell and thus to ferroptosis sensitivity (**Suppl. Figure 9I**). The cell line HT, one of the few GCB DLBCL cell lines that lacks 5-LOX expression, exhibited rather high GSH levels and was resistant towards both DMF-induced lipid peroxidation and cytotoxicity (**Figure 3A-B**, **Suppl. Figure 1A** and **Suppl. Figure 10A-C**). Forced expression of FLAG-tagged 5-LOX in HT cells promoted DMF-induced lipid peroxidation, indicating that 5-LOX expression in GCB DLBCL sensitizes to DMF-mediated ferroptosis induction (**Suppl. Figure 10D-E**). Taken together, high 5-LOX expression in GCB DLBCLs was correlated with their sensitivity towards DMF-induced ferroptosis.

DMF reduces NF- κ B activity by inhibition of the IKK complex

Unlike in GCB DLBCL, low doses of DMF were unable to induce ferroptosis in ABC DLBCL cell lines (**Figure 2D-E**). To elucidate the molecular mechanism of its anti-lymphoma effect in ABC DLBCL, we quantified DMF-induced alterations in the global gene expression profile of HBL-1 cells by RNA-seq (**Figure 4A**). Gene set enrichment

analysis identified several NF- κ B gene signatures down-regulated upon DMF treatment, comprising classical NF- κ B target genes, such as *NFKBIA*, *NFKBIZ*, *TNFAIP3*, *BIRC3* and *CFLAR* (**Figure 4A-C** and **Suppl. Figure 11A-C**).

To unravel the molecular basis of the DMF-dependent NF- κ B inhibition in ABC DLBCL, we assessed the functionality of the IKK complex, an essential player in canonical NF- κ B signaling. DMF treatment impaired the phosphorylation of I κ B α at S32/36, indicating that DMF disrupted the chronic activation of the IKK complex in ABC DLBCL (**Figure 4D** and **Suppl. Figure 12A**). Consistent with the established inhibitory role of I κ B α , DMF treatment resulted in markedly decreased RelA translocation to the nucleus as well as in impaired binding of RelA and c-Rel to their consensus DNA sequence (**Figure 4E** and **Suppl. Figure 12B**).

Since many genes that were up-regulated in response to DMF treatment represented classical Nrf2-target genes (e.g. *GCLM*, *TXNRD1*, *NQO1*, *SLC7A11* and *FTH1*), we explored a potential role of Nrf2 in the DMF-dependent NF- κ B inhibition (**Figure 4A** and **Suppl. Figure 11C**). However, neither inhibition of IKK activity nor DMF-induced cytotoxicity were affected by Nrf2 silencing, demonstrating that DMF-mediated NF- κ B inhibition and cell death are independent of Nrf2 (**Suppl. Figure 12C-E**). Accordingly, even though treatment of ABC DLBCL cell lines with the DMF metabolite MMF provoked an Nrf2 response, it failed to impair I κ B α phosphorylation (**Suppl. Figure 12F**). Since the GPX4 inhibitor RSL3 as well as BSO and erastin, which deplete the GSH pool and induce a pro-oxidative state in the cell, were also unable to inhibit IKK activity in ABC DLBCL, we concluded that protein or lipid oxidation is not involved in the DMF-mediated inhibition of NF- κ B signaling (**Suppl. Figure 12G**).

Also, DMF treatment did not impair upstream BCR and MAPK signaling, as DMF treatment did not reduce the phosphorylation of BLNK, PLC γ 2, ERK1/2, AKT, JNK1/2

and p38 (**Suppl. Figure 13A**). BCR-mediated NF- κ B activation critically relies on the assembly of the CARD11-BCL10-MALT1 (CBM) complex, which upon polyubiquitination not only recruits and activates the IKK complex but also promotes MALT1 protease activation, which in turn supports NF- κ B signaling by cleavage and inactivation of negative regulators, such as A20 or RelB.^{10,46} Neither K63-linked polyubiquitination of BCL10 nor MALT1-mediated RelB cleavage were affected by DMF treatment (**Figure 4F** and **Suppl. Figure 13B-C**).

To investigate whether IKK2 was directly modified by DMF, proteins with reactive cysteines were labeled with biotin-coupled iodoacetamide (IA-biotin) and isolated using streptavidin beads. In solvent-treated cells, IKK2 was precipitated due to its accessible reactive cysteine residues. DMF treatment prior to labeling, however, significantly reduced the reaction of the iodoacetamide probe with IKK2 and KEAP1, the latter a key sensor of oxidative and electrophilic stress which harbors several reactive cysteine residues (**Figure 4G**).⁴⁷ Mass spectrometric analysis of endogenous IKK complex in DMF-treated ABC DLBCL cells identified succination of several cysteine residues, e.g. C179 in the kinase domain and C464 in the leucine zipper domain of IKK2 as well as C347 in the ubiquitin-binding domain of NEMO (**Suppl. Figure 14A-B**).⁴⁸⁻⁵⁰ Interestingly, the cysteines found to be succinated by DMF are highly conserved across various species (**Suppl. Figure 15A-B**). To evaluate the importance of C179 and C464 in DMF-dependent IKK2 inhibition, we assessed the capacity of the respective cysteine-to-alanine mutants of IKK2 to catalyze the phosphorylation of I κ B α . As previously reported, the IKK2^{C179A} mutant exhibited impaired kinase activity, while the activity of IKK2^{C464A} was similar to that of the wildtype protein.⁵⁰ Strikingly, whereas the kinase activity of wildtype IKK2 and the IKK2^{C464A} variant was reduced by DMF treatment, the residual activity of the IKK2^{C179A} mutant was resistant to DMF, indicating

that succination of this cysteine residue is key for the observed DMF-mediated IKK2 inhibition (**Figure 4H**). Collectively, DMF did not alter upstream BCR signaling or CBM complex formation in ABC DLBCL, but impaired NF- κ B signaling by inhibiting IKK activity.

Janus kinases are inhibited directly by DMF

In addition to I κ B α phosphorylation, DMF treatment simultaneously decreased the constitutive STAT3 phosphorylation observed in ABC DLBCL cell lines, indicating a direct role of DMF in STAT3 inhibition (**Figure 5A** and **Suppl. Figure 16A**). DMF treatment also strongly impaired STAT3 phosphorylation in ABC DLBCL cell lines that were activated with exogenous IL-6 or IL-10 (**Figure 5B** and **Suppl. Figure 16B-C**). Similar to IKK inhibition, neither MMF, DMS, BSO, erastin nor RSL3 affected the STAT3 phosphorylation status (**Suppl. Figure 16D-E**). As we noticed that both the steady-state and the IFN α -induced phosphorylation of STAT1 were also impaired by DMF treatment, we hypothesized that DMF might directly inhibit the activity of Janus kinases (**Figure 5A, C**). Indeed, DMF treatment decreased the auto-phosphorylation of JAK1 and TYK2 in untreated or IFN α -stimulated ABC DLBCL cell lines (**Figure 5D**). Strikingly, all Janus kinases investigated showed reduced labeling with IA-biotin upon DMF treatment, indicating a DMF-mediated succination of these kinases (**Figure 5E**). To identify which cysteine residues were modified by DMF, we immunoprecipitated JAK1 from solvent- or DMF-treated ABC DLBCL cells and analyzed potential succination events by mass spectrometry. Succination of two cysteine residues of JAK1 (i.e. C257 and C731) was detected in the DMF-treated samples only (**Figure 5F** and **Suppl. Figure 17A**). While C731 is located in the catalytically inactive protein kinase 1 domain, we hypothesized that succination of the strongly conserved C257 within the FERM domain, which mediates the interaction with cytokine receptors, may

be responsible for the observed inhibitory effect of DMF on JAK1 activity (**Figure 5F**).⁵¹ Structural analysis confirmed the accessibility of C257 and thus corroborated the idea of a direct modification of JAK1 by DMF (**Figure 5G**). Strikingly, DMF treatment indeed weakened the interaction of the alpha subunit of the IL-10 receptor (IL10RA) with wildtype JAK1 but not with the JAK1^{C257A} mutant (**Figure 5H** and **Suppl. Figure 17B**). Since the activity of the JAK1^{C257A} mutant was still partially impaired by DMF treatment, further modifications of JAK1 might contribute to the DMF-mediated inhibition of the JAK/STAT pathway (**Suppl. Figure 17C**). HBL-1 cells that were transduced to express a hyperactive STAT3 mutant (STAT3C) and treated with exogenous IL-6/IL-10 exhibited an increased resistance to DMF-mediated cytotoxicity, confirming the importance of JAK inhibition for DMF-mediated toxicity (**Figure 5I**). Collectively, our data identify the direct modification and inhibition of Janus kinases by DMF as an important mechanism for its toxicity in ABC DLBCL.

Inhibition of FSP1 and BCL-2 synergizes with DMF treatment

To investigate the therapeutic potential of DMF *in vivo*, we transplanted human DLBCL cell lines into zebrafish embryos that were subsequently incubated in solvent- or DMF-supplemented medium. A dose of 5 μ M DMF was sufficient to prevent tumor formation in more than 50% (SU-DHL-6) or 70% (DOHH2) of the animals (**Figure 6A-B**).

To further sensitize DLBCL cells to ferroptotic cell death, we pharmacologically targeted the GSH-independent ferroptosis suppressor protein 1 (FSP1).⁵² Strikingly, combined treatment with DMF and iFSP1 synergistically induced cytotoxicity in GCB DLBCL cell lines (**Figure 6C** and **Suppl. Figure 18A**). Moreover, the BCL-2 inhibitor ABT-199, but neither the PI3K inhibitor AZD8835 nor the tubulin polymerization inhibitor vincristine, showed promising combinatorial effects with DMF treatment in ABC DLBCL cells (**Figure 6D**, **Suppl. Figure 18B** and **Suppl. Figure 19A-B**). To

validate the efficacy of the combinatorial treatment with DMF and ABT-199 *in vivo*, we used HBL-1 and patient-derived (VFN-D1) xenograft mouse models. While DMF treatment alone was sufficient to significantly reduce tumor growth, combination with ABT-199 strongly enhanced its anti-lymphoma effect (**Figure 6E-F**). Collectively, our data reveal a potent anti-tumor activity of DMF both *in vitro* and *in vivo* and suggest that combined treatment of DMF with either FSP1 inhibitors or BH3 mimetics might represent a promising novel strategy in DLBCL therapy.

Discussion

Here we demonstrate a broad anti-lymphoma effect of DMF, an established, approved and even during long-term application well-tolerated drug, which is currently used for the treatment of psoriasis and RRMS.^{30,53} Although DMF treatment was found to diminish lymphocyte numbers in the blood of patients, clinical trials failed to provide any evidence for an increased susceptibility to infections, even though single cases of progressive multifocal leukoencephalopathy (PML) were reported. Despite its profound cytotoxicity in both major DLBCL subtypes, we uncovered different modes of action underlying the broad cytotoxic effect of DMF: While DMF-induced cell death in GCB DLBCL exhibits all typical hallmarks of ferroptosis, i.e. lipid peroxidation, iron dependency and protection by lipophilic radical-trapping antioxidants, DMF-induced cytotoxicity in ABC DLBCL is mainly characterized by inhibition of NF- κ B and JAK/STAT survival signaling.¹⁹⁻²¹

In contrast to BSO and erastin, which directly or indirectly inhibit glutathione synthesis, DMF potently and rapidly depletes GSH by succination.⁵⁴ Due to its distinct mode of action, DMF cannot be easily incorporated into the currently defined classes of ferroptosis inducers (FINs), which include cystine import inhibitors, GPX4 inhibitors, GPX4/CoQ₁₀ depleters and lipid peroxidation inducers. We therefore propose a new group of FINs comprising electrophilic substances that potently deplete the cellular GSH pool.⁵⁵

Our data suggest that GCB DLBCL cell lines are highly susceptible to DMF-induced ferroptosis because of their inherent low glutathione levels in concert with low GPX4 and high 5-LOX expression. The nuclear localization of 5-LOX observed in GCB DLBCL cell lines and in approximately 50% of GCB DLBCL biopsies indicates that 5-LOX may be enzymatically active, which requires its recruitment to the 5-LOX-

activating protein (FLAP) residing at the nuclear membrane.^{43,44} Even though the transcription factor Sp1 contributes to 5-LOX expression, it remains unclear why a subset of GCB DLBCL shows high 5-LOX levels. Interestingly, B-cell activation seems to play an important role in the regulation of 5-LOX expression, because PKC activity inversely correlates with 5-LOX levels. In B cells, PKC controls amongst others the activation of the transcription factors NF- κ B and AP-1, but it is still unknown whether these are involved in 5-LOX regulation.¹⁰ The contribution of Sp1 to the ferroptosis susceptibility of DLBCL also requires further clarification, particularly since it has been associated with 5-LOX and GPX4 expression.^{45,56,57} We propose a model in which 5-LOX expression is driven by constitutively active transcription factors, but simultaneously suppressed by chronic B-cell activation in ABC DLBCL cells.

Our data suggest that inhibition of classical NF- κ B and STAT3 activity, both essential for ABC DLBCL survival, contributes to the DMF-induced cytotoxicity observed in this subtype.^{10,17,41} Inhibition of NF- κ B signaling by DMF has been previously reported in various cellular systems, but the proposed modes of action differed substantially and included HO-1-mediated NF- κ B inhibition, reduction of K63-linked polyubiquitination as well as direct modification of RelA or upstream regulators of NF- κ B, such as PKC.^{32,58-61} In ABC DLBCL cell lines, DMF does not affect upstream BCR signaling, CBM complex formation, MALT1 protease activity and K63-linked polyubiquitination of BCL10. Instead, DMF directly succinates a reactive cysteine residue, which resides in the activation loop of the IKK2 kinase domain, and thus inhibits IKK activity in DLBCL cell lines.⁵⁰

In addition to its inhibitory effect on NF- κ B, we were able to demonstrate that DMF directly modifies JAKs. We propose that succination of the highly conserved C257 located in the FERM domain of JAK1 weakens the interaction between JAK1 and the

IL-10 receptor and possibly other cytokine receptors. Expression of STAT3C, a STAT3 mutant with an increased DNA-binding affinity, and its activation with exogenous IL-6/IL-10 partially protected ABC DLBCL cell lines from DMF-mediated cytotoxicity. Thus, we propose a model in which the DMF-dependent cytotoxicity observed in ABC DLBCL relies on the inhibition of both NF- κ B and JAK/STAT survival signaling.

As 40-80% of primary DLBCL samples exhibit high levels of BCL-2 expression, the combination of BH3 mimetics, such as ABT-199, with DMF represents an attractive novel therapeutic strategy.⁶²⁻⁶⁶ This seems especially promising in ABC DLBCL, since BCL-2 is an established regulator of apoptosis but not of ferroptosis. In GCB DLBCL, the simultaneous pharmacological inhibition of the GSH-GPX4 axis and the FSP1-CoQ₁₀-NAD(P)H system, which cooperate in the prevention of excessive lipid peroxidation, synergistically induced cell death.^{52,67} Thus, combining DMF with other drugs impairing the cellular capacity to detoxify lipid peroxides might provide an attractive option for the future treatment of DLBCL patients.

Acknowledgments

We thank Margot Thome, Dirk Schwarzer, Georg Zocher, Franziska Klose, Corinna Kosnopfel and Marcus Conrad for helpful discussion and technical advice. This work was supported by the Collaborative Research Center Transregio SFB/TR 156 (to SH), SFB/TR 209 (to KSO and SH), the Emmy-Noether program of the DFG and the DFG under Germany's Excellence Strategy EXC2180 (both to SH), the Deutsche Krebshilfe (to GL and SH), the Ministry of Health of the Czech Republic (grant NV19-08-00144), the Grant Agency of the Czech Republic (grant GA20-25308S) (both to PK) and the Swiss National Science Foundation (SNF, 310030 179239) (to CL).

Authorship

Contribution: AS, P. Bucher, M. Grimm, P. Berning, MB, WX, MK, MZ, MJ, CS, HH, PV and PK performed experiments; AS, MK, MZ, M. Grau, PK, KB, AR, GO, CL, KSO, GL and SH analyzed data; AS, GL and SH wrote the manuscript which all other authors commented on; AS, GL and SH conceived and coordinated the study.

Conflict-of-interest disclosure: GL declares the following potential conflict of interests with respect to the current study. GL has received honoraria from Bayer, AstraZeneca, NanoString, Celgene, Gilead, Janssen and Roche, has participated in a consulting or advisory role for AstraZeneca, Bayer, Celgene, Gilead, Janssen, NanoString and Roche, has been on a speaker's bureau for Bayer, Celgene, Gilead, Janssen and Roche, has received research funding from AQUINOX, AstraZeneca, Bayer, Celgene, Gilead, Janssen and Roche, and has had travel, accommodation and expenses reimbursed by Bayer, Celgene, Gilead, Janssen, Roche and Verastem.

References

1. Nogai H, Dorken B, Lenz G. Pathogenesis of non-Hodgkin's lymphoma. *J Clin Oncol*. 2011;29(14):1803-1811.
2. Swerdlow SH, Campo E, Pileri SA, et al. The 2016 revision of the World Health Organization classification of lymphoid neoplasms. *Blood*. 2016;127(20):2375-2390.
3. Coiffier B, Lepage E, Briere J, et al. CHOP chemotherapy plus rituximab compared with CHOP alone in elderly patients with diffuse large-B-cell lymphoma. *N Engl J Med*. 2002;346(4):235-242.
4. Pfreundschuh M, Trumper L, Osterborg A, et al. CHOP-like chemotherapy plus rituximab versus CHOP-like chemotherapy alone in young patients with good-prognosis diffuse large-B-cell lymphoma: a randomised controlled trial by the MabThera International Trial (MInT) Group. *Lancet Oncol*. 2006;7(5):379-391.
5. Gisselbrecht C, Glass B, Mounier N, et al. Salvage regimens with autologous transplantation for relapsed large B-cell lymphoma in the rituximab era. *J Clin Oncol*. 2010;28(27):4184-4190.
6. Alizadeh AA, Eisen MB, Davis RE, et al. Distinct types of diffuse large B-cell lymphoma identified by gene expression profiling. *Nature*. 2000;403(6769):503-511.
7. Lenz G, Wright G, Dave SS, et al. Stromal gene signatures in large-B-cell lymphomas. *N Engl J Med*. 2008;359(22):2313-2323.
8. Rosenwald A, Wright G, Chan WC, et al. The use of molecular profiling to predict survival after chemotherapy for diffuse large-B-cell lymphoma. *N Engl J Med*. 2002;346(25):1937-1947.
9. Wright G, Tan B, Rosenwald A, Hurt EH, Wiestner A, Staudt LM. A gene expression-based method to diagnose clinically distinct subgroups of diffuse large B cell lymphoma. *Proc Natl Acad Sci U S A*. 2003;100(17):9991-9996.
10. Grondona P, Bucher P, Schulze-Osthoff K, Hailfinger S, Schmitt A. NF-kappaB Activation in Lymphoid Malignancies: Genetics, Signaling, and Targeted Therapy. *Biomedicines*. 2018;6(2).
11. Compagno M, Lim WK, Grunn A, et al. Mutations of multiple genes cause deregulation of NF-kappaB in diffuse large B-cell lymphoma. *Nature*. 2009;459(7247):717-721.
12. Davis RE, Ngo VN, Lenz G, et al. Chronic active B-cell-receptor signalling in diffuse large B-cell lymphoma. *Nature*. 2010;463(7277):88-92.
13. Lenz G, Staudt LM. Aggressive lymphomas. *N Engl J Med*. 2010;362(15):1417-1429.
14. Lenz G, Davis RE, Ngo VN, et al. Oncogenic CARD11 mutations in human diffuse large B cell lymphoma. *Science*. 2008;319(5870):1676-1679.
15. Schmitz R, Wright GW, Huang DW, et al. Genetics and Pathogenesis of Diffuse Large B-Cell Lymphoma. *N Engl J Med*. 2018;378(15):1396-1407.
16. Chapuy B, Stewart C, Dunford AJ, et al. Molecular subtypes of diffuse large B cell lymphoma are associated with distinct pathogenic mechanisms and outcomes. *Nat Med*. 2018;24(5):679-690.
17. Lam LT, Wright G, Davis RE, et al. Cooperative signaling through the signal transducer and activator of transcription 3 and nuclear factor- κ B pathways in subtypes of diffuse large B-cell lymphoma. *Blood*. 2008;111(7):3701-3713.
18. Salas A, Hernandez-Rocha C, Duijvestein M, et al. JAK-STAT pathway targeting for the treatment of inflammatory bowel disease. *Nat Rev Gastroenterol Hepatol*. 2020;17(6):323-337.
19. Li J, Cao F, Yin HL, et al. Ferroptosis: past, present and future. *Cell Death Dis*. 2020;11(2):88.
20. Friedmann Angeli JP, Krysko DV, Conrad M. Ferroptosis at the crossroads of cancer-acquired drug resistance and immune evasion. *Nat Rev Cancer*. 2019;19(7):405-414.
21. Dixon SJ, Lemberg KM, Lamprecht MR, et al. Ferroptosis: an iron-dependent form of nonapoptotic cell death. *Cell*. 2012;149(5):1060-1072.
22. Yang WS, Kim KJ, Gaschler MM, Patel M, Shchepinov MS, Stockwell BR. Peroxidation of polyunsaturated fatty acids by lipoxygenases drives ferroptosis. *Proc Natl Acad Sci U S A*. 2016;113(34):E4966-4975.
23. Kagan VE, Mao G, Qu F, et al. Oxidized arachidonic and adrenic PEs navigate cells to ferroptosis. *Nat Chem Biol*. 2017;13(1):81-90.

24. Haeggstrom JZ, Funk CD. Lipoxygenase and leukotriene pathways: biochemistry, biology, and roles in disease. *Chem Rev.* 2011;111(10):5866-5898.
25. Friedmann Angeli JP, Conrad M. Lipoxygenases-Killers against Their Will? *ACS Cent Sci.* 2018;4(3):312-314.
26. Shah R, Shchepinov MS, Pratt DA. Resolving the Role of Lipoxygenases in the Initiation and Execution of Ferroptosis. *ACS Cent Sci.* 2018;4(3):387-396.
27. Friedmann Angeli JP, Schneider M, Proneth B, et al. Inactivation of the ferroptosis regulator Gpx4 triggers acute renal failure in mice. *Nat Cell Biol.* 2014;16(12):1180-1191.
28. Yang WS, SriRamaratnam R, Welsch ME, et al. Regulation of ferroptotic cancer cell death by GPX4. *Cell.* 2014;156(1-2):317-331.
29. Linker RA, Lee DH, Ryan S, et al. Fumaric acid esters exert neuroprotective effects in neuroinflammation via activation of the Nrf2 antioxidant pathway. *Brain.* 2011;134(Pt 3):678-692.
30. Bruck J, Dringen R, Amasuno A, Pau-Charles I, Ghoreschi K. A review of the mechanisms of action of dimethylfumarate in the treatment of psoriasis. *Exp Dermatol.* 2018;27(6):611-624.
31. Brennan MS, Matos MF, Li B, et al. Dimethyl fumarate and monoethyl fumarate exhibit differential effects on KEAP1, NRF2 activation, and glutathione depletion in vitro. *PLoS One.* 2015;10(3):e0120254.
32. Blewett MM, Xie J, Zaro BW, et al. Chemical proteomic map of dimethyl fumarate-sensitive cysteines in primary human T cells. *Sci Signal.* 2016;9(445):rs10.
33. Zhao G, Liu Y, Fang J, Chen Y, Li H, Gao K. Dimethyl fumarate inhibits the expression and function of hypoxia-inducible factor-1alpha (HIF-1alpha). *Biochem Biophys Res Commun.* 2014;448(3):303-307.
34. Gillard GO, Collette B, Anderson J, et al. DMF, but not other fumarates, inhibits NF-kappaB activity in vitro in an Nrf2-independent manner. *J Neuroimmunol.* 2015;283:74-85.
35. Vandermeeren M, Janssens S, Wouters H, et al. Dimethylfumarate is an inhibitor of cytokine-induced nuclear translocation of NF-kappa B1, but not RelA in normal human dermal fibroblast cells. *J Invest Dermatol.* 2001;116(1):124-130.
36. Kornberg MD, Bhargava P, Kim PM, et al. Dimethyl fumarate targets GAPDH and aerobic glycolysis to modulate immunity. *Science.* 2018;360(6387):449-453.
37. Hanson J, Gille A, Offermanns S. Role of HCA(2) (GPR109A) in nicotinic acid and fumaric acid ester-induced effects on the skin. *Pharmacol Ther.* 2012;136(1):1-7.
38. Hanson J, Gille A, Zwykiel S, et al. Nicotinic acid- and monomethyl fumarate-induced flushing involves GPR109A expressed by keratinocytes and COX-2-dependent prostanoid formation in mice. *J Clin Invest.* 2010;120(8):2910-2919.
39. Chen H, Assmann JC, Krenz A, et al. Hydroxycarboxylic acid receptor 2 mediates dimethyl fumarate's protective effect in EAE. *J Clin Invest.* 2014;124(5):2188-2192.
40. Tang H, Lu JY, Zheng X, Yang Y, Reagan JD. The psoriasis drug monomethylfumarate is a potent nicotinic acid receptor agonist. *Biochem Biophys Res Commun.* 2008;375(4):562-565.
41. Davis RE, Brown KD, Siebenlist U, Staudt LM. Constitutive nuclear factor kappaB activity is required for survival of activated B cell-like diffuse large B cell lymphoma cells. *J Exp Med.* 2001;194(12):1861-1874.
42. Lingappan K. NF-kappaB in Oxidative Stress. *Curr Opin Toxicol.* 2018;7:81-86.
43. Luo M, Jones SM, Peters-Golden M, Brock TG. Nuclear localization of 5-lipoxygenase as a determinant of leukotriene B4 synthetic capacity. *Proc Natl Acad Sci U S A.* 2003;100(21):12165-12170.
44. Mandal AK, Jones PB, Bair AM, et al. The nuclear membrane organization of leukotriene synthesis. *Proc Natl Acad Sci U S A.* 2008;105(51):20434-20439.
45. Radmark O, Samuelsson B. 5-Lipoxygenase: mechanisms of regulation. *J Lipid Res.* 2009;50 Suppl:S40-45.
46. Thome M, Charton JE, Pelzer C, Hailfinger S. Antigen receptor signaling to NF-kappaB via CARMA1, BCL10, and MALT1. *Cold Spring Harb Perspect Biol.* 2010;2(9):a003004.
47. Jaramillo MC, Zhang DD. The emerging role of the Nrf2-Keap1 signaling pathway in cancer. *Genes Dev.* 2013;27(20):2179-2191.

48. Zandi E, Rothwarf DM, Delhase M, Hayakawa M, Karin M. The I κ B kinase complex (IKK) contains two kinase subunits, IKK α and IKK β , necessary for I κ B phosphorylation and NF- κ B activation. *Cell*. 1997;91(2):243-252.
49. Rahighi S, Ikeda F, Kawasaki M, et al. Specific recognition of linear ubiquitin chains by NEMO is important for NF- κ B activation. *Cell*. 2009;136(6):1098-1109.
50. Byun MS, Choi J, Jue DM. Cysteine-179 of I κ B kinase beta plays a critical role in enzyme activation by promoting phosphorylation of activation loop serines. *Exp Mol Med*. 2006;38(5):546-552.
51. Villarino AV, Kanno Y, O'Shea JJ. Mechanisms and consequences of Jak-STAT signaling in the immune system. *Nat Immunol*. 2017;18(4):374-384.
52. Doll S, Freitas FP, Shah R, et al. FSP1 is a glutathione-independent ferroptosis suppressor. *Nature*. 2019;575(7784):693-698.
53. Methner A, Zipp F. Multiple sclerosis in 2012: Novel therapeutic options and drug targets in MS. *Nat Rev Neurol*. 2013;9(2):72-73.
54. Zheng L, Cardaci S, Jerby L, et al. Fumarate induces redox-dependent senescence by modifying glutathione metabolism. *Nat Commun*. 2015;6:6001.
55. Feng H, Stockwell BR. Unsolved mysteries: How does lipid peroxidation cause ferroptosis? *PLoS Biol*. 2018;16(5):e2006203.
56. Ufer C, Borchert A, Kuhn H. Functional characterization of cis- and trans-regulatory elements involved in expression of phospholipid hydroperoxide glutathione peroxidase. *Nucleic Acids Res*. 2003;31(15):4293-4303.
57. Alim I, Caulfield JT, Chen Y, et al. Selenium Drives a Transcriptional Adaptive Program to Block Ferroptosis and Treat Stroke. *Cell*. 2019;177(5):1262-1279 e1225.
58. Bellezza I, Tucci A, Galli F, et al. Inhibition of NF- κ B nuclear translocation via HO-1 activation underlies alpha-tocopheryl succinate toxicity. *J Nutr Biochem*. 2012;23(12):1583-1591.
59. Kastrati I, Siklos MI, Calderon-Gierszal EL, et al. Dimethyl Fumarate Inhibits the Nuclear Factor κ B Pathway in Breast Cancer Cells by Covalent Modification of p65 Protein. *J Biol Chem*. 2016;291(7):3639-3647.
60. McGuire VA, Ruiz-Zorrilla Diez T, Emmerich CH, et al. Dimethyl fumarate blocks pro-inflammatory cytokine production via inhibition of TLR induced M1 and K63 ubiquitin chain formation. *Sci Rep*. 2016;6:31159.
61. Nicolay JP, Muller-Decker K, Schroeder A, et al. Dimethyl fumarate restores apoptosis sensitivity and inhibits tumor growth and metastasis in CTCL by targeting NF- κ B. *Blood*. 2016;128(6):805-815.
62. Green TM, Young KH, Visco C, et al. Immunohistochemical double-hit score is a strong predictor of outcome in patients with diffuse large B-cell lymphoma treated with rituximab plus cyclophosphamide, doxorubicin, vincristine, and prednisone. *J Clin Oncol*. 2012;30(28):3460-3467.
63. Hu S, Xu-Monette ZY, Tzankov A, et al. MYC/BCL2 protein coexpression contributes to the inferior survival of activated B-cell subtype of diffuse large B-cell lymphoma and demonstrates high-risk gene expression signatures: a report from The International DLBCL Rituximab-CHOP Consortium Program. *Blood*. 2013;121(20):4021-4031; quiz 4250.
64. Johnson NA, Slack GW, Savage KJ, et al. Concurrent expression of MYC and BCL2 in diffuse large B-cell lymphoma treated with rituximab plus cyclophosphamide, doxorubicin, vincristine, and prednisone. *J Clin Oncol*. 2012;30(28):3452-3459.
65. Tsuyama N, Sakata S, Baba S, et al. BCL2 expression in DLBCL: reappraisal of immunohistochemistry with new criteria for therapeutic biomarker evaluation. *Blood*. 2017;130(4):489-500.
66. Froehlich TC, Muller-Decker K, Braun JD, et al. Combined inhibition of Bcl-2 and NF κ B synergistically induces cell death in cutaneous T-cell lymphoma. *Blood*. 2019;134(5):445-455.
67. Bersuker K, Hendricks JM, Li Z, et al. The CoQ oxidoreductase FSP1 acts parallel to GPX4 to inhibit ferroptosis. *Nature*. 2019;575(7784):688-692.

Figure legends

Figure 1. DMF treatment induces cytotoxicity in DLBCL.

GCB DLBCL (**A**), ABC DLBCL (**B**) or myeloid lymphoma/leukemia (**C**) cell lines were treated daily with DMSO or 20 μ M DMF. Cell numbers were determined as indicated and normalized to the solvent control. Error bars correspond to the mean \pm SD. Data is representative of at least three (**A-C**) independent experiments.

Figure 2. DMF treatment induces ferroptosis in DLBCL.

A) Reduced glutathione (GSH) levels were quantified in various DLBCL cell lines and normalized to the myeloid cell line THP-1. **B**) The indicated cell lines were treated with 20 μ M DMF for 2 h. The ratio of reduced (GSH) to oxidized (GSSG) glutathione was determined and normalized to the respective solvent-treated controls. **C**) Lipid peroxidation was quantified by flow cytometry using the oxidation-sensitive fluorescent probe BODIPY C11. GCB DLBCL cell lines were treated with solvent or the indicated amounts of DMF and erastin for 2 h and 8 h, respectively. **D, E**) GCB DLBCL (**D**) and ABC DLBCL (**E**) cell lines were treated with solvent, 20 μ M DMF alone or in combination with 5 μ M ferrostatin-1 (Fer-1) for 24 h (**D**) and 48 h (**E**). Cell numbers were determined and normalized to the solvent control. **F**) DOHH2 and SU-DHL-6 cells were treated with 20 μ M DMF alone or in combination with 5 μ M Fer-1, 100 μ M α -tocopherol, 100 μ M deferoxamine (DFX) or 20 μ M Q-VD. Survival was quantified by MTS assay after 24 h. **G, H**) Quantification of lipid peroxidation in DMF-treated control and FLAG-RelA overexpressing GCB DLBCL cells. The mean fluorescence intensity (MFI) of oxidized BODIPY C11 in DMF-treated cells was normalized to the MFI of the respective solvent-treated samples. **I**) DOHH2 cells expressing FLAG-RelA or control vector were counted and treated daily with 20 μ M DMF for 6 days. Cell counts were

normalized to the solvent control. Error bars correspond to the mean \pm SD. Data is representative of at least two (**A, B**) or three (**C-I**) independent experiments. Statistical significance was calculated using t-test (* $p < 0.05$, ** $p < 0.01$, *** $p < 0.001$).

Figure 3. 5-Lipoxygenase sensitizes GCB DLBCL cells to DMF-induced ferroptosis.

A) Protein expression of 5-LOX, FSP1 and system x_c^- in the indicated cell lines was visualized by immunoblot analysis. ERK1/2, Tom20 and GAPDH served as loading controls. **B)** *ALOX5* transcript levels in DLBCL or myeloid cell lines were quantified by qPCR and normalized to the expression in U937 cells. *SDHA* served as reference gene. **C)** Immunohistochemical staining of 5-LOX in human GCB and ABC DLBCL biopsies. Scale bar corresponds to 50 μ m. **D)** Quantification of nuclear 5-LOX staining in DLBCL biopsies (GCB DLBCL: $n=89$, ABC DLBCL: $n=64$). **E)** The indicated ABC DLBCL cell lines were treated with 5 μ M sotrastaurin (STN), 0.1 μ M ibrutinib, 4 μ M GS-9973 or 1 μ M dasatinib for 24 h. Transcript levels of *ALOX5* and *TNFAIP3* were quantified and normalized to the solvent control. *SDHA* served as reference gene. **F)** *ALOX5* and *TNFAIP3* mRNA expression in the indicated GCB DLBCL cell lines activated for 8 h with PMA/ionomycin (P/I). *SDHA* served as reference gene. **G)** The survival of SU-DHL-6 cells treated with 20 μ M DMF alone or in combination with 10 μ M zileuton, 2.5 μ M CJ-13610, 5 μ M CAY10649 or 10 μ M MK-886 was assessed after 24 h by MTS assay. **H)** Quantification of lipid peroxidation in DMF-treated control and *ALOX5*-silenced DOHH2 cells. The mean fluorescence intensity (MFI) of oxidized BODIPY C11 in DMF-treated cells was normalized to the MFI of the respective solvent-treated samples. Error bars correspond to the mean \pm SD. Data is representative of at least two (**E**) or three independent experiments (**A-B, F-H**). Statistical significance was calculated using t-test (** $p < 0.01$, *** $p < 0.001$).

Figure 4. DMF potently inhibits IKK activity.

A) Heatmaps of differentially expressed genes in HBL-1 cells treated with DMF for 12, 24, 36 and 48 h compared to the solvent control. Gene expression changes are depicted according to the color scale. **B)** Gene set enrichment analysis identified a gene set describing NF- κ B targets to be down-regulated by DMF treatment. **C)** The indicated ABC DLBCL cell lines were treated with solvent or 20 μ M DMF for 6 h. Transcript levels of *TNFAIP3*, *CD40*, *BIRC3* and *NFKBIA* were quantified by qPCR. Expression of DMF-treated cells was normalized to the respective solvent control. *SDHA* served as reference gene. **D)** ABC DLBCL cell lines were treated with 40 μ M DMF for 4 h. S32/36 phosphorylation of I κ B α was visualized by immunoblot analysis. GAPDH served as loading control. **E)** After treatment with either solvent or DMF for 16 h, nuclear fractions were isolated and binding of the NF- κ B members RelA, c-Rel and p50 to their consensus nucleotide sequence was quantified by TransAM assay. **F)** HBL-1 cells were treated with the indicated DMF concentrations or with the MALT1 inhibitor LVSR-fmk (2 μ M) for 4 h in combination with the proteasome inhibitor MG-132 (5 μ M) 90 min prior to cell lysis. MALT1-mediated RelB cleavage was visualized by immunoblot analysis. GAPDH served as loading control. **G)** HBL-1 cells were treated with solvent, 40 μ M DMF or 40 μ M DMS for 4 h. After lysis, proteins containing reactive cysteine residues were labeled with biotin-coupled iodoacetamide (IA-biotin) and subsequently pulled-down with streptavidin (SA) agarose. The accessibility of cysteine residues in IKK2 and KEAP1 was analyzed by immunoblotting. **H)** HEK293T cells were transfected with the indicated IKK2 constructs, treated for 1 h with solvent or DMF and analyzed for I κ B α phosphorylation by immunoblotting. GAPDH served as loading control. Data is representative of at least two (**E**, **G**) or three independent experiments (**C-D**, **F**, **H**). Statistical significance was calculated using t-test (* p < 0.05, ** p < 0.01).

Figure 5. DMF impairs the activity of Janus kinases.

A) The ABC DLBCL cell line OCI-Ly10 was treated with 40 μ M DMF for the specified times and the phosphorylation of STAT3, STAT1 and I κ B α was assessed by immunoblot analysis. GAPDH served as loading control. **B, C)** ABC DLBCL cell lines were treated with solvent, 40 μ M DMF and/or 3 ng/ml recombinant human IL-6 (**B**) or 1 ng/ml IFN α (**C**), as indicated. Phosphorylation of STAT1/3 was visualized by immunoblot analysis. GAPDH served as loading control. **D)** Analysis of JAK1 and TYK2 auto-phosphorylation in solvent-, IFN α - and/or DMF-treated ABC DLBCL cell lines. Arrowhead indicates phosphorylated TYK2 (P-TYK2). GAPDH served as loading control. **E)** HBL-1 cells treated with solvent, 40 μ M DMF or 40 μ M DMS were lysed and reactive cysteine-containing proteins were labeled with biotin-coupled iodoacetamide (IA-biotin), isolated using streptavidin (SA) agarose and analyzed by immunoblotting. **F)** Schematic representation of JAK1 domain structure including FERM domain, Src homology 2 (SH2) domain and kinase domains. Alignment of JAK1 sequences surrounding the conserved C257 from various species. **G)** Using PDB entry 5IXI, human JAK1 was pictured around the modified cysteine residue (C257) to emphasize its solvent accessibility. The sulfur atom of the cysteine side chain is marked by a pink sphere. The protein chain (grey) is shown in cartoon representation. The close proximity of C257 to the receptor (dark blue) binding site is shown. **H)** HEK293T cells were transiently transfected with V5-tagged IL-10 receptor (alpha subunit, IL10RA-V5) alone or in combination with Strep-tagged JAK1. 24 h after transfection, cells were treated with solvent or DMF for 1 h, lysed and JAK1 was pulled-down using Strep-Tactin beads. The interaction between IL10RA-V5 and JAK1-Strep was visualized by immunoblot analysis. **I)** HBL-1 cells expressing control vector, FLAG-RelA or FLAG-STAT3C were treated daily with solvent or 20 μ M DMF in combination with

recombinant human IL-6 and IL-10 (3 ng/ml each), as indicated. Cell numbers were determined after 48 h and normalized to the respective controls lacking DMF. Data is representative of at least two (**E, I**) or three independent experiments (**A-D, H**). Statistical significance was calculated using t-test (** $p < 0.01$).

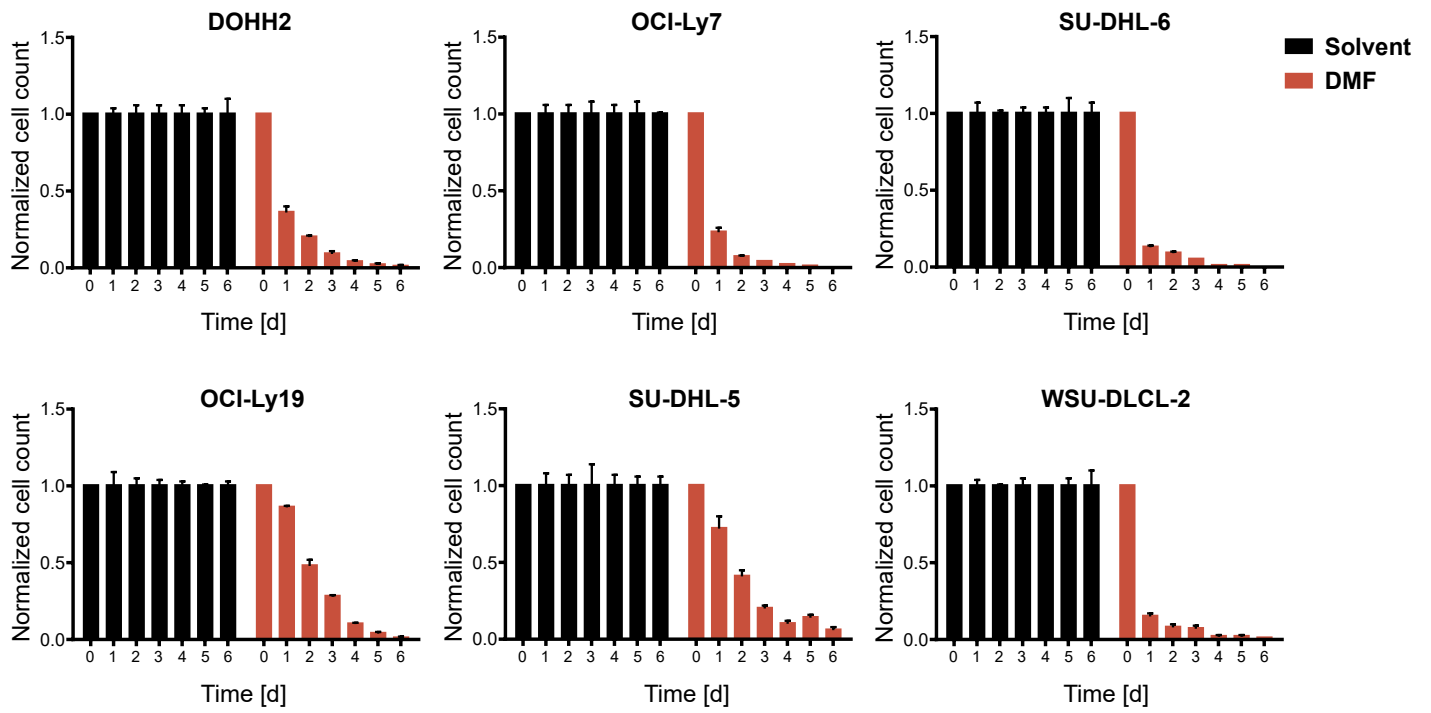
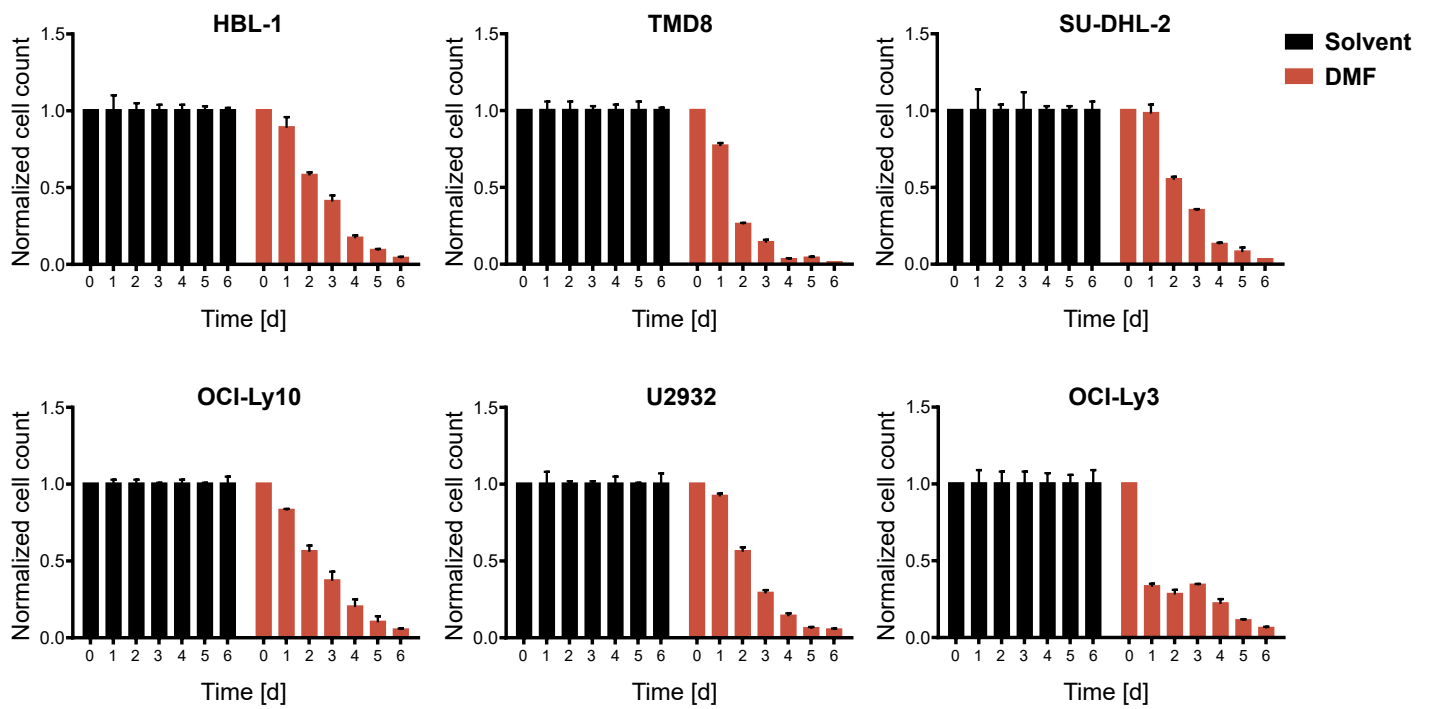
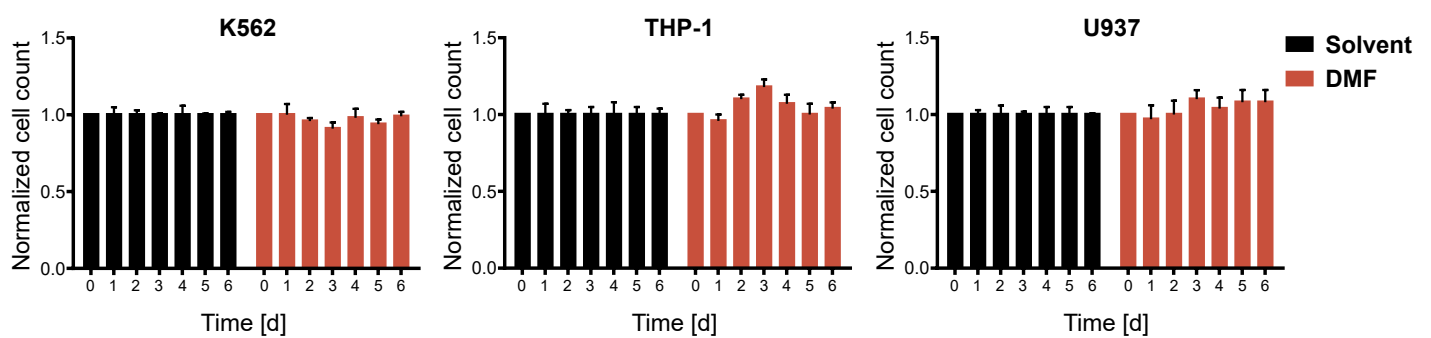
Figure 6. Inhibition of FSP1 and BCL-2 synergizes with DMF treatment.

A) SU-DHL-6 and DOHH2 cells were transplanted into zebrafish embryos. Tumor formation in animals treated with either solvent or 5 μ M DMF was quantified by microscopy after 3 d ($n \geq 21$). DMF treatment significantly reduced the frequency of tumor-bearing animals ($p=0.001$ for SU-DHL-6, $p=0.043$ for DOHH2).

B) Representative images of transplanted zebrafish embryos after solvent or DMF treatment. The respective tumor cells were fluorescently labeled and visualized by microscopy. The pictures on the right represent magnified sections of the zebrafish embryos. Scale bar in the lower right corner corresponds to 100 μ m.

C, D) SU-DHL-6 or HBL-1 cells were treated with DMF alone (top panels) or in combination with either the FSP1 inhibitor iFSP1 (**C**) or ABT-199 (**D**) (bottom panels). Cell survival was quantified by MTS assay after 24 h (**C**) or 72 h (**D**). The combination index (CI) for DMF and iFSP1 in SU-DHL-6 is ≤ 0.55 and for DMF and ABT-199 in HBL-1 ≤ 0.75 .

E, F) HBL-1 (**E**) or VFN-D1 patient-derived (**F**) xenograft mice were treated either with vehicle, ABT-199, DMF or the combination of ABT-199 and DMF, as indicated. Tumor volume was quantified by caliper measurements up to 14 days after start of the treatment. Each group consists of at least 7 animals. Statistical significance was calculated by the comparison of each treatment group to the vehicle control (* $p < 0.05$, *** $p < 0.001$). Data is representative of at least three independent experiments (**A-D**).

A**B****C****Figure 1**

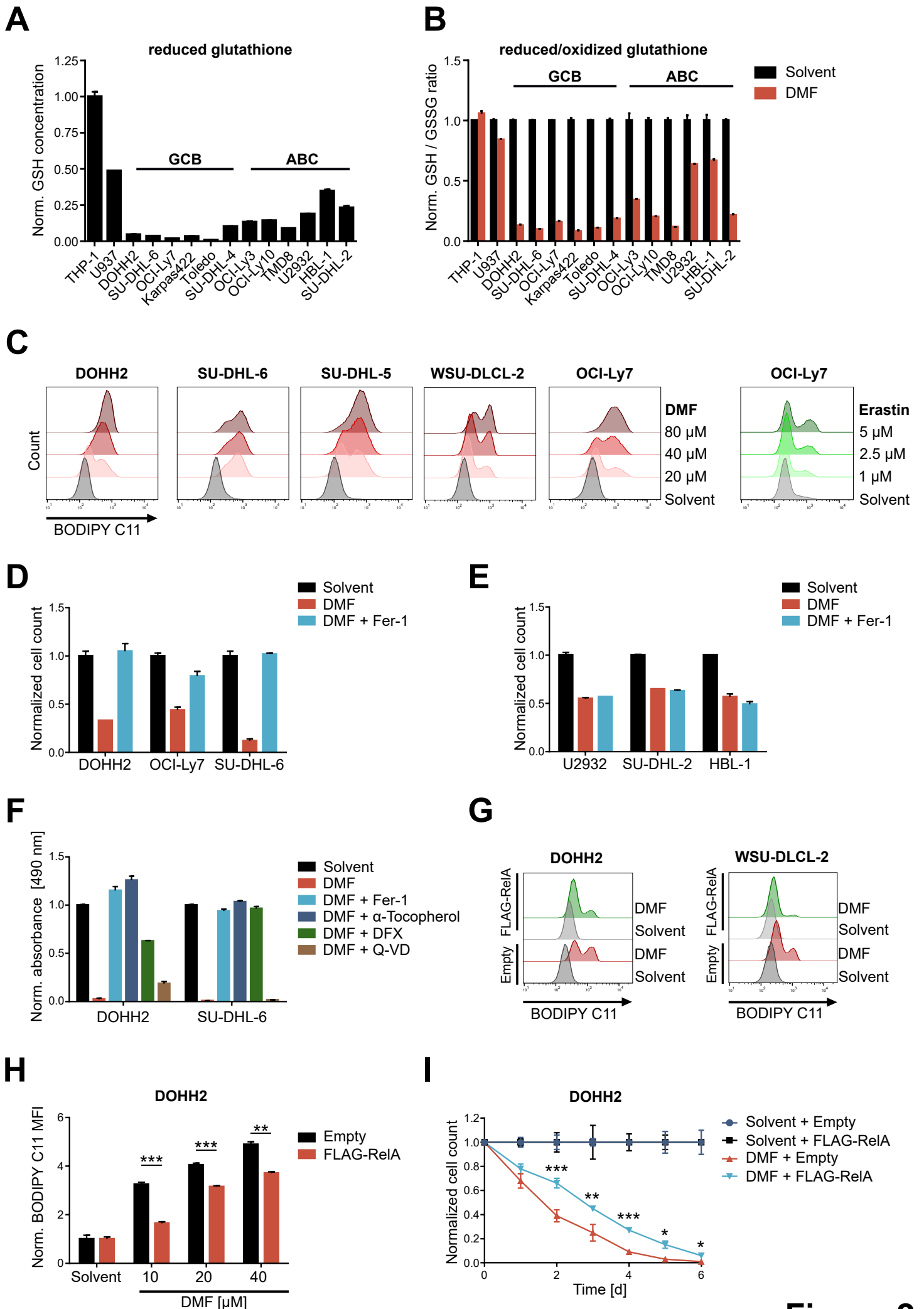


Figure 2

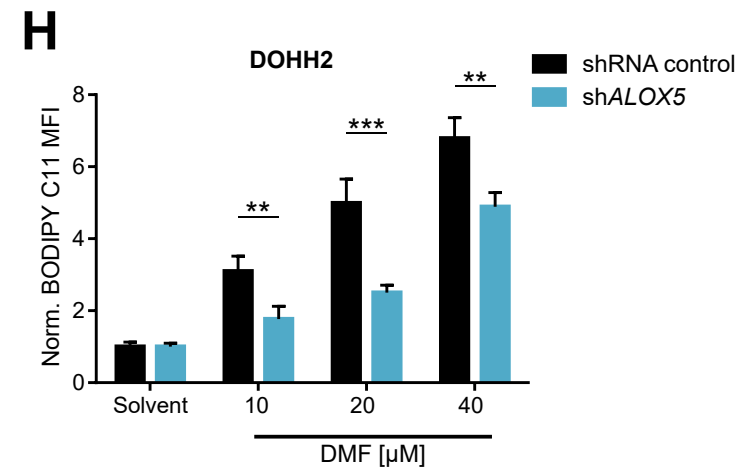
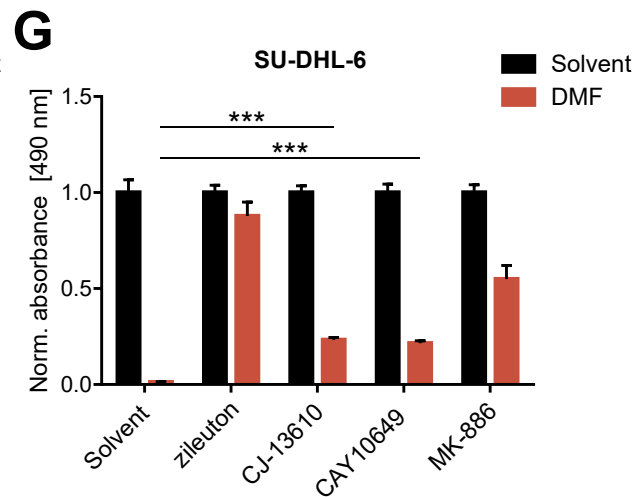
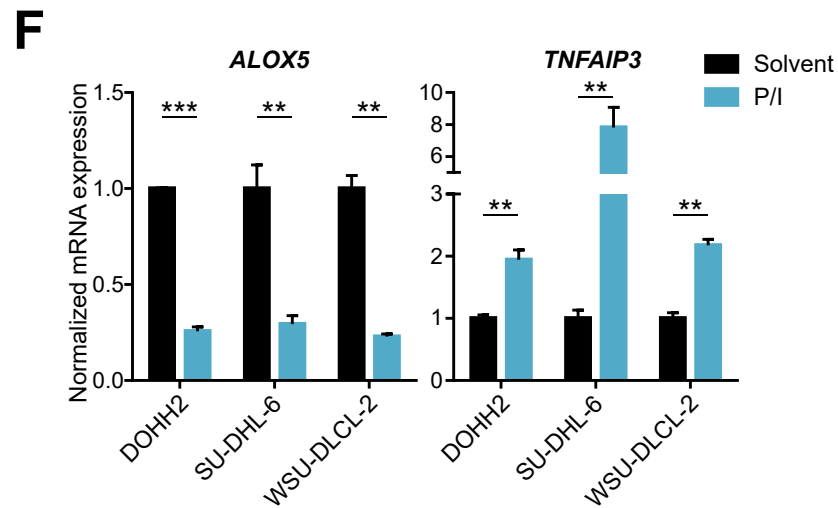
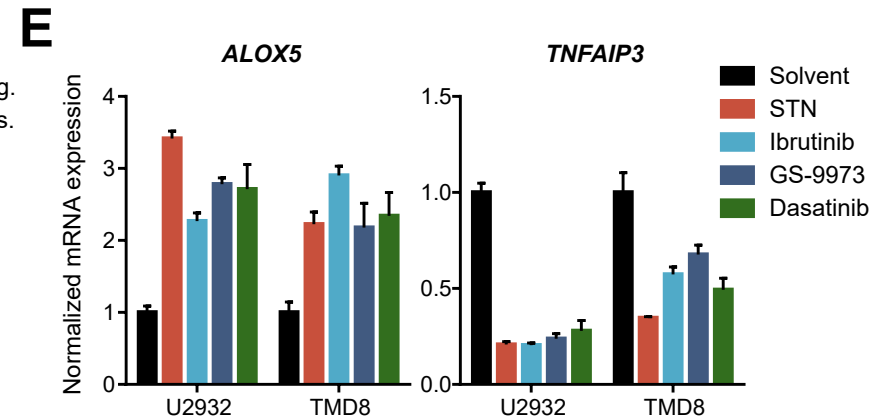
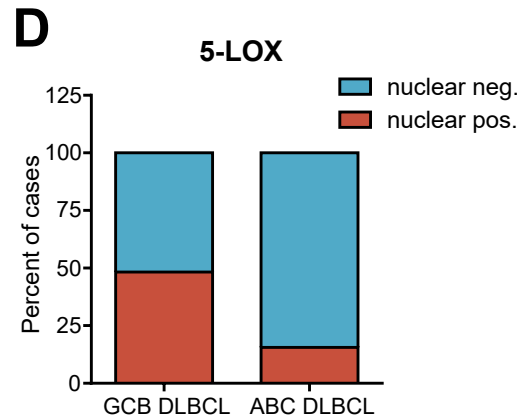
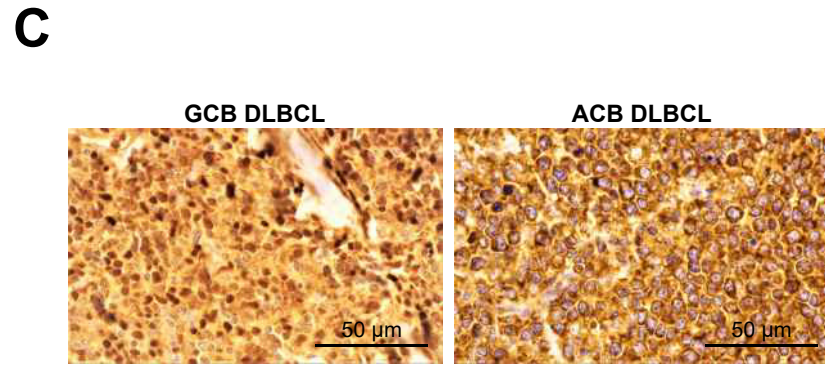
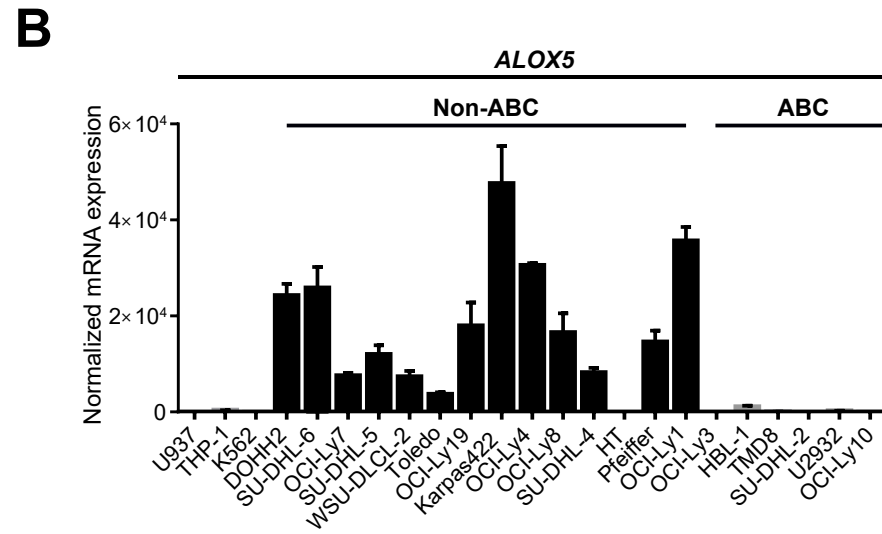
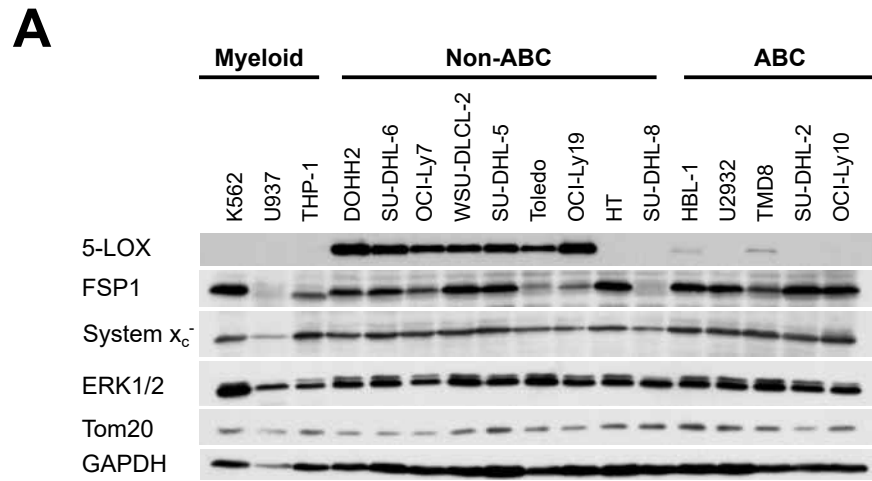


Figure 3

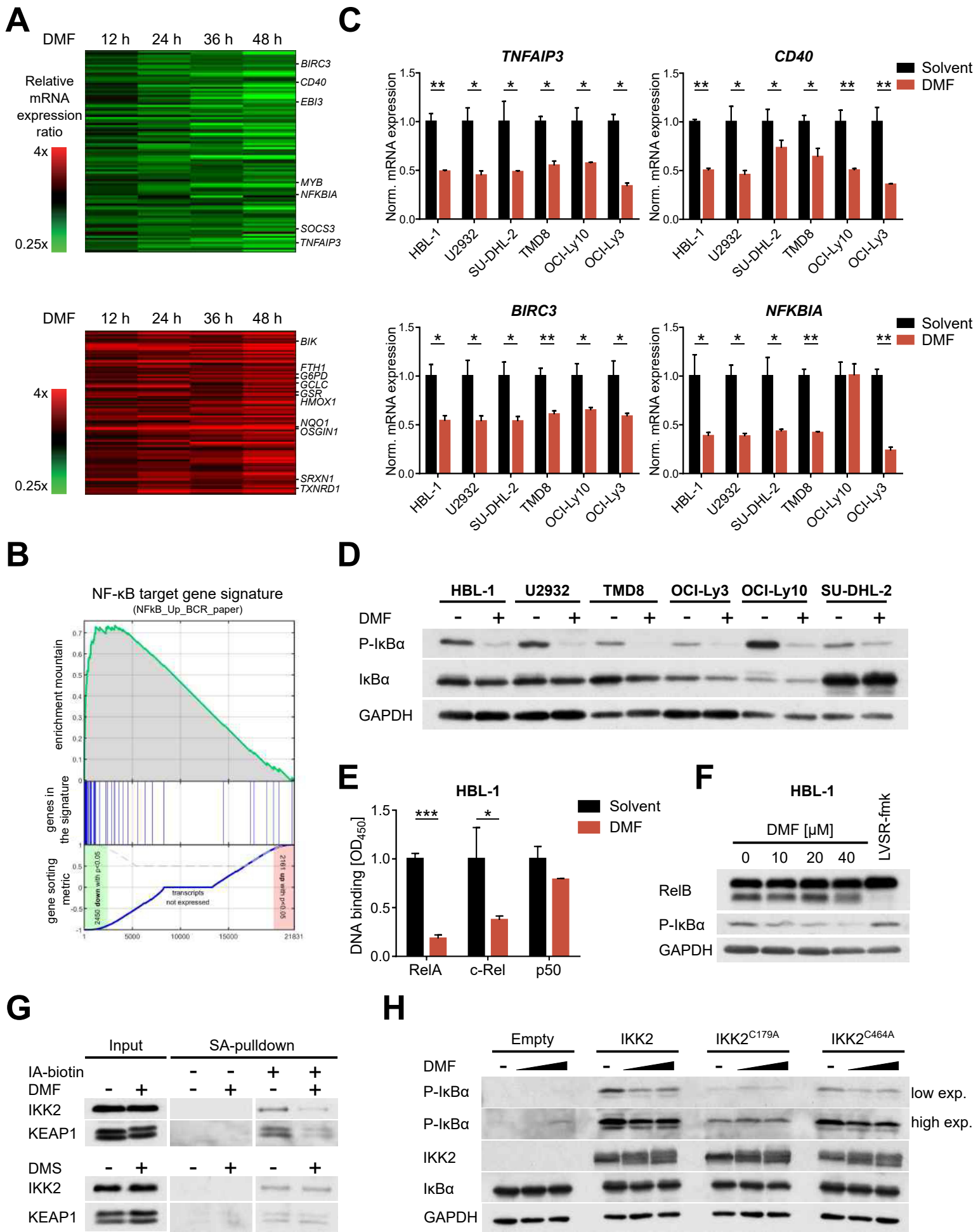
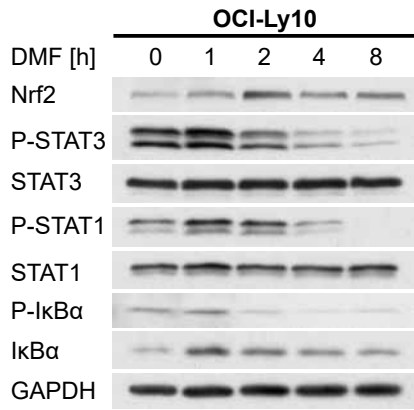
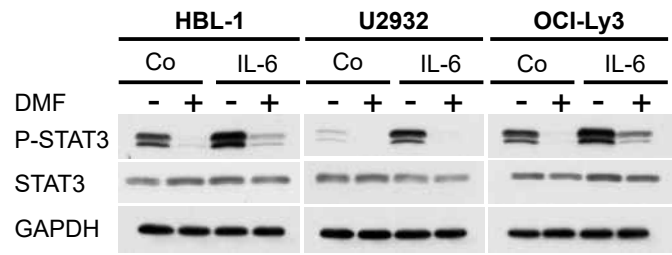
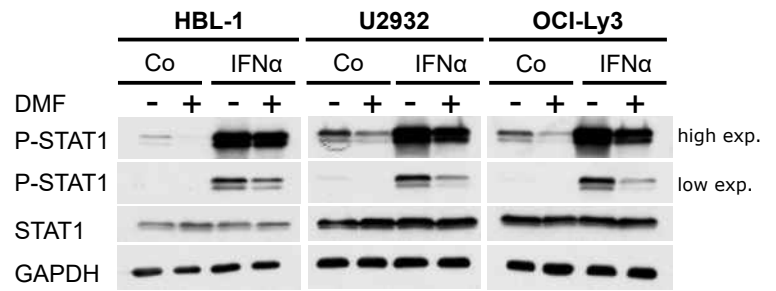
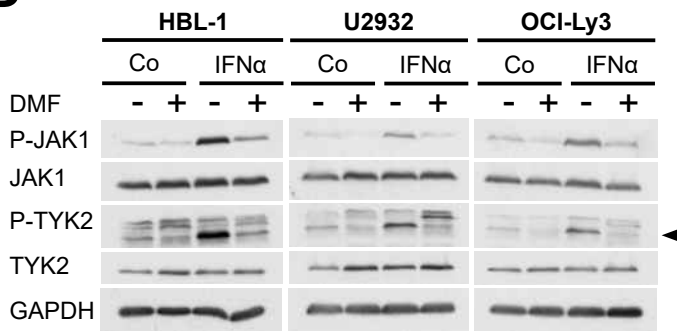
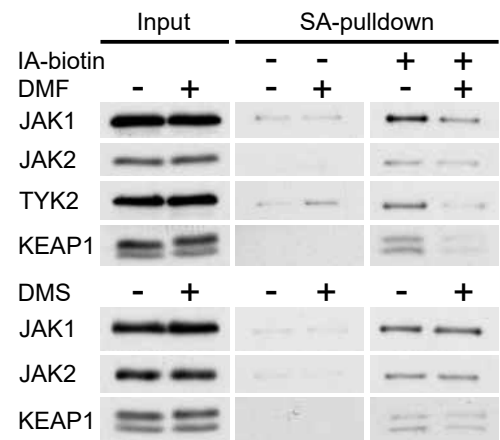
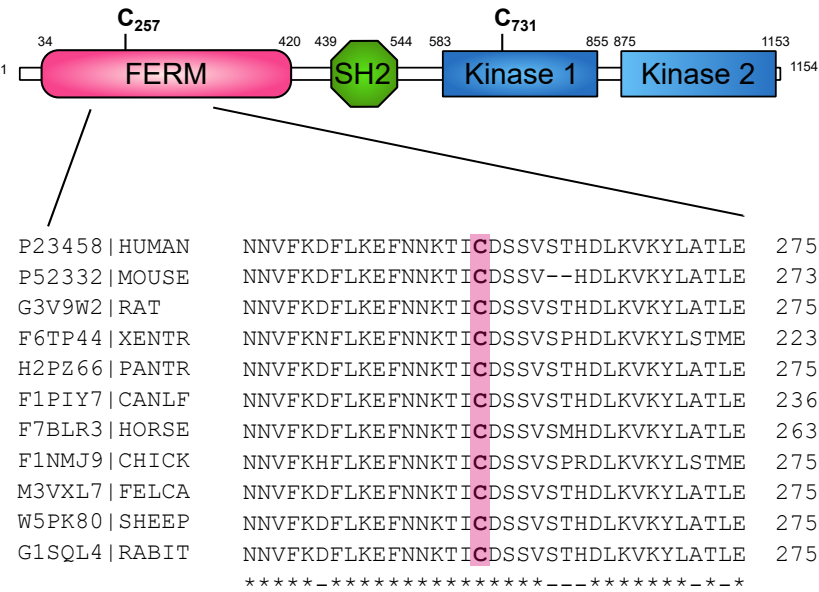
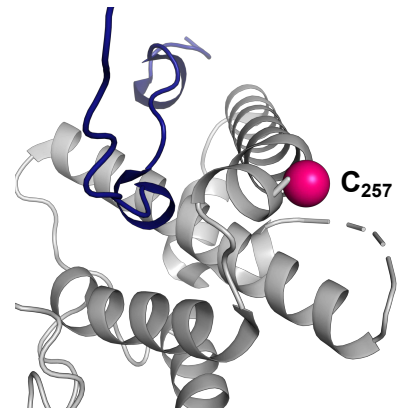
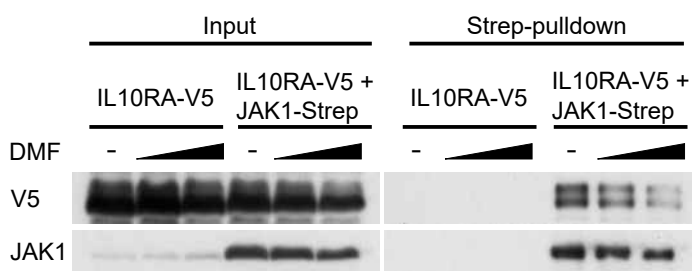
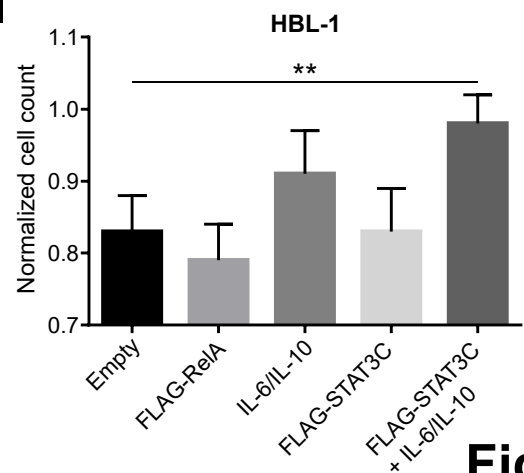


Figure 4

A**B****C****D****E****F****G****H****I****Figure 5**

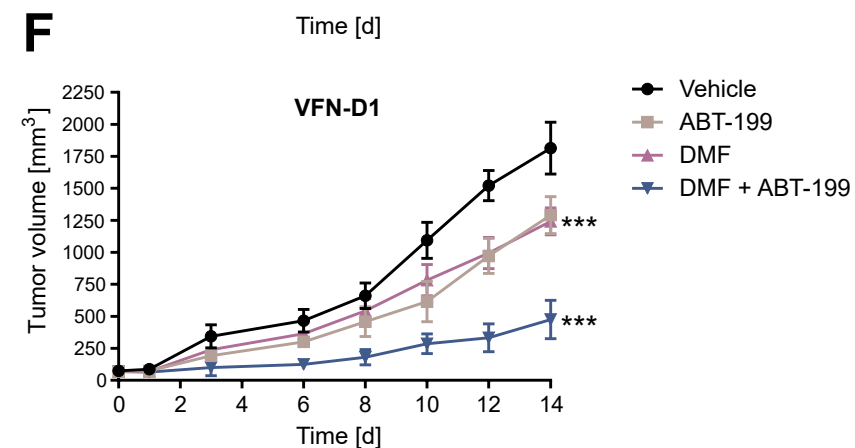
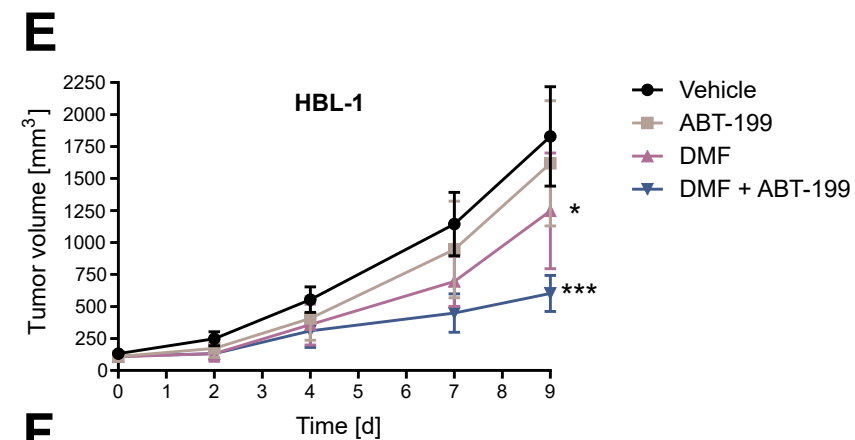
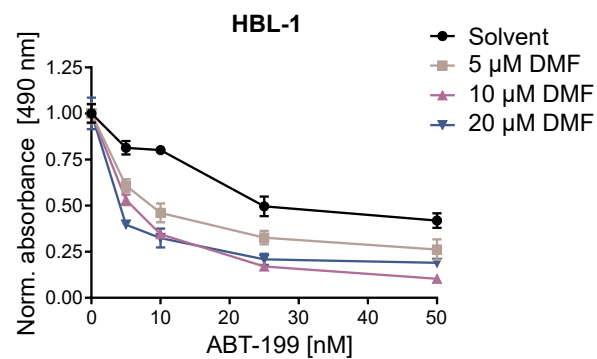
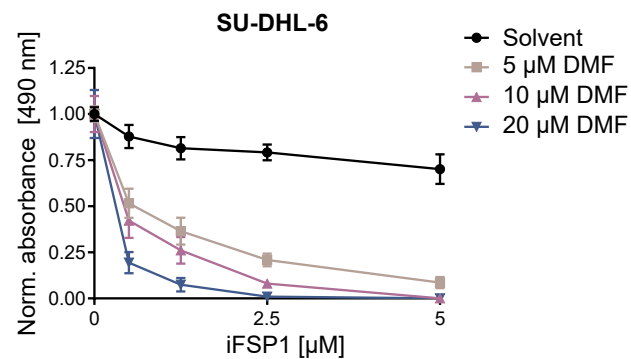
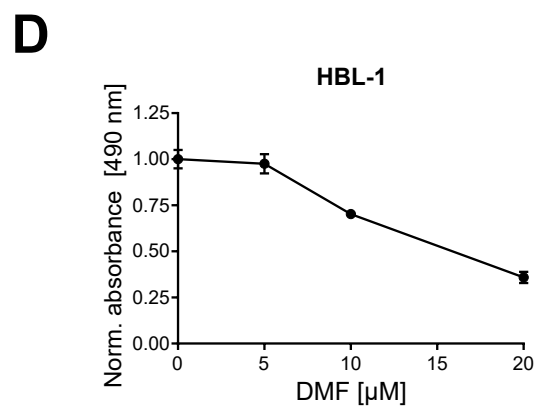
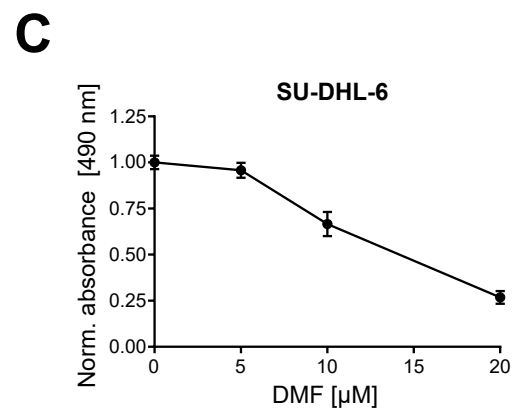
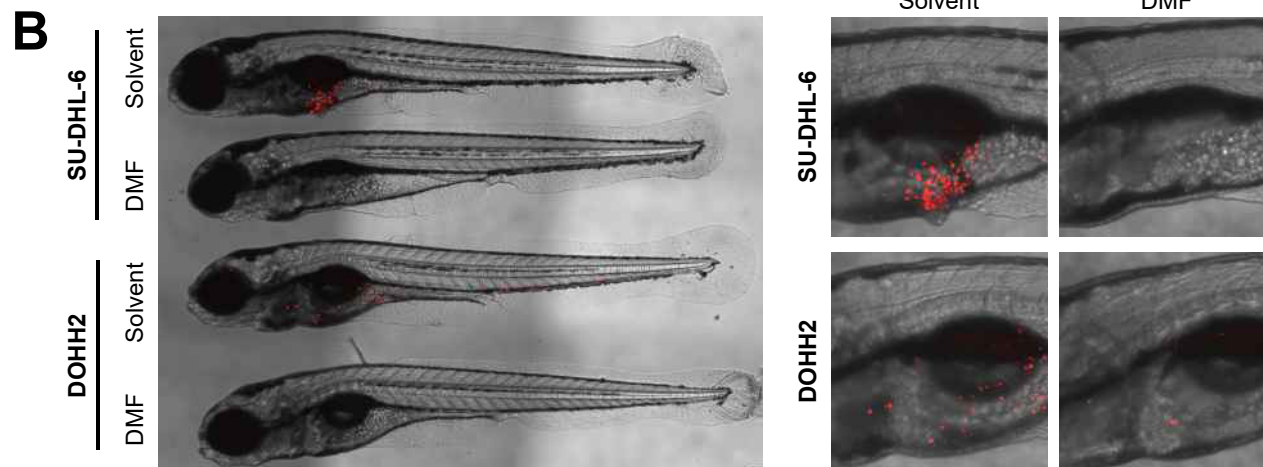
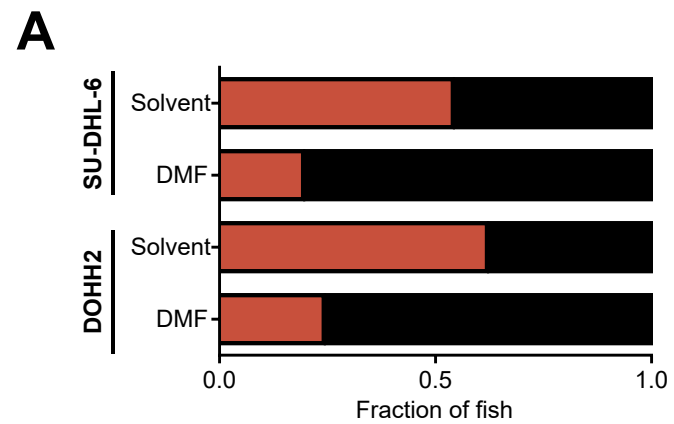
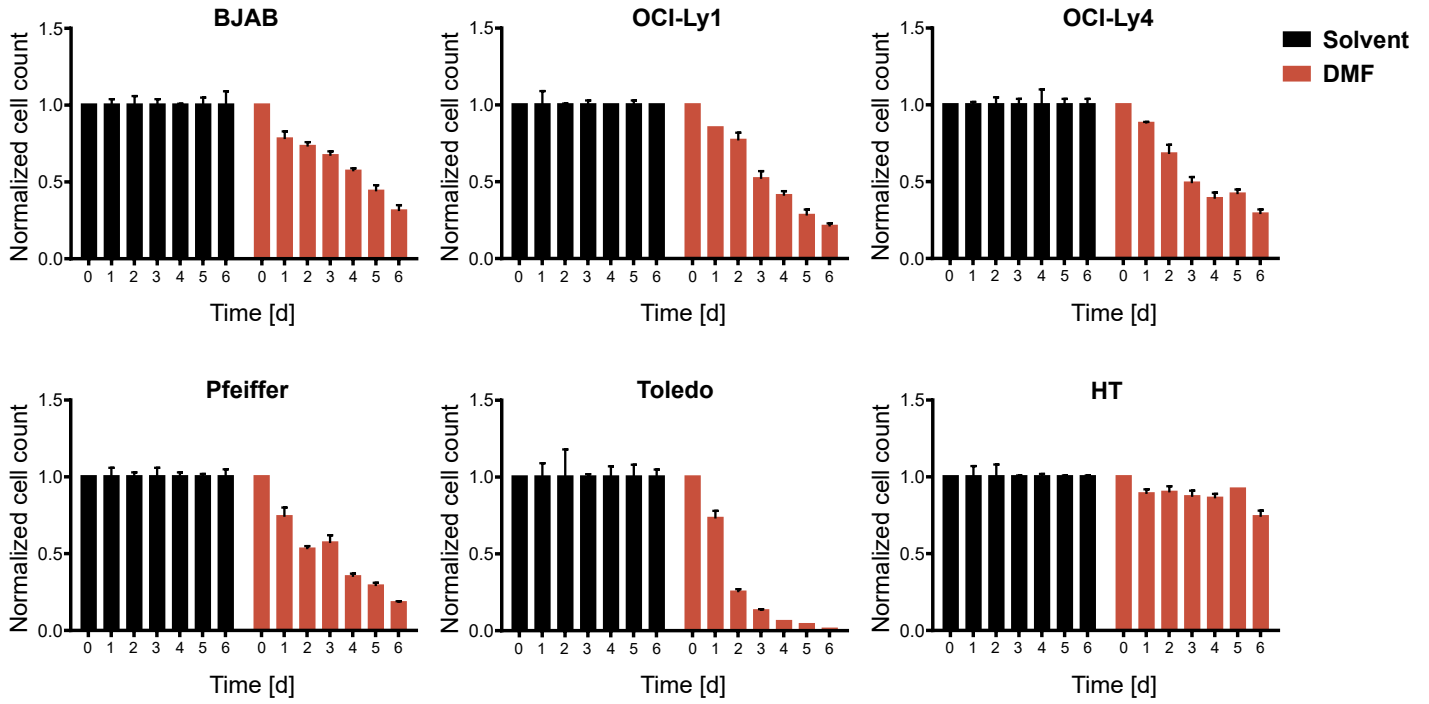
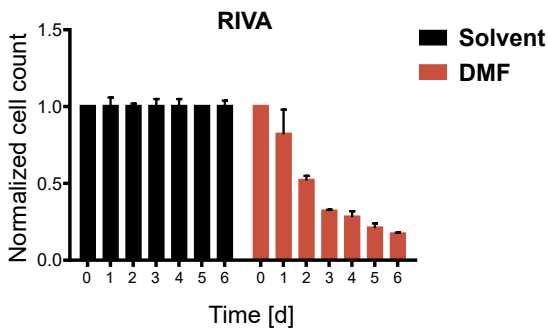
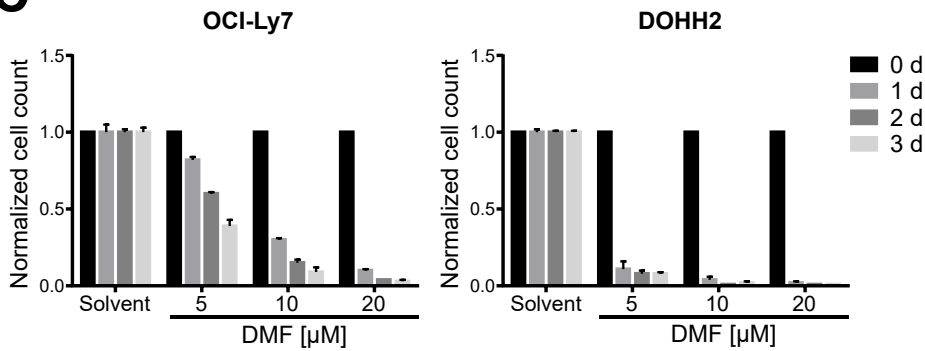
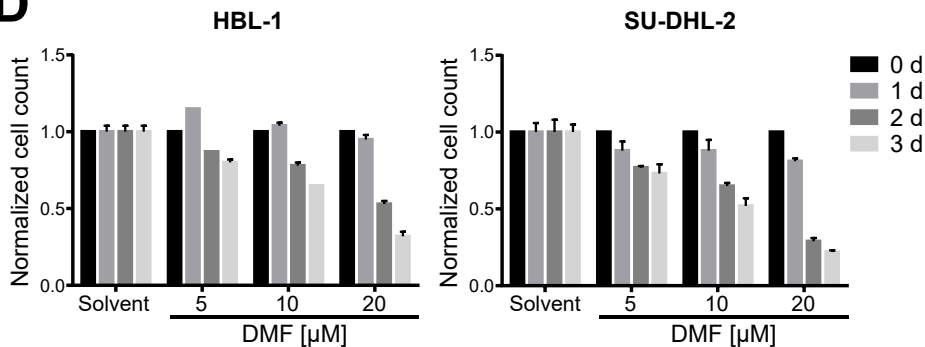
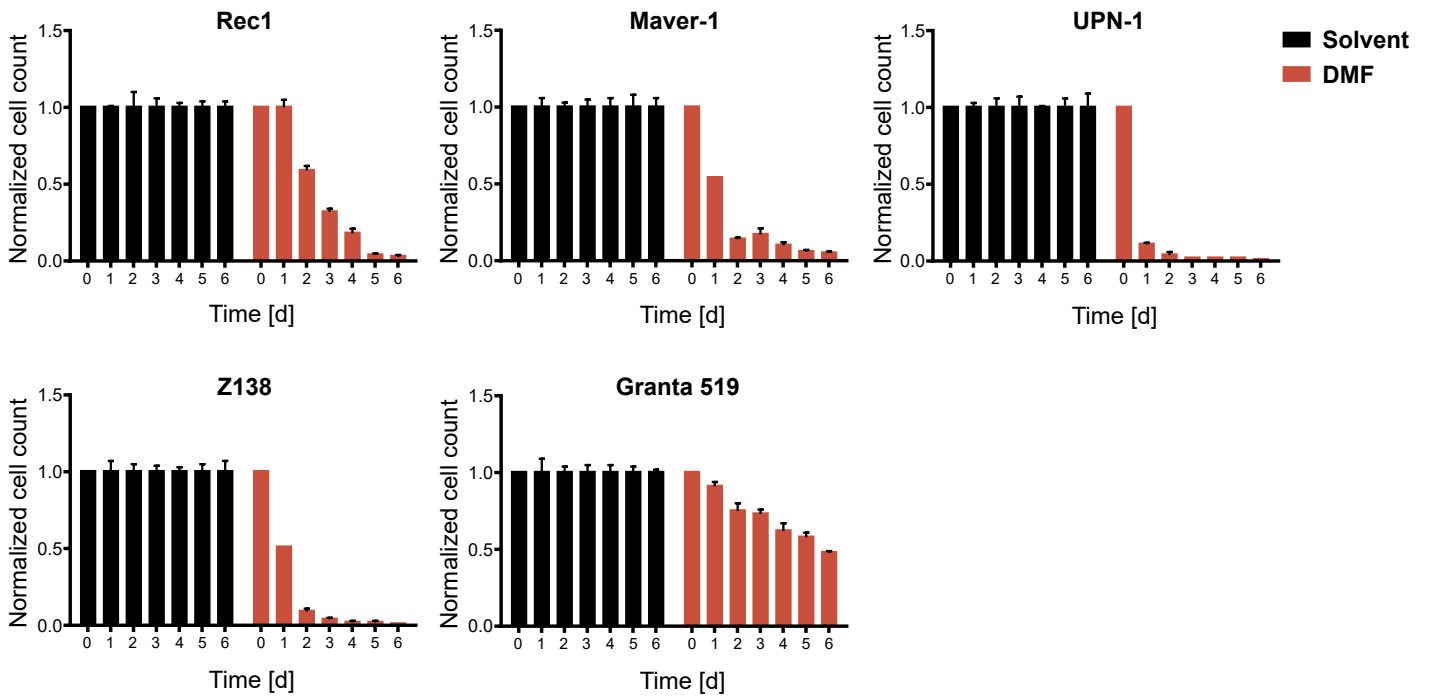
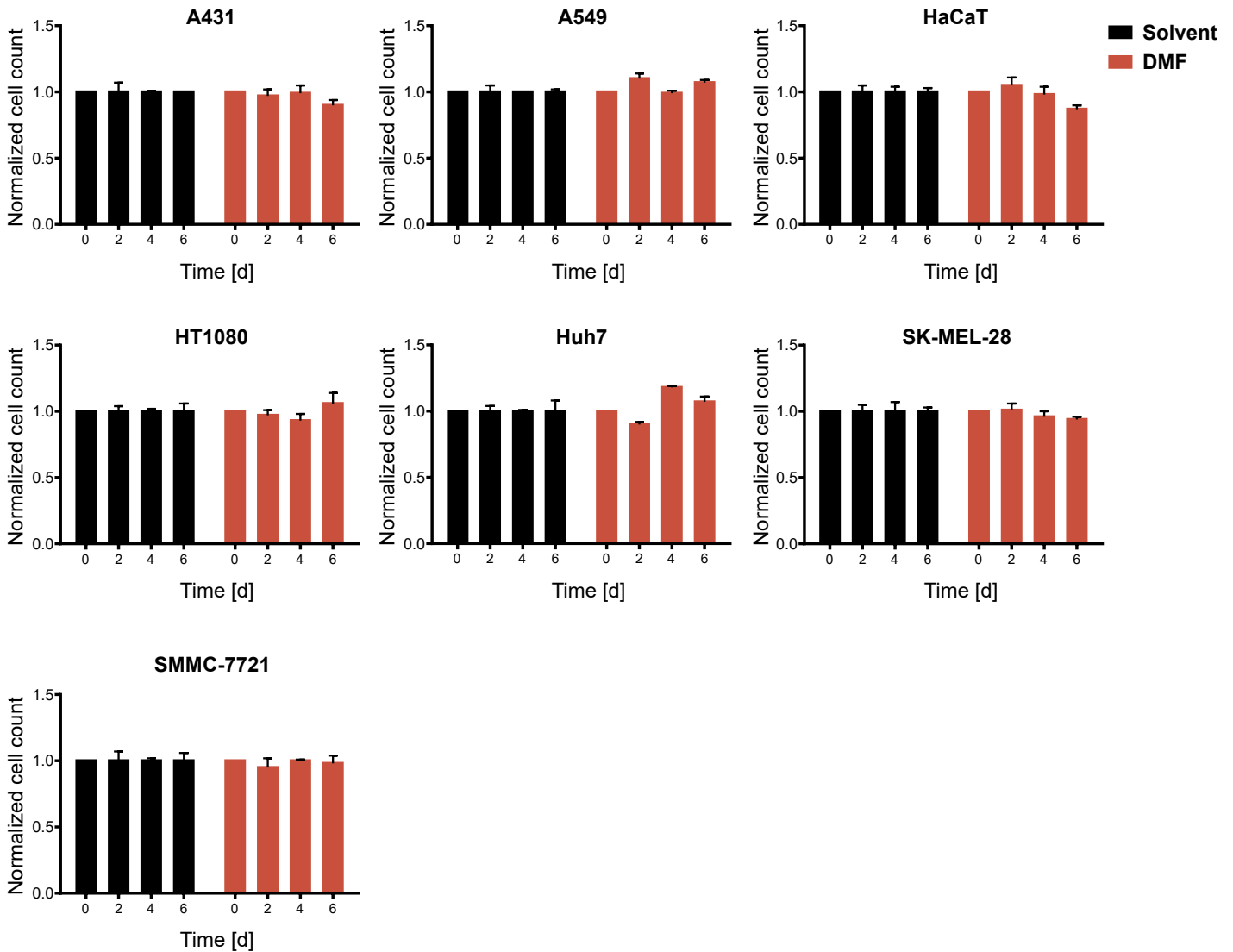
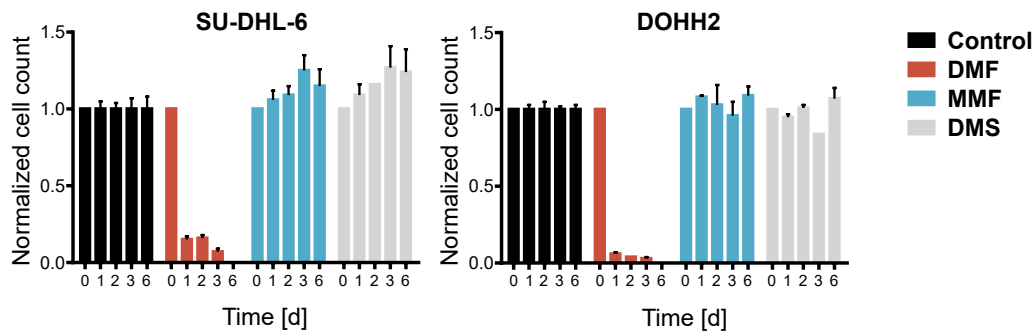
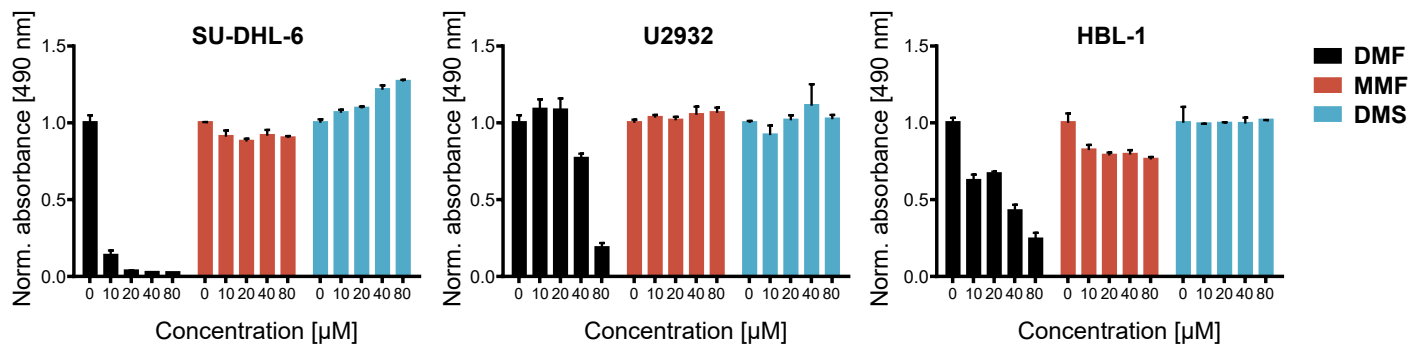
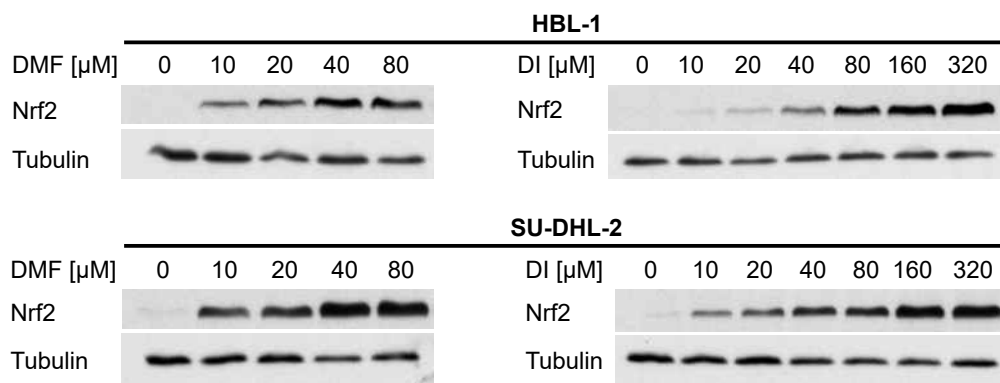
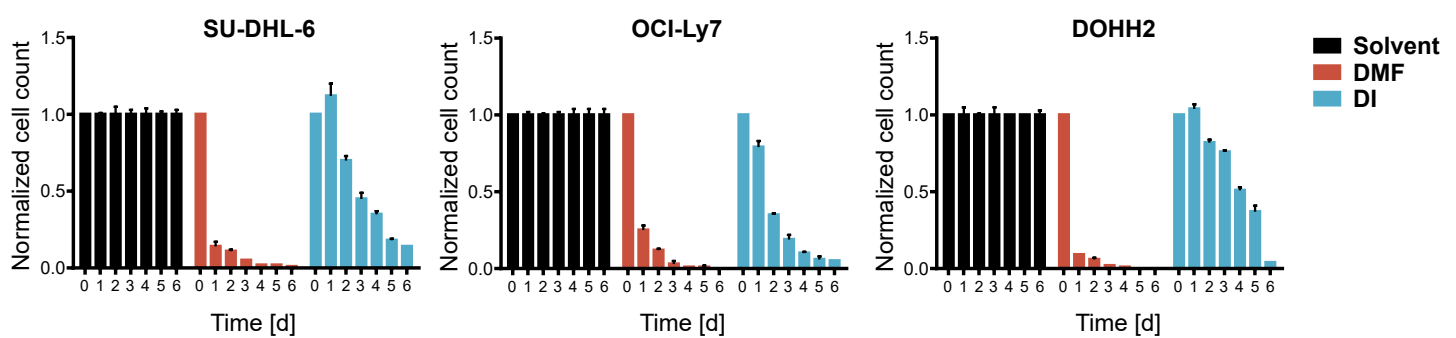
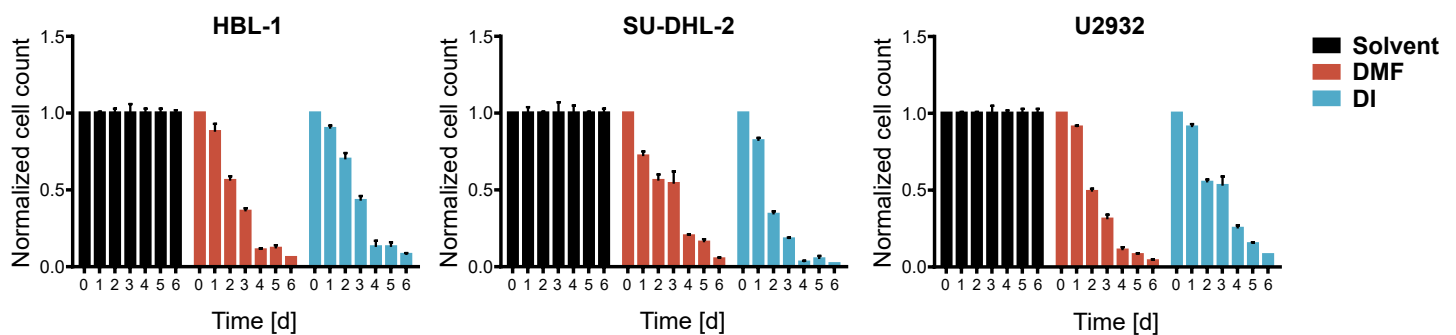
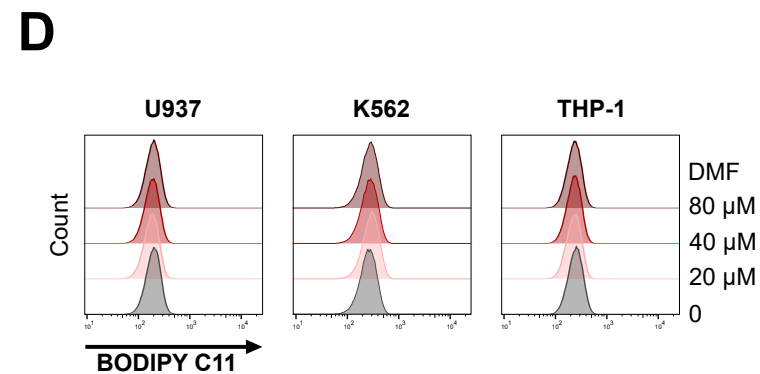
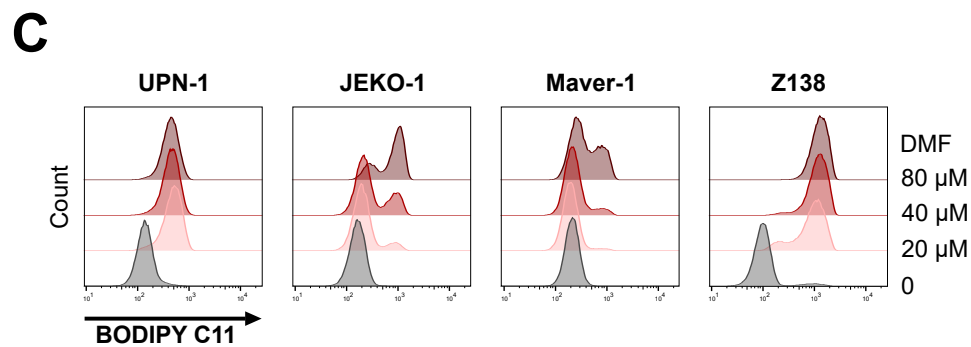
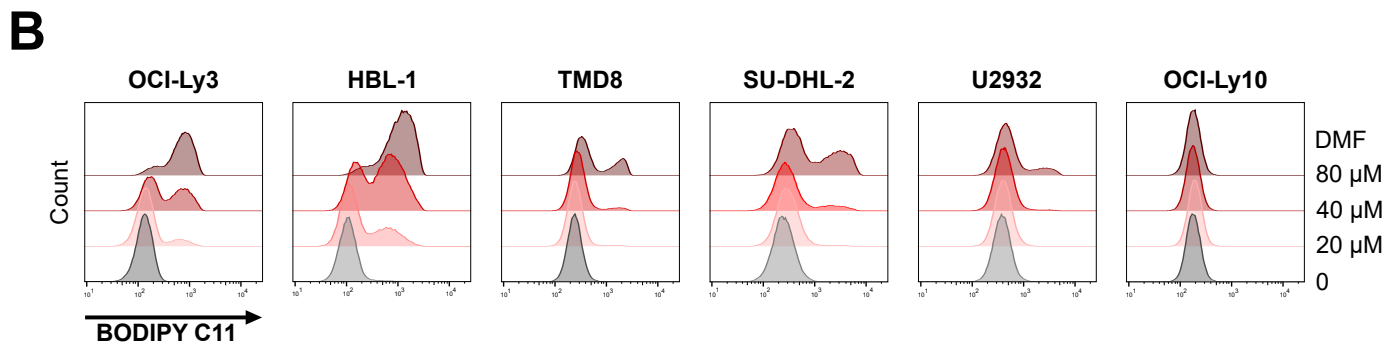
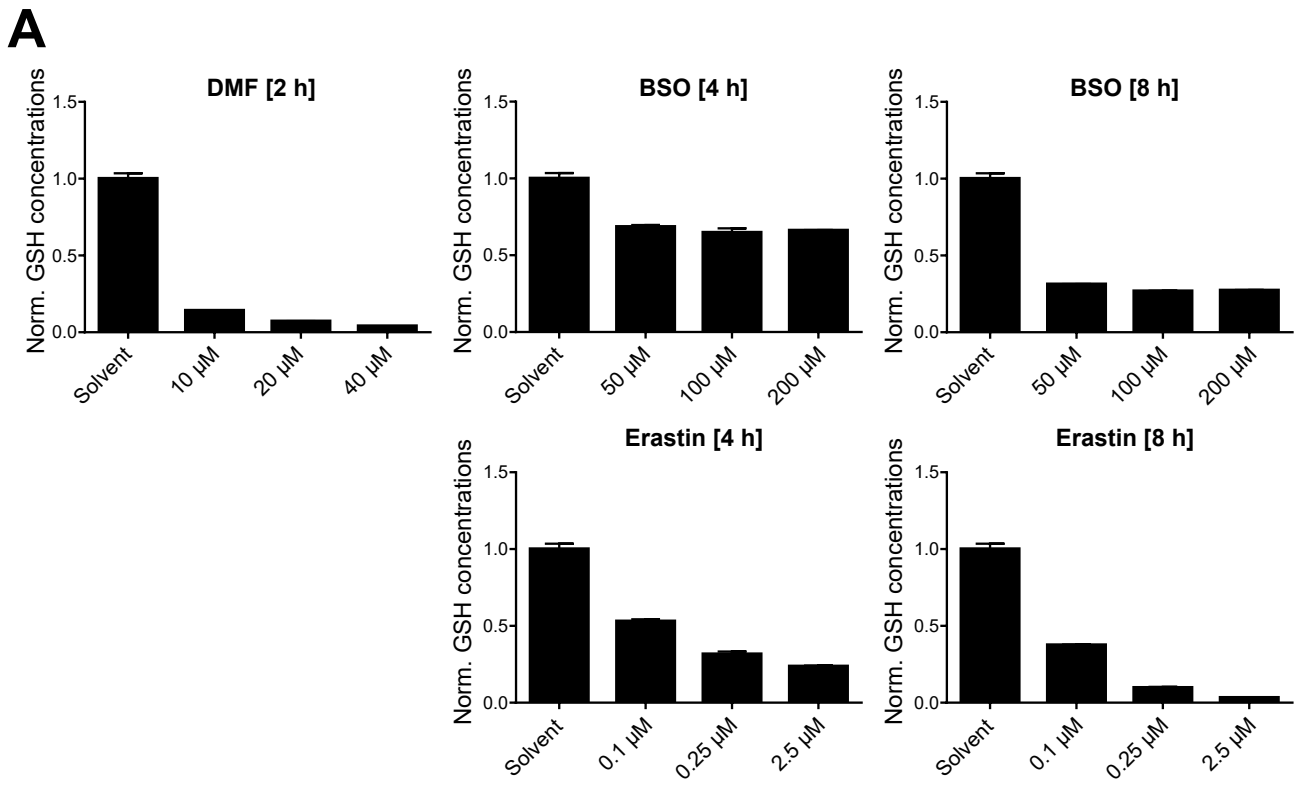


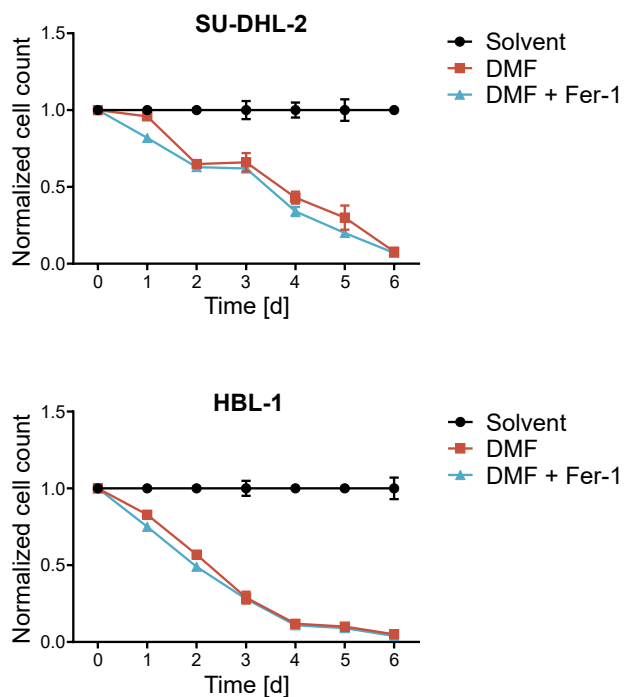
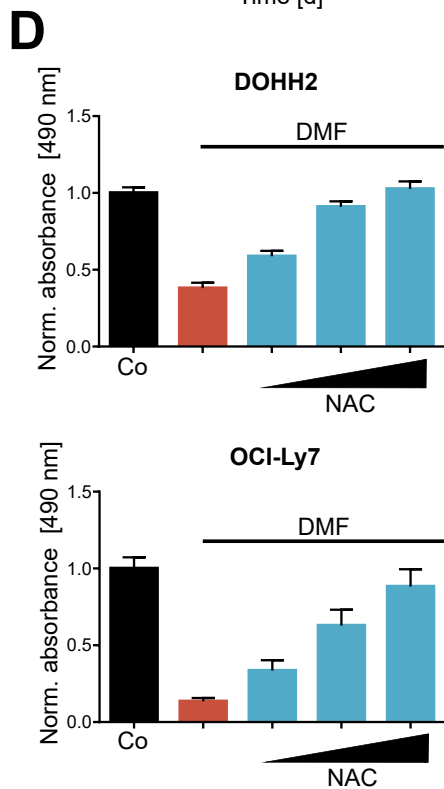
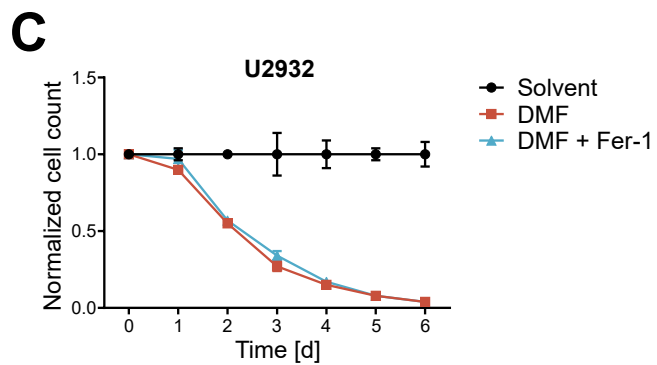
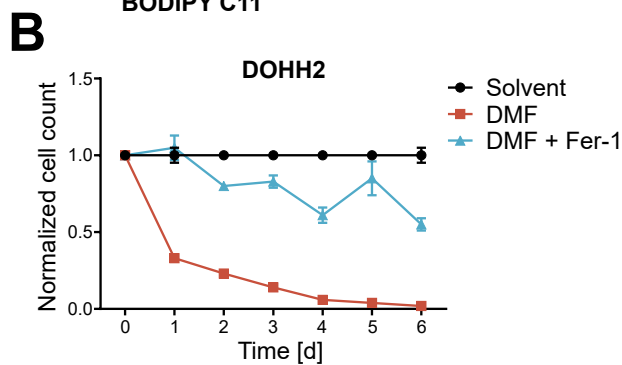
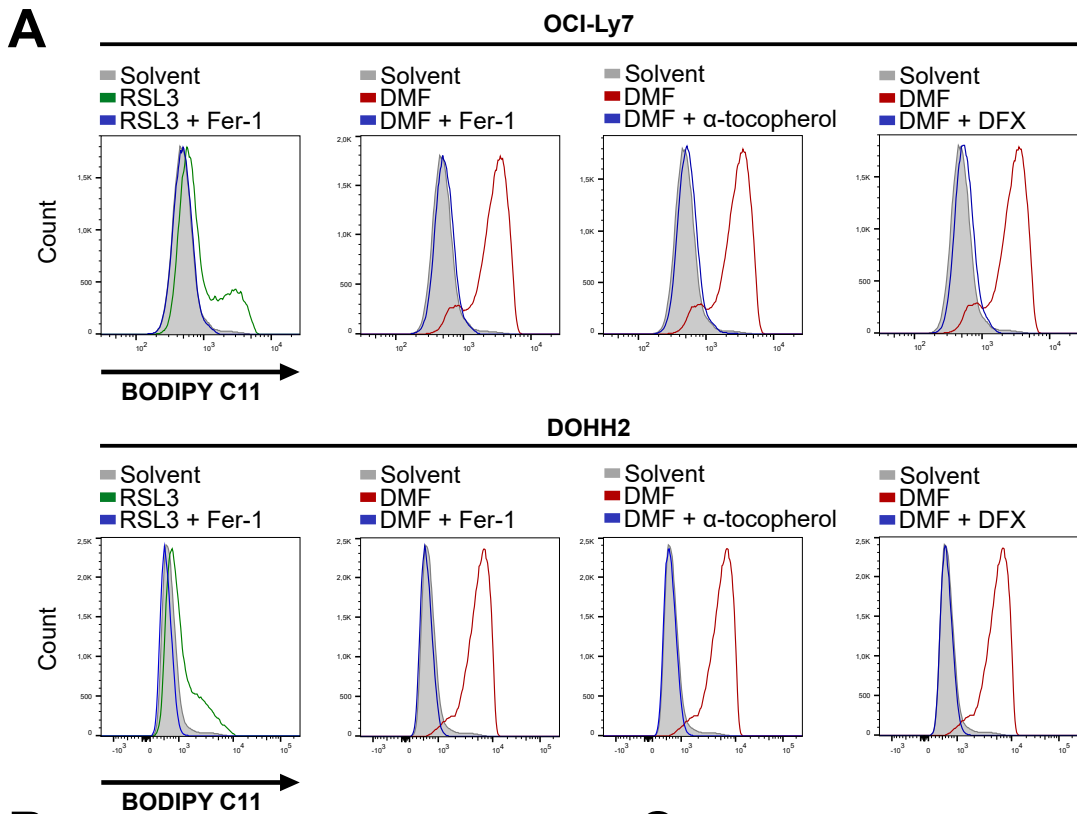
Figure 6

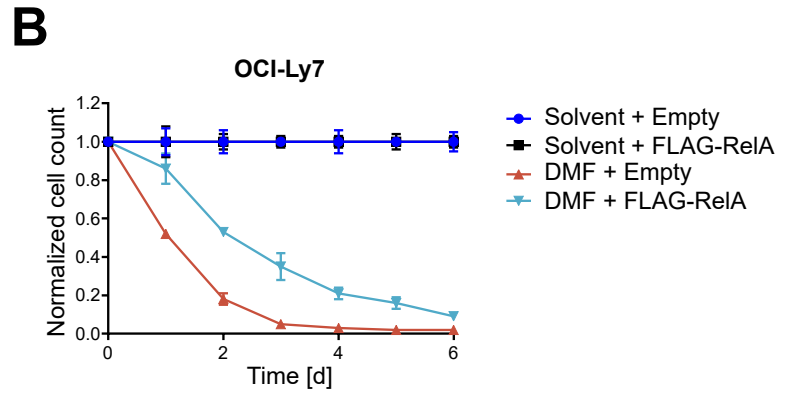
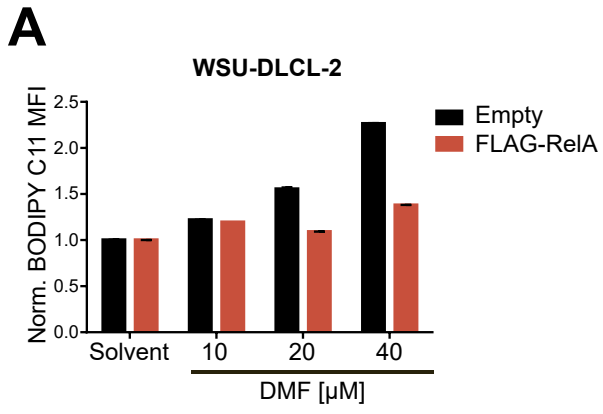
A**B****C****D**

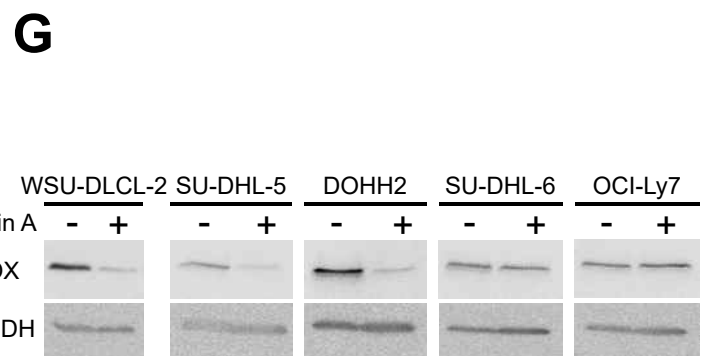
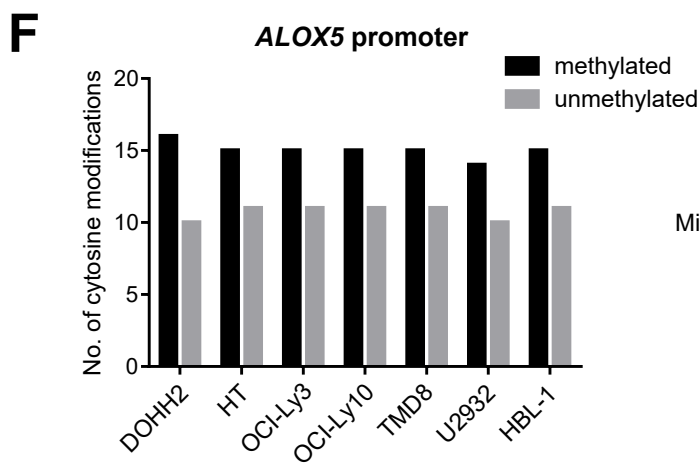
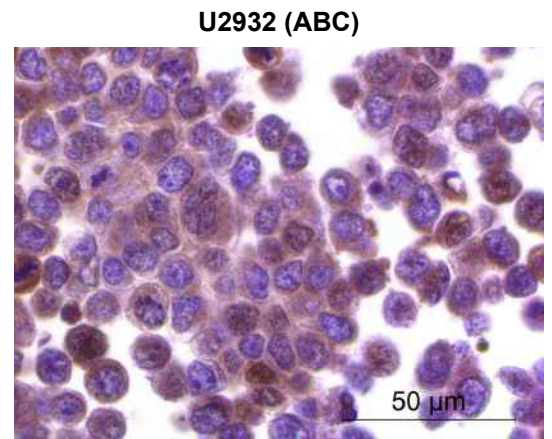
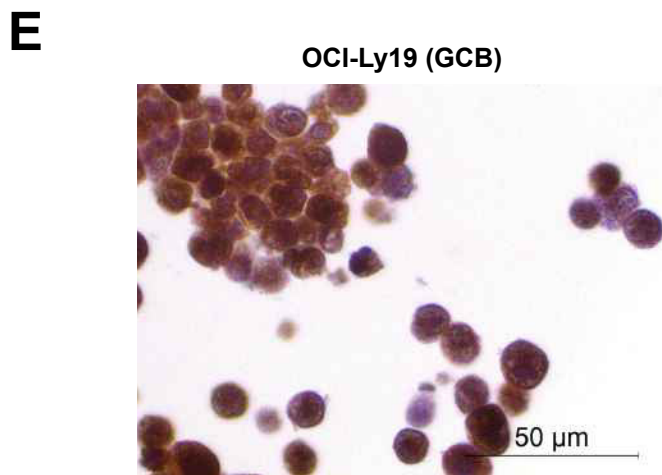
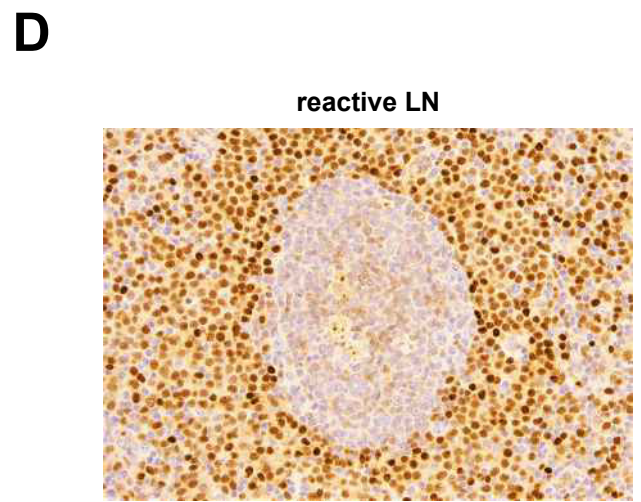
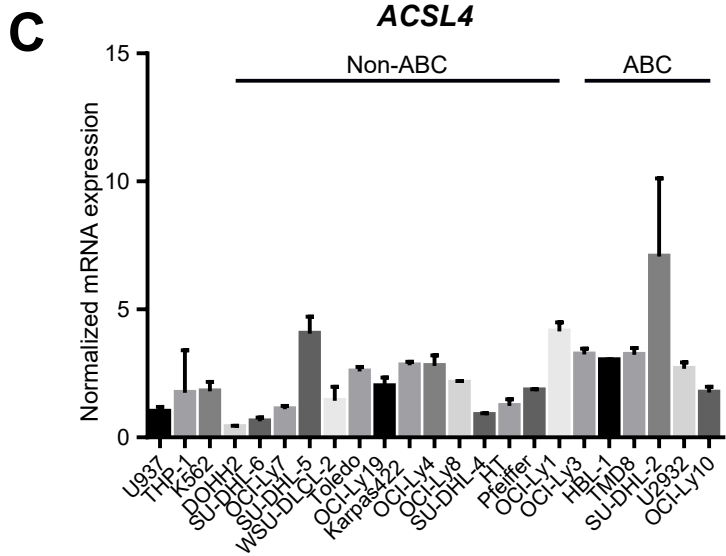
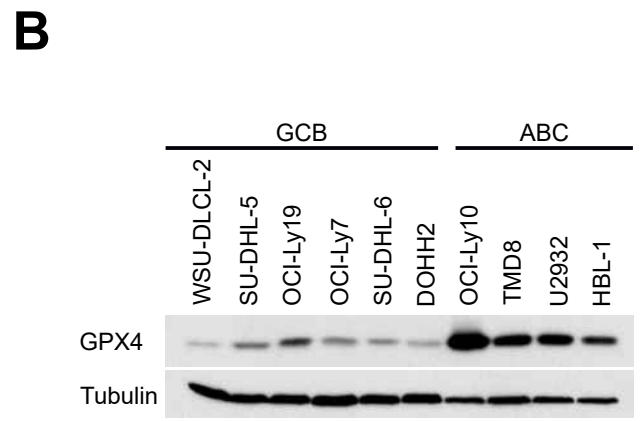
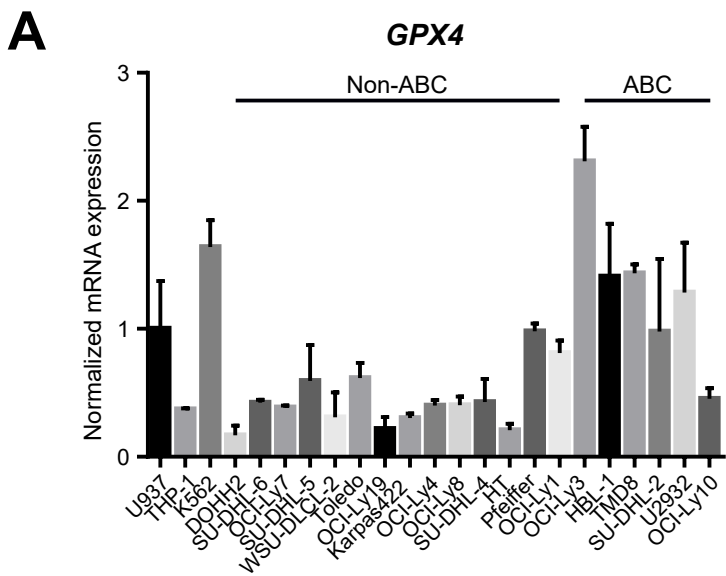
A**B**

A**B****C****D****E**

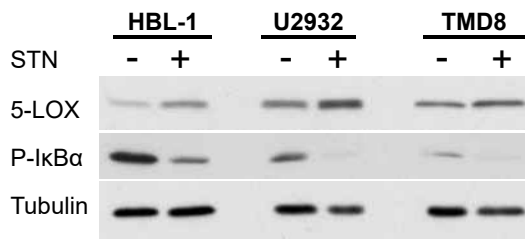
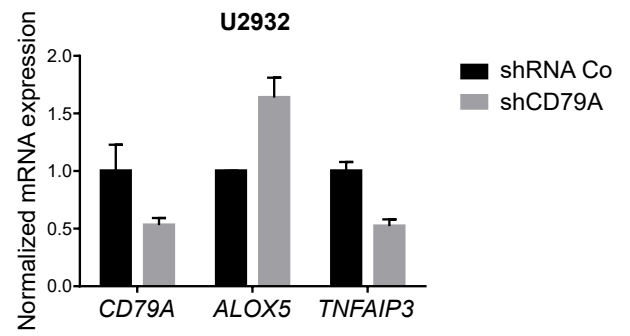
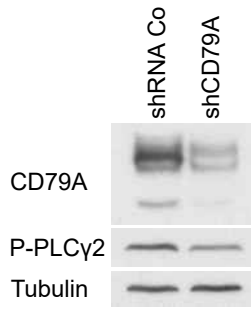
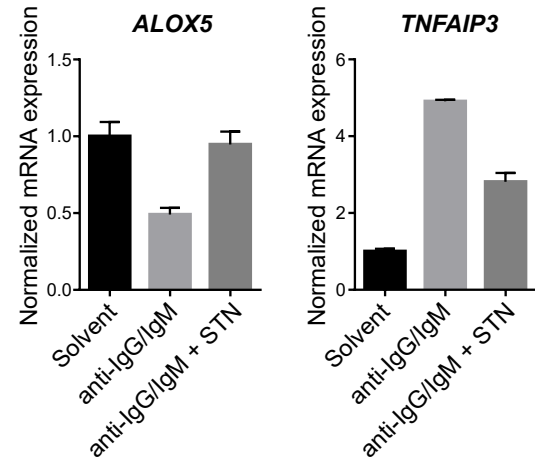
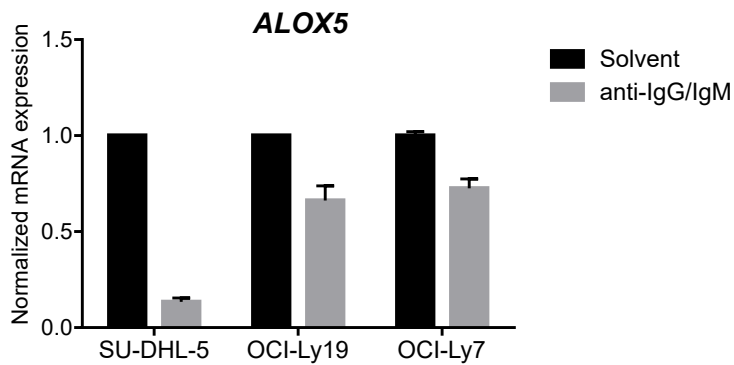


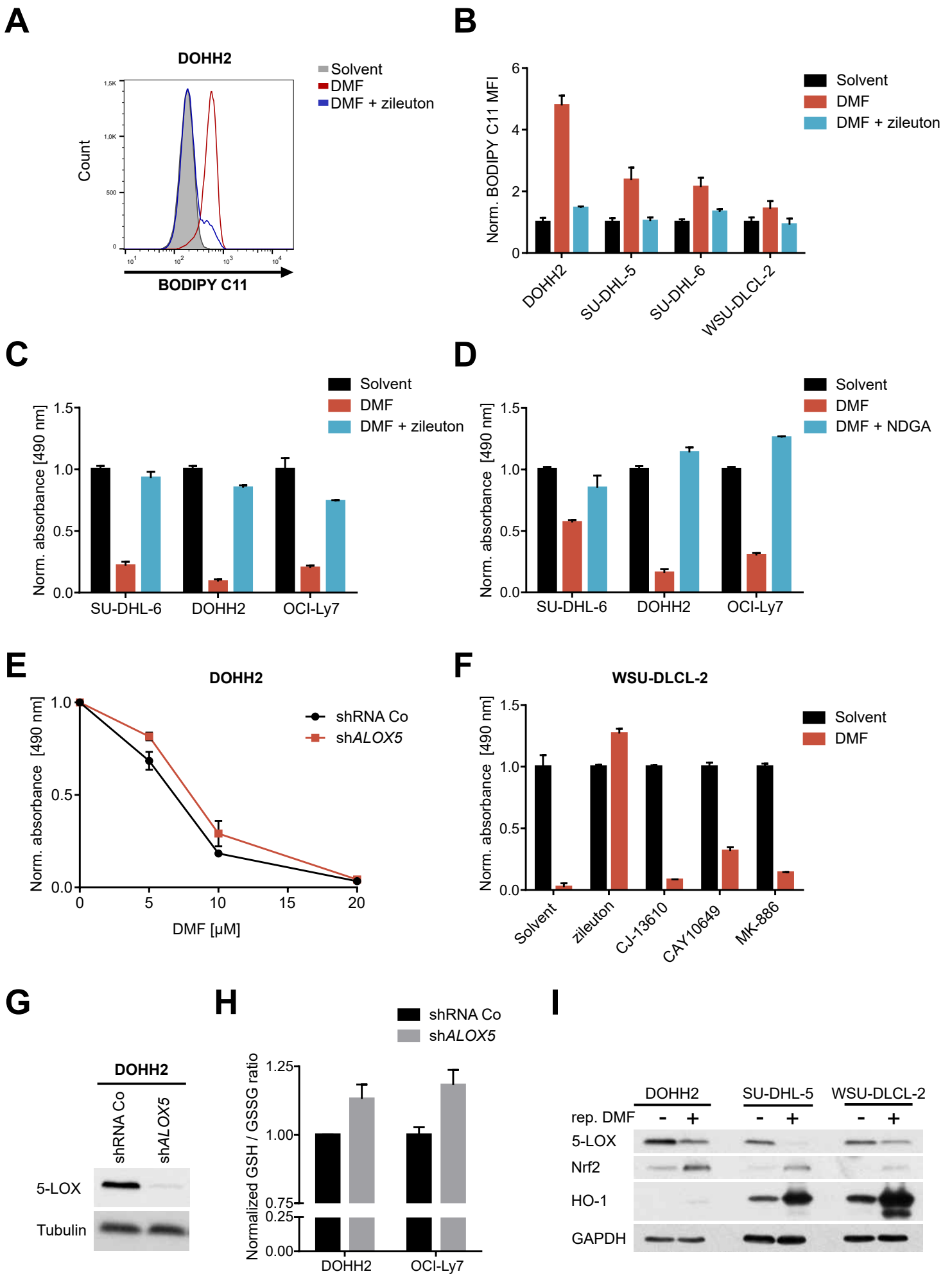




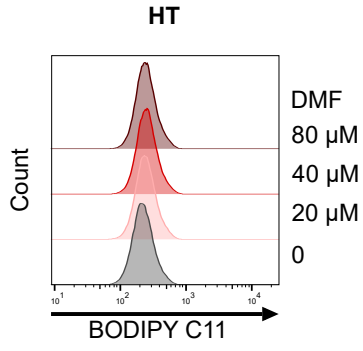
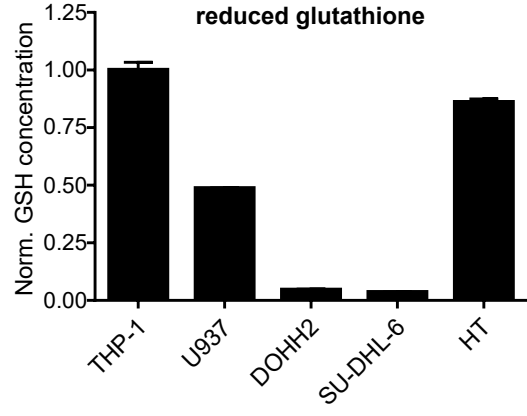
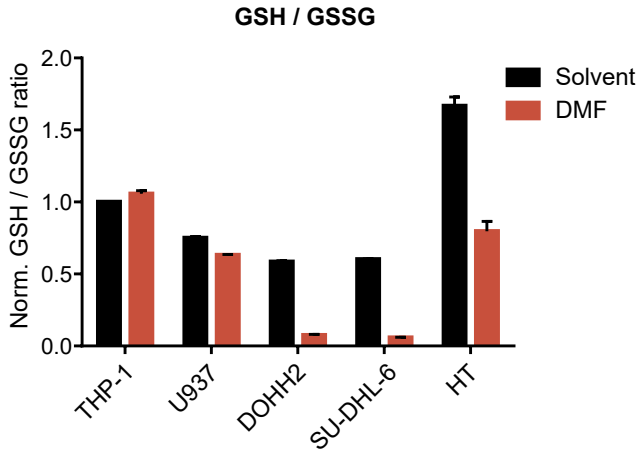
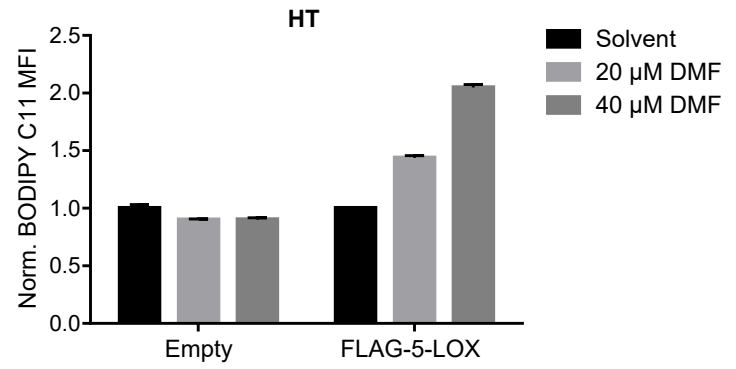
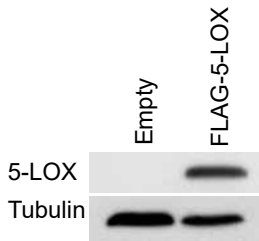


Supplemental Figure 7

A**B****C****D****E**

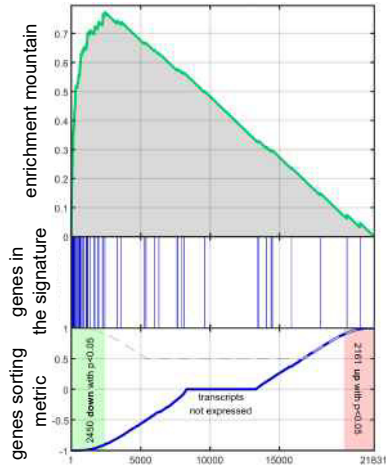


Supplemental Figure 9

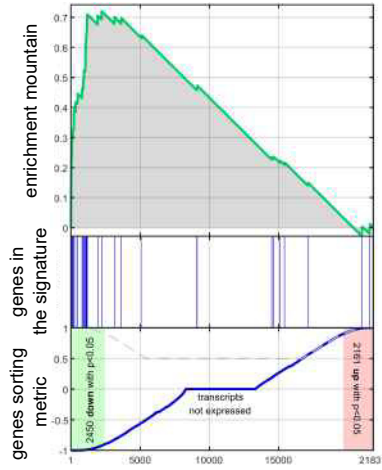
A**B****C****D****E**

A

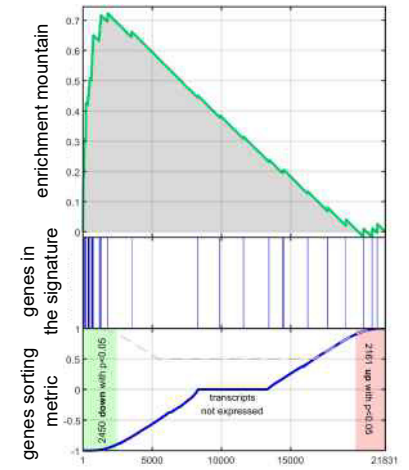
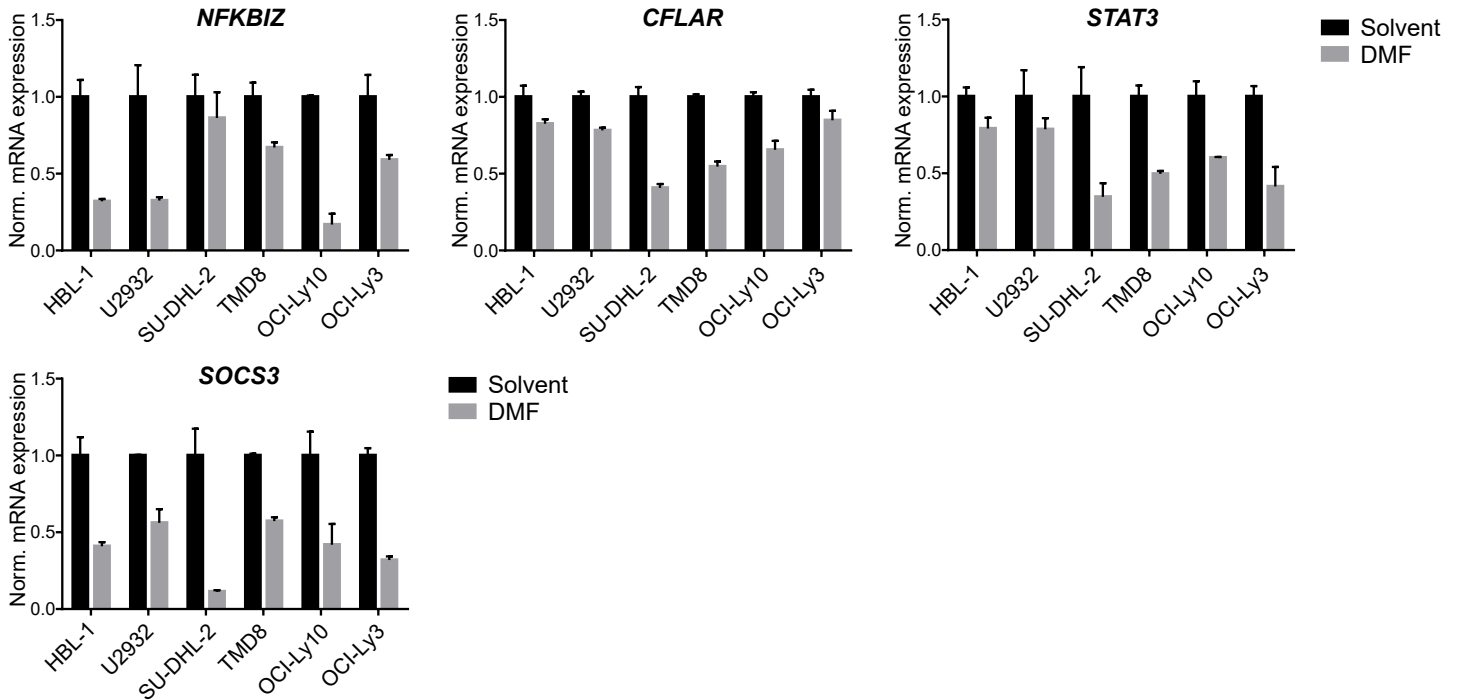
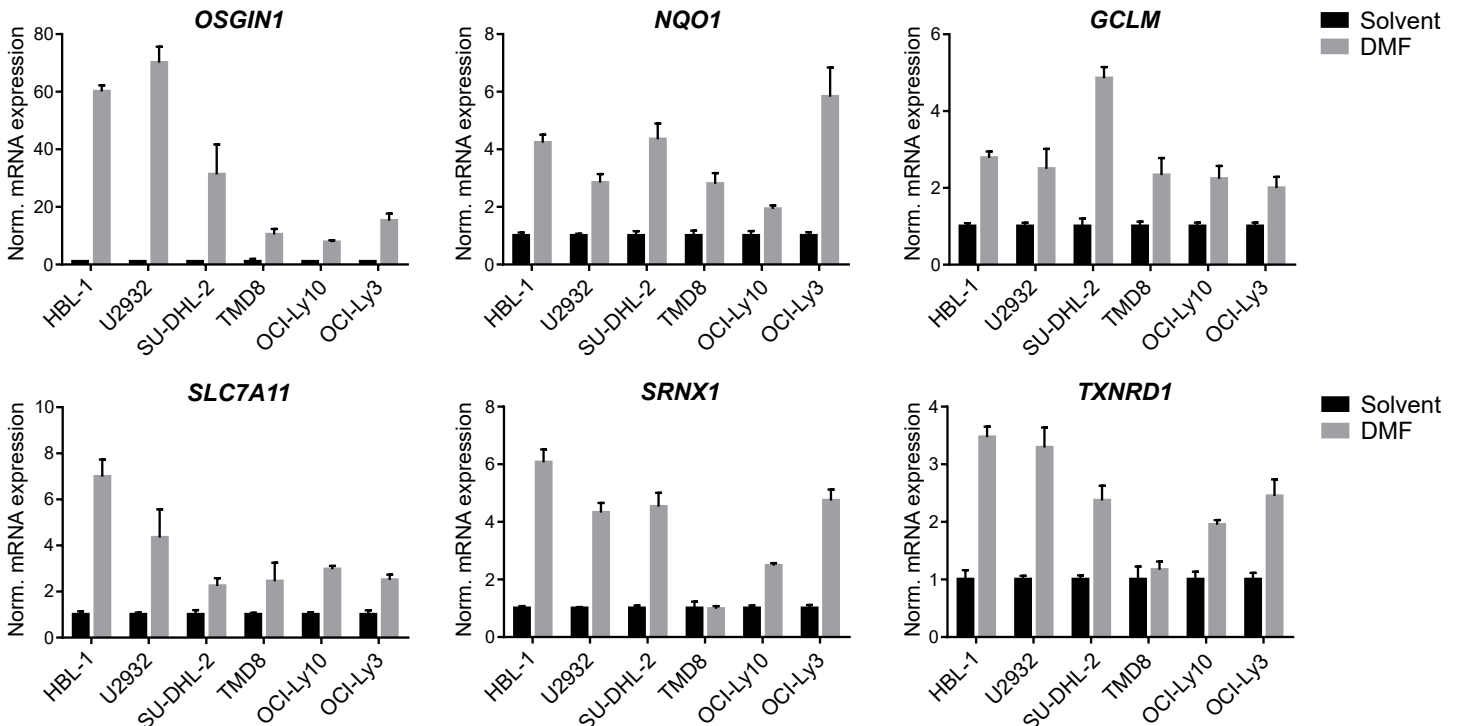
MALT1 inhibitor target gene signature
(Downregulated genes following z-VRPR-fmk treatment)

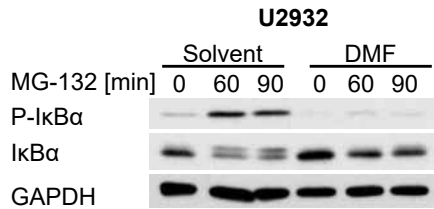
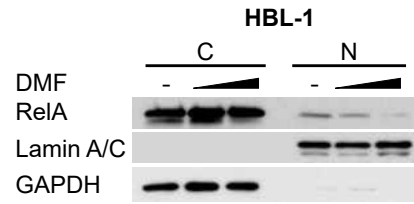
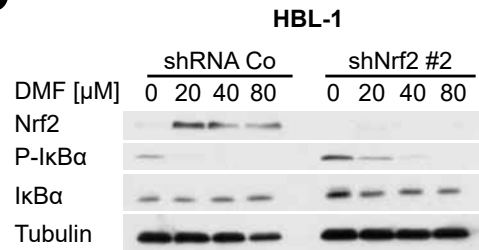
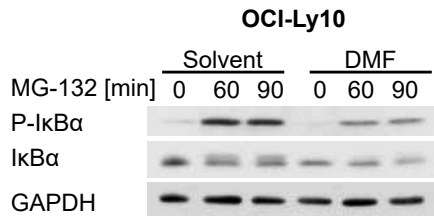
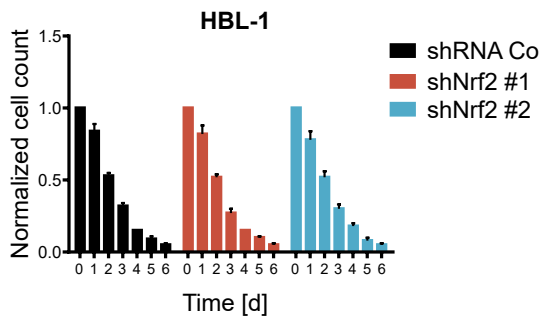
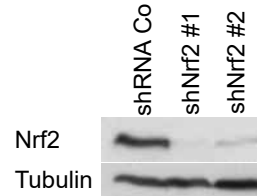
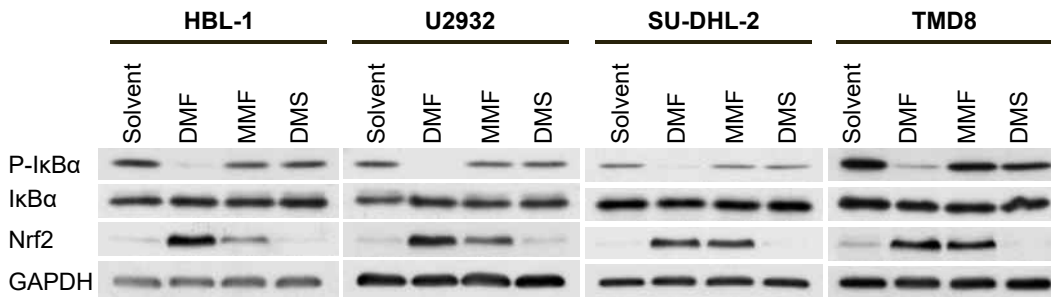
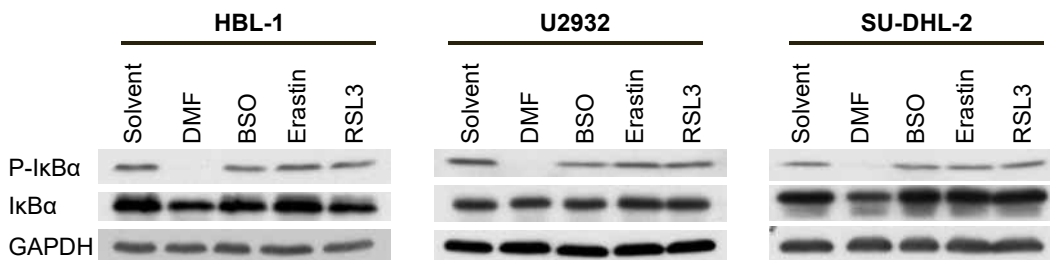


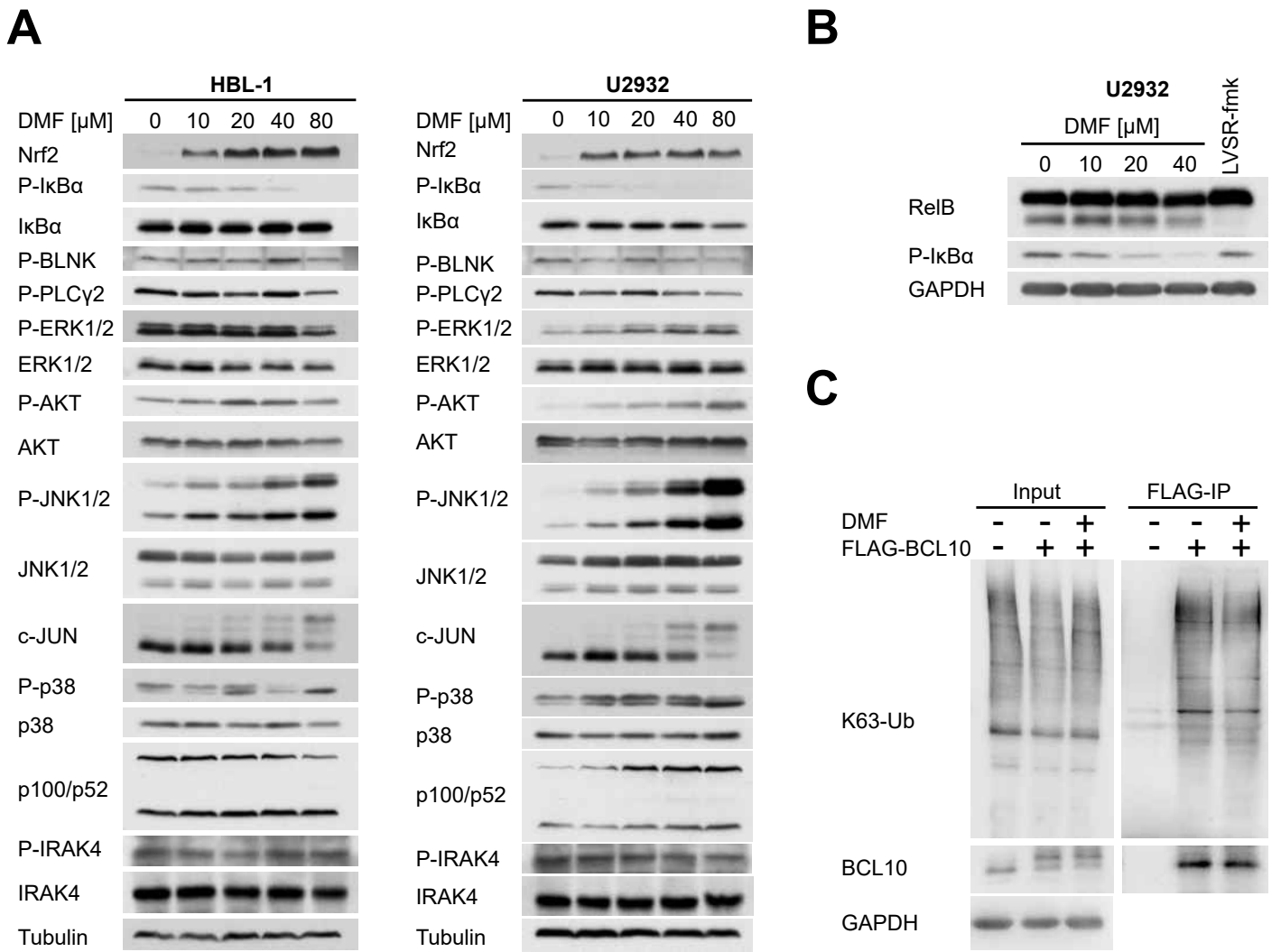
NF- κ B target gene signature
(NF κ B_Up_bothOCILy3andLy10)

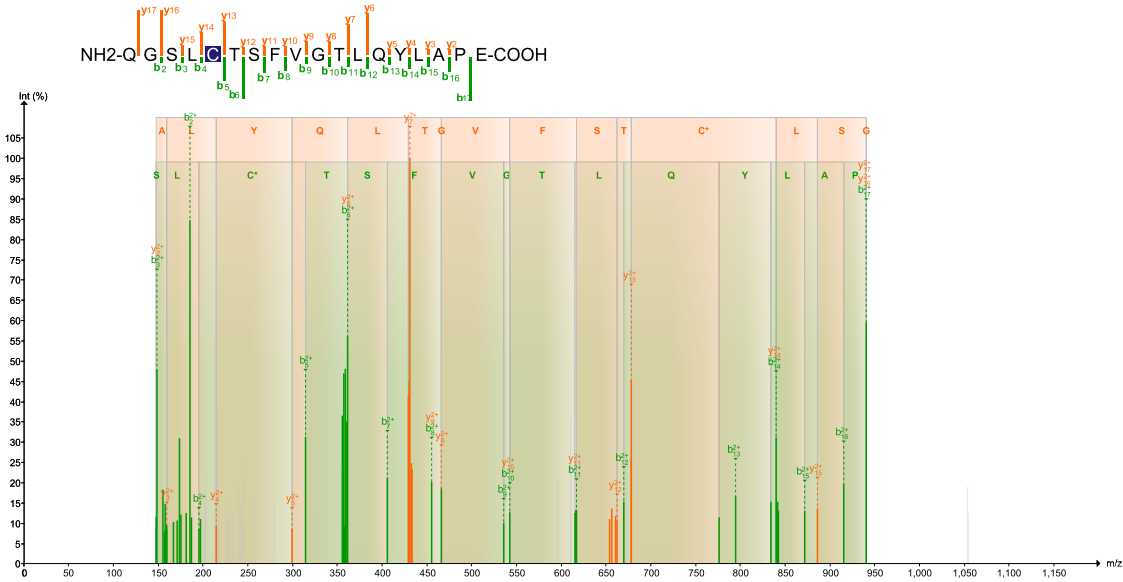
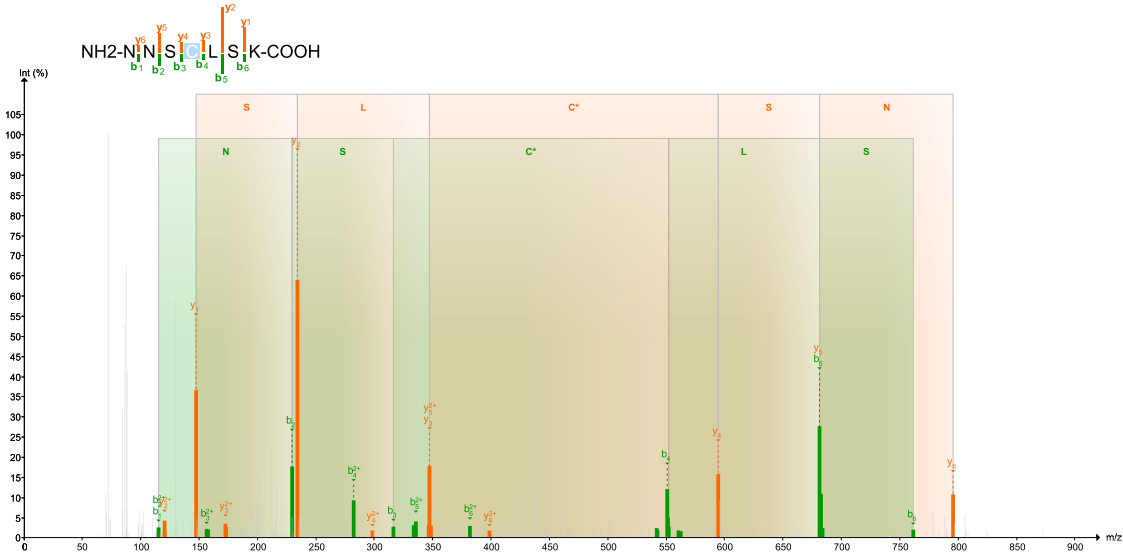
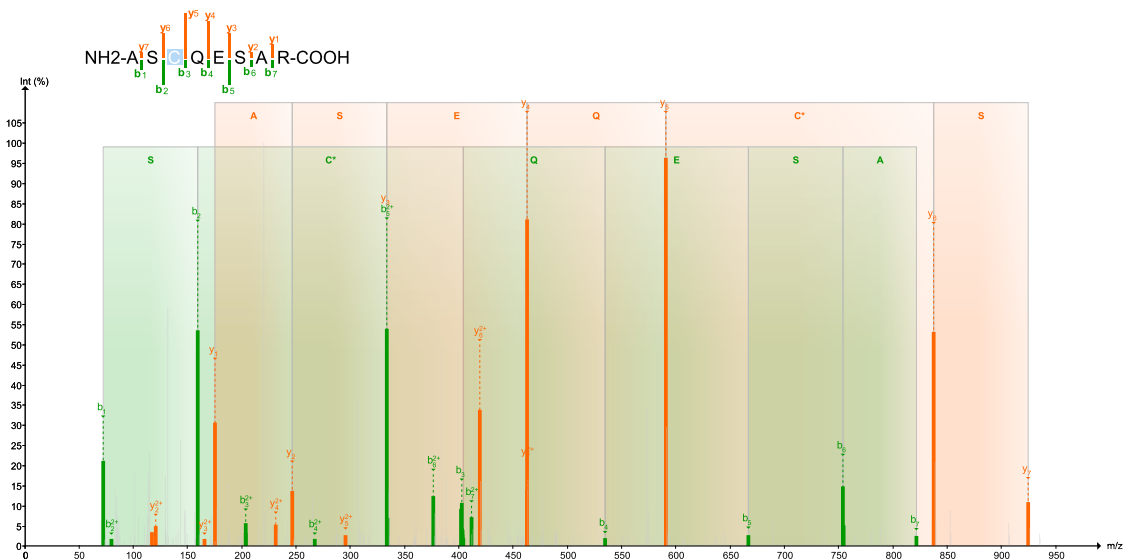


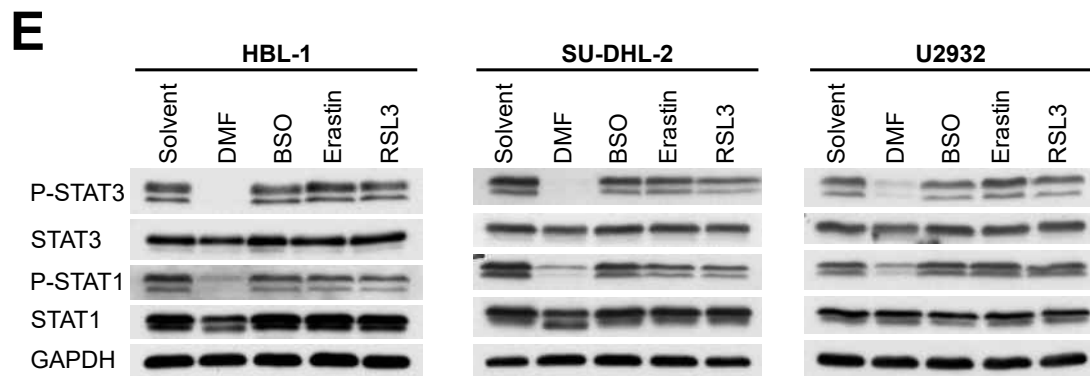
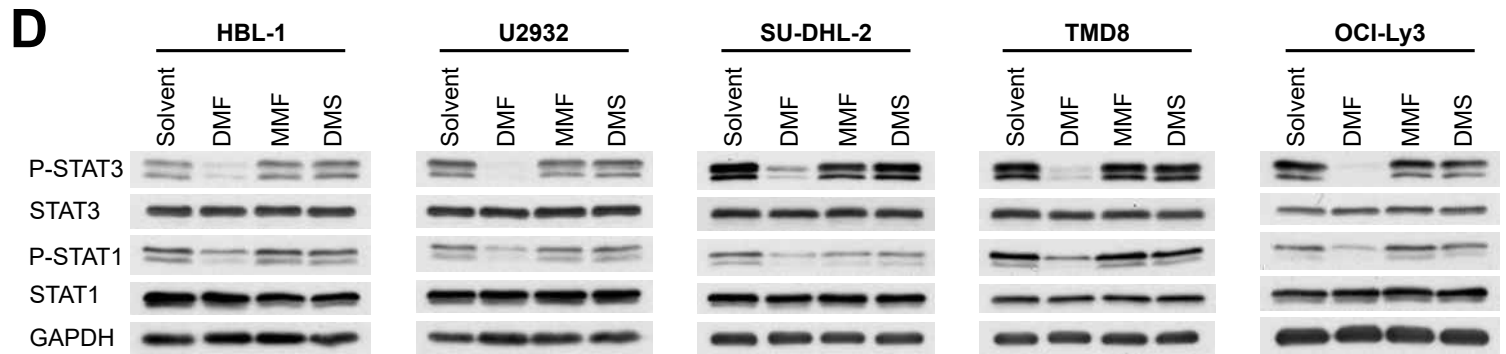
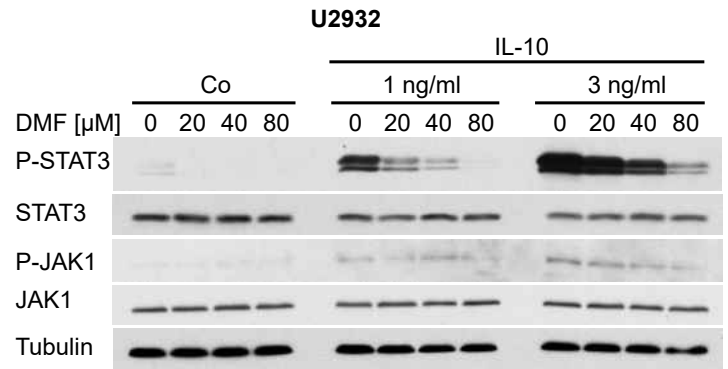
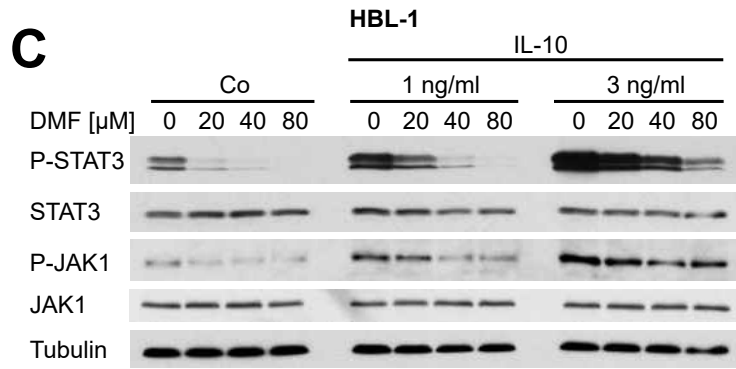
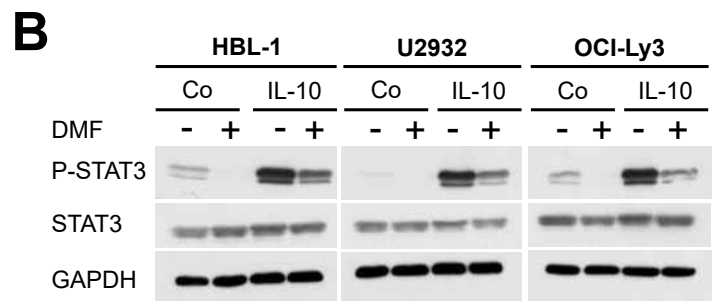
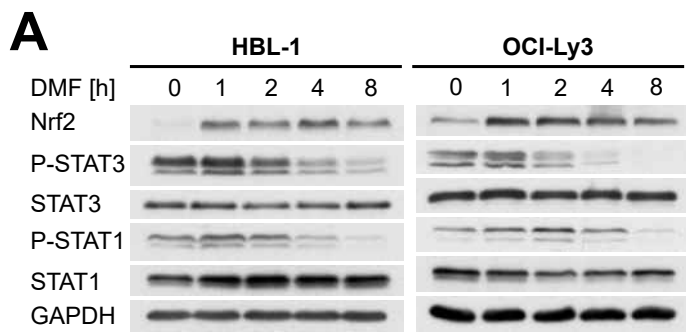
NF- κ B target gene signature
(Regulated genes in HBL-1 after specific IKK β inhibitor MLN120B)

**B****C**

A**B****C****D****E****F****G**

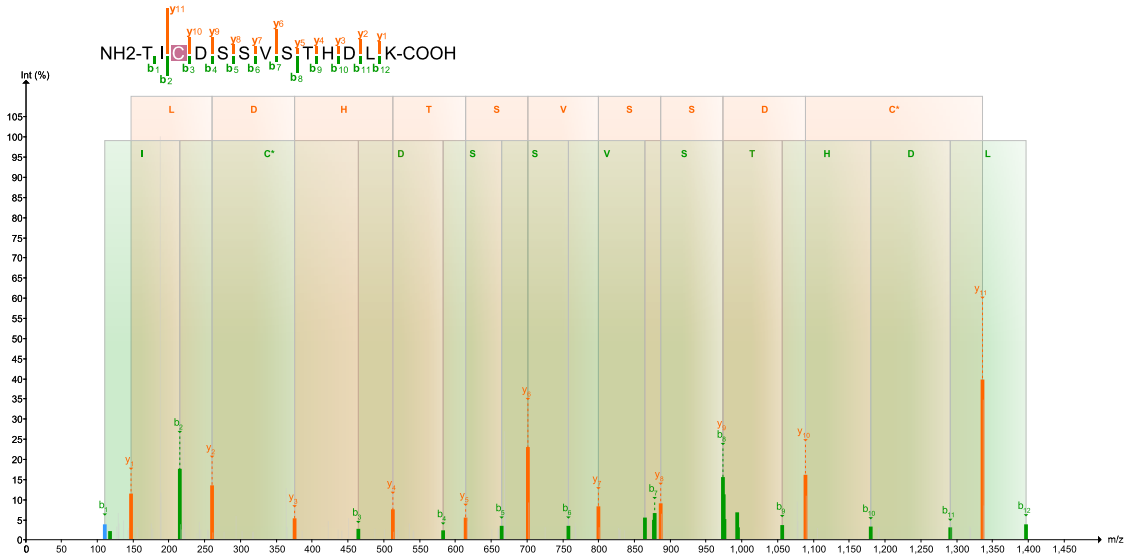


A**IKK2 C179****IKK2 C464****B****NEMO C347**

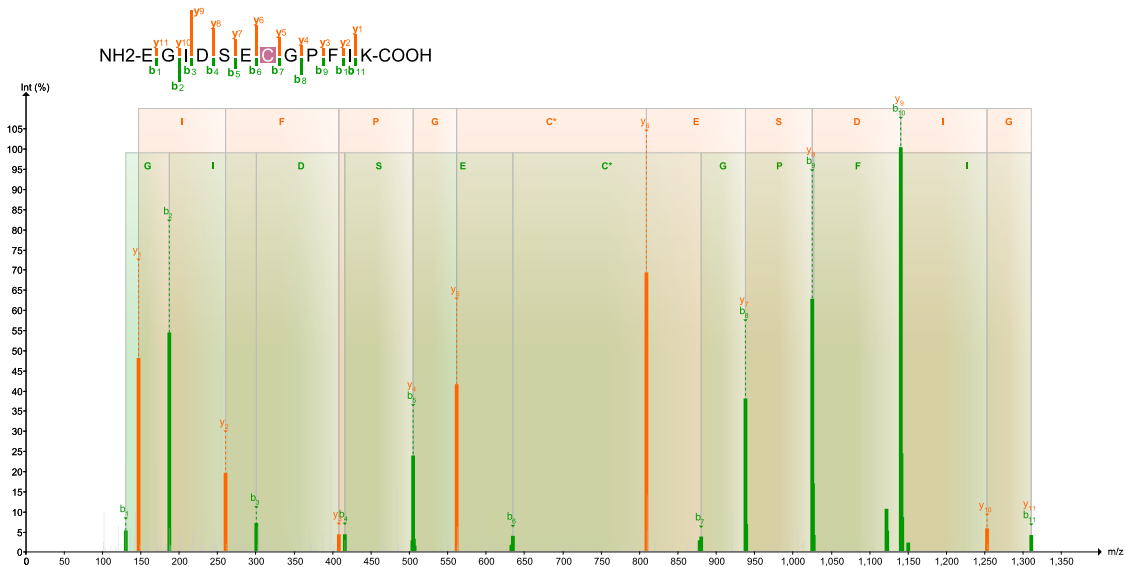


A

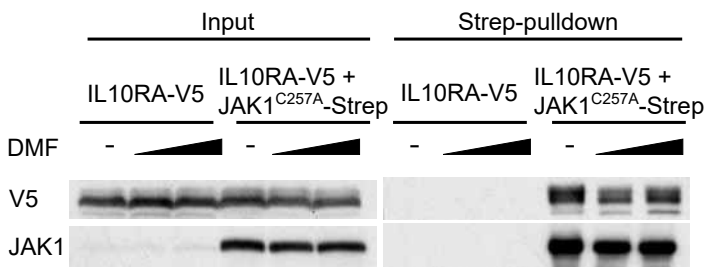
JAK1 C257



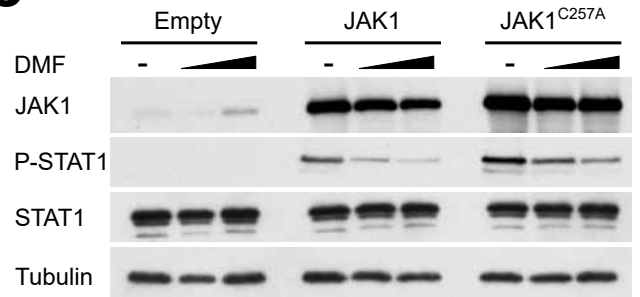
JAK1 C731

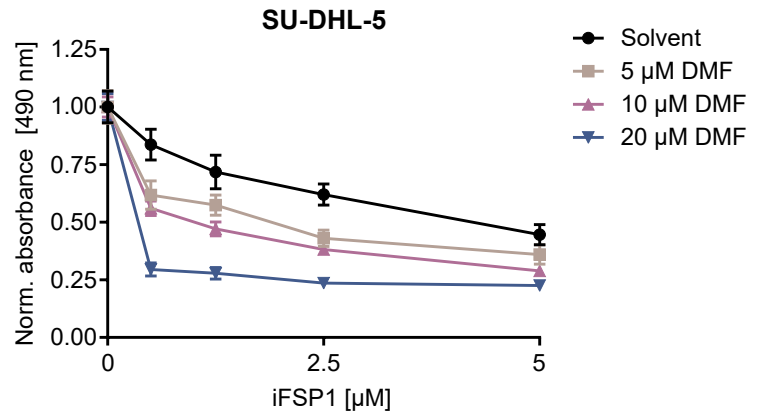
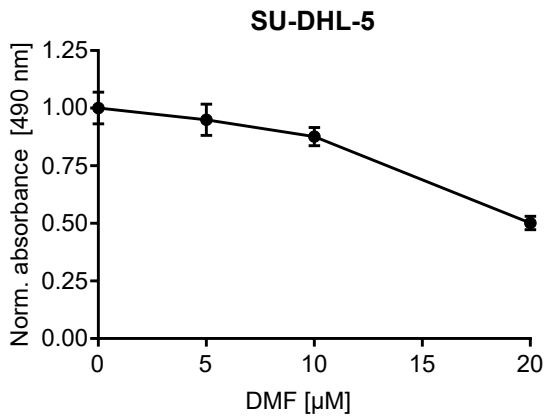
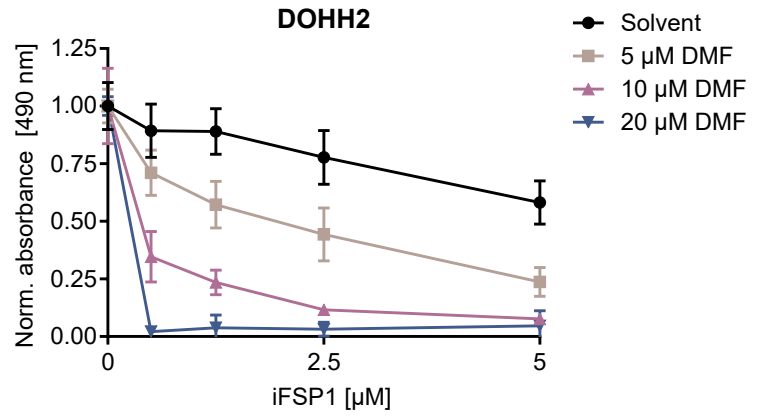
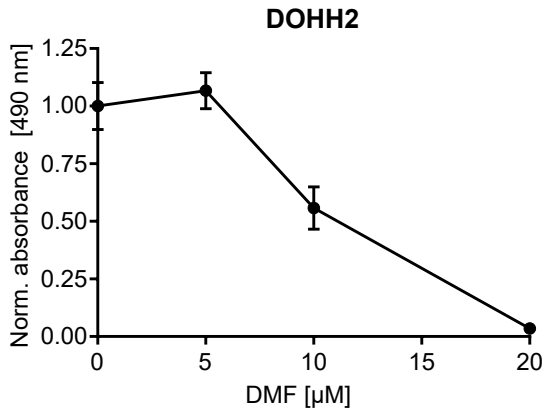
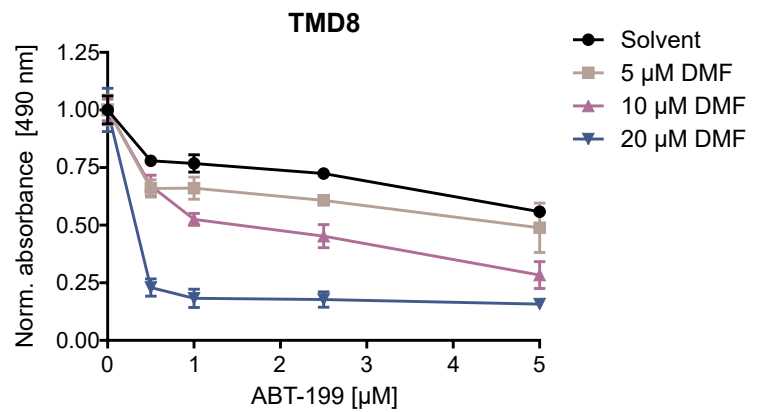
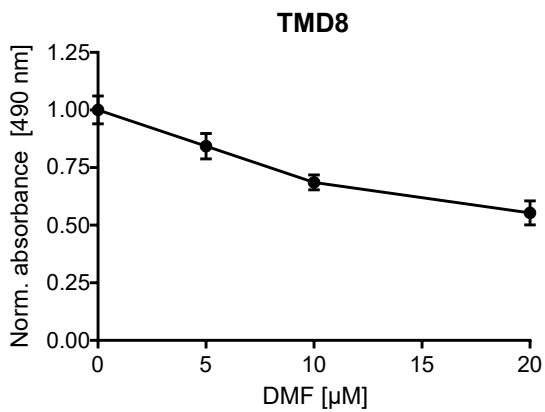
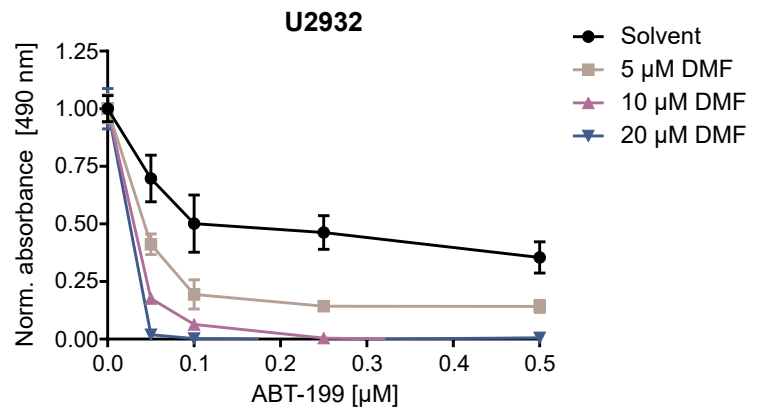
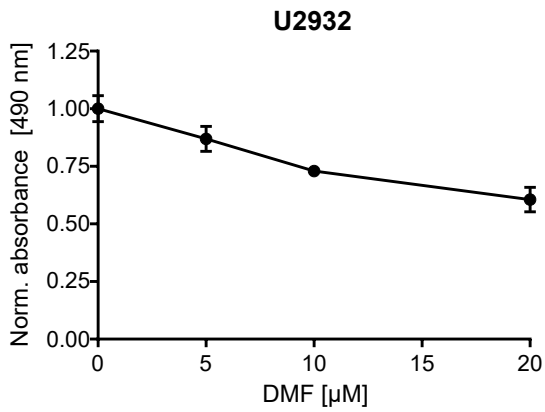


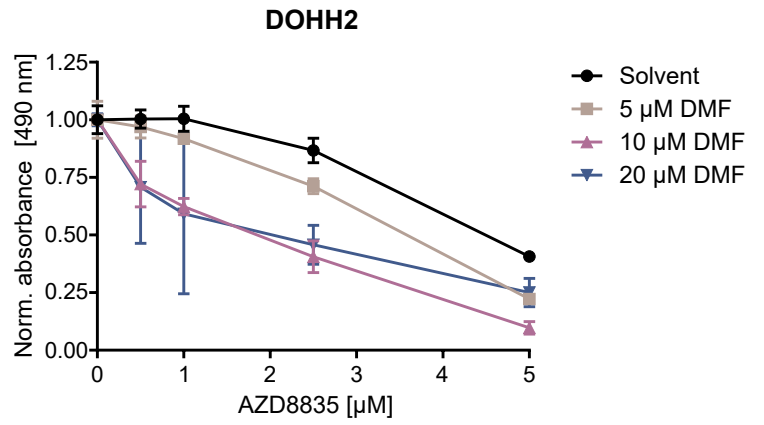
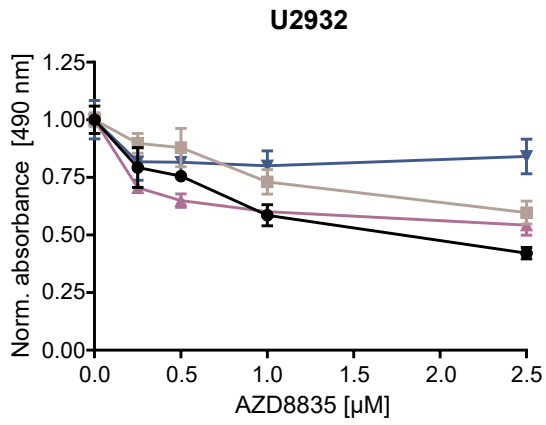
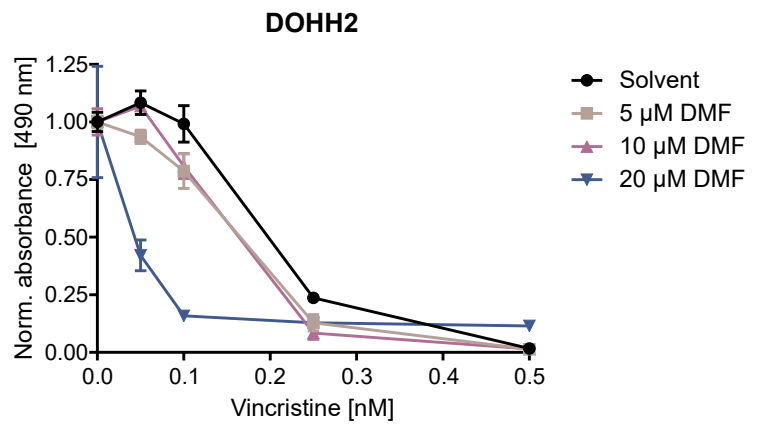
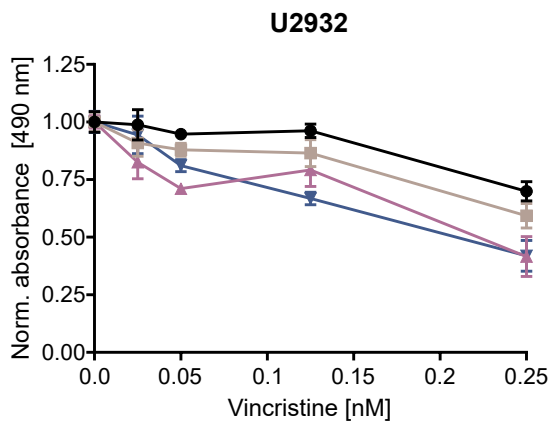
B



C



A**B**

A**B**

Dimethyl fumarate induces ferroptosis and impairs NF- κ B/STAT3 signaling in DLBCL

Supplemental Materials and Methods

Cell culture, transfection, lentiviral and retroviral transduction

Cell lines used in this study were cultivated in the appropriate medium supplemented with fetal calf serum (FCS) or human serum (**Suppl. Table 1**) at 37°C and 5% CO₂ in a humidified atmosphere.

Cells were treated with the following substances as indicated in the text and/or figure legends: dimethyl fumarate, monomethyl fumarate, dimethyl succinate, dimethyl itaconate, α -tocopherol, deferoxamine, MG-132, N-acetyl-L-cysteine (all Sigma-Aldrich), erastin, Q-VD, AZD8835, vincristine sulfate, sotrastaurin, zileuton, nordihydroguaiaretic acid, MK-886, ibrutinib, GS-9973, dasatinib (all Selleckchem), RSL3, buthionine sulfoximine, ferrostatin-1, mithramycin A, ABT-199, iFSP1, CJ-13610, CAY10649 (all Cayman Chemical) and LVSR-fmk (Bachem). GCB DLBCL cells were stimulated with PMA (80 ng/ml; Sigma-Aldrich) and ionomycin (1 μ M; Cayman Chemical) or with 10 μ g/ml of an agonistic anti-IgG/IgM antibody fragment F(ab')₂-goat anti-human IgG, IgM (H+L) secondary antibody, ThermoFisher). Recombinant human (rh) IL-6, IL-10 and IFN α (all Immunotools) were used to activate JAK/STAT signaling in DLBCL cells.

For co-immunoprecipitation experiments, HEK293T cells were transfected by the calcium phosphate precipitation method to express Strep-tagged JAK1 and IL10RA-V5. The pLX302 IL10RA-V5 puro construct was a gift from Kevin Janes (Addgene plasmid #47552). Expression constructs encoding variants of IKK2 (i.e. C179A or C464A) and JAK1 (C257A) were generated by site-directed mutagenesis using Q5

polymerase (NEB) and primers specific for the desired mutation. For functional analysis, cysteine-to-alanine variants of IKK2 and JAK1 as well as the respective wild-type constructs were transiently expressed in HEK293T cells.

Lentiviral transduction of DLBCL cells was performed as described previously.¹ In brief, lentiviral particles were produced in HEK293T cells using the helper plasmids psPAX2 and pMD2.G as well as a vector encoding the protein of interest (FLAG-5-LOX, FLAG-RelA, FLAG-BCL10) or a small hairpin RNA (shRNA; pLKO.1 plasmid) for knockdown experiments. The clone IDs and respective targeting sequences of the shRNA vectors are provided in **Suppl. Table 2**. Stably transduced cells were selected using the appropriate selection medium supplemented with puromycin (Invivogen).

For efficient retroviral transductions, cell lines were engineered to express a murine ecotropic receptor as previously described.² Additionally, the cell lines were engineered to express a bacterial tetracycline repressor allowing doxycycline-inducible complementary DNA (cDNA) expression. FLAG-tagged RelA or a constitutively active STAT3 mutant cDNA (STAT3C, A662C and N664C) was ligated into a modified version of the inducible pRetroCMV vector. The retroviral transduction experiments were performed as previously described.^{1,3}

Biotin-coupled iodoacetamide labeling and streptavidin-pulldown

To determine the accessibility of free thiol groups in the protein of interest after DMF treatment, cell lysates at a concentration of 2 µg protein/ml were incubated with 20 µM biotin polyethyleneoxide iodoacetamide (Sigma-Aldrich) for 1 h at room temperature. Subsequently, labeled proteins were pulled-down using streptavidin agarose beads and analyzed by immunoblotting.

Survival assays (cell counting, MTS assay)

For long-term survival assays, cells were seeded at a density of 0.2×10^6 cells/ml. For 6 days, viable cells were counted using a cell analyzer (NucleoCounter NC-250, Chemometec) and treated daily with inhibitors or the respective solvent. Every second day the cells were seeded in fresh medium. To assess short-term toxicity (1-3 d) and to determine potential synergism between two inhibitors, cells were seeded at 0.1 to 0.2×10^6 cells/ml, treated and quantified using an MTS assay (Promega) according to the manufacturer's instructions. The combination index (CI) was calculated with the CompuSyn software.⁴

Quantitative real-time PCR

Total RNA was extracted using the RNeasy Mini Kit (Qiagen) and transcribed into cDNA employing the Biozym cDNA synthesis kit (Biozym) with random hexamer primers according to the manufacturer's instructions. Transcript levels were determined by qPCR using a LightCycler 480 II system (Roche) and SYBR Fast qPCR master mix (Genaxxon). Relative transcript expression was calculated with the $2(-\Delta\Delta Ct)$ method. Succinate dehydrogenase complex subunit A (*SDHA*) was used as a reference gene. Sequences of primers used for qPCR are provided in **Suppl.**

Table 3.

Gene expression profiling and GSEA

Gene expression profiling was performed in HBL-1 cells after 12, 24, 36 and 48 h treatment with 40 μ M DMF. Briefly, total RNA was isolated using the RNeasy Mini Kit

(Qiagen) following the manufacturer's protocol. RNA was amplified and labeled with the TotalPrep RNA Amplification Kit (ThermoFisher) and labeled samples were hybridized on HumanHT-12 v4 Expression BeadChips (Illumina) according to the manufacturer's protocol. Sequenced reads of mRNA were aligned against the human transcriptome using HISAT2.⁵ Aligned sequence counts were then aggregated for genes using RSEM.⁶

A non-negative binomial test (Bioinformatics Toolbox of MATLAB® R2019a, The MathWorks® Inc., USA) was used to calculate p-values of gene regulation comparing DMF and solvent over all time points. To analyze in an unbiased fashion which biological processes were affected by DMF, we performed gene set enrichment analysis (GSEA), testing an integrated database of 21,466 gene expression signatures for enrichment with respect to the gene ranking by DMF regulation.⁷ This database contained signatures from the Molecular Signatures Database v6.2, the GeneSigDB v4, HGCN gene families and the Staudt laboratory library.⁸⁻¹¹ GSEA p-values were computed by permutation tests and FDRs were computed relative to respective signature families.

The gene expression data are available from the Gene Expression Omnibus of the National Center for Biotechnology Information (www.ncbi.nlm.nih.gov/geo) through GEO accession number GSE164267.

Analysis of *ALOX5* promoter methylation

To analyze the DNA methylation status of the *ALOX5* promoter, genomic DNA from various cell lines was isolated using the Wizard Genomic DNA Purification Kit (Promega) according to the manufacturer's protocol. Non-methylated cytosines were

converted using the MethylEdge Bisulfite Conversion System (Promega) according to the manufacturer's instructions. A part of the *ALOX5* promoter was amplified by standard PCR (primers: fw: GTTAGGGATTAGTGGTGGGAG; rev: AAAACTTATCCAACAATACTTCTC), sequenced and methylation surrounding the transcription start site (-48 to +120) was analyzed.

Immunohistochemistry

5-LOX expression was evaluated in three reactive lymph node specimens, in formalin-fixed, paraffin-embedded DLBCL cell lines and in 153 human DLBCL specimens on tissue microarray (TMA) format. Cell of origin (COO) was assigned by digital gene expression profiling, indicating 89 GCB and 64 non-GCB DLBCLs. Paraffin sections were immunostained with the monoclonal anti-ALOX5 antibody (OTI2C5; dilution 1:150; ThermoFisher) according to standard protocols with the Lab Vision Autostainer 720 (ThermoFisher).

Nuclear fractionation and DNA-binding of NF- κ B (TransAM)

Nuclear extracts were prepared using the Nuclear Extract Kit (Active Motif) according to the instructions of the manufacturer. DNA binding of RelA, c-Rel and p50 was quantified employing the NF- κ B family TransAM kit (Active Motif) according to the manufacturer's protocol.

Cell lysis, immunoprecipitation and immunoblotting

Cells were lysed in lysis buffer (50 mM Tris-HCl pH 7.4, 150 mM NaCl, 1% NP-40, 50 mM NaF, 10 mM Na₄P₂O₇, 10 mM Na₄V₂O₇ and Complete protease inhibitor cocktail; Roche). To assess K63-linked polyubiquitination of FLAG-BCL10, the lysis buffer was supplemented with protease inhibitors, 50 mM N-ethyl maleimide (NEM; Sigma-Aldrich) and 100 μM PR619 (Merck). Anti-FLAG M2 Affinity Gel (Sigma-Aldrich) was used for the immunoprecipitation of FLAG-tagged BCL10. Pulldown of JAK1-Strep in HEK293T lysates was performed in lysis buffer containing 1% Brij-96 using Strep-Tactin sepharose resin (IBA). SDS-PAGE and immunoblotting were performed as described previously.¹ A list of primary antibodies used for Western blot is available in **Suppl. Table 4**. Antibodies raised against FSP1 and system x_c⁻ were a kind gift of M. Conrad.

Mass spectrometry and structural analysis

For mass spectrometric analysis of the DMF-induced succination of cysteine residues, endogenous JAK1 and IKK2 were immunoprecipitated from solvent and DMF-treated HBL-1 cells. Following several washing steps, the immunoprecipitated proteins were on-bead digested with 5 μg/ml modified sequencing-grade trypsin (Promega) or using a combination of Trypsin and GluC (Promega) in 2 M urea, 50 mM Tris-HCl pH 7.5 and 1 mM DTT overnight at 28°C. Peptides were alkylated using iodoacetamide (5 mg/ml) and incubated in the dark for 30 min at room temperature. Samples were desalted using C18 Stage Tips as described.¹² Peptide mixtures were injected automatically and loaded at a flow rate of 30 μl/min in 0.1% trifluoroacetic acid in high performance liquid chromatography (HPLC)-grade water onto a nano trap column (300 μm inner diameter × 5 mm pre-column, packed with Acclaim PepMap100 C18, 5 μm, 100 Å; ThermoFisher). After 3 min, peptides were eluted and separated on the analytical

column (75 μm inner diameter \times 25 cm, Acclaim PepMap RSLC C18, 2 μm , 100 \AA ; ThermoFisher) by a linear gradient from 2% to 30% of buffer B (80% acetonitrile and 0.08% formic acid in HPLC-grade water) in buffer A (2% acetonitrile and 0.1% formic acid in HPLC-grade water) at a flow rate of 300 nl/min over 107 min. Remaining peptides were eluted by a short gradient from 30% to 95% buffer B in 10 min. Analysis of the eluted peptides was performed on a QExactive Plus mass spectrometer (ThermoFisher). From the high-resolution MS pre-scan with a mass range of 335 to 1,500, the ten most intense peptide ions were selected for fragment analysis in the Orbitrap depending on intensity (at least 200 counts) and if they were at least doubly charged. The normalized collision energy for higher-energy collisional dissociation was set to a value of 35 or 30 and the resulting fragments were detected with a resolution of 70,000. The lock mass option was activated; the background signal with a mass of 445.12003 was used as lock mass. Every ion selected for fragmentation was excluded for 60 s by dynamic exclusion. MS/MS data were analyzed using the Mascot software (version 2.5.1) and visualized using the Scaffold software (version 4.11.0). As a digesting enzyme, Trypsin/P or Trypsin-GluC was selected with maximal two missed cleavages. Cysteine carbamidomethylation was set for fixed modifications, and oxidation of methionine and N-terminal acetylation was specified as variable modifications. To identify peptides with succination sites on JAK1 and IKK2 we used as variable modifications 2-succinyl, 2-dimethylsuccinyl or 2-monomethylsuccinyl. Identified peptides with and without succinyl modification were selected and entered in an inclusion list for targeted mass spectrometry analysis using Parallel Reaction Monitoring (PRM) performed on a QExactive Plus mass spectrometer. For data analysis of targeted mass spectrometry, obtained raw data were processed using the open source software tool Skyline for targeted proteomics and the evaluation of the

resulting data.¹³ The MS2 spectra obtained from Mascot searches were integrated and visualised using the PDV software suite.¹⁴

All mass spectrometry RAW data files were made available publicly in the proteomexchange database (proteomexchange.org) under the project ID accession number PXD024441.

For visualization of selected cysteines in the protein structure, Pdb entries were obtained from the protein data bank (www.rcsb.org). Structure figures were generated and rendered with pymol (The PyMOL Molecular Graphics System, Version 2.0 Schrödinger, LLC.).

Xenograft mouse model, zebrafish husbandry and yolk sac transplantation

For the VFN-D1 patient-derived and the HBL-1 xenograft mouse models, adult female NOD.Cg-Prkdc^{scid} Il2rg^{tm1Wjl}/SzJ (NSG) mice were implanted subcutaneously with 1×10^7 cells in PBS (300 μ l). Once mice developed palpable tumors, the animals were randomized into control, DMF (daily i.p. treatment with 500 μ l of 3 mg/ml DMF in PBS), ABT-199 (daily p.o. treatment with 100 mg/kg in ethanol/PhosalG/PEG400) or DMF+ABT-199 treated groups. Tumor volumes were measured at the indicated times with a caliper in three perpendicular dimensions and calculated with $V = 1/2 \times (\text{length} \times \text{width}^2)$. The animal experiment was approved by the institutional Animal Welfare Committee (Czech Republic, Approval MSMT-19427/2019-4).

Zebrafish experiments and husbandry were approved by the “Kantonales Veterinäramt Basel-Stadt” (Haltebewilligung: 1024H) in Switzerland. Zebrafish wild-type Tübingen strains were bred and maintained as described previously and according to FELASA

and Swiss federal law guidelines.¹⁵ Xenotransplantation was performed using SU-DHL-6 and DOHH2 cell lines. After harvesting, cells were labeled with a lipophilic red fluorescent dye (CellTracker™ CM-Dil, ThermoFisher), according to the manufacturer's instructions. Zebrafish were maintained, collected, grown and staged in E3 medium at 28.5°C according to standard protocols.¹⁶ For xenotransplantation experiments, zebrafish embryos were anesthetized in 0.4% tricaine at 48 hpf (hours post-fertilization) and 200 SU-DHL-6 or DOHH2 cells were micro-injected into the vessel-free area of the yolk sac. After injection, embryos were incubated for 1 h at 28.5-29°C for recovery. Cell transfer was then verified by examining the presence of a fluorescent cell mass localized at the injection site in the yolk sac via fluorescence microscopy. Afterwards, fish were treated with DMF or solvent as indicated for three consecutive days. At 5 dpf (days post-fertilization), embryos were screened by fluorescence microscopy for a normal morphology as well as a visible cell mass in the yolk using a Zeiss SteREO Discovery V20 microscope and the number of tumor-bearing fish was quantified. For each condition, at least 20 fish were analyzed over 3-4 biological replicates. Representative pictures were taken using a Nikon CSU-W1 spinning disk microscope.

Supplemental Figures

Supplemental Figure 1. DMF treatment induces cytotoxicity in DLBCL cells.

A, B) GCB (**A**) and ABC (**B**) DLBCL cell lines were treated daily with DMSO or 20 μ M DMF. Cell numbers were determined as indicated and normalized to the solvent control. **C, D)** GCB (**C**) and ABC (**D**) DLBCL cell lines were treated for 3 days with solvent or the indicated DMF concentrations. Error bars correspond to the mean \pm SD. Data is representative of at least three (**A, B**) independent experiments.

Supplemental Figure 2. Low-dose DMF is toxic for MCL but not for other tumor cell lines.

A, B) MCL cell lines (**A**) or A431 (epidermoid carcinoma), A549 (adenocarcinomic alveolar basal epithelial), HaCaT (aneuploid immortal keratinocyte), HT1080 (fibrosarcoma), Huh7 (hepatocarcinoma), SK-MEL-28 (melanoma) and SMMC-7721 (hepatocarcinoma) cells (**B**) were treated daily with DMSO or 20 μ M DMF. Cell numbers were determined as indicated and normalized to the solvent control. Error bars correspond to the mean \pm SD. Data is representative of at least two independent experiments.

Supplemental Figure 3. Dimethyl itaconate but not the DMF metabolite MMF exhibits anti-lymphoma activity.

A) The indicated DLBCL cell lines were treated daily with 20 μ M DMF, monomethyl fumarate (MMF) or dimethyl succinate (DMS). Cell numbers were determined and normalized to the solvent control. **B)** Titration of DMF, MMF and DMS in the indicated DLBCL cell lines. Cell numbers were quantified by MTS assay 48 h after treatment and normalized to the respective solvent control (0 μ M). **C)** Nrf2 induction by DMF or

dimethyl itaconate (DI) treatment (4 h) of DLBCL cell lines was visualized by immunoblot analysis. Tubulin served as loading control. **D, E**) Cell counts of GCB (**D**) and ABC (**E**) DLBCL cell lines upon daily treatment with 20 μ M DMF or 80 μ M DI were normalized to the solvent control. Error bars correspond to the mean \pm SD. Data is representative of at least two independent experiments.

Supplemental Figure 4. DMF depletes GSH and induces lipid peroxidation in DLBCL and MCL cell lines.

A) Quantification of reduced glutathione (GSH) in DOHH2 cells treated with solvent, DMF, buthionine sulfoximine (BSO) or erastin for the indicated times and concentrations. GSH levels were normalized the respective solvent controls. **B-D)** Lipid peroxidation was quantified by flow cytometry using BODIPY C11 in DMF-treated ABC DLBCL (**B**), MCL (**C**) or myeloid (**D**) cell lines. Error bars correspond to the mean \pm SD. Data is representative of at least two (**A, C-D**) or three (**B**) independent experiments.

Supplemental Figure 5. Ferrostatin-1 protects from DMF-induced lipid peroxidation and cytotoxicity.

A) Oxidation of BODIPY C11 in GCB DLBCL cells treated with RSL3 or DMF was quantified by flow cytometry. Lipid peroxidation was prevented by co-treatment with ferrostatin-1 (Fer-1, 10 μ M), α -tocopherol (100 μ M) or deferoxamine (DFX, 100 μ M). **B, C)** The GCB DLBCL cell line DOHH2 (**B**) and the ABC DLBCL cell lines U2932, SU-DHL-2 and HBL-1 (**C**) were treated daily with either 20 μ M DMF alone or in combination with 5 μ M Fer-1. Cell numbers were determined and normalized to the solvent control. **D)** The GCB DLBCL cell lines DOHH2 and OCI-Ly7 were treated either

with 20 μ M DMF alone or in combination with increasing concentrations of N-acetyl-L-cysteine (NAC; 5, 10 and 25 μ M). Survival of the cells was determined by MTS assay 24 h after treatment and normalized to the solvent control. Error bars correspond to the mean \pm SD. Data is representative of at least two **(B-D)** or three **(A)** independent experiments.

Supplemental Figure 6. Forced expression of RelA reduces DMF-mediated cytotoxicity in GCB DLBCL.

A) Quantification of lipid peroxidation by flow cytometry (BODIPY C11) in DMF-treated control and FLAG-RelA overexpressing WSU-DLCL-2 cells. The mean fluorescence intensity (MFI) of oxidized BODIPY C11 in DMF-treated cells was normalized to the MFI of the respective solvent-treated samples. **B)** OCI-Ly7 cells expressing control vector or FLAG-RelA were counted and treated daily with 20 μ M DMF for 6 days. Cell numbers were normalized to the respective solvent control. Error bars correspond to the mean \pm SD. Data is representative of at least two independent experiments.

Supplemental Figure 7. GPX4 and 5-LOX expression in DLBCL.

A) *GPX4* mRNA levels were determined by qPCR in the indicated cell lines. Expression was normalized to the myeloid cell line U937. *SDHA* served as reference gene. **B)** *GPX4* protein levels in GCB and ABC DLBCL cell lines were visualized by immunoblotting. Tubulin served as loading control. **C)** *ACSL4* mRNA levels were determined by qPCR in the indicated cell lines. Expression was normalized to the myeloid cell line U937. *SDHA* served as reference gene. **D, E)** Immunohistochemical staining of 5-LOX in a section of a reactive lymph node (LN) **(D)** or in the GCB DLBCL cell line OCI-Ly19 and the ABC DLBCL cell line U2932 **(E)**. **F)** Analysis of CpG island methylation of the *ALOX5* promoter in the indicated DLBCL cell lines. **G)** Visualization

of 5-LOX expression levels in GCB DLBCL cell lines treated with solvent or 300 nM mithramycin A. GAPDH served as loading control. Error bars correspond to the mean \pm SD. Data is representative of at least two (**A-C**) or three (**F, G**) independent experiments.

Supplemental Figure 8. B-cell activation regulates 5-LOX expression.

A) Immunoblot analysis of 5-LOX protein levels in ABC DLBCL cell lines treated with solvent or 5 μ M sotrastaurin (STN) for 24 h. Tubulin served as loading control. **B)** Quantification of *ALOX5* mRNA levels in U2932 cells transduced with either non-targeting vector control or an shRNA targeting CD79A. *SDHA* served as reference gene. **C)** The efficacy of the shRNA-mediated knockdown of CD79A was controlled by immunoblotting. Tubulin served as loading control. **D)** The GCB DLBCL cell line SU-DHL-6 was treated with agonistic anti-IgG/IgM antibodies for 8 h in the absence or presence of 5 μ M STN. *ALOX5* and *TNFAIP3* transcript levels were quantified by qPCR and normalized to the unstimulated control. *SDHA* served as reference gene. **E)** The indicated GCB DLBCL cell lines were activated with anti-IgG/IgM for 8 h and analyzed for *ALOX5* mRNA expression. *SDHA* served as reference gene. Error bars correspond to the mean \pm SD. Data is representative of at least two (**B-E**) or three (**A**) independent experiments.

Supplemental Figure 9. Lipoxygenase inhibitors alleviate DMF-mediated toxicity.

A, B) Lipid peroxidation in the indicated GCB DLBCL cell lines treated with solvent, 20 μ M DMF alone or in combination with 10 μ M zileuton was quantified by flow cytometry using BODIPY C11. The mean fluorescence intensity (MFI) of oxidized BODIPY C11 in DMF-treated cells was normalized to the MFI of the respective solvent-treated samples. **C, D)** The indicated GCB DLBCL cell lines were treated with either

20 μ M DMF alone or in combination with 10 μ M zileuton (**C**) or 1 μ M nordihydroguaiaretic acid (NDGA) (**D**) for 2 days. Cell numbers were determined by MTS assay and normalized to the solvent control. **E**) Control or *ALOX5*-silenced DOHH2 cells were incubated with increasing concentrations of DMF for 24 h. Cell survival was quantified by MTS assay. **F**) The survival of WSU-DLCL-2 cells treated with 20 μ M DMF alone or in combination with 10 μ M zileuton, 2.5 μ M CJ-13610, 5 μ M CAY10649 or 10 μ M MK-886 was assessed by MTS assay. **G**) The shRNA-mediated knockdown of 5-LOX expression was verified by immunoblot analysis. Tubulin served as loading control. **H**) Quantification of the GSH/GSSG ratio in the indicated control and *ALOX5*-silenced GCB DLBCL cell lines. **I**) The indicated cell lines were treated with 5 μ M DMF consecutively six times within 3 weeks and analyzed for Nrf2, HO-1 and 5-LOX expression by immunoblot analysis. GAPDH served as loading control. Error bars correspond to the mean \pm SD. Data is representative of at least two (**B**, **E-I**) or three (**A**, **C-D**) independent experiments.

Supplemental Figure 10. DMF induces lipid peroxidation in 5-LOX overexpressing HT cells.

A) Quantification of BODIPY C11 oxidation in DMF-treated HT cells by flow cytometry. **B**) Glutathione (GSH) levels in the indicated cell lines. GSH content was normalized to the myeloid cell line THP-1. **C**) The ratio of reduced GSH to oxidized GSSG was quantified in solvent- and DMF-treated cells. **D**, **E**) HT cells were lentivirally transduced with an expression construct encoding FLAG-5-LOX. BODIPY C11 oxidation upon DMF treatment in empty vector or FLAG-5-LOX transduced cells was analyzed by flow cytometry. MFI of oxidized BODIPY C11 was normalized to the MFI of its reduced form and subsequently to solvent-treated control cells (**D**). FLAG-5-LOX expression in HT

cells was visualized by immunoblot analysis. Tubulin served as loading control (**E**). Error bars correspond to the mean \pm SD. Data is representative of at least two (**B-C**) or three (**A, D-E**) independent experiments.

Supplemental Figure 11. DMF regulates NF- κ B target gene expression in ABC DLBCL.

A) In HBL-1 cells gene set enrichment analysis identified various NF- κ B gene sets down-regulated by DMF treatment. **B, C)** The indicated ABC DLBCL cell lines were treated for 6 h with solvent or 20 μ M DMF and mRNA expression of the indicated genes was assessed by qPCR. Expression levels of DMF-treated cells were normalized to the respective solvent control. *SDHA* served as reference gene. Error bars correspond to the mean \pm SD. Data is representative of at least two (**B-C**) independent experiments.

Supplemental Figure 12. DMF-mediated IKK inhibition is independent of Nrf2.

A) I κ B α phosphorylation of solvent or DMF-treated ABC DLBCL cell lines was visualized by immunoblot analysis in the presence of the proteasome inhibitor MG-132. GAPDH served as loading control. **B)** Nuclear (N) and cytoplasmic (C) fractions of solvent or DMF-treated HBL-1 cells were analyzed by immunoblotting for RelA translocation to the nucleus. Lamin A/C served as marker for the nuclear, GAPDH as marker for the cytoplasmic fraction, respectively. **C)** HBL-1 cells were transduced with control vector or an shRNA targeting Nrf2 and treated for 4 h with solvent or the indicated DMF doses. The phosphorylation of I κ B α and the efficacy of Nrf2 silencing were visualized by immunoblot analysis. Tubulin served as loading control. **D, E)** The ABC DLBCL cell line HBL-1 was lentivirally transduced with a control vector or two

independent Nrf2-targeting shRNAs. Upon daily treatment with 20 μ M DMF, cell numbers were determined and normalized to the untreated controls **(D)**. Knockdown of Nrf2 expression was verified by immunoblot analysis. GAPDH served as loading control **(E)**. **F, G)** The indicated ABC DLBCL cell lines were treated for 16 h with solvent, 20 μ M DMF, 20 μ M monomethyl fumarate (MMF), 20 μ M dimethyl succinate (DMS) **(F)** or solvent, 20 μ M DMF, 100 μ M buthionine sulfoximine (BSO), 0.5 μ M erastin, 100 nM RSL3 **(G)**, as indicated. The phosphorylation of I κ B α was assessed by immunoblot analysis, GAPDH served as loading control. Data is representative of at least two independent experiments.

Supplemental Figure 13. Upstream BCR and TLR signaling is not affected by DMF treatment.

A) The ABC DLBCL cell lines HBL-1 and U2932 were treated for 4 h with the indicated concentrations of DMF. The phosphorylation of signaling proteins was visualized by immunoblot analysis. Tubulin served as loading control. **B)** U2932 cells were treated with the indicated DMF concentrations or with the MALT1 protease inhibitor LVSR-fmk (2 μ M) for 4 h and the proteasome inhibitor MG-132 (5 μ M) 90 min prior to harvesting. MALT1-mediated RelB cleavage was visualized by immunoblot analysis. GAPDH served as loading control. **C)** HBL-1 cells were transduced with a control or an expression vector encoding FLAG-tagged BCL10 and incubated with solvent or 40 μ M DMF for 4 h. BCL10 was immunoprecipitated using anti-FLAG beads and analyzed for K63-linked polyubiquitination. GAPDH served as loading control. Data is representative of at least two independent experiments.

Supplemental Figure 14. Succination of IKK2 C179, C464 and NEMO C347 by DMF treatment.

A, B) The ABC DLBCL cell line HBL-1 was treated with 50 μ M DMF for 4 h. IKK2 was immunoprecipitated and analyzed for the presence of succinated peptides. Tryptic digestion of the immunoprecipitate yielded succinated peptides comprising IKK2 C464 and NEMO C347 that were subsequently identified by mass spectrometry. Additionally, GluC digestion of the IKK2 immunoprecipitate revealed succination of IKK2 at C179. The mass-to-charge ratios in relation to their intensities of the IKK2 (**A**) and NEMO (**B**) peptide fragments are shown. All succinated peptides were identified in at least three independent samples.

Supplemental Figure 15. The succinated cysteines in IKK2 and NEMO are conserved.

A) Schematic representation of IKK2 domain structure including its protein kinase, leucine zipper (LZ) and NEMO-binding (NBD) domains. Alignment of IKK2 sequences surrounding the conserved C179 and C464 from various species. **B)** Alignment of NEMO sequences surrounding the conserved C347 from various species.

Supplemental Figure 16. DMF treatment reduces the phosphorylation of STAT1 and STAT3.

A) The ABC DLBCL cell lines HBL-1 and OCI-Ly3 were incubated with 40 μ M DMF and the phosphorylation of STAT3 and STAT1 at the indicated time points was assessed by immunoblot analysis. GAPDH served as loading control. **B)** ABC DLBCL cell lines were treated with solvent, 40 μ M DMF and/or 3 ng/ml recombinant human IL-10. Phosphorylation of STAT1/3 was visualized by immunoblot analysis. GAPDH served as loading control. **C)** ABC DLBCL cells were treated with solvent, DMF and/or

recombinant human IL-10 as indicated. The phosphorylation of JAK1 and STAT3 was revealed by Western blot. Tubulin served as loading control. **D, E)** The indicated ABC DLBCL cell lines were treated for 16 h with solvent, 20 μ M DMF, 20 μ M monomethyl fumarate (MMF), 20 μ M dimethyl succinate (DMS) (**D**) or solvent, 20 μ M DMF, 100 μ M buthionine sulfoximine (BSO), 0.5 μ M erastin, 100 nM RSL3 (**E**). STAT1/3 phosphorylation was analyzed by immunoblot analysis. GAPDH served as loading control. Data is representative of at least two independent experiments.

Supplemental Figure 17. Succination of JAK1 C257 and C731 by DMF treatment.

A) The ABC DLBCL cell line HBL-1 was treated with 50 μ M DMF for 4 h. JAK1 was immunoprecipitated, subjected to tryptic digestion and analyzed for the presence of succinated peptides. The MS spectra revealed succination of JAK1 at C257 and C731. All succinated peptides were identified in at least three independent samples. **B)** HEK293T cells were transiently transfected with V5-tagged IL-10 receptor (alpha subunit, IL10RA-V5) alone or in combination with Strep-tagged JAK1^{C257A}. 24 h after transfection, cells were treated with solvent or DMF for 1 h, lysed and JAK1 was pulled-down using Strep-Tactin beads. The interaction between IL10RA-V5 and JAK1-Strep was visualized by immunoblot analysis. **C)** HEK293T cells were transiently transfected with either expression constructs encoding JAK1 wildtype, JAK1^{C257A} or an empty control vector. After 24 h, cells were treated with DMF or solvent for 1.5 h and analyzed for STAT1 phosphorylation by immunoblotting. Tubulin served as loading control. Data is representative of at least two (**B-C**) independent experiments.

Supplemental Figure 18. FSP1 and BCL-2 inhibition synergizes with DMF treatment.

A) The indicated GCB DLBCL cell lines were treated with DMF alone (left panels) or in combination with the FSP1 inhibitor iFSP1 (right panels). Survival was quantified after 24 h by MTS assay. **B)** The ABC DLBCL cell lines U2932 and TMD8 were treated either with DMF alone (left panels) or with DMF and the BCL-2 inhibitor ABT-199 (right panels). Cells were treated once with ABT-199 and twice with DMF (at timepoints 0 and 24 h). Survival was quantified after 72 h by MTS assay. Error bars correspond to the mean \pm SD. Data is representative of three independent experiments.

Supplemental Figure 19. Neither the PI3K inhibitor AZD8835 nor the tubulin polymerization inhibitor vincristine synergizes with DMF.

A-B) The indicated DLBCL cell lines were treated with DMF alone or in combination with the PI3K inhibitor AZD8835 (**A**) or vincristine (**B**), as indicated. Cells were treated twice with DMF (0, 24 h) and cell survival was quantified after 72 h by MTS assay. Error bars correspond to the mean \pm SD. Data is representative of at least two independent experiments.

Supplemental Tables

Cell line	Medium
A431	DMEM + 10% FCS
A549	DMEM + 10% FCS
BJAB	RPMI + 10% FCS
DOHH2	RPMI + 10% FCS
Granta 519	RPMI + 10% FCS
HaCaT	DMEM + 10% FCS
HBL-1	RPMI + 20% FCS
HEK293T	DMEM + 10% FCS
HT	RPMI + 10% FCS
HT1080	DMEM + 10% FCS
Huh7	DMEM + 10% FCS
JEKO-1	RPMI + 20% FCS
Karpas 422	RPMI + 20% FCS
K562	RPMI + 10% FCS
Maver-1	RPMI + 20% FCS
OCI-Ly1	IMDM + 10% FCS
OCI-Ly3	RPMI + 20% FCS
OCI-Ly4	RPMI + 10% FCS
OCI-Ly7	IMDM + 10% FCS
OCI-Ly8	IMDM + 10% FCS
OCI-Ly10	IMDM + 20% human serum
OCI-Ly19	IMDM + 10% FCS
Pfeiffer	RPMI + 10% FCS
Rec1	RPMI + 10% FCS
RIVA	RPMI + 20% FCS
SK-MEL-28	DMEM + 10% FCS
SMMC-7721	DMEM + 10% FCS
SU-DHL-2	RPMI + 20% FCS
SU-DHL-4	RPMI + 10% FCS
SU-DHL-5	RPMI + 20% FCS
SU-DHL-6	RPMI + 10% FCS
SU-DHL-8	RPMI + 20% FCS
Toledo	RPMI + 20% FCS
THP-1	RPMI + 10% FCS
TMD8	RPMI + 20% FCS
U2932	RPMI + 20% FCS
U937	RPMI + 10% FCS
UPN-1	RPMI + 10% FCS
WSU-DLCL-2	RPMI + 10% FCS
Z138	RPMI + 10% FCS

Suppl. Table 1: Cell lines and cell culture media used in this study.

Target gene	Clone ID	Sequence (5'>3')
<i>NFE2L2</i> #1	TRCN0000273494	AGTTTGGGAGGAGCTATTATC
<i>NFE2L2</i> #2	TRCN0000007555	GCTCCTACTGTGATGTGAAAT
<i>ALOX5</i>	TRCN0000056568	CCTGTTTCATCAACCGCTTCAT
<i>CD79A</i>	TRCN0000057514	ACTTCCAATGCCCGCACAATA

Suppl. Table 2: Clone ID and sequence of shRNA vectors used.

Target	Primer	Sequence (5'>3')
<i>SDHA</i>	SDHA_F	CAAACAGGAACCCGAGGTTTT
	SDHA_R	CAGCTTGGTAACACATGCTGTAT
<i>ALOX5</i>	ALOX5_F	CTCAAGCAACACCGACGTAAT
	ALOX5_R	CCTTGTGGCATTGTTGGCATCG
<i>GPX4</i>	GPX4_F	GAGGCAAGACCGAAGTAAACTAC
	GPX4_R	CCGAACTGGTTACACGGGAA
<i>ACSL4</i>	ACSL4_F	ACTGGCCGACCTAAGGGAG
	ACSL4_R	GCCAAAGGCAAGTAGCCAATA
<i>TNFAIP3</i>	TNFAIP3_F	TCCTCAGGCTTTGTATTTGAGC
	TNFAIP3_R	TGTGTATCGGTGCATGGTTTTA
<i>CD40</i>	CD40_F	ACTGAAACGGAATGCCTTCCT
	CD40_R	CCTCACTCGTACAGTGCCA
<i>BIRC3</i>	BIRC3_F	AAGCTACCTCTCAGCCTACTTT
	BIRC3_R	CCACTGTTTTCTGTACCCGGA
<i>NFKBIA</i>	NFKBIA_F	CTCCGAGACTTTTCGAGGAAATAC
	NFKBIA_R	GCCATTGTAGTTGGTAGCCTTCA
<i>NFKBIZ</i>	NFKBIZ_F	CCAGCCTGGGAGCATGATTG
	NFKBIZ_R	GCCGTAGAAGTAGCTCAGGTTG
<i>CFLAR</i>	CFLAR_F	TCAAGGAGCAGGGACAAGTTA
	CFLAR_R	GACAATGGGCATAGGGTGTATC
<i>STAT3</i>	STAT3_F	CAGCAGCTTGACACACGGTA
	STAT3_R	AAACACCAAAGTGGCATGTGA
<i>SOCS3</i>	SOCS3_F	CCTGCGCCTCAAGACCTTC
	SOCS3_R	GTCCTGCGCTCCAGTAGAA
<i>OSGIN1</i>	OSGIN1_F	CCCGGTCATCATTGTGGGTAA
	OSGIN1_R	GCTTCGTGTAGGGTGTGTAGC
<i>NQO1</i>	NQO1_F	GAAGAGCACTGATCGTACTGGC
	NQO1_R	GGATACTGAAAGTTCGCAGGG
<i>GCLM</i>	GCLM_F	CATTTACAGCCTTACTGGGAGG
	GCLM_R	ATGCAGTCAAATCTGGTGGCA
<i>SLC7A11</i>	SLC7A11_F	TCTCAAAGGAGGTTACCTGC
	SLC7A11_R	AGACTCCCCTCAGTAAAGTGAC
<i>SRNX1</i>	SRNX1_F	CAGGGAGGTGACTACTTCTACTC
	SRNX1_R	CAGGTACACCCTTAGGTCTGA
<i>TXNRD1</i>	TXNRD1_F	ATATGGCAAGAAGGTGATGGTCC
	TXNRD1_R	GGGCTTGTCTAACAAGCTG
<i>CD79A</i>	CD79A_F	CAAGAACCGAATCATCACAGCC
	CD79A_R	TCTGCCATCGTTTCCTGAACA

Suppl. Table 3: Primer sequences used for qPCR.

Target	Source	Provider	Catalogue no.
Nrf2	rabbit monoclonal	Cell Signaling	#12721
Tubulin	mouse monoclonal	Sigma-Aldrich	T9026
5-LOX	rabbit monoclonal	Cell Signaling	#3289
GPX4	rabbit polyclonal	Cell Signaling	#52455
GAPDH	rabbit monoclonal	Cell Signaling	#5174
P-IkB α S32/S36	mouse monoclonal	Cell Signaling	#9246
IkB α	mouse monoclonal	Cell Signaling	#4814
HO-1	rabbit monoclonal	Cell Signaling	#43966
RelA	rabbit monoclonal	Cell Signaling	#8242
Lamin A/C	rabbit polyclonal	Cell Signaling	#2032
CD79A	rabbit monoclonal	Cell Signaling	#13333
P-BLNK Y96	rabbit polyclonal	Cell Signaling	#3601
P-PLC γ 2 Y1217	rabbit polyclonal	Cell Signaling	#3871
P-ERK1/2 Y204/Y187	mouse monoclonal	Santa Cruz	sc-7383
ERK1/2	mouse monoclonal	Santa Cruz	sc-514302
P-AKT S473	rabbit monoclonal	Cell Signaling	#4058
AKT	rabbit monoclonal	Cell Signaling	#4691
P-JNK1/2 T183/Y185	rabbit monoclonal	Cell Signaling	#4668
JNK1/2	rabbit monoclonal	Cell Signaling	#9258
c-JUN	rabbit monoclonal	Cell Signaling	#9165
P-p38 T180/Y182	rabbit monoclonal	Cell Signaling	#4511
p38	rabbit monoclonal	Cell Signaling	#8690
p100/p52	rabbit polyclonal	Cell Signaling	#4882
P-IRAK4 T345/S346	rabbit monoclonal	Cell Signaling	#11927
IRAK4	rabbit polyclonal	Cell Signaling	#4363
K63-Ubiquitin	rabbit monoclonal	Cell Signaling	#5621
BCL10	rabbit polyclonal	Santa Cruz	sc-5611
P-STAT3 Y705	rabbit polyclonal	Cell Signaling	#9145
STAT3	mouse monoclonal	Cell Signaling	#9139
P-STAT1 Y701	rabbit monoclonal	Cell Signaling	#9167
STAT1	rabbit monoclonal	Cell Signaling	#14994
P-JAK1 Y1034/Y1035	rabbit monoclonal	Cell Signaling	#74129
JAK1	mouse monoclonal	Cell Signaling	#50996
P-TYK2 Y1054/Y1055	rabbit monoclonal	Cell Signaling	#68790
TYK2	rabbit monoclonal	Cell Signaling	#14193
JAK2	rabbit monoclonal	Cell Signaling	#3230
Tom20	mouse monoclonal	BD Biosciences	612278
IKK2	rabbit polyclonal	Cell Signaling	#2678
KEAP1	rabbit polyclonal	Cell Signaling	#4678
V5 epitope tag	rabbit polyclonal	Diagenode	C15410270

Suppl. Table 4: Primary antibodies used for immunoblotting.

Supplemental References

1. Bucher P, Erdmann T, Grondona P, et al. Targeting chronic NFAT activation with calcineurin inhibitors in diffuse large B-cell lymphoma. *Blood*. 2020;135(2):121-132.
2. Ngo VN, Young RM, Schmitz R, et al. Oncogenically active MYD88 mutations in human lymphoma. *Nature*. 2011;470(7332):115-119.
3. Wenzel SS, Grau M, Mavis C, et al. MCL1 is deregulated in subgroups of diffuse large B-cell lymphoma. *Leukemia*. 2013;27(6):1381-1390.
4. Chou TC. Theoretical basis, experimental design, and computerized simulation of synergism and antagonism in drug combination studies. *Pharmacol Rev*. 2006;58(3):621-681.
5. Kim D, Langmead B, Salzberg SL. HISAT: a fast spliced aligner with low memory requirements. *Nat Methods*. 2015;12(4):357-360.
6. Li B, Dewey CN. RSEM: accurate transcript quantification from RNA-Seq data with or without a reference genome. *BMC Bioinformatics*. 2011;12:323.
7. Subramanian A, Tamayo P, Mootha VK, et al. Gene set enrichment analysis: a knowledge-based approach for interpreting genome-wide expression profiles. *Proc Natl Acad Sci U S A*. 2005;102(43):15545-15550.
8. Culhane AC, Schroder MS, Sultana R, et al. GeneSigDB: a manually curated database and resource for analysis of gene expression signatures. *Nucleic Acids Res*. 2012;40(Database issue):D1060-1066.
9. Gray KA, Daugherty LC, Gordon SM, Seal RL, Wright MW, Bruford EA. Genenames.org: the HGNC resources in 2013. *Nucleic Acids Res*. 2013;41(Database issue):D545-552.
10. Liberzon A, Birger C, Thorvaldsdottir H, Ghandi M, Mesirov JP, Tamayo P. The Molecular Signatures Database (MSigDB) hallmark gene set collection. *Cell Syst*. 2015;1(6):417-425.
11. Shaffer AL, Wright G, Yang L, et al. A library of gene expression signatures to illuminate normal and pathological lymphoid biology. *Immunol Rev*. 2006;210:67-85.
12. Kennedy SA, Jarboui MA, Srihari S, et al. Extensive rewiring of the EGFR network in colorectal cancer cells expressing transforming levels of KRAS(G13D). *Nat Commun*. 2020;11(1):499.
13. MacLean B, Tomazela DM, Shulman N, et al. Skyline: an open source document editor for creating and analyzing targeted proteomics experiments. *Bioinformatics*. 2010;26(7):966-968.
14. Li K, Vaudel M, Zhang B, Ren Y, Wen B. PDV: an integrative proteomics data viewer. *Bioinformatics*. 2019;35(7):1249-1251.
15. Nüsslein-Volhard C, Dahm R. Zebrafish : a practical approach (ed 1st). Oxford: Oxford University Press; 2002.
16. Kimmel CB, Ballard WW, Kimmel SR, Ullmann B, Schilling TF. Stages of embryonic development of the zebrafish. *Dev Dyn*. 1995;203(3):253-310.